

F. HOBLIT

Gust Loads on Aircraft: Concepts and Applications



Education Series

J. S. PRZEMIENIECKI EDITOR-IN-CHIEF

Gust Loads on Aircraft: Concepts and Applications

Frederic M. Hoblit
Consultant

Formerly,
Senior Research and Development Engineer
Lockheed-California Company

AIAA EDUCATION SERIES

J. S. Przemieniecki
Series Editor-in-Chief
Air Force Institute of Technology
Wright-Patterson Air Force Base, Ohio

This volume was sponsored by the Lockheed Aeronautical Systems Company and was originally published in whole as a Lockheed Report

Published by
American Institute of Aeronautics and Astronautics, Inc.
370 L'Enfant Promenade, S.W., Washington, D.C. 20024

Texts Published in the AIAA Education Series

Re-Entry Vehicle Dynamics

Frank J. Regan, 1984

Aerothermodynamics of Gas Turbine and Rocket Propulsion

Gordon C. Oates, 1984

Aerothermodynamics of Aircraft Engine Components

Gordon C. Oates, Editor, 1985

Fundamentals of Aircraft Combat Survivability Analysis and Design

Robert E. Ball, 1985

Intake Aerodynamics

J. Seddon and E. L. Goldsmith, 1985

Composite Materials for Aircraft Structures

Brian C. Hoskin and Alan A. Baker, Editors, 1986

Gasdynamics: Theory and Applications

George Emanuel, 1986

Aircraft Engine Design

Jack D. Mattingly, William Heiser, and Daniel H. Daley, 1987

An Introduction to the Mathematics and Methods of Astrodynamics

Richard H. Battin, 1987

Radar Electronic Warfare

August Golden Jr., 1988

Advanced Classical Thermodynamics

George Emanuel, 1988

Aerothermodynamics of Gas Turbine and Rocket Propulsion, Revised and Enlarged

Gordon C. Oates, 1988

Re-Entry Aerodynamics

Wilbur L. Hankey, 1988

Mechanical Reliability: Theory, Models and Applications

B. S. Dhillon, 1988

Aircraft Landing Gear Design: Principles and Practices

Norman S. Currey, 1988

American Institute of Aeronautics and Astronautics, Inc., Washington, DC

Library of Congress Cataloging-in-Publication Data

Hoblit, Frederic M.

Gust loads on aircraft: concepts and applications

p. cm.—(AIAA education series)

Bibliography: p.

Includes index.

1. Airplanes—Design and construction. 2. Gust loads. I. Title. II. Series.

TL671.2.H58 1988 629.132'3—dc19 88-8146 CIP

ISBN 0-930403-45-2

Copyright © 1988 by the American Institute of Aeronautics and Astronautics, Inc. All rights reserved. Printed in the United States of America. No part of this publication may be reproduced, distributed, or transmitted, in any form or by any means, or stored in a data base or retrieval system, without prior written permission of the publisher.

To My Lockheed Mentors,
Melcon A. Melcon, Jack Wignot, and Warren Stauffer

This page intentionally left blank

FOREWORD

One of the objectives of the AIAA Education Series is to provide archival documentation of the established practices in aircraft design. *Gust Loads on Aircraft: Concepts and Applications* by Frederic M. Hoblit is in this special category; it provides an authoritative exposition of the current engineering practice of determining gust loads on airplanes, especially the continuous-turbulence gust loads.

The author begins with the older concept of discrete-gust idealization of the gust structure, including the subject of static and dynamic discrete-gust loads, and then moves on to the more modern power-spectral, or continuous-turbulence, concepts and methods. This newer approach has gained wide acceptance and is being used today as the primary method of determining the dynamic loads due to gust encounters that are subsequently used to verify structural integrity of the airplane.

Because of the relative unfamiliarity of an average reader with the power-spectral methods, all the necessary mathematical concepts and methods are provided in the text. The continuous-turbulence gust loads criteria are discussed with reference to Federal Aviation Authority requirements and military specifications. This is followed by a detailed discussion of loads combination and design criteria, gust-response equations of motion, various short-cut methods, spanwise variation of vertical gust velocity, treatment of nonlinear systems, and analysis of gust-response flight-test data. The final chapter addresses the overall philosophy of discrete-gust concepts and their present applications.

This latest text in the AIAA Education Series provides a unique source of the design criteria and analysis of aircraft in turbulent air. It should be useful as a reference material for structural-loads engineers and as a supplementary text for courses in aeroelasticity, flight mechanics, and flight controls.

J. S. PRZEMIENIECKI
Editor-in-Chief
AIAA Education Series

This page intentionally left blank

TABLE OF CONTENTS

- xi Preface**

- 1 Chapter 1. Gust Loads Fundamentals**
 - 1.1 Mechanism of Gust Loads Generation
 - 1.2 Characteristics of Turbulence

- 7 Chapter 2. Discrete-Gust Static Loads**
 - 2.1 One-Minus-Cosine Idealization
 - 2.2 FAR Static Gust Requirement
 - 2.3 FAR Gust Loads Formula
 - 2.4 History of FAR Static Gust Requirements
 - 2.5 Effect of Static Aeroelastic Deformation on $C_{L\alpha}$
 - 2.6 Corresponding Military Requirements

- 15 Chapter 3. Discrete-Gust Dynamic Loads**
 - 3.1 Definition
 - 3.2 When, Where, and Why Considered
 - 3.3 Ingredients of the Discrete-Gust Dynamic Loads
Differential Equations
 - 3.4 Sample Results
 - 3.5 Criteria Considerations

- 21 Chapter 4. Basic PSD Concepts and Application to Gust Loads**
 - 4.1 Gust Profile as a Stationary Gaussian Random Process
 - 4.2 Measure of Intensity: RMS Value of y
 - 4.3 Probability Distribution
 - 4.4 Frequency Content and Power-Spectral Density (PSD)
 - 4.5 Gust PSD for Use in Design
 - 4.6 Frequency of Exceedance
 - 4.7 Application of Frequency of Exceedance to Gust Loads
 - 4.8 Determination of P 's and b 's from Flight Data
 - 4.9 Relation Between Frequency of Exceedance and
Probability of Exceedance
Problems

- 69 Chapter 5. Continuous Turbulence Gust Loads Criteria**
- 5.1 FAR Requirements
 - 5.2 Military Requirements
 - 5.3 Basic Forms of Criterion
 - 5.4 Design Levels
 - 5.5 Flight Profile Generation
 - 5.6 Modification of Design Envelope Criterion to Account for N_0
 - 5.7 Combined Vertical and Lateral Gust Loads
 - 5.8 Stability Augmentation or Active Control System (ACS)
- 97 Chapter 6. Load Combinations and Design Conditions**
- 6.1 The Phasing Problem
 - 6.2 Loads for Stress Analysis
- 115 Chapter 7. Gust Response Equations of Motion: Formulation and Solution**
- 7.1 Generalized Coordinates
 - 7.2 Grid Systems
 - 7.3 Basic Data
 - 7.4 Use of Matrices and Matrix Algebra
 - 7.5 Loads as Functions of Generalized Coordinate Response
 - 7.6 Solution for Frequency-Response Functions
 - 7.7 Inclusion of an Active Control System
 - 7.8 Computation of \bar{A} , N_0 , and ρ
 - 7.9 Checks for Error
- 123 Chapter 8. Short-Cut Methods**
- 8.1 Plunge-Only Curves
 - 8.2 Plunge-Pitch Curves: Hoblit Parameters
 - 8.3 Plunge-Pitch Curves: Peele Parameters
 - 8.4 Qualitative Relations Between Peele and $1/(1 + 2\pi k)$ Lift Growth Assumptions and Definition of an Effective \bar{c} for Use in Secs. 8.1.1 and 8.2
 - 8.5 Use of Plunge-Pitch Curves to Give Plunge-Only Data
 - 8.6 Use of Simplified Equations of Motion
 - 8.7 Empirical Adjustments Problems
- 165 Chapter 9. Spanwise Variation of Vertical Gust Velocity**
- 9.1 Introduction
 - 9.2 Applications of Three-Dimensional Gust Analysis
 - 9.3 Effect of Three-Dimensional Gust Analysis on Loads
 - 9.4 Effect of L on Three-Dimensional Gust Response

- 169 Chapter 10. Treatment of Nonlinear Systems**
- 10.1 Sources of Nonlinearities
 - 10.2 Use of Time-History Analysis
 - 10.3 Simplifications Made
 - 10.4 Gust Velocity Time History
 - 10.5 Interpretation of Results
- 173 Chapter 11. Analysis of Gust-Response Flight-Test Data**
- 11.1 Purpose of Gust-Response Flight Testing
 - 11.2 Basic Approach
 - 11.3 Selection of Samples for Analysis
 - 11.4 Gust Velocity Determination
 - 11.5 Use of PSD's
 - 11.6 PSD Determination: Parameter Selection
 - 11.7 Other Considerations in PSD Determination
 - 11.8 Effects of Computing Options on PSD's and Frequency-Response Functions
- 187 Chapter 12. Adequacy of the Stationary-Gaussian Idealization of the Gust Structure**
- 12.1 Evidence of Possible Inadequacies in the Stationary-Gaussian Model
 - 12.2 Non-Gaussian Turbulence vs Nonstationary Turbulence
 - 12.3 Evaluation of the Adequacy of the Stationary-Gaussian Model
 - 12.4 Other Models
- 197 Chapter 13. Present Place of Discrete-Gust Load Requirements**
- 13.1 Nature of Atmospheric Turbulence
 - 13.2 Tuned Discrete-Gust Analysis
 - 13.3 Static Discrete-Gust Loads
 - 13.4 Computational Considerations
- 203 Appendix A: Plunge-Only Equation of Motion for an Airplane Encountering a One-Minus-Cosine Vertical Gust**
- 209 Appendix B: Elementary Introduction to Some Concepts in Probability Theory and Statistics**
- B.1 Probability of a Single Event
 - B.2 Some Basic Rules of Probability
 - B.3 Probability Distribution
 - B.4 Frequency of Exceedance

- 217 **Appendix C: Gaussian Probability Distribution Plots**
 - C.1 Plots
 - C.2 Sources of Data: y/σ Less than 5.0
 - C.3 Sources of Data: y/σ Greater than 5.0

- 227 **Appendix D: Ratio of von Kármán to Dryden Gust PSD's**

- 229 **Appendix E: Upper Limit of Integration in Computation of \bar{A} , N_0 , and ρ**
 - E.1 Problem
 - E.2 Factors Tending to Make Φ Drop Off Faster than Indicated by Simple Theory
 - E.3 Effect of N_0 on Loads
 - E.4 Usual Practice in Selecting Upper Limit
 - E.5 Houbolt Criterion

- 237 **Appendix F: Plots of σ_w Probability Distributions**

- 241 **Appendix G: Derivation of Generalized Frequency of Exceedance Equation**

- 243 **Appendix H: Relative Ultimate Gust Capabilities for Upbending, Downbending, and Lateral Gust**

- 253 **Appendix I: Most Likely σ_w Value Associated with a Particular Load Level**
 - I.1 Introduction and Results
 - I.2 Integrations of Joint Probability Density of w and σ_w
 - I.3 Integrations of Rice's Equation $\times p(\sigma_w)$
 - I.4 Derivation of Formulas for Fitting Parabolic Curves to Tabulated Data

- 275 **Appendix J: Matrices and Matrix Algebra**
 - J.1 Matrix Evaluation of Generalized Mass, $\Sigma \phi^2 \Delta M$
 - J.2 Basic Formulation of Gust Equations and Method of Solution
 - J.3 Typical Vertical Gust Equations of Motion in Frequency-Response Form

- 283 **Appendix K: C.G. Acceleration PSD's for an Idealized Rigid Airplane Free to Pitch and Plunge**

- 287 **Appendix L: Annotated Bibliography**

- 297 **References**

- 303 **Subject Index**

PREFACE

The primary purpose of this book is to provide a comprehensive introduction to the subject of gust loads on airplanes, especially continuous-turbulence gust loads, with emphasis on understanding basic concepts. A secondary purpose is to provide detailed information on certain gust loads subjects not adequately covered elsewhere or for which this book would be a convenient reference.

The intended users fall into two categories:

1) Persons with limited experience in gust loads determination, such as —

- New loads engineers.
- Loads engineers whose specialization has been outside the area of gust loads determination.
- Engineers in other disciplines, such as flutter, control systems, etc. that must interface with the gust loads discipline.
- Engineering supervision in loads and related disciplines.
- Aeronautical engineering instructors at all levels.
- Engineering students.

The structural loads discipline is such a narrow one that virtually no loads engineers receive their education in this specialty other than on the job. Accordingly, this book has been written primarily with the practicing engineer in mind. Nevertheless, it could serve admirably as auxiliary material for courses in aeroelasticity, flight dynamics, and flight controls. In this capacity, it would provide a deeper understanding of how the mathematical techniques covered in such courses relate to real airplanes flying in real turbulence and how these techniques are used in engineering practice. It would also be appropriate as auxiliary material for courses in airplane structures.

2) Persons with more extensive experience in gust loads determination, but who may not be aware of particular aspects of the subject not used in everyday work.

This book had its origins in notes developed for the gust loads portion of a loads course given to FFA airframe engineers in 1975. Those notes, however, were mostly in outline form and required expanding into coherent prose. This was accomplished as the notes evolved first into a proprietary Lockheed report in 1982. At that time, too, the scope of the material covered was considerably expanded. For this book, the many references to Lockheed proprietary material have been removed; a limited amount

of new material has been added; and some of the original material has been updated and otherwise reworked to improve the presentation.

A major emphasis has been placed on power-spectral, or continuous-turbulence, concepts and methods. The first published material on the application of power-spectral methods to gust loads studies appeared in 1952 and 1953. Since that time, the continuous-turbulence approach to gust loads determination has undergone extensive development and has gained wide acceptance. At Lockheed, for the purpose of assuring adequate strength with respect to gust encounter, primary reliance is placed—and has been for 25 years—on dynamic loads obtained using the continuous-turbulence approach.

Some use continues to be made of the older discrete-gust idealization of the gust structure. For this reason, and because of its historical importance, the subject of static and dynamic discrete-gust loads is also covered in some detail.

One of the long-standing needs that this work is intended to fill is for a brief, practical introduction to the use of power-spectral methods in loads work generally. The author has long held that the mathematical introduction to power-spectral theory often found is not only overwhelming to the average engineer, but totally unnecessary for understanding the concepts and putting them to work.

Chapter 4 provides such an introduction. It involves accepting on faith a few plausible relationships—for example, Eqs. (4.7), (4.15), and (4.19)—and proceeding from there. The reader interested only in power-spectral methods may find all he or she needs in Chapters 1 and 4. Chapters 5 and 6, however, provide additional material that is fundamental to gust-loads applications of these methods. Chapters 7 through 12 cover material that is more specialized, although still of practical and conceptual importance.

The material presented herein draws heavily on the author's firsthand knowledge of Lockheed-California Company practices and experience. (The Lockheed-California Company was one of several Lockheed companies that were combined in 1987 to form the Lockheed Aeronautical Systems Company.) The material also may reflect the author's prejudices. This is inevitable and no apology is made.

Although only gust loads applications are dealt with explicitly herein, the basic concepts discussed in Chapter 4—especially in Secs. 4.1, 4.2, 4.3, 4.4, and 4.6—have found wide use in many fields of science and engineering. Specific mention might be made of application to taxi loads (response to runway bumps), buffet loads, ship motions in waves, noise in electronic circuits, and the theory of Brownian motion.

Virtually nothing is said about the important subject of repeated loads spectra—in other words, fatigue. Repeated loads spectra are basically exceedance curves, and these are covered thoroughly in Secs. 4.6, 4.7, and 5.5, but the practical generation of realistic spectra of local stresses, or of jack load sequences for an airplane fatigue test, is not covered. This subject

is comparable in scope to the generation of matching conditions to define loads at the limit design level, covered in Sec. 6.2.3.

Also, there is virtually no discussion of the application of power-spectral methods to the determination of airplane motions, as distinct from loads. The same concepts, techniques, and computer programs that are effective in predicting airplane loads will also predict airplane motions. The criteria for evaluating the acceptability of these motions, however, require separate treatment. Prediction of airplane motions also has application with respect to functioning of equipment, especially in military applications.

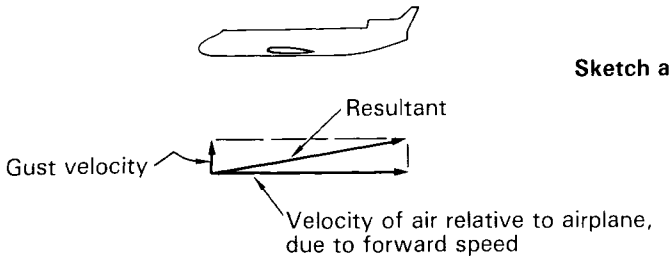
FREDERIC M. HOBLIT
Studio City, California

GUST LOADS FUNDAMENTALS

1.1 MECHANISM OF GUST LOADS GENERATION

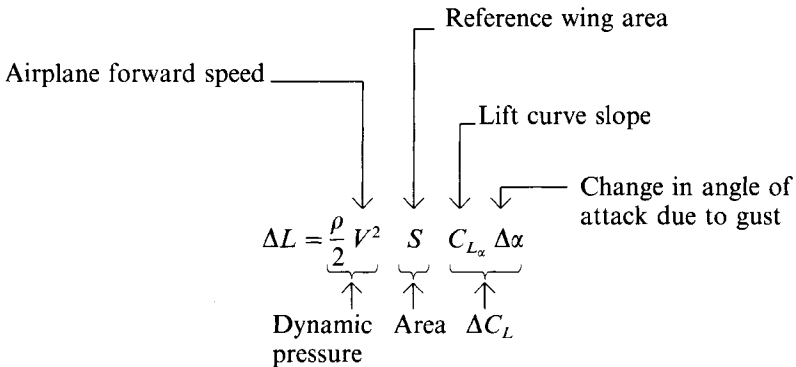
1.1.1 Vertical and Lateral Gust

Gust loads, whether due to discrete gusts or continuous turbulence, are ordinarily considered to be the result of a change in angle of attack due to a component of gust velocity at right angles to the flight path. Vertical and lateral gusts fall into this category. The change in angle of attack, in radians, is equal to the gust velocity divided by the forward speed.



Sketch a

If we consider, for example, a vertical gust, the change in lift due to the gust is



$$\Delta L = \frac{\rho}{2} V^2 S C_{L\alpha} \frac{U}{V} = \frac{\rho}{2} UV S C_{L\alpha} \quad (1.1)$$

\downarrow Gust velocity

Dividing by W (airplane weight) gives the incremental load factor Δn

$$\Delta n = \frac{\Delta L}{W} = \frac{\frac{\rho}{2} UV C_{L\alpha}}{W/S} = \frac{\frac{\rho}{2} UV}{\left(\frac{W}{C_{L\alpha} S}\right)} \quad (1.2)$$

Usual expression

Expression separating speed-altitude parameters (numerator) from other airplane parameters (denominator)

1.1.2 Head-On Gust

This case can also be important. Here, all that changes is the dynamic pressure. (The angle of attack is simply the constant pitch attitude of the airplane.)



Sketch b

Velocity V due to forward speed



Gust velocity U

$$\Delta L = \frac{\rho}{2} [(V + U)^2 - V^2] S C_L = \frac{\rho}{2} (2UV + U^2) S C_L$$

$$\Delta L = \frac{\rho}{2} (2UV) \left(1 + \frac{1}{2} \frac{U}{V}\right) S C_L \approx \frac{\rho}{2} (2UV) S C_L \quad (1.3)$$

Note that ΔL now depends on steady-flight C_L instead of on $C_{L\alpha}$. It still depends on the product UV . Dividing by W gives Δn

$$\Delta n = \frac{\Delta L}{W} = \frac{\frac{\rho}{2} (2UV) C_L}{W/S} = \frac{\frac{\rho}{2} (2UV)}{\left(\frac{W}{C_L S}\right)} \quad (1.4)$$

GUST LOADS FUNDAMENTALS

3

An alternate equation for Δn is given by substituting

$$C_L = \frac{W}{\frac{\rho}{2} V^2 S} \quad \text{or} \quad \frac{W}{C_L S} = \frac{\rho}{2} V^2$$

to give

$$\Delta n = \frac{\frac{\rho}{2} (2UV)}{\frac{\rho}{2} V^2} = 2 \frac{U}{V} \tag{1.5}$$

The head-on gust, it should be noted, produces only a lift, not a side force, inasmuch as in steady-flight $C_y = 0$.

1.1.3 Ratio of Lifts, Head-On to Vertical Gust

Combining Eqs. (1) and (3), we obtain

$$\frac{\Delta L_{\text{head-on}}}{\Delta L_{\text{vertical}}} = \frac{\frac{\rho}{2} (2UV) S C_L}{\frac{\rho}{2} (UV) S C_{L\alpha}} = 2 \frac{C_L}{C_{L\alpha}} \tag{1.6}$$

Values of this ratio for typical situations are shown in the next to last column of the following table:

Line	Airplane	Condition	$C_{L\alpha}$	C_L	$2 \frac{C_L}{C_{L\alpha}}$	Total Vertical
1	L-1011	Cruise: $h = 32,000$ ft $W = 390,000$ lb $M = 0.85$	7.16	0.39	0.11	1.006
2	L-1011	Approach: 45-deg flaps, $W = 330,000$ lb $V_e = 165$ kts	6.47	1.04	0.32	1.050

Because of the probabilistic nature of atmospheric turbulence or gusts, and in particular the fact that vertical and head-on gusts are uncorrelated, it is realistic to combine lifts due to vertical and head-on gusts on a root-sum-square basis. The root-sum-square addition can also be shown to give maximum lift due to a gust of constant velocity as its direction varies. Accordingly, in the last column of the table, the ratio of total lift, at any

given probability level, to lift due to vertical gust alone is given as $\sqrt{1 + [2(C_L/C_{L_0})^2]}$.

The figures in the preceding Table are only approximate, in that they do not take account of the airplane motions in response to the gust encounter. These motions will be somewhat different for vertical and head-on gusts (see Sec. 1.1.4).

1.1.4 Effect of Airplane Motions

The *net* change in angle of attack felt by the airplane depends not only on the gust velocity, but also on the airplane motion induced by the gust as the airplane traverses the gust profile. A gust will never reach its maximum velocity instantaneously; during the period of buildup, the airplane will have time to acquire motion. The pertinent airplane motions, in response to a *vertical gust*, are as follows:

Plunge. The airplane will translate vertically in the direction of the gust velocity, so that the net gust velocity felt is reduced (see also Sec. 2.2).

Pitch. The airplane, because of its natural pitch stability, will tend to weathervane so as to reduce the gust increment in angle of attack.

The differential equation for motion of a rigid airplane in response to a vertical gust can be written in terms of a single variable α . This variable α is the *increment* in angle of attack due to the *airplane motions*, $\theta + \dot{z}/V$; it does *not* include the angle of attack $\alpha_g = U/V$ associated with the gust velocity directly, which appears in the equation of motion as the forcing function. This equation is a second-order linear differential equation, so the response is analogous to that of a single-mass mass-spring-damper system.* Consequently, factors that affect the response of such a system also affect airplane response to gusts in much the same way. These would include, for example, damping, forcing-function “rise time,” and resonant response to repeated load application. The forcing function, however, consists not only of the gust velocity itself, but also its first and second derivatives. Because the differential equation is of second order, the airplane motions can result not only in load alleviation (reduction),† but also in a load increase due to dynamic overshoot.

Loads due to *lateral gust* are affected by airplane motions in a manner comparable to that described for vertical gusts.

For a *head-on gust*, the alleviation effect of plunge motion is the same as

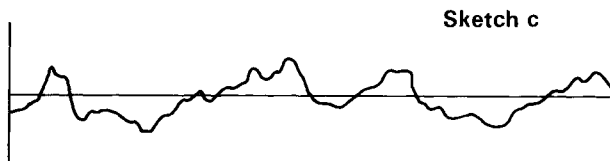
*The actual equation can be derived, for example, starting with Eqs. 4.15,7 p. 133, of Ref. 1. Only Eqs. (b) and (c) are used, representing equilibrium in plunge and pitch, respectively. The \ddot{u} , $\dot{\eta}$, and $\ddot{\eta}$ terms are deleted as not pertinent, and the θ term in Eq. (b) is deleted as negligible. An α_g term is added to each of the equations. The force equation is then solved for $\dot{\theta}$ and the resulting expression substituted into the pitch equation, which then contains the single variable α .

†The load reduction is due primarily to the fact that loads are proportional to $(\alpha_g + \alpha)$, and at low frequencies α tends to subtract from α_g , so that $|\alpha_g + \alpha| < |\alpha_g|$.

for a vertical gust; the motion will depend only on the lift produced, not on its source. The pitch motion will be different, however, inasmuch as the increment in lift due to a vertical gust will act at the airplane aerodynamic center, whereas the lift due to a head-on gust will act at the 1-g flight center of pressure, that is, the c.g. (These can differ substantially, for example, as the result of a difference between wing and tail angles of attack in 1-g flight; in fact, they must differ if the airplane is to be "statically stable.") In addition, in the case of a head-on gust, there is probably some very small alleviating effect due to slowdown resulting from the drag increase associated with the increase in dynamic pressure.

1.2 CHARACTERISTICS OF TURBULENCE

1.2.1 Typical Gust Profile



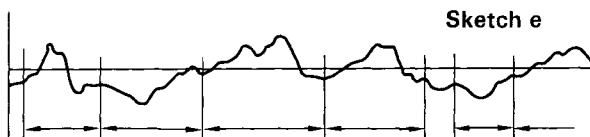
A gust profile in space becomes a gust velocity time history when the distance scale is divided by the airplane forward speed to become a time scale. Typically, gust profiles tend to be continuous and irregular, as illustrated by foregoing Sketch c.

1.2.2 Terminology

Generally, when the profile is continuous, the gust structure is spoken of as turbulence. When the gust structure consists of more or less isolated pulses, the single pulse is referred to as a gust.



Also, a continuous turbulence profile can be thought of, loosely, as consisting of a series of individual gusts.



Expressions such as “gust structure,” “gust profile,” or “gust loads” refer equally to continuous turbulence and individual gusts.

1.2.3 *Isotropy*

Typically, atmospheric turbulence tends to be not only continuous, but also isotropic—the same in all directions. Thus, 1) along a given path through a patch of turbulence, the *lateral gust* profile will tend to have the same general characteristics as the *vertical gust* profile, including roughly the same peak values; 2) in *traverses in various directions* through the same patch of turbulence, the resulting profiles will tend to have the same general characteristics; and 3) in terms of individual gusts, a given gust is equally likely to occur as a vertical gust, a lateral gust, or a gust in any other direction, and it is equally likely to be found in any direction of traverse—north-south, east-west, upwind, downwind, crosswind, etc.

1.2.4 *Sources of Turbulence*

The usual breakdown is as follows:

1) *Storm* (especially thunderstorm): The most common source of severe turbulence.

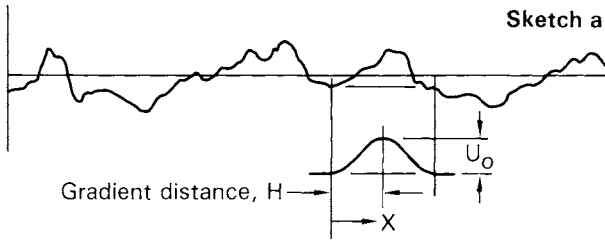
2) *Cumulus cloud*: The same mechanism as thunderstorm, but less severe.

3) *Clear air*: Usually much less severe; particular sources include wind shear; jet stream (can be severe due to high wind shear); wind over ground (wind shear in the Earth’s boundary layer); wind over and between mountains (can be extremely severe close to the ground); and convection due to morning warming of air close to the ground, especially over the desert.

DISCRETE-GUST STATIC LOADS

2.1 ONE-MINUS-COSINE IDEALIZATION

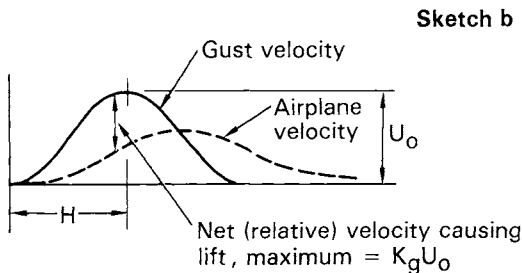
The usual individual gust, or “discrete gust,” idealization of the gust structure consists of a one-minus-cosine pulse:



$$U = \frac{1}{2} U_0 \left(1 - \cos \frac{2\pi x}{2H} \right)$$

2.2 FAR STATIC GUST REQUIREMENT

For the purpose of obtaining static gust loads, FAR 25 (Federal Aviation Regulations, Part 25²) specifies the one-minus-cosine shape and an airplane motion confined to plunge only. The gust velocity and airplane vertical velocity then relate as shown in Sketch b:



(Actually, the use of K_g in Sketch b is an over-simplification. K_g as normally used in gust loads calculations is taken to include not only the effect of the airplane motion, indicated in the sketch, but also the lag in buildup of lift in response to gust entry and sudden changes in angle of attack. See the next section and Appendix A.)

2.3 FAR GUST LOADS FORMULA

The FAR gust loads formula, for vertical gust loads, is, essentially,

$$\Delta n = K_g \frac{U_{de} V_e C_{L_\alpha}}{498 \frac{W}{S}} \quad (2.1)$$

“Sharp-edge-gust” response

in combination with

$$K_g = \frac{0.88 \mu_g}{5.3 + \mu_g} \quad (2.2)$$

$$\mu_g = \frac{2W}{\rho g S \bar{c} C_{L_\alpha}} \quad (2.3)$$

where

Δn = incremental load factor.

K_g = factor to account for airplane motion (Sketch b) and lag in buildup of lift.

U_{de} = derived equivalent gust velocity, fps.

V_e = airplane equivalent airspeed, knots.

C_{L_α} = airplane lift curve slope (per rad).

$$498 = \frac{1}{\frac{\rho_0}{2} 1.689}$$

where ρ_0 is the sea-level air density and 1.689 converts V_e in knots to fps.

W = airplane weight.

S = reference wing area.

μ_g = “mass parameter” as defined by Eq. (2.3).

ρ = air density.

\bar{c} = wing mean geometric chord.

g = acceleration due to gravity.

Equation (2.1) is equivalent to Eq. (1.2), except for the addition of the coefficient K_g to account for the airplane motion and lag in buildup of lift.

U_{de} corresponds to U_0 in Sketch b. It is equal to $U_0 \sqrt{\rho/\rho_0}$; hence, the subscript e for “equivalent.” The subscript d for “derived” reflects the fact that values of U_{de} can be derived from accelerations recorded in operational flight, by solving Eq. (2.1) for U_{de} . In this sense, U_{de} is not an actual velocity, but a fictitious gust velocity derived from the acceleration according to highly arbitrary assumptions as to gust shape.

DISCRETE-GUST STATIC LOADS

Values of U_{de} are specified as functions of altitude. At altitudes from sea level to 20,000 ft, the values are

- at V_B (design rough-air speed) $U_{de} = 66$ fps
- at V_C (design cruise speed) $U_{de} = 50$ fps
- at V_D (design dive speed) $U_{de} = 25$ fps

The lower gust velocity at V_C than at V_B reflects the expectation that the airplane can be slowed down (to V_B) prior to encountering a gust of over 50 fps. The still lower gust velocity at V_D reflects the very low probability that the airplane will be flying at V_D , resulting from the fact that purposely flying in excess of V_C is illegal.

At altitudes above 20,000 ft, U_{de} decreases linearly to the following values at 50,000 ft: At V_B , 38 fps; at V_C , 25 fps; and at V_D , 12.5 fps. The design-load factor is considered to vary linearly between V_B and V_C and between V_C and V_D . (This is not necessarily the same as considering the gust velocities to vary linearly, because of the variation of $C_{L\alpha}$ with both Mach number and equivalent airspeed.)

K_g is specified to be determined on the basis of a one-minus-cosine gust shape with a gust gradient distance* H (sketch b) of 12.5 chordlengths (mean geometric). Equation (2.2) is an acceptable empirical equation that

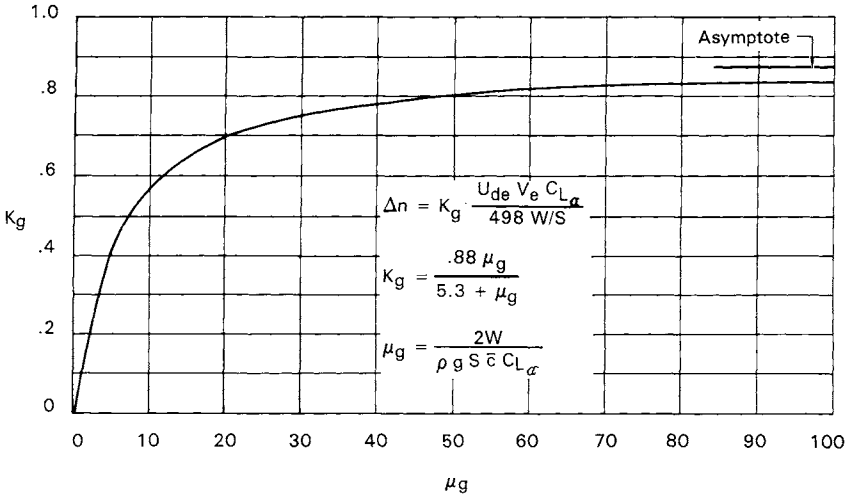


Fig. 2.1 Gust factor K_g , current FAR gust loads formula.

*The term *gradient distance* originated at a time when the gust profile was considered to be of a linear-ramp shape (sketch b) so that there was a clearly defined portion of constant gradient. The usage has carried over to other shapes.

Downloaded by RMIT UNIV BUNDOORA on June 4, 2013 | http://arc.aiaa.org | DOI: 10.2514/6.861888

approximates the values that have been computed at a series of values of μ_g . K_g as given by this equation is plotted in Fig. 2.1.

The gradient distance H is specified in chordlengths instead of feet for two reasons. The first is somewhat obscure, the precise details having become blurred with the passage of time. It appears to involve, however, a combination of qualitative reasoning and experimental evidence. The qualitative reasoning is that the gradient distance felt by the airplane in its plunge motion will depend on how rapidly it weathervanes in pitch. As a very rough approximation, the greater the wing chord, the slower the airplane response. The experimental evidence is shown in Fig. 2.2, taken from NACA Report 997.³ When gust velocity is plotted versus gradient distance for a variety of

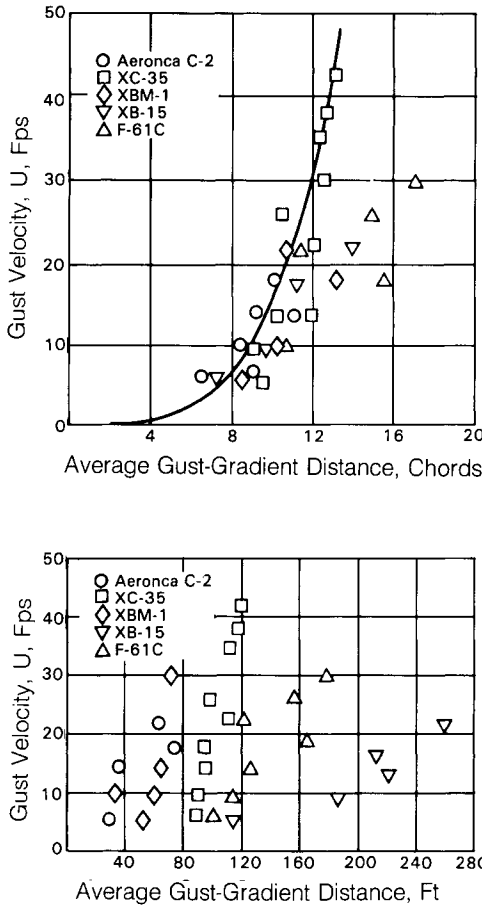
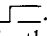


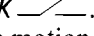
Fig. 2.2 Correlation of gust velocity with gradient distance expressed in feet and chords.

airplanes, the scatter is much less when the gradient distance is expressed in chordlengths than when expressed in feet. The second reason is that the determination of K_g is greatly simplified. The formulation and solution of the equation of motion for determining K_g is discussed in detail in Appendix A. The treatment there of a relatively simple case illustrates various facets of gust response determination in general, as well as providing concrete background relative to the FAR gust loads formula.

2.4 HISTORY OF FAR STATIC GUST REQUIREMENTS

The FAR static gust loads formula in its present form is discussed in Sec. 2.3. The evolution of the civil airworthiness gust loads requirements from their first appearance to their present form occurred gradually over a period of some 20 years, from the early 1930's to the mid-1950's. Before that time, gust loads were not considered in design; the flight maneuver conditions alone were considered to provide adequate strength. As design speeds increased, however, it was evident that gust loadings would likewise increase [Eq. (2.2)] and there was growing concern that gust loads should be considered explicitly in design. Knowledge pertinent to gust loads had been growing for some time; indeed, Part 2 of NACA Report 1, published in 1915, was entitled "Theory of an Aeroplane Encountering Gusts."⁴ (This extraordinary paper, prepared by E.B. Wilson of MIT, is discussed at some length in Ref. 4.)

Sharp-edge gust . The first U.S. civil requirements relating to gust loads were included in the 1934 "Airworthiness Requirements for Aircraft" issued by the Bureau of Air Commerce. This first requirement was based on a sharp-edge-gust concept. Loads were given, in effect, by Eq. (1.2); no consideration was given to the effects of airplane motion. The design gust velocity was taken as 30 fps; the corresponding airplane speed was the equivalent of what would now be the design cruise speed. Apparently, there was also a requirement for a 15 fps gust velocity at a design dive speed.

U_e and K . By the late 1930's, a need to account for the differences in airplane motion due to gust encounter from one airplane to another had become apparent. This need was most strikingly apparent in the design of gliders. A glider, with its very low wing loading, will quickly acquire vertical velocity as it penetrates the gust; accordingly, the net gust velocity felt by the glider (Sketch b) would be far less than for a typical airplane. As a result, the gust loads would be vastly over-predicted. The regulations that resulted are contained in the February 1941 issue of the Civil Aeronautics Manual (CAM 04); they may actually have first appeared two or three years earlier.

In CAM 04 the design gust velocity is designated U_e (e for equivalent). It is specified as 40, 30, and 15 fps for speeds V_B , V_C , and V_D , respectively. The gust velocities do not vary with altitude (although because the equivalent

GUST LOADS ON AIRCRAFT

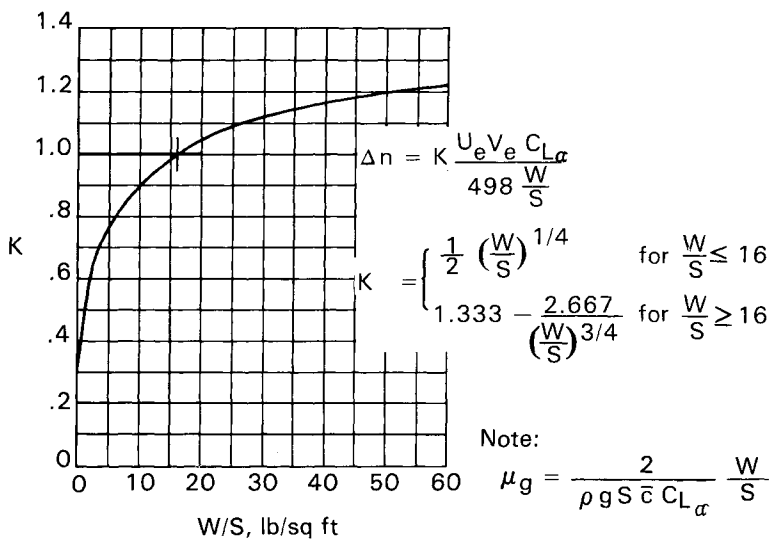


Fig. 2.3 Gust “alleviation factor,” pre-1953 gust loads formula.

gust velocities are constant, the true gust velocities do indeed vary.) The effect of airplane motions is indicated in Fig. 2.3. The alleviation factor K is defined as a function of wing loading W/S . The curve was initially derived on the basis of theory, on the assumption of a linear-ramp gust shape; it was then simplified to the form shown, essentially by assuming typical values for particular airplane and flight parameters. To preserve continuity with past practice with respect to design gust velocities, the curve was adjusted to a value of unity for a typical existing airplane, the Boeing B247.

U_{de} and K_g . The current regulations utilize theoretical work undertaken by the NACA for this purpose and published in 1953 in NACA TN 2964.⁵ They became effective with the publication of CAR 4b-3 in 1956. In the current regulations, the linear-ramp shape was replaced by a one-minus-cosine pulse. The resulting alleviation factor, now designated the gust factor K_g , was determined directly on the basis of simple theory without further approximations; thus, the appearance of the mass parameter μ_g in Fig. 2.1 in place of the simpler parameter W/S . The gust velocities were selected to give approximately the same load factors as the previous regulation for then current airplanes; actually, the loads came out generally a few percent higher. The chosen gust velocities, 66, 50, and 25 fps at V_B , V_C , and V_D , respectively, were held constant to an altitude of 20,000 ft and then decreased with further increasing altitude.

A comparison of the old and new criteria for a typical airplane of the time,

the Lockheed Model 1649 Constellation at design cruise speed, is obtained as follows:

$$\begin{aligned}
 W &= 116,000 \text{ lb} \\
 S &= 1850 \text{ ft}^2 \\
 \bar{c} &= 13.3 \text{ ft} \\
 h &= 20,000 \text{ ft} \\
 \rho &= 0.001267 \text{ lb s}^2/\text{ft}^4 \\
 V_e &= 261 \text{ knots} \\
 C_{L_\alpha} &= 6.59/\text{rad} \\
 W/S &= (116,000 \text{ lb})/(1850 \text{ ft}^2) = 63 \text{ lb/ft}^2 \\
 K &= 1.214 \text{ (Fig. 2.3)} \\
 KU_e &= (1.214)(30 \text{ fps}) = \underline{36.4 \text{ fps}} \\
 \mu_g &= \frac{2(W/S)}{\rho g \bar{c} C_{L_\alpha}} = \frac{2(63)}{(0.001267)(32.2)(13.3)(6.59)} = 35.2 \\
 K_g &= 0.765 \text{ (Fig. 2.1)} \\
 K_g U_{de} &= (0.765)(50 \text{ fps}) = \underline{38.3 \text{ fps}}
 \end{aligned}$$

2.5 EFFECT OF STATIC AEROELASTIC DEFORMATION ON C_{L_α}

As an airplane encounters a gust, the structure deforms statically in response to the forces developed. Consequently, the aerodynamic forces are different from those for a rigid airplane. In using the gust loads formula, it is reasonable to use the appropriately modified value of C_{L_α} . For a swept wing transport, the effect is a reduction in C_{L_α} . This reduction is the result of the bending deformation of the wing; as the wing bends up, a streamwise section will experience a greater deflection at the trailing edge than at the leading edge, because the trailing edge corresponds to a more outboard location along the wing structural axis.

Although use of a flexible-airplane C_{L_α} is reasonable in concept, some care is appropriate in order to maintain consistency in practice. To the extent that a rigid-airplane assumption may have been utilized in establishing the design gust velocities, it could be unconservative to take advantage of aeroelastic relief in a new design. Actually, however, the current design gust velocities were established at a time when virtually all airplanes were straight wing and static aeroelastic effects were small. Accordingly, in the design of the L-1011, for example, it was considered appropriate to use the flexible-airplane C_{L_α} in the gust loads formula.

Determination of stability derivative “flex-to-rigid” ratios is a well-developed art, at least at the Lockheed-California Company. Two aspects of these calculations, however, are not always appreciated and bear emphasis at this point. Firstly, in computing the deformed shape, inertia forces as well as aerodynamic forces must be included. In this respect, an airplane in flight is different from a model in a wind tunnel. For the wind-tunnel case, in contrast to the free-airplane case, inertia forces do not change, remaining at their

1-g values regardless of what happens to the aerodynamic forces as a result of the change in α . As a corollary, the flex-to-rigid ratios are different, depending on the airplane weight and weight distribution. Secondly, *in defining* α , the airplane reference must be the “phantom rigid airplane” with respect to which the aeroelastic deflections would occur if considered to be given by superposition of the free-vibration elastic modes. This is the reference with respect to which, for each mode and hence for the total deflected shape,

$$\int \phi x \, dm = 0$$

where x is the distance of the mass element from the pitch axis through the cg , and ϕ is the deflection of the mass element relative to the reference.

This requirement follows from the concept that, as the airplane deforms, it does so without pitch rotation of the airplane as a whole. Any pitch rotation of the airplane as a whole, if it is to be accounted for in the analysis, must be calculated from the airplane equations of motion, considering the pitching moments acting and integrating the pitching accelerations with respect to time.

2.6 CORRESPONDING MILITARY REQUIREMENTS

Although Eq. (2.1) is sometimes referred to simply as “the FAR gust loads formula,” the identical equation is, in fact, equally well established in U.S. Air Force (USAF) and U.S. Navy specifications. It was initially developed, in its present form, as a joint project of the regulating agencies and the NACA in about 1953.⁵

The military discrete-gust loads requirements do, however, differ from FAR with respect to designation and definition of the design speeds at which the three design gust velocities apply, with V_G , V_H , and V_L corresponding to V_B , V_C , and V_D , respectively. In addition, the reduction of design gust velocity with altitude above 20,000 ft is different in the U.S. Navy requirements than in FAR. (The USAF requirement agrees with FAR.)

DISCRETE-GUST DYNAMIC LOADS

3.1 DEFINITION

The term “dynamic loads” is used at the Lockheed-California Company—and probably rather generally elsewhere—to indicate loads that include the inertia forces associated with elastic-mode accelerations.

3.2 WHEN, WHERE, AND WHY CONSIDERED

Discrete-gust dynamic loads are not now required by FAR nor by the Federal Aviation Authority (FAA). They are superseded by the continuous turbulence loads requirement of FAR 25.305 (d) and FAR Appendix G² (see Chapters 4 and 5). The determination of discrete-gust dynamic loads in connection with FAA certification reached its high point at the Lockheed-California Company in 1955–1960, in conjunction with design of the Model 1649 Constellation and the Electra, including the 1960 Electra structural reevaluation. The British Civil Aviation Authority (CAA) is reluctant to rely on a continuous turbulence gust loads analysis. Accordingly, the British Civil Airworthiness Requirements⁶ (BCAR) still requires that design loads include discrete-gust dynamic loads. Extensive discrete-gust dynamic loads calculations have been performed for British certification of the L-1011, for example, for all production versions to date.

It is the author’s understanding that some other U.S. companies still perform discrete-gust dynamic loads calculations for their own information, in addition to the continuous turbulence loads on which primary reliance is based. One advantage of the discrete-gust approach is the easier visualization of how the airplane is responding. At Lockheed-California, however, the continuous turbulence loads are considered fully adequate in themselves.

3.3 INGREDIENTS OF THE DISCRETE-GUST DYNAMIC LOADS DIFFERENTIAL EQUATIONS

3.3.1 *Elastic and Rigid-Body Modes*

The differential equations use as generalized coordinates the pertinent rigid-body and elastic (free-vibration) modes. In the 1955–1960 analyses, only two generalized coordinates were used, airplane plunge and the first wing-bending elastic mode. In the 1960 Electra work, the actual first wing-bending-mode shape was used, including the fairly substantial wing twist

present in this mode. In the L-1011 analyses, the same generalized coordinates are used as in the continuous turbulence analysis, two rigid-airplane and 20 elastic modes in the vertical gust analysis and three rigid-airplane and 30 elastic modes in the lateral gust analysis (see Chapter 7).

3.3.2 Aerodynamics and Coupling

Aerodynamic forces are included in the analysis as produced both by the gust velocity directly and by the airplane motions. Lag in buildup of lift is accounted for. These forces result in the coupling of the various modes, that is, motions in one mode result in generalized forces on all the others.

3.3.3 Time-History Solutions

The essential feature of the analysis is the determination of time-history solutions of the differential equations.

3.3.4 Integrated Loads

Time histories of shears, bending moments, and torsions, as well as of generalized coordinate displacements, velocities, and/or accelerations, are included in the solution. The integrated-load time histories are computed from the time histories of the gust input and the motions in the various rigid-airplane and elastic modes.

3.4 SAMPLE RESULTS

Time histories of wing-bending moment for the L-1011 at BL 150 are shown for several gradient distances in Fig. 3.1. Peak values as a function of gradient distance are shown in Fig. 3.2 for both the flexible airplane and the statically responding airplane. For the statically responding airplane, forces due to accelerations and velocities in the elastic modes are set equal to zero in the time-history solutions, but forces due to elastic mode displacements are retained.

3.5 CRITERIA CONSIDERATIONS

3.5.1 Tuning

In the calculation of static-gust loads, a single gradient distance of 12.5 chords is specified. This does not say that all actual gusts are of the same gradient distance, but the actual gradient distance, from a static gust standpoint, is not very important. As can be seen from Fig. 3.2, the gradient distance can vary over a wide range with only a very small effect on the static gust loads.

The dynamic response, however, also as shown in Fig. 3.2, is indeed sensitive to gradient distance. Because of the presence in the atmosphere of

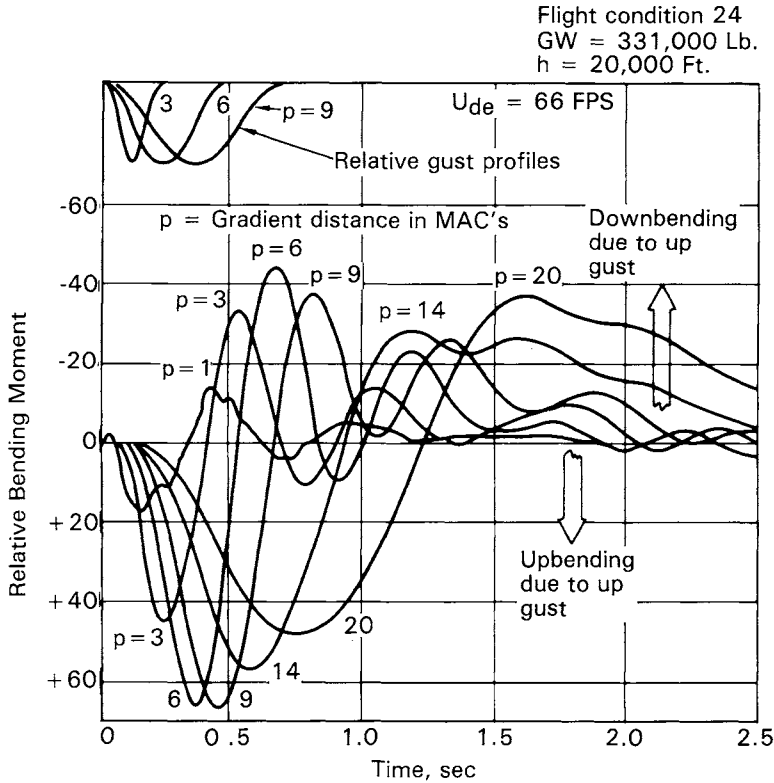


Fig. 3.1 Incremental wing bending moment time histories due to one-minus-cosine discrete gust; L-1011-1 at BL 150.

gusts having a wide range of gradient distance, it is important to tune the gust to give maximum response. Hence, the familiar designation, “tuned discrete-gust analysis.”

FAR has never spelled out explicitly how a discrete-gust dynamic analysis should be carried out. The requirement follows entirely from the brief general statement, “Where structural flexibility is such that any rate of load application likely to occur in the operating conditions might produce transient stresses appreciably higher than those corresponding to static loads, the effects of this rate of application must be considered.” [FAR 25 305(c)]. Sometimes, FAR has been interpreted literally as requiring the dynamic loads to be determined only for the 12.5 chord gust. This, of course, makes no sense at all, and both the FAA and the CAA have generally required that a range of gradient distances be included.

GUST LOADS ON AIRCRAFT

Flight condition 24 GW = 331,000 Lb. h = 20,000 Ft. V _e = 278 KEAS (V _{TP})	Flight condition 6 GW = 233,600 Lb. h = 20,000 Ft. V _e = 278 KEAS
---	---

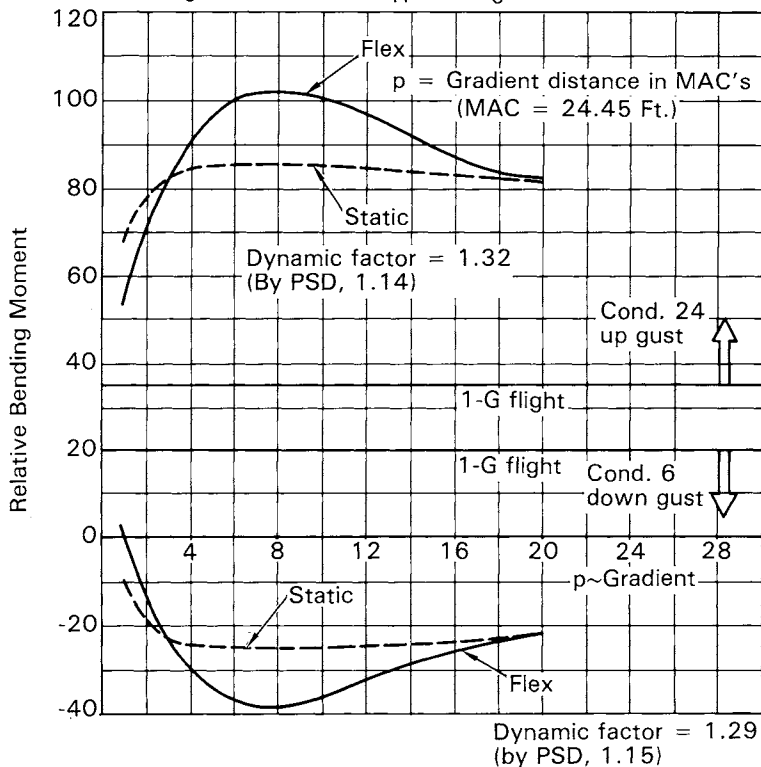


Fig. 3.2 Variation of maximum wing bending moment with gust gradient distance; L-1011-1, BL 150.

3.5.2 Variation of Gust Velocity with Gradient Distance

There seems to be a general consensus, based on both intuition and evidence, that gusts of shorter gradient distance tend to be of lower gust velocity. J. G. Jones of the Royal Aircraft Establishment (RAE), as a result of power-spectral density considerations, has proposed

$$U_0 \propto H^{1/3}$$

and this seems quite reasonable (see Ref. 7). BCAR, however, does not yet provide for other than a constant U_0 ; no constant of proportionality has yet been established for design use of the aforementioned relationship.

3.5.3 Comparative Analysis

Prior to the early 1950's, no explicit consideration had been given to the dynamic response of elastic modes in establishing gust loads for design. By the late 1940's and early 1950's, however, concern regarding the possible magnitude of dynamic effects led to numerous studies of various existing aircraft by the NACA, the individual aircraft manufacturers, and others. These studies were sufficient to establish that dynamic amplification factors on wing bending moment of 1.2–1.3, determined by varying the discrete-gust gradient distance, were not uncommon on the then existent large piston-engine aircraft. It was also apparent, however, that those airplanes had satisfactory service and safety records, even though no provision had been made in their design loads for the dynamic effects that were by then known to be present. Thus, it became evident that the design gust velocities had been set high enough so that, for these airplanes, no increase in design loads for dynamic effects was needed. On the other hand, it was apparent that as airplanes became larger, faster, and more flexible, the relative dynamic effects might well increase; and sooner or later, design to static loads alone could lead to a structure of inadequate strength.

Consequently, to prevent any deficiency in strength that might otherwise have resulted from this trend, it became the practice, and a specific requirement of the FAA, that if a manufacturer showed that for his new model the percentage increase in load, due to transient effects, was no greater than that of his previous models, it would not be necessary to design for the increased load; however, if the increase were greater than for the previous models, the difference would be designed for. Hence, the expression “comparative analysis.”

This policy was applied in the design of the Lockheed Model 1649 Constellation and the Electra in the mid-1950's. In the analyses of these airplanes, primary emphasis was placed on a comparison of wing-bending moment dynamic amplification factors with those obtained from similar analyses of earlier Constellation series aircraft. Even in these analyses, however, it was recognized that comparison of dynamic magnification factors alone would not assure that the new airplane would have as great a gust capability as the previous models. Consequently, consideration was also given to the effects of

- 1) Differences in the margin between design speed and normal operational speed.
- 2) Differences in the static-gust loads criteria to which those airplanes had been designed.
- 3) Positive margins of safety for gust loads in the reference airplanes.

In connection with the 1960 structural reevaluation of the Electra, it became evident that a simple comparison of wing bending moment dynamic amplification factors was not sufficient to assure compatibility of gust strength with an earlier successful design. Rather, complete wing loads (shear, bending moment, and torsion, in proper phase) for a level of gust severity that would just take the reference airplane to limit strength, with

dynamic effects fully accounted for, was needed. Such an approach was utilized in the Electra reevaluation and also in all of the discrete-gust dynamic loads work done in connection with BCAA certification of the various L-1011 models.

Throughout these applications, it has been customary to refer to the factor by which the nominal design gust velocities must be divided, in order to just take the reference airplane to limit strength, as the “dynamic accountability factor” (DAF). Ordinarily, the loads are obtained first based on the nominal design gust velocities (i.e., the design static-gust velocities as stated in FAR or BCAR); these loads, rather than the gust velocity, are then divided by the DAF.

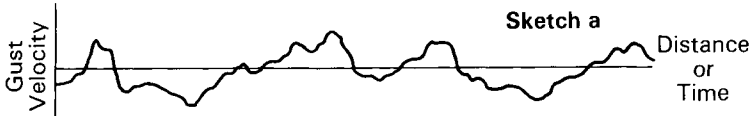
4

BASIC PSD CONCEPTS AND APPLICATION TO GUST LOADS

4.1 GUST PROFILE AS A STATIONARY GAUSSIAN RANDOM PROCESS

4.1.1 Typical Gust Profile

As noted in Sec. 1.2, gust profiles typically tend to be continuous and irregular, as illustrated by Sketch a.



4.1.2 Idealization as a "Stationary Gaussian Random Process"

Such a profile can be idealized as a "stationary Gaussian random process." The profile, or time history, as thus idealized is *stationary* in that it is considered to be of infinite duration and its statistical properties are the same wherever it may be sampled. The time history is also *Gaussian* because if the time history is sampled at random—or, in practice, at many equally spaced points in time—the resulting probability distribution is Gaussian, often called "normal," and defined by a probability density function

$$p(y) = \frac{1}{\sqrt{2\pi}\sigma_y} e^{-\frac{1}{2}\left(\frac{y}{\sigma_y}\right)^2}$$

where σ_y is a constant. A more complete discussion is provided in Sec. 4.3, and especially in 4.3.4. The time history is *random* in that it has no apparent pattern or regularity. As a result, it can be defined only in terms of its statistical characteristics. The term *process*, in the present context, can be thought of simply as another word for time history.

4.1.3 Why the Stationary-Gaussian Idealization?

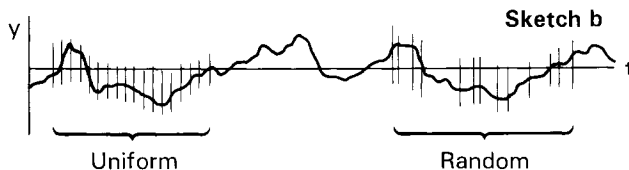
There are two basic reasons why this idealization is in such wide use. Firstly, it is vastly more realistic than the simple discrete-gust idealizations

described in earlier sections. In particular, it provides inherently for: 1) The infinite variation in the shape of individual gusts; 2) the variation of gust magnitude with gradient distance; 3) the proper superposition of very-short-gradient gusts that excite the various elastic modes with the longer-gradient gusts that give the largest rigid-airplane loads; and 4) the reduced gust velocity properly associated (on an equal-probability basis) with a resonant series of gusts.

Secondly, easy-to-apply mathematical techniques are available to use this idealization. These are the techniques referred to as generalized harmonic analysis or power-spectral analysis. *They permit determining the statistical characteristics of the airplane response (accelerations, loads, etc.) directly from the statistical description of the gust velocity profile.* With these techniques available, the stationary-Gaussian idealization is vastly simpler to apply than any discrete-gust idealization that is competitive in terms of realism. (Efforts to develop a more realistic discrete-gust idealization are discussed briefly in Sec. 12.4.)

4.2 MEASURE OF INTENSITY: RMS VALUE OF y

Let y be any stationary random function of time, such as a gust velocity or airplane response.



The magnitude of the fluctuations of y about the mean value is measured by a special kind of average, the root-mean-square (rms) value, designated σ_y and given by

$$\sigma_y = \sqrt{\overline{y^2}} = \sqrt{\lim_{T \rightarrow \infty} \frac{1}{2T} \int_{-T}^T [y(t)]^2 dt} \quad (4.1)$$

Bar denotes average

This equation applies only when the mean value of y is zero. If the mean value of y is not, in fact, zero, then for the purpose of Eq. (4.1), y is to be taken as the *increment* in y relative to its mean value. If y is the gust velocity, the mean is, in fact, zero; if y is a response, y is taken to be the increment relative to the 1-g level flight value.*

*In gust loads applications, the term rms is universally taken as applying to the gust increment only. In statistics generally, the term *rms* applies to the result given by Eq. (4.1) when y in the equation includes the mean. This quantity also can be useful; for example, it is what is indicated by an ac ammeter when measuring a current consisting of an alternating and a direct

To evaluate σ_y from a time history, the time history can be read at small uniform intervals, or it can be sampled randomly.* In either case, Eq. (4.1) becomes

Bar denotes average

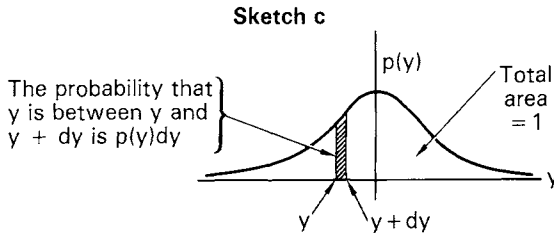
$$\sigma_y = \sqrt{\overline{y^2}} = \sqrt{\lim_{N \rightarrow \infty} \frac{1}{N} \sum_{i=1}^N [y(t_i)]^2} \quad (4.2)$$

One obvious motivation for squaring y before averaging [Eqs. (4.1) and (4.2)] is that otherwise positive and negative fluctuations will offset each other to give a value of zero. Thus, the purpose of measuring the magnitude of the fluctuations of y would be defeated.

4.3 PROBABILITY DISTRIBUTION

4.3.1 Probability Density and Probability Distribution

A more detailed picture of the magnitude of y is given by the probability density or probability distribution. The *probability density* $p(y)$ is defined by the relation:



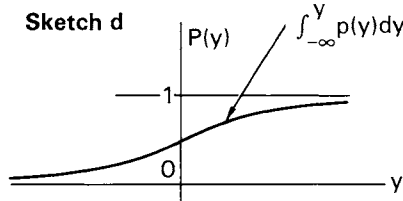
current superimposed. When the mean is subtracted out, the resulting rms value is called the “standard deviation.” Before taking the square root, the result is called the “variance.” The term standard deviation is seldom used in a gust loads context. Its more usual application is when the mean is not something separately identifiable, such as a 1-g level flight value, but instead is just one value that might be assumed by the variable. For example, the average height of a certain group of students is 69.0 in., with a standard deviation of 2.6 in.

*The random-sampling concept applies more rigorously when many separate time histories are generated simultaneously, all inherently identical in statistical properties. If every time history of this “ensemble” is sampled once, all at the same given time, each is, in effect, sampled randomly. The average and the rms value can legitimately be determined from this kind of sampling. In practice, however, in the sampling of actual measured gust velocity and gust loads time histories, we are usually confined to dealing with one time history at a time—and all too short in duration at that!

The *probability distribution* $P(y)$ is defined as the probability that $y < y_1$, where y_1 is a particular value of y , written

$$P(y) = P\{y < y_1\}$$

↑ ↑
Two different meanings of P ,
distinguished by context.*



$P(y)$ is given by

$$P(y) = \int_{-\infty}^{y_1} p(y) dy \tag{4.3}$$

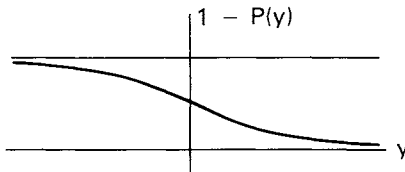
The term probability distribution is also used in a general sense to include the probability density. To distinguish $P(y)$ from $p(y)$, $P(y)$ is often referred to as the cumulative probability distribution, although this term is sometimes reserved for the quantity $1 - P(y)$; see Eq. (4.3a).

In the example illustrated by sketches c and d, $p(y)$ is symmetrical about $y = 0$. This symmetry is characteristic of a stationary Gaussian random process but is not necessary in general.

An alternate means of defining a probability distribution is the function $1 - P(y)$; that is, the probability that y is greater than y_1 (Sketch e):

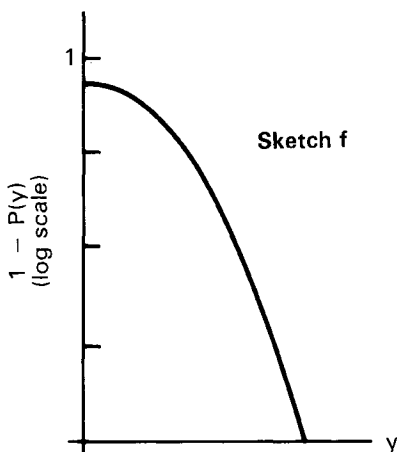
$$1 - P(y) = \int_{y_1}^{\infty} p(y) dy \tag{4.3a}$$

Sketch e



*A more common notation, apparently, is one in which $f(y)$ and $F(y)$ replace $p(y)$ and $P(y)$. Here, f and F are thought of as standing for frequency of occurrence or function. The alternate notation, $p(y)$ and $P(y)$, is used here to avoid confusion with f as a cycles per second (cps) kind of frequency.

This is usually plotted on semilog coordinates:



This form of plot is especially useful in connection with selection of design values of y , in that one is inherently interested in values that are exceeded with low probability. A value of 0.00026, for example, is simpler both to comprehend and to plot than 0.99974. Also, it avoids the impression of five-significant-figure accuracy when it is really a two-significant-figure number.

The reader without previous background in the theory of probability may be interested in the somewhat different treatment of this material in Appendix B.

4.3.2 Gaussian Probability Distribution

A particular probability distribution of great importance is the Gaussian probability distribution, often referred to as the normal distribution.

Definition. This distribution is defined by a probability density given by the expression

$$p(y) = \frac{1}{\sqrt{2\pi}} \frac{1}{\sigma_y} e^{-\frac{1}{2}\left(\frac{y}{\sigma_y}\right)^2} \quad (4.4)$$

where σ_y is the rms value of y . This plots as shown in Fig. 4.1. In Eq. (4.4) and Fig. 4.1, y is the difference between y and its mean. If y is taken as the quantity itself, y should be replaced with $(y - y_{\text{mean}})$ in Eq. (4.4).

Plots. The cumulative Gaussian probability distribution $P(y)$ is not expressible in closed form. A plot of $1 - P(y)$, which can be used as a source of numerical values, is given in Fig. 4.2. A more comprehensive set of plots is provided in Appendix C.

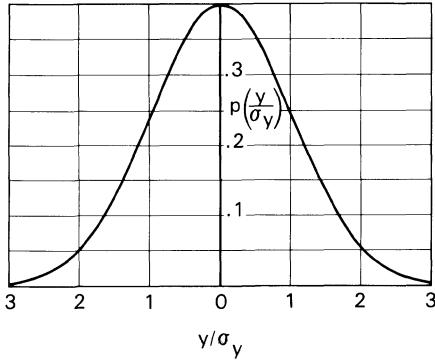


Fig. 4.1 Gaussian probability density.

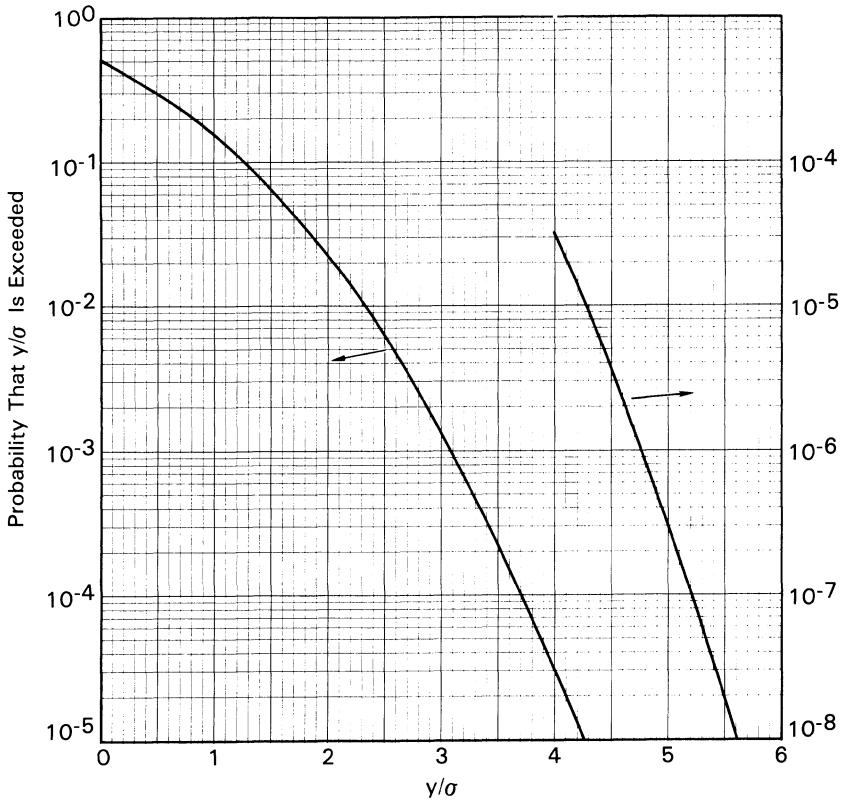


Fig. 4.2 Gaussian cumulative probability distribution.

4.3.3 Significance of the Gaussian Distribution

The Gaussian probability density is far more than an empirical mathematical expression that happens to be a good fit for a great deal of experimental data. The following two examples will give some appreciation of its basic theoretical importance.

1) Suppose that a person stands at the origin on the x axis, facing in the positive direction, and tosses a coin a number of times. Each time it comes up heads, he takes a step forward; and each time it comes up tails, a step backward. (This is known as the “random-walk” experiment.) Where will he be, in terms of probability, after any given number of tosses? The probabilities are shown in Fig. 4.3. Each probability is written as a fraction. The total number of possible sequences appears in the denominator (2^n where n is the number of tosses), and the number of sequences that lead to the given final position appears in the numerator. (Readers with limited exposure to the theory of probability may find Appendix B helpful at this point.)

As the number of tosses increases, the shape suggested by the bars looks more and more like a Gaussian probability density. It can be shown that as the number of tosses increases without limit, the shape defined by the bars approaches *exactly* the Gaussian probability density. The mathematical demonstration is rather long and complex and depends on several fortunate guesses along the way, but utilizes only mathematics available at the undergraduate engineering level.

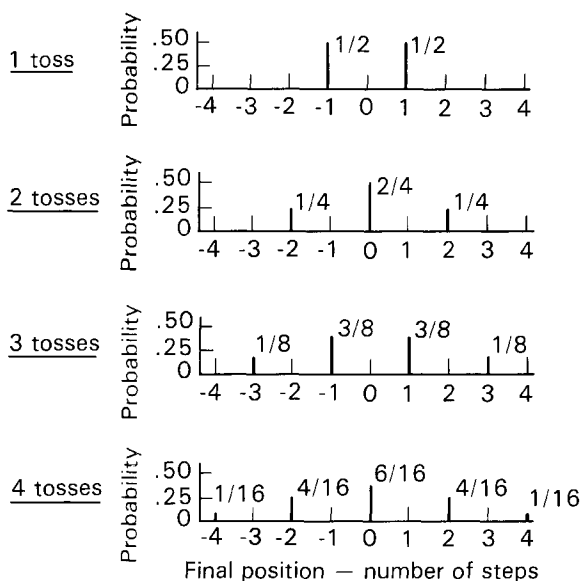
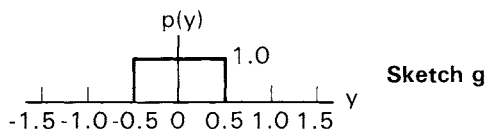
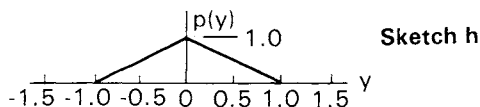


Fig. 4.3 Random-walk probabilities.

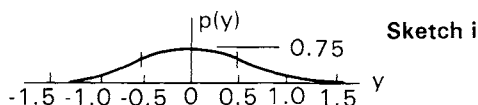
2) Suppose a single sample is taken of each of three random variables, each with the following probability density:



and the three values added. What is the probability density of the sum? If only two of the samples are added, the probability density can be calculated to be



and if all three are added,



(Each of the three segments in Sketch i is a portion of a second-degree parabola.)

It is seen that, even if we add only three variables, the probability density bears a striking resemblance to the Gaussian probability density. The resemblance is even more impressive when an accurately plotted Gaussian curve is actually superimposed. It can be shown that as the number of variables sampled and summed increases without limit, the probability does indeed approach the Gaussian. Further, this can be shown to occur for any probability density of the individual variables within rather broad limits, not just the "boxcar" distribution from which the probability densities in Sketches g, h, and i were obtained.

4.3.4 Stationary Gaussian Random Process

It was noted in Sec. 4.2 that one characteristic of a stationary Gaussian random process, the obvious one, is that the probability density of y is Gaussian [(Eq. 4.4)]. An additional requirement, however, is that the probability density of \dot{y} also be Gaussian and that \dot{y} be independent of y . An alternate to this additional requirement, apparently, is that the process be "joint Gaussian," which means that the joint probability density of y_1 and y_2 , where y_1 and y_2 are values of y separated by a given time increment τ , be Gaussian. A joint probability density is defined analogously to a single-variable probability density, that is, the probability that x is between x and $x + dx$ and at the same time y is between y and $y + dy$ is $p(x,y) dx dy$. A

Gaussian joint probability density is one representable by

$$p(x,y) = \frac{1}{2\pi\sigma_x\sigma_y\sqrt{1-r^2}} \exp \left\{ -\frac{1}{1-r^2} \left[\frac{1}{2} \left(\frac{x}{\sigma_x} \right)^2 - r \left(\frac{x}{\sigma_x} \right) \left(\frac{y}{\sigma_y} \right) + \frac{1}{2} \left(\frac{y}{\sigma_y} \right)^2 \right] \right\} \quad (4.5)$$

Apparently, it can be shown that if this more fundamental requirement is met—that is, if the process is joint Gaussian—then the previously stated additional requirement, that y be Gaussian, is also met.

Still another variant of the additional requirement, derived by Chen⁸ from the joint Gaussian requirement, is that the probability distribution of $(y_1 - y_2)$ be Gaussian, where again y_1 and y_2 are values of y separated by any given time increment τ .

The practical importance of any such additional requirement—that is, any requirement over and above the obvious one that the distribution of y itself be Gaussian—is that it is necessary in the derivation of Rice's equation. Rice's equation is introduced in Sec. 4.6 and is the basis for the analytical determination of frequency of exceedance curves.

Presumably, random processes do occur for which these requirements are indeed closely met. Internally generated noise in electronic circuits appears to be one of these. The ramifications of these requirements with respect to atmospheric turbulence are discussed in Chapter 12.

4.4 FREQUENCY CONTENT AND POWER-SPECTRAL DENSITY (PSD)

4.4.1 Frequency Content: Superposition of Sinusoids

The *magnitude* of a stationary Gaussian random process is seen to be defined statistically by its rms value and its probability distribution (Gaussian). To complete the statistical description of the random process requires, in addition, the definition of its *frequency content*.

A stationary Gaussian random process can be considered to be generated by the superposition of an infinite number of sinusoidal components. These components differ infinitesimally in frequency from one to the next. Each component is of prescribed infinitesimal amplitude and each is randomly phased relative to the others.

This superposition can be expressed mathematically as

$$y(t) = \sum_{m=1}^{\infty} \underbrace{\sqrt{\Phi(\omega_m) \Delta\omega}}_{\text{Infinitesimal amplitude}} \cos(\omega_m t + \underbrace{\psi_m}_{\text{Random phase}}) \quad (4.6)$$

where ω_m is the radian frequency of each component, and it is understood

that all values of ω_m from zero to ∞ , differing infinitesimally from one to another, are to be included.

The quantity $\Phi(\omega_m)$ is called the power-spectral density (psd) and will be discussed more fully in Sec. 4.4.2. It can be seen to provide a measure of the amplitude of each of the many sinusoids that are superimposed. As a continuous function of frequency, $\Phi(\omega)$ provides the complete measure of the frequency content of the process.

The phase angle ψ is random, with a boxcar probability density over the range 0–360 deg.

How sinusoids superimpose to form a stationary Gaussian random process is illustrated very crudely in Fig. 4.4. Here only five sinusoids are used, but the sum of just these five has very much the appearance of a stationary Gaussian random process.

The superposition of sinusoids to form a stationary Gaussian random process is in some respects similar to the superposition of sinusoids to form a Fourier series, with which the reader may be familiar. The differences, however, are important. These are

1) The Fourier series consists of components at discrete frequencies, $\omega_1, 2\omega_1, 3\omega_1, 4\omega_1, \dots$. Although there are, in general, an infinite number of components, the frequencies are not infinitesimally spaced.

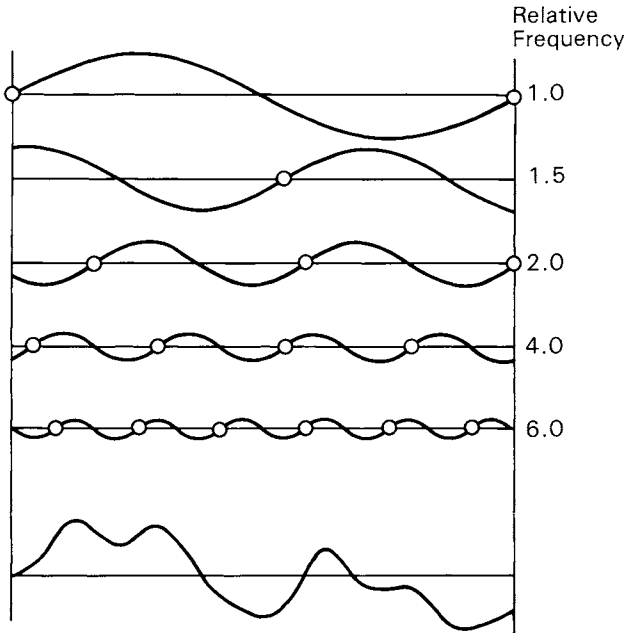


Fig. 4.4 Example of superposition of sinusoids to approximate a stationary random process.

Downloaded by RMIT UNIV BUNDOORA on June 4, 2013 | http://arc.aiaa.org | DOI: 10.2514/4.861888

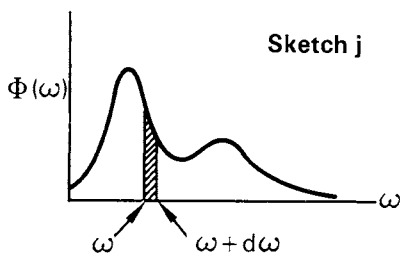
2) In a Fourier series, at time zero, the components are all at a phase angle of 0, 90, 180, or 270 deg. The phase angles are prescribed, not random.

3) The Fourier series may be formed to match an arbitrary function over a finite time interval, beyond which it may be of no interest; or, beyond this interval or twice this interval, it may repeat indefinitely. The stationary Gaussian time history never repeats.

4.4.2 PSD

Physical significance. The psd function will be denoted by $\Phi(\omega)$. Thus, it is indicated to be a function of the radian frequency ω .

If $\Phi(\omega)$ is the psd of the quantity $y(t)$, then $\Phi(\omega) d\omega$ is the contribution to y^2 , or σ_y^2 , of frequencies between ω and $\omega + d\omega$.



Relation of σ_y to $\Phi(\omega)$. As a corollary to the aforementioned, the rms value of y is equal to the square root of the area under the psd curve

$$\sigma_y = \sqrt{\int_0^{\infty} \Phi(\omega) d\omega} \quad (4.7)$$

Significance of terminology. In the expression “power-spectral density”—

1) *Spectral* indicates a measure of frequency content.

2) *Power* indicates, somewhat by analogy, that the quantity to which the various frequency components contribute is the mean square value of the variable. Electrical power is given, for example, by $P = I^2R$ or $P = E^2/R$. More loosely, mechanical energy is given by $E = (1/2)MV^2$ (kinetic) or $E = (1/2)Kx^2$ (elastic).

3) *Density* indicates that the frequencies are not discrete but continuously distributed, so one cannot speak of the contribution of a single frequency ω but only of the contribution of a band of frequencies between ω and $\omega + d\omega$.

Definitions of PSD. The quantity $\Phi(\omega)$, the psd, can be defined in various ways. Four of these are indicated next. It is somewhat a matter of personal preference which of these is considered the definition and which are considered derived properties.

- 1) $\Phi(\omega)$ is the constant $\Phi(\omega_m)$ in Eq. (4.6).
- 2) $\Phi(\omega)$ is the quantity such that $\Phi(\omega) d\omega$ is the contribution to $\overline{y^2}$ of frequencies between ω and $\omega + d\omega$.

$$3) \quad \Phi(\omega) = \lim_{T \rightarrow \infty} \frac{1}{\pi} \frac{1}{T} \left| \int_{-T}^T y(t) e^{-i\omega t} dt \right|^2 \quad (4.8)$$

|| denotes modulus of the complex quantity.

↑
Fourier transform of $y(t)$,

$$\int_{-\infty}^{\infty} y(t) e^{-i\omega t} dt$$

where $y(t)$ has been truncated to have zero value outside the range $-T$ to T .

- 4) $\Phi(\omega)$ is the Fourier transform of the autocovariance function [see Sec. 4.4.3, Eq. (4.10)].

One-Sided vs Two-Sided PSD's. It might be remarked that the psd's defined and used in this report and in gust loads work fairly generally, are "one-sided" spectra; that is, they are considered to exist for positive values of ω only. Power spectra, however, are often treated in the literature as "two-sided" spectra; these are defined for negative as well as positive frequencies, with $\Phi(-\omega) = \Phi(\omega)$. In Eq. (4.7), the integration is then from $-\infty$ to ∞ , instead of from 0 to ∞ ; for this equation to hold, $\Phi(\omega)$ must be divided by 2. Thus, psd values for a two-sided spectrum are just half of those for a one-sided spectrum, and equations defining the psd, such as Eqs. (4.6), (4.8), and (4.10), must be modified accordingly.

4.4.3 Mathematical Relation Between PSD and Time History

Given $\Phi(\omega)$, an infinite number of time histories can be generated by means of Eq. (4.6). Conversely, given a time history, a single psd can be calculated, for example, by means of Eq. (4.8).

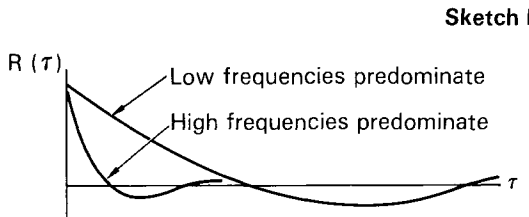
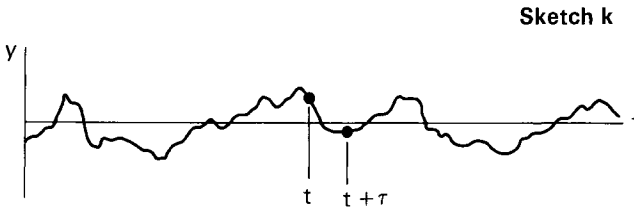
In practice, of course, Eq. (4.8) can be applied only over a finite length of record. The actual limit as $T \rightarrow \infty$ cannot be determined. We speak of the psd of a particular finite record. Conceptually, however, this finite record is only one sample of a time history of infinite duration. Various finite samples thereof will yield psd's that differ slightly from one to another, with the likely amount of difference depending on the length of the samples.

An alternate mathematical path to that expressed by Eq. (4.8) for the calculation of psd's from time histories, which has been widely employed in practical applications, utilizes the "autocovariance function" as an intermediate

step. The autocovariance function or “autocorrelation function” is defined as

$$R(\tau) = \overline{y(t)y(t+\tau)} = \lim_{T \rightarrow \infty} \frac{1}{2T} \int_{-T}^T y(t)y(t+\tau) dt \quad (4.9)$$

This expresses the correlation of a function with itself (“auto”) at points separated by various times τ :



It can readily be seen from Eq. (4.9) that when $\tau = 0$, $R = \overline{y^2} = \sigma_y^2$. From this relation, it is clear that autocovariance is a more appropriate term than autocorrelation although the latter is in more common use. The quantity y^2 , which $R(\tau)$ is equal to at $\tau = 0$, is often referred to in statistics as the variance. In contrast, correlation is invariably a normalized quantity, with a value of unity indicating perfect correlation, as occurs at $\tau = 0$. Accordingly, the term autocorrelation function should more properly refer to $R(\tau)/\sigma_y^2$.

The psd is determined from $R(\tau)$ as follows:

$$\Phi(\omega) = \frac{2}{\pi} \int_0^\infty R(\tau) \cos\omega\tau d\tau \quad (4.10)$$

Conversely,

$$R(\tau) = \int_0^\infty \Phi(\omega) \cos\omega\tau d\omega \quad (4.11)$$

Equations (4.10) and (4.11) are a special form of Fourier transform.

A practical procedure for the computation of psd's from time histories

following the path of Eqs. (4.9) and (4.10) was introduced by Tukey in 1949 (see Appendix L). This has come to be called the Blackman–Tukey method and was standard for many years.

More recently, the Blackman–Tukey method has been largely displaced by the fast Fourier transform (FTT) method.* This method takes the Eq. (4.8) route, but utilizes an ingenious scheme that vastly reduces the amount of computation. This involves dividing the time history into a number of blocks, each containing L equally spaced points, where L must be an integer power of 2; for example, 32, 64, 128, etc.

Determination of psd's from time histories is treated in much more detail in Chapter 11.

4.4.4 Changes in the Frequency Argument

To this point, functions of frequency have been expressed as functions of ω , the frequency in rad/s. Other frequency arguments are often useful. These include, with ω listed as well for completeness,

ω	rad/s	
f	cps or Hz	
Ω	rad/ft	} spatial frequency
$\Omega/2\pi$, or $1/\lambda$	cycles/ft	
k	rad/semichord	} $\lambda = \text{wavelength}$

Gust psd's are usually compared and specified as functions of Ω or $\Omega/2\pi$, inasmuch as the gust structure in the atmosphere must be independent of the speed with which it is traversed. Ω and $\Omega/2\pi$ are often referred to as spatial frequencies, in contrast to ω and f , which, correspondingly, are temporal frequencies. At the Lockheed-California Company, gust response psd's are ordinarily expressed as functions of f , inasmuch as loads engineers think most easily in terms of cps or Hz.

Numerical values of psd are different depending on the frequency argument. Inasmuch as

$$\int_0^{\infty} \Phi(\omega) d\omega = \int_0^{\infty} \Phi(f) df = \int_0^{\infty} \Phi(\Omega) d\Omega = \sigma^2$$

whenever the frequency argument is changed, so that its numerical values go up or down, Φ must be changed in the reciprocal ratio. Sometimes, the symbol Φ is changed to $\bar{\Phi}$, $\hat{\Phi}$, $\tilde{\Phi}$, etc. to identify the frequency argument with which it is used. This more complex notation is not used here, it being understood that $\Phi(\omega)$, $\Phi(f)$, etc. are, in fact, different functions.

*At the Lockheed-California Company, gust-response flight-test data obtained in 1971 were processed using the Blackman–Tukey method. Similar data obtained in 1977 were processed by the FFT method.

Some of the relations among the various frequency arguments are

$$\omega = 2\pi f = \Omega V = \frac{kV}{b_0} \quad (\text{where } b_0 \text{ is the reference semichord and } V \text{ is the true airspeed})$$

$$\Omega = \frac{\omega}{V} = \frac{2\pi f}{V} = \frac{k}{b_0}$$

$$f = \frac{\omega}{2\pi} = \frac{\Omega V}{2\pi} = \frac{kV}{2\pi b_0} = \left(\frac{\Omega}{2\pi}\right)V$$

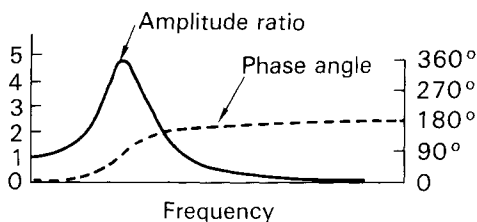
$$k = \frac{\omega b_0}{V} = \Omega b_0 = \frac{2\pi f b_0}{V}$$

$$\frac{\Omega}{2\pi} = \frac{f}{V}$$

4.4.5 Frequency-Response Function

This is the key ingredient in the determination of the psd of the response from the psd of the input. Consider any dynamic system whose action can be represented by linear differential equations with constant coefficients. Apply a steady-state sinusoidal excitation, or input, of unit amplitude and at a given frequency. The response, or output, at any given point in the system will be at the frequency of the excitation. The relation of output to input is characterized by an amplitude ratio and a phase angle. These can be plotted against frequency. The resulting relation is known as the “frequency-response function,” also referred to as the “transfer function.”

Sketch m



The frequency-response function and transfer function are closely related, and the two terms are often used interchangeably. Actually, frequency-response function is the more precise term in the present application. As noted, it expresses a relation between steady-state input and output—*response* as a function of *frequency*. On the other hand, the transfer function is an input-output *ratio* that arises in the operational or Laplace transform solution for transient response. However, the mathematical expressions for the two are essentially identical, the frequency-response function being obtained by

substituting $i\omega$ for s in the mathematical expression for the transfer function. Consequently, the distinction is somewhat academic.

If rotating vectors are used to represent periodic phenomena, and complex notation then used to describe the rotating vectors, the frequency-response function becomes a single complex quantity given by

$$H = \frac{\text{Output}}{\text{Input}} \tag{4.12}$$

H can be written as either

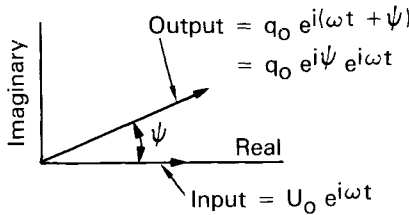
$$H = a + bi \tag{4.13}$$

or as

$$H = |H|e^{i\psi} \tag{4.14}$$

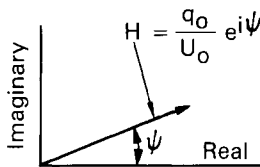
where $|H|$, the modulus of the complex quantity, is the amplitude ratio and ψ the phase angle.

More specifically, in terms of a gust velocity input U and a response output q , the input and output rotating vectors are as shown in the following sketch. The vectors are shown in the position corresponding to $t = 0$ and are considered to rotate counterclockwise at a rotational velocity ω (rad/s). The actual input and output physical quantities are given by the projections of the respective vectors on the real axis.



The frequency-response function is then given as

$$\begin{aligned} H &= \frac{\text{Output}}{\text{Input}} = \frac{q_0 e^{i\psi} e^{i\omega t}}{U_0 e^{i\omega t}} \\ &= \frac{q_0}{U_0} e^{i\psi} \end{aligned}$$

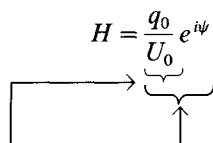


which can also, if desired, be expressed as

$$H = a + bi$$

This form is usually used in computations because it greatly facilitates adding and subtracting.

Note that in the expression

$$H = \frac{q_0}{U_0} e^{i\psi}$$


This is the “amplitude ratio,” or ratio of output to input amplitudes, q_0/U_0 ...

whereas the entire expression is the *complex* amplitude ratio, output/input, that includes both the amplitude ratio q_0/U_0 and the phase angle ψ .

Sign conventions for phase angle. When the frequency-response function is defined in accordance with Eqs. (4.12), (4.13), and (4.14), a positive value of ψ indicates that the output leads the input. This is not a universal sign convention, however; a positive ψ can be taken to indicate either a lead or a lag of the output relative to the input. Both signs conventions have been widely used. Too often, however, the sign convention is not stated, and confusion can easily result.

Calculations of frequency-response function. In the determination of design gust loads, the frequency-response function is obtained by solution of the differential equations of motion of the airplane. The input is a sinusoidally varying (steady state) gust velocity, and the various outputs are the corresponding sinusoidally varying shears, bending moments, torsions, accelerations, concentrated inertia forces, and/or whatever else may be of interest. Thus, the simple expression $H(\omega)$ may represent, in fact, the results of a developmental and computational task of great magnitude and complexity. A glimpse of what may be involved is provided in Chapter 7.

4.4.6 Input-Output Relation

For a linear system, with subscripts i and o denoting input and output, respectively, the input-output relation is as indicated by Fig. 4.5. Thus, the input spectrum (Φ_i) is multiplied, frequency by frequency, by the square of the modulus of the frequency-response function, to give the output spectrum.

$$\Phi_o(f) = \Phi_i(f) |H(f)|^2 \tag{4.15}$$

This gives the output psd. The output probability distribution, if the input

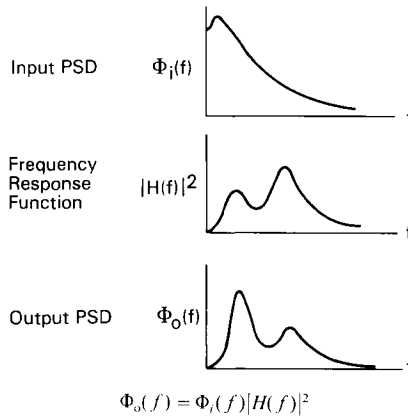


Fig. 4.5 Input-output relationship

probability distribution is Gaussian, will also be Gaussian. The output rms value is given by the square root of the area under the output psd curve [Eq. (4.7)].

It should be duly noted that the power-spectral input-output relation requires solution of the differential equations of motion only for frequency-response functions. This involves algebra only (Chapter 7). In contrast, the determination of a time-history response to a discrete gust requires step-by-step numerical integration; in other words, calculus, which is inherently more complicated.

4.4.7 A Simple Application of Power-Spectral Methods

It now becomes evident how power-spectral methods can be used to give useful answers to gust loads questions. For example: For a given airplane, by what percent do gust loads increase due to structural flexibility, including elastic-mode dynamic effects? The solution is straightforward. Start with a gust psd; see Sec. 4.5. Determine the frequency response function for both the rigid and the flexible airplane. This will be the frequency-response function relating a given load quantity, such as a bending moment at a given wing station, as an output, to the gust velocity as an input. Separately for the rigid and flexible airplanes, multiply the gust psd by the square of the modulus of the frequency-response function [Eq. (4.15)] to give the bending moment, or output, psd. Determine the area under the output psd curve for each case and take the square root of this area [Eq. (4.7)] to give σ_y , the rms value of the output.

The ratio of flexible-airplane to rigid-airplane bending moments is then given by the ratio of the rms values. This ratio applies, of course, not only at the one-sigma probability level ($y/\sigma = 1.0$, Fig. 4.2) but also at *any* fixed probability level.

In Chapter 5 we shall see how actual design gust loads can be determined, on an absolute instead of a comparative basis.

4.4.8 Typical PSD Shapes

A typical gust velocity psd, obtained from the L-1011 1971 gust response flight-test program, is shown in Fig. 4.6. Note that both the horizontal and the vertical scale are logarithmic, so that a slope of $-5/3$ indicates that Φ varies inversely as the $5/3$ power of frequency. The inserted frequency scale in Hz corresponds to the particular true airspeed of the test, 584 fps. The time-history sample shown is an artificially generated stationary-Gaussian-time history, rather than the actual time history from which the plotted psd was obtained. Its frequency content, however, is very similar to that indicated by the plotted psd.*

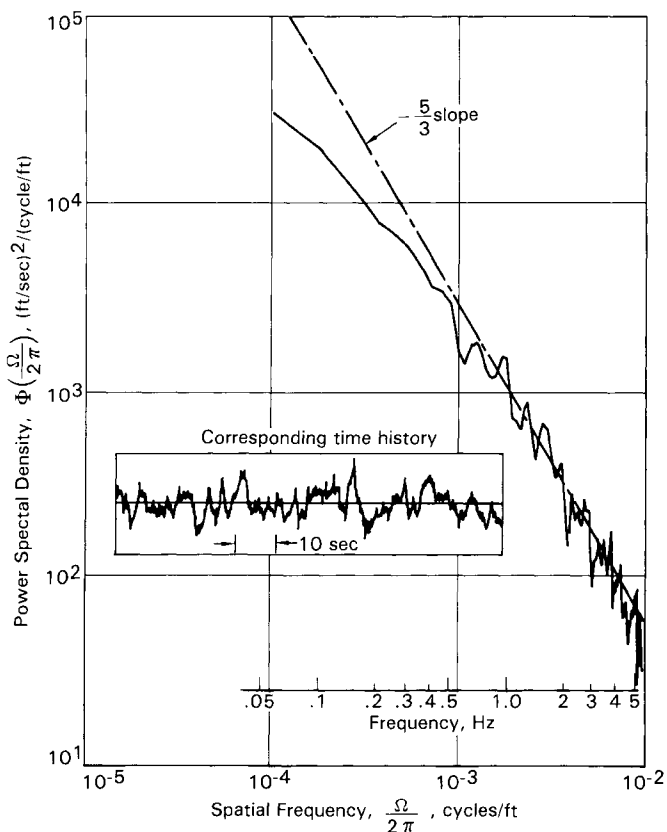
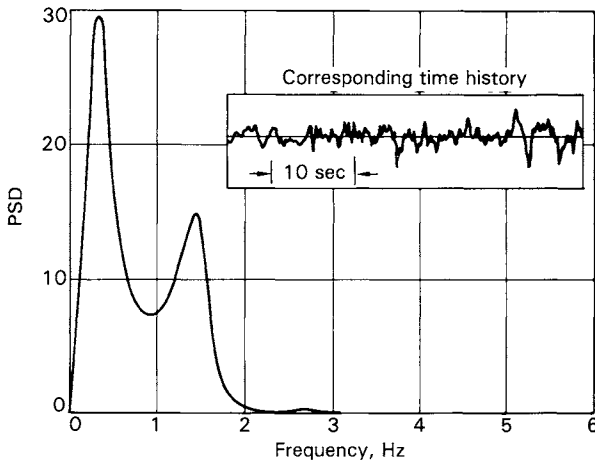


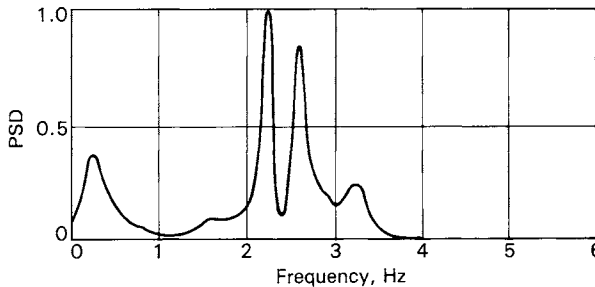
Fig. 4.6 Typical gust velocity psd; flight-measured.

*The psd shown is of Burst 12d1 of the 1971 L-1011 gust-response flight-test program. The time history shown is a portion of Turbulence Sample A, vertical gust, used in a 1978 L-1011 Visual Flight Simulator study.

Typical response psd's are shown in Fig. 4.7. Both were obtained theoretically. The bending-moment psd in Fig. 4.7a clearly reflects the airplane short-period natural frequency of about 0.3 Hz and the first wing-bending frequency of about 1.5 Hz. The torsion psd in Fig. 4.7b shows a less dominant short-period peak at 0.3 Hz, a bare hint of the first wing-bending resonance at 1.5 Hz, pronounced peaks at the engine frequencies at 2.3 and 2.7 Hz, and a smaller peak reflecting the first fuselage bending mode between 3 and 3.5 Hz. The bending-moment time history shown in Fig. 4.7a is for a comparable flight condition.* It clearly shows the 1.5 Hz oscillations related



a) L-1011 wing bending moment of BL 183.



b) L-1011 wing torsion at BL 183.

Fig. 4.7 Typical response psd's; theoretical.

*The theoretical psd's in both Figs. 4.7a and 4.7b are for the flight condition of Burst 12d1 of the 1971 L-1011 flight-test program. The time history shown is a portion of Burst 1b of the 1977 L-1011 active controls flight-test program (Ref. 9). The two flight conditions are similar.

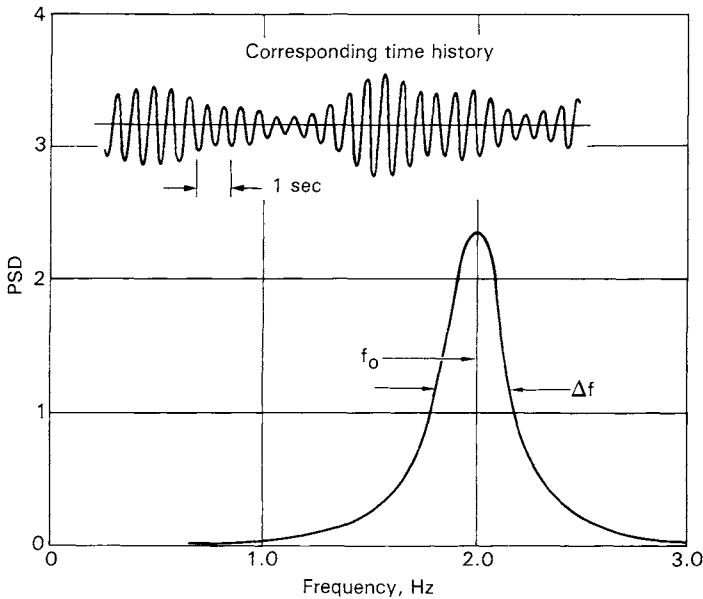


Fig. 4.8 Typical psd; narrow band noise.

to the first bending-mode dynamic response. For a reason that will be pointed out next, the short-period frequency is less conspicuous.

A typical “narrow-band-noise” psd and its related time history are shown qualitatively in Fig. 4.8. The narrowness of the band is measured by the ratio of its band width Δf to its center frequency f_0 . The time history has the general appearance of a high-frequency “carrier” (at approximately f_0) with random low-frequency amplitude modulation. In comparison, two equal signals of frequencies $f + \frac{1}{2}\Delta f$ and $f - \frac{1}{2}\Delta f$, respectively, would “beat” sinusoidally at a frequency of $\frac{1}{2}\Delta f$, that is, lower than the carrier frequency in the ratio $\Delta f/2f_0$.

A time history having a narrow-band-noise characteristic is most likely to occur, in a gust loads context, as the response of a lightly damped elastic or rigid-airplane mode. In fact, the damping constant ζ (ratio of actual to dead-beat damping) can be calculated approximately as $\Delta f/2f_0$, where Δf is measured (as in the figure) at the “half-power point”—that is, at a psd of one-half the peak value.

4.5 GUST PSD FOR USE IN DESIGN

4.5.1 Equations

Two shapes of gust velocity psd have been in wide use, the von Kármán and the Dryden.* These are defined by mathematical expressions as follows.

For vertical and lateral gust (the usual application):

<p><i>von Kármán</i></p> <p>(Use for design, $L = 2500$ feet)</p> $\Phi(\Omega) = \sigma_w^2 \frac{L}{\pi} \frac{1 + \frac{8}{3}(1.339L\Omega)^2}{[1 + (1.339L\Omega)^2]^{11/6}}$	<p><i>Dryden</i></p> $\Phi(\Omega) = \sigma_w^2 \frac{L}{\pi} \frac{1 + 3L^2\Omega^2}{[1 + L^2\Omega^2]^2}$	(4.16)
--	---	--------

Corresponding equations for longitudinal (fore-aft) gust (seldom needed):

<p><i>von Kármán</i></p> $\Phi(\Omega) = \sigma_w^2 \frac{2L}{\pi} \frac{1}{[1 + (1.339L\Omega)^2]^{5/6}}$	<p><i>Dryden</i></p> $\Phi(\Omega) = \sigma_w^2 \frac{2L}{\pi} \frac{1}{[1 + L^2\Omega^2]^2}$	(4.17)
--	---	--------

In Eqs. (4.16) and (4.17) σ_w = rms gust velocity and L = scale of turbulence (discussed in Secs. 4.5.3 and 4.5.5). (The subscript w in σ_w , in its original usage, indicated the vertical component of gust velocity; σ_w is now often used, and is here, to refer to any specified component of the gust velocity.)

The constant $\sigma_w^2(L/\pi)$ in Eq. (4.16) changes to the following for other frequency arguments:

$\Phi(\Omega) : \sigma_w^2(L/\pi)$	$\Phi(\omega) : \sigma_w^2 \frac{L}{\pi V}$
$\Phi\left(\frac{\Omega}{2\pi}\right) : \sigma_w^2 \cdot 2L$	$\Phi(f) : \sigma_w^2 \frac{2L}{V}$
$\Phi(L\Omega) : \sigma_w^2 \frac{1}{\pi}$	$\Phi(k) : \sigma_w^2 \frac{L}{\pi b_0}$

*The von Kármán spectrum first gained the attention of the gust loads community, apparently, as a result of its inclusion in a 1962 AGARD paper later published as NASA TR R-199,¹⁰ where it was referred to simply as the "isotropic-turbulence" spectrum. This designation was used at the Lockheed-California Company for several years thereafter, until the "von Kármán" designation gained general acceptance. Earlier, the von Kármán spectrum was one of six defined in Ref. 11, published in 1957, and used therein for calculating two-dimensional gust response. The Dryden spectrum was proposed for gust loads use in a 1952 paper by Liepmann.¹² This spectrum, accordingly, was referred to at the Lockheed-California Company for many years as the Liepmann spectrum.

In Eq. (4.17), the constant in each case is twice that just shown for Eq. (4.16).

4.5.2 Plots

Plots of the von Kármán and Dryden psd's for the vertical-lateral gust case with $L = 2500$ ft are shown in Fig. 4.9. For a plot indicating ratios of von Kármán to Dryden gust psd for $L = 2500$ ft, as a function of frequency in Hz for a family of true airspeeds, see Appendix D. A comparison between the von Kármán spectra for the vertical-lateral and longitudinal gust cases is shown in Fig. 4.10.

In Figs. 4.9 and 4.10, the psd is plotted as a function of a frequency argument $\Omega/2\pi$. It might be remarked that when the frequency argument is chosen instead to be $L\Omega$, then the psd $\Phi(L\Omega)$ is a function of a single variable only, $L\Omega$. For all of the other frequency arguments listed earlier, Φ is a

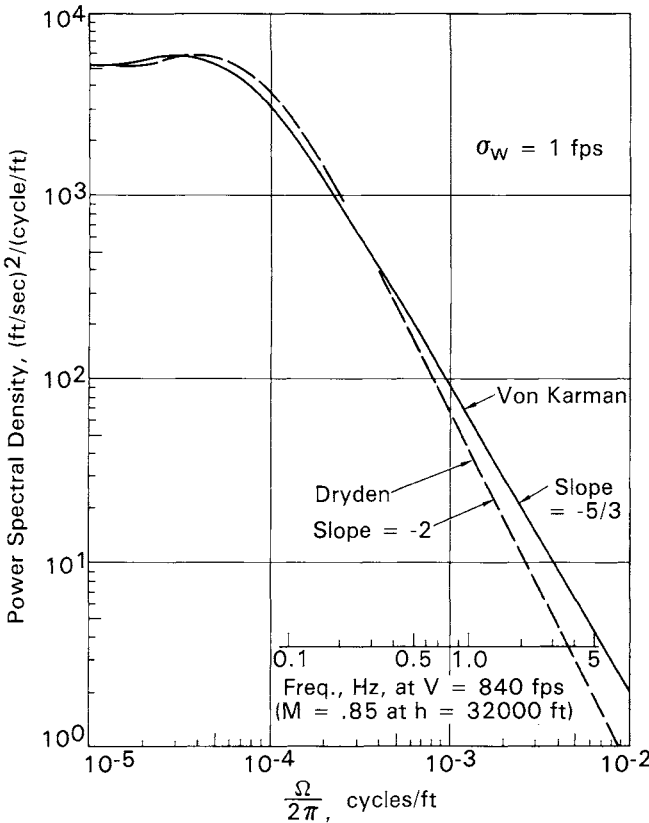


Fig. 4.9 Von Kármán and Dryden gust psd's; $L = 2500$ ft.

Downloaded by RMIT UNIV BUNDOORA on June 4, 2013 | http://arc.aiaa.org | DOI: 10.2514/4.861888

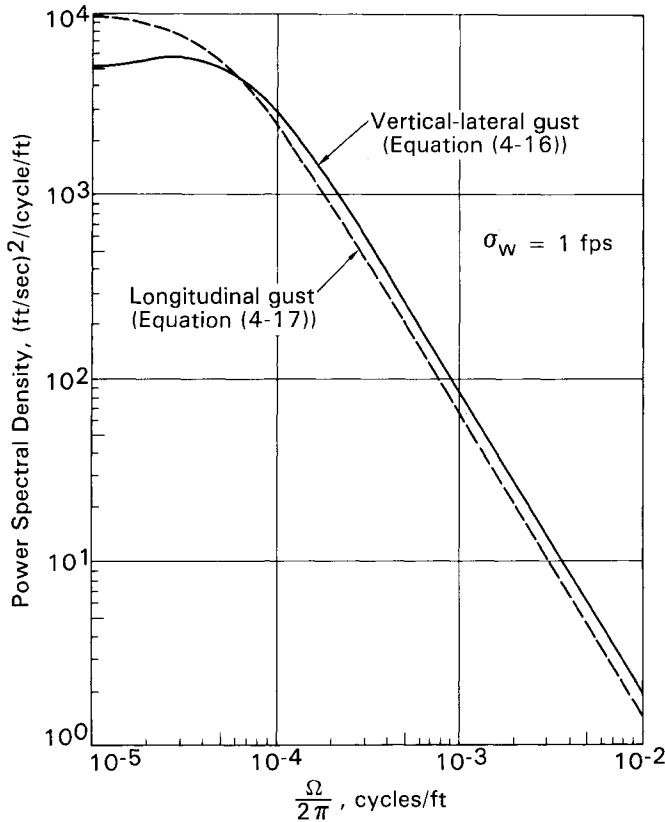


Fig. 4.10 Von Kármán vertical-lateral and longitudinal gust psd's; $L = 2500$ ft.

function of *two* variables, the frequency argument and L .* In Figs. 4.9 and 4.10, therefore, each different value of L would give a different curve. If, however, in either figure the frequency scale is changed to an $L\Omega$ scale (by multiplying by $2\pi \cdot 2500$) and the vertical scale modified accordingly (by dividing by $2\pi \cdot 2500$) then the single curve shown for each spectrum will apply for all values of L . $\Phi(L\Omega/2\pi)$ would, of course, also be a function of a single variable, in this case $L\Omega/2\pi$.

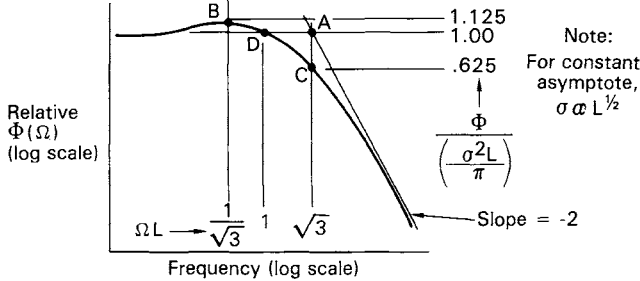
*These conclusions follow from Eqs. (4.16) and (4.17), from which it is seen that, except for the initial coefficient in which only L appears, L and Ω each occur only in combination with the other. The presence or absence of L in the coefficient is indicated by the list of expressions following Eqs. (4.16) and (4.17).

4.5.3 Significance of L

The constant L in Eqs. (4.16) and (4.17) is called the *scale of turbulence*. The value of L determines the frequency at which the knee of the psd curve occurs, at approximately $L\Omega = 1$.* The geometry of both the von Kármán and the Dryden psd shapes in the vicinity of the knee is indicated in some detail in Fig. 4.11.

DRYDEN

$$\Phi(\Omega) = \frac{\sigma^2 L}{\pi} \frac{1 + 3L^2\Omega^2}{(1 + L^2\Omega^2)^2}$$



VON KARMAN

$$\Phi(\Omega) = \frac{\sigma^2 L}{\pi} \frac{1 + 4.78L^2\Omega^2}{[1 + 1.79L^2\Omega^2]^{11/6}}$$

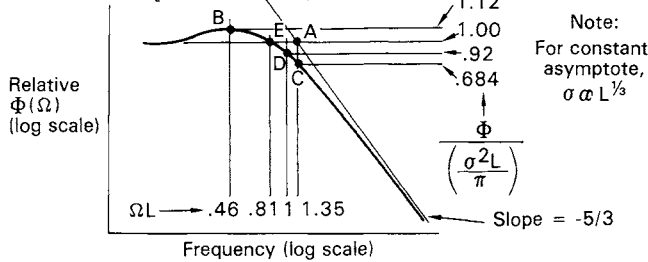


Fig. 4.11 Geometric properties of gust psd curves.

* L has sometimes been defined in terms of the autocovariance function (Sec. 4.4.3) as

$$L = \frac{\int_0^\infty R(\tau) d\tau}{R(0)} \tag{4.18}$$

In terms of Sketch 1 in Sec. 4.4.3, L is thus seen to be the length of a rectangle of height $R(0)$ and area equal to that under the $R(\tau)$ curve. Unfortunately, for a given patch of isotropic

Downloaded by RMIT UNIV BUNDOORA on June 4, 2013 | http://arc.aiaa.org | DOI: 10.2514/4.861888

4.5.4 Von Kármán vs Dryden PSD's

Of the two spectra, the von Kármán gives the better fit to observed data and also is supported, with respect to the $-5/3$ exponent at the higher frequencies, by theory. It is the standard for design use. The Dryden spectrum has retained its importance primarily because of the ease of deriving a filter that will convert a white-noise time history (constant psd, easily generated) to a time history having this spectral shape. For the Dryden spectrum, an exact filter can be derived. For the von Kármán spectrum, the desired filter can only be approximated; nevertheless, excellent approximations are available that are not overly complex. For further discussion, see Chapter 10.

Although the fit to observed data is better for the von Kármán spectrum than for the Dryden, both spectra show a sharper knee than is usually indicated by actual measurements of atmospheric gust velocities.

4.5.5 Values of L for Design

In civil aircraft gust loads determination, L is taken to be equal to 2500 ft for all altitudes. This value was selected in FAA-ADS-53¹³ and has been accepted generally. For altitudes less than about 2500 ft above the ground, the scale of turbulence probably tends to be less, especially for the vertical component. Military specifications, because of the possible importance of high-speed flight at very low altitudes, usually attempt to reflect this variation by specifying reduced values of L at altitudes less than 2500 ft above the ground [see, for example, MIL-A-008861A (USAF)]¹⁴. This reduction may take the form of a linear variation with h (altitude) for vertical gust velocity ($L = h$) and some lesser reduction for lateral and longitudinal gust velocities. Such a reduction is also usual in automatic landing system studies, where the most realistic possible representation at very low altitudes is obviously desirable.

4.5.6 Significance of Design Value of L

Several comments are pertinent with respect to the significance of the value $L = 2500$ ft selected for use in design. One sometimes comes across

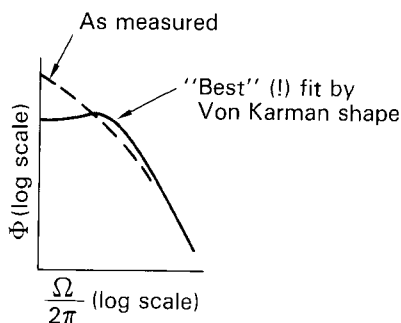
turbulence, L as defined by Eq. (4.18) is twice as great for the longitudinal gust velocity as for the vertical and lateral gust velocities. In Eqs. (4.16) and (4.17), in contrast, L is defined simply as a constant in the equations; and the equations are so written that use of the same value in both equations will properly describe a given patch of isotropic turbulence. Thus, L is considered to describe the turbulence as a whole rather than vertical-lateral or longitudinal components individually.

Furthermore, if a given single value of L is substituted into both Eqs. (4.16) and (4.17), and if $R(\tau)$ is then computed by means of Eq. (4.11), and L , in turn, by means of Eq. (4.18), then the value of L obtained from Eq. (4.18) for the longitudinal gust case will agree with the value initially substituted into Eq. (4.17). On the other hand, the value obtained from Eq. (4.18) for the vertical-lateral case will be one-half of the value initially substituted into Eq. (4.16).

remarks suggesting that a “controversy” exists regarding the “correct” value of L . Such remarks are misleading. They are misleading first because of the vague inference that selection of the correct value of L is vital in order to arrive at realistic design loads. The fact is that the gust response depends hardly at all on L —any value, as long as it is not too small, can be selected as long as it is used consistently (see discussion on Fig. 4.12).

Such remarks are misleading also because they imply that there is some single correct value of L . Instead, L probably varies over a considerable range from one turbulence patch to another. Even more important, L has meaning only in terms of a particular mathematically defined spectral shape; for example, the von Kármán shape. More often than not, however, the psd of a particular patch of turbulence does not fit the equation very well for any value of L (see Sketch n). Therefore, even for a single patch of turbulence, there may be no correct value.

Sketch n



So the pertinent question is not, “What is the correct value of L ?” but rather, “What is an appropriate value for design use?” This question makes sense. Whatever value is picked, even though it need not in practice be precise, should be related, as closely as practicable, to the actual turbulence that airplanes will encounter. There is indeed difficulty in accurately measuring gust psd’s at the low-frequency end.

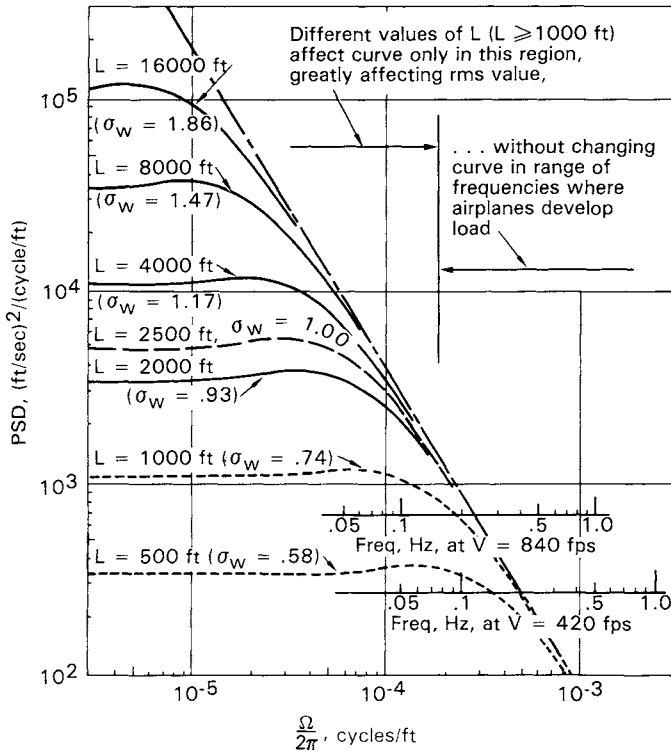
Gust velocity psd’s are determined experimentally from time histories of gust velocity encountered by an airplane flying through turbulence. The gust velocity relative to the airplane is obtained by means of a vane or a differential pressure probe. The absolute gust velocity is then obtained by adjusting for the effect of the airplane motions, which are measured simultaneously (Sec. 11.4). At the higher frequencies, say above 0.25–0.50 Hz, the airplane motions are relatively small and can be removed accurately. However, at the much lower frequencies which establish the value of L (if indeed it exists at all; see Sketch n), adjusting for the effect of airplane motions involves taking a small difference of large numbers; consequently, maintaining accuracy becomes very difficult. So there is indeed considerable uncertainty even in

establishing L on a statistical basis, or in establishing spectral shapes in the low-frequency region in terms of whatever other parameters might be appropriate. As Etkin⁴ puts it, “the deformation of L at altitude remains an unresolved difficulty.”

Now, why is a rather arbitrary value of L satisfactory?

Two families of von Kármán psd curves are shown in Fig. 4.12. In Fig. 4.12a, the curves all have the same high-frequency asymptote. (The asymptote selected is that corresponding to $L = 2500$ ft and $\sigma_w = 1.00$.) As indicated on the figure, over the frequency range at which airplanes develop gust loads, the curves virtually coincide for all values of L down to about 2000 ft and perhaps even lower. Thus, whichever of these curves might be selected for design (as long as L is no less than about 2000 ft), the loads would be the same.

There is a trap, however! The curves do differ significantly at lower

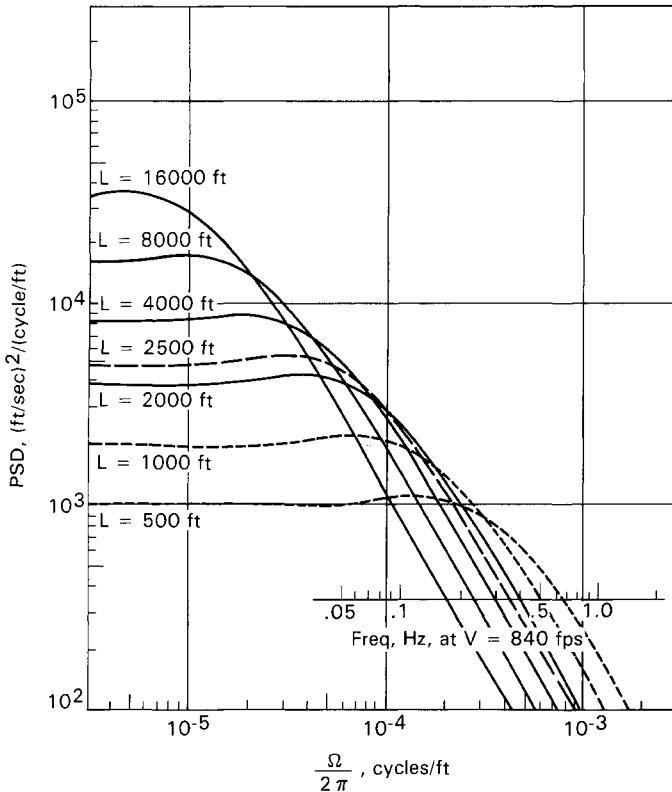


a) Constant asymptote.

Fig. 4.12 Effect of L on psd curves: von Kármán shape, vertical-lateral gust.

frequencies, so that their σ_w values are different. If, for example, an appropriate design σ_w with $L = 2500$ ft is 30 fps, then with $L = 8000$ ft, the design σ_w must be increased to $30(1.47/1.00) = 44$ fps to keep the asymptote, and the loads, the same. (The general rule is that to keep the asymptote the same, σ_w must vary as the cube root of L .) The quantity σ_w is the accepted measure of gust intensity, but what it must measure is the height of the asymptote; it provides this measure only after L has been specified. To describe a given asymptote will require different values of σ_w , depending on L .

One helpful point of view (refer again to Fig. 4.12a) is that we *cannot* know what the psd is at very low frequencies, because we cannot measure the gust velocities; and *we do not care* because there is no effect on the airplane response. So we arbitrarily define the psd shape in this region—it could have been von Kármán with $L = 8000$ ft, for example, just as well as the $L = 2500$ ft von Kármán spectrum actually chosen—in order that whenever



b) Constant rms; $\sigma_w = 1.00$ fps.

Fig. 4.12 (continued). Effect of L on psd curves: von Kármán shape, vertical-lateral gust.

we call out a particular value of σ_w , we establish the location of the psd curve in the higher frequency region that governs the airplane response.

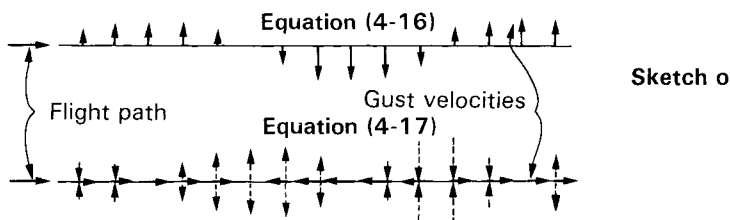
Figure 4.12b shows the effect on the psd plots of holding *constant* σ_w . For computing convenience, psd's are usually normalized to a unit σ_w value; and it is just as well to be aware of how the psd's for various L 's would compare when thus normalized. Physically, as pointed out in the preceding paragraphs, constant σ_w has no meaning because σ_w is so heavily influenced by the very low-frequency gust velocity components, which are unknown and unimportant. If one were to attribute, foolishly, some sort of basic significance to σ_w , then one could see from Fig. 4.12b that for an airplane responding primarily at, say, a frequency corresponding to $\Omega/2\pi = 3 \times 10^{-4}$, the loads would indeed depend on L , actually varying as $1/L^{1/3}$.*

A statement or inference that loads depend on L always requires qualification. If based on the relations indicated by Fig. 4.12a, such a statement or inference makes sense. If based on the relations indicated by Fig. 4.12b, it does not!

Now that all this has been said, it should be added that the situation is not quite as clear-cut as suggested. Even with $L = 2500$ ft, there are sometimes situations in which the responding frequencies reach down to or below the knee in the psd curve. These involve either flight at very high speeds (e.g., supersonic cruise) or modes with very low natural frequencies (e.g., the Dutch-roll mode on some airplanes).

4.5.7 Why PSD's Are Different for Vertical-Lateral and Longitudinal Components of Turbulence

The source of the difference between the vertical-lateral and longitudinal psd's in a given patch of isotropic turbulence [Eq. (4.16) vs (4.17)] is the difference in the orientation of the gust velocity component relative to the flight path:



*From Eq. (4.16), when $L\Omega \gg 1$,

$$\Phi(\Omega) = \sigma_w^2 \frac{L}{\pi} \frac{\frac{8}{3}(1.339L\Omega)^2}{[(1.339L\Omega)]^{11/6}} \propto \frac{L \cdot L^2}{L^{11/3}} \propto \frac{1}{L^{2/3}}; \quad \sqrt{\Phi(\Omega)} \propto \frac{1}{L^{1/3}}$$

It is seen that Eq. (4.16) applies to a shearing type of gust velocity variation. Equation (4.17), in contrast, applies to what appears superficially to be an extension-compression type of variation, although it must actually involve, instead, a lateral inflow-outflow variation as indicated by the dotted arrows. In view of the differences noted, it is reasonable to expect a difference in frequency content between the two cases. In fact, one might even guess, correctly, that the second of the two patterns would display a more gradual variation of gust velocity than the first, leading to a greater proportion of low-frequency components in the psd. It is to be emphasized that the difference between Eqs. (4.16) and (4.17) has nothing to do with wind direction. The turbulence is assumed to be fully isotropic, and the reasoning applies equally to any flight path through the turbulence.

4.5.8 Other Mathematically Defined PSD Shapes

To assist in finding simple mathematically defined curves that best fit the various shapes obtained from actual gust velocity measurements, several families of curves have been developed. These are described and presented in AFFDL-TR-68 127,¹⁵ pp. 70 and 205–217. The plots in the reference are to a small scale, however; four plots to a page. Unreduced plots, together with a full set of transparencies for overlaying the measured data, are much more helpful in comparing with flight-measured psd's.

4.6 FREQUENCY OF EXCEEDANCE

In loads applications, the rms value σ_y and the probability distribution— $p(y)$, $P(y)$, or $1 - P(y)$ (Sec. 4.3)—do not provide entirely adequate measures of load magnitude.

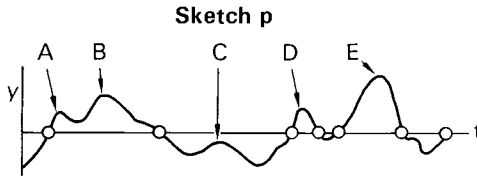
The probability distribution of any load quantity y , if expressed in the form $1 - P(y)$, is the probability that y as sampled at a single instant will be in excess of y_1 . This probability can also be thought of as equivalent to the fraction of time, over a very long sample, that y will be in excess of y_1 . This probability, however, tells us nothing at all about the probability that the highest peak within some finite time interval, such as the duration of a flight, or the lifetime of an airplane, will be in excess of y_1 . Nor does it indicate the numbers of peaks to be expected, in excess of various values of y_1 , within such an interval. For this kind of information, we need frequency of exceedance data.

4.6.1 What Is a Peak?

Two simple definitions are available:

1) *An algebraic maximum.* All of A , B , C , D , E in Sketch p would qualify. C might be ruled out arbitrarily as being less than zero. This is an obvious definition, but one not often used in practice.

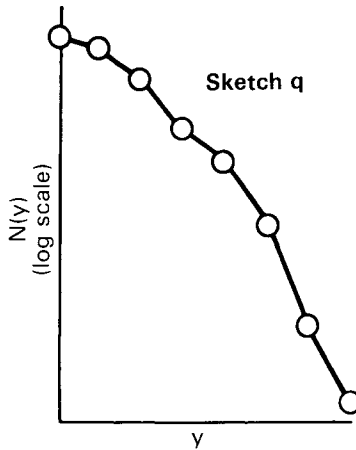
2) *The highest value between successive zero crossings.* Only B, D, and E qualify. This definition has been widely used.



Both of these definitions apply also to negative peaks.

4.6.2 Peak Count Data

Peak count data are obtained from recorded time histories by measuring each peak, counting the numbers of peaks within arbitrarily defined bands, accumulating these counts from the high to low values of y , dividing by the duration of the record (in hours) to give $N(y)$, and plotting as indicated in Sketch q. In this plot, $N(y)$ is the number of peaks per hour in excess of y .



4.6.3 Rice's Equation

Corresponding, but not identical, data can be obtained theoretically for a stationary Gaussian random process by means of "Rice's Equation," first published in Ref. 16 (Eqs. 3.3-11 and 3.3-14 there).

Rice's equation is

$$N(y) = N_0 e^{-\frac{1}{2} \left(\frac{y}{\sigma_y}\right)^2} \tag{4.19}$$

Downloaded by RMIT UNIV BUNDOORA on June 4, 2013 | http://arc.aiaa.org | DOI: 10.2514/4.861888

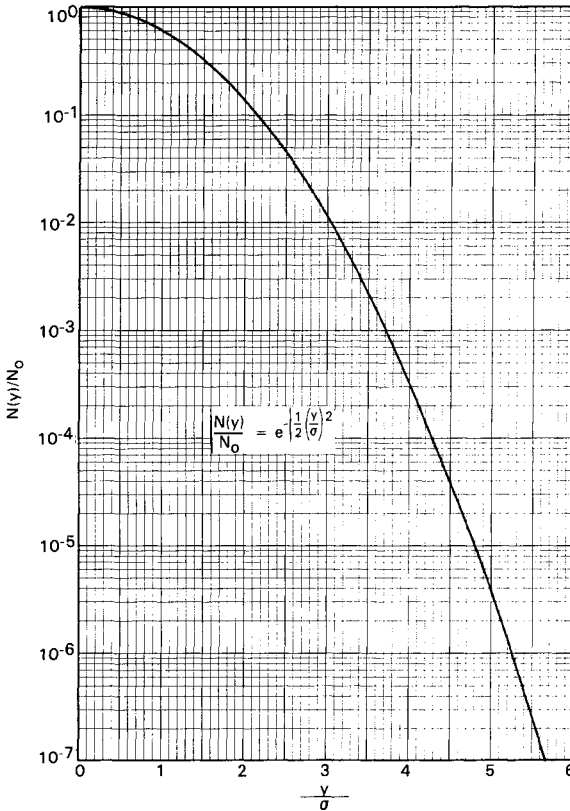


Fig. 4.13 Rice's equation.

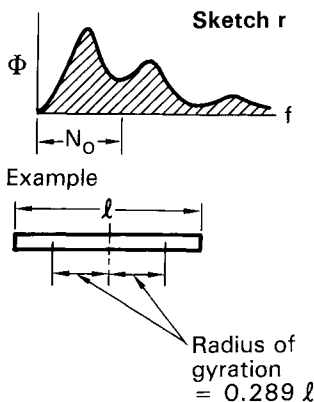
This equation gives the number of crossings of a given level y , per unit time, with positive slope. N_0 , it can be seen, is therefore the number of zero crossings per unit time with positive slope. This equation is plotted in Fig. 4.13. On the semilog coordinates, the curve is a parabola.

As can be seen by reference to Sketch p (with a little thought), this approximates the cumulative peak count (Sketch q) obtained by defining peaks according to the second definition given in Sec. 4.6.10. The approximation is fairly good for values y/σ greater than 2. It is especially good, even at lower values of y/σ , for narrow band noise (Fig. 4.8).

The number of negative-slope crossings is, of course, equal to the number of positive-slope crossings: what goes up must come down! The reason for counting positive-slope crossings only (or negative only) is to obtain the same number of crossings (approximately) as there are positive peaks, instead of twice as many.

N_0 in Eq. (4.19) can be thought of as a “characteristic frequency.” It is given by

- 1) Radius of gyration of the psd about zero frequency



$$2) N_0 = \sqrt{\int_0^\infty f^2 \Phi(f) df / \int_0^\infty \Phi(f) df} \tag{4.20}$$

$$3) N_0 = \frac{1}{2\pi} \frac{\sigma_{dy/dr}}{\sigma_y} \tag{4.21}$$

A practical problem sometimes arises in that the numerator in Eq. (4.20) may not converge, that is,

$$\lim_{f \rightarrow \infty} \int_0^f f^2 \Phi(f) df = \infty$$

This occurs when $\Phi(f)$ decreases less steeply than as f^{-3} as $f \rightarrow \infty$. This problem is discussed in detail in Appendix E.

4.7 APPLICATION OF FREQUENCY OF EXCEEDANCE TO GUST LOADS

4.7.1 Concept

The following discussion addresses the determination, by analysis, of frequency-of-exceedance curves for various load quantities y for typical overall operation of an airplane. This determination will involve

- 1) Establishing a *mission profile* (or flight profile).
- 2) Breaking the mission profile into *mission segments* for analysis. This segmentation will be such that, over each segment, altitude, speed, and

airplane weight can be considered constant (at a midsegment value) for the purpose of analysis.

3) Accounting for the *various* σ_w levels expected to be encountered in each segment.

Within each segment, the atmosphere is first considered to be made up of discrete patches of continuous turbulence of different rms intensities σ_w , each of which is stationary and Gaussian. This discrete-patch model is then replaced by a model that has a continuously varying distribution of σ_w . This variation is considered to be gradual enough in time, however, so that the relations of output to input developed for a stationary Gaussian process still apply.

4.7.2 Introduction of \bar{A} into Rice's Equation

Definition:

$$\bar{A} \equiv \frac{\sigma_y}{\sigma_w} \quad (4.22)$$

\bar{A} is obtained by dynamic analysis, by utilizing Eqs. (4.7) and (4.15) and solving the airplane equations of motion to give $H(f)$. A single gust psd shape is used, considered to be independent of σ_w .

Solving Eq. (4.22) to give $\sigma_y = \bar{A}\sigma_w$ and substituting into Eq. (4.19), Rice's equation, gives

$$\begin{aligned} N(y) &= N_0 \exp\left[-\frac{1}{2}\left(\frac{y}{\sigma_y}\right)^2\right] = N_0 \exp\left[-\frac{1}{2}\left(\frac{y}{\bar{A}\sigma_w}\right)^2\right] \\ &= N_0 \exp\left[-\frac{1}{2}\frac{(y/\bar{A})^2}{\sigma_w^2}\right] \end{aligned} \quad (4.23)$$

This step replaces σ_y with σ_w , and y with y/\bar{A} ; it thus paves the way for accounting for the known probability distribution of σ_w in the atmosphere.

4.7.3 Superposition of Many Turbulence Patches of Various σ_w Levels to Give Overall $N(y)$ for a Segment

Applying Eq. (4.23) to each of many σ_w levels σ_{w_i} , in turn, and superimposing gives

$$N(y) = \sum_{\sigma_{w_i}} t_i N_0 \exp\left[-\frac{1}{2}\frac{(y/\bar{A})^2}{\sigma_{w_i}^2}\right] \quad (4.24)$$

Fraction of time that $\sigma_w = \sigma_{w_i}$

If we now consider a continuous variation of σ_w , Eq. (4.24) is replaced by

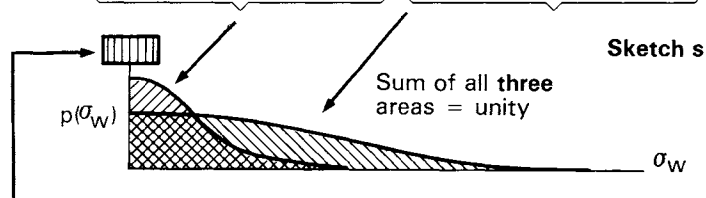
$$N(y) = \int_{\sigma_w=0}^{\infty} N_0 \exp\left[-\frac{1}{2} \frac{(y/\bar{A})^2}{\sigma_w^2}\right] \underbrace{p(\sigma_w) d\sigma_w}_{t_i} \quad (4.25)$$

Probability density

Here, the probability, $p(\sigma_w) d\sigma_w$, that σ_w has a value between σ_w and $\sigma_w + d\sigma_w$ is considered to be equivalent to the fraction of time that σ_w is between σ_w and $\sigma_w + d\sigma_w$.

4.7.4 Convenient Mathematical Form for Probability Density of σ_w

$$p(\sigma_w) = P_1 \sqrt{\frac{2}{\pi}} \frac{1}{b_1} \exp\left[-\frac{1}{2} \left(\frac{\sigma_w}{b_1}\right)^2\right] + P_2 \sqrt{\frac{2}{\pi}} \frac{1}{b_2} \exp\left[-\frac{1}{2} \left(\frac{\sigma_w}{b_2}\right)^2\right] \quad (4.26)$$



“Signboard” or delta function—area indicates probability that $\sigma_w = 0$. This is not included explicitly in Eq. (4.26), which will be utilized only over the range $\sigma_w > 0$.

Equation (4.26) was first introduced in NACA TN 4332.¹⁷ It is now used almost universally.

Originally, the two terms were regarded as applying to nonstorm and storm turbulence, respectively. Equation (4.26) can also be considered, however, to be simply an empirical equation covering all types of turbulence collectively.

P_1 , P_2 , b_1 , and b_2 are constants depending on altitude. Values recommended for design, for use with a von Kármán gust spectrum with $L = 2500$ ft, are given in Figs. 4.14 and 4.15. These are taken from FAA-ADS-53¹³. Figures 4.14 and 4.15 cover only the altitude range 0–50,000 ft. The curves in Ref. 13 go on up to 80,000 ft. P_1 and P_2 are fractions of time in nonstorm and storm turbulence, respectively, and b_1 and b_2 are constants indicative of probable intensities.

Each of the two terms in Eq. (4.26), without the P_1 or P_2 coefficient, is seen to represent the positive half of a Gaussian probability density, with a factor of 2 in front to account for the missing negative half. Thus, each term, prior to multiplication by P_1 or P_2 , is by itself a probability density, with area under the curve equal to unity. By comparison of Eq. (4.26) with Eq. (4.4),

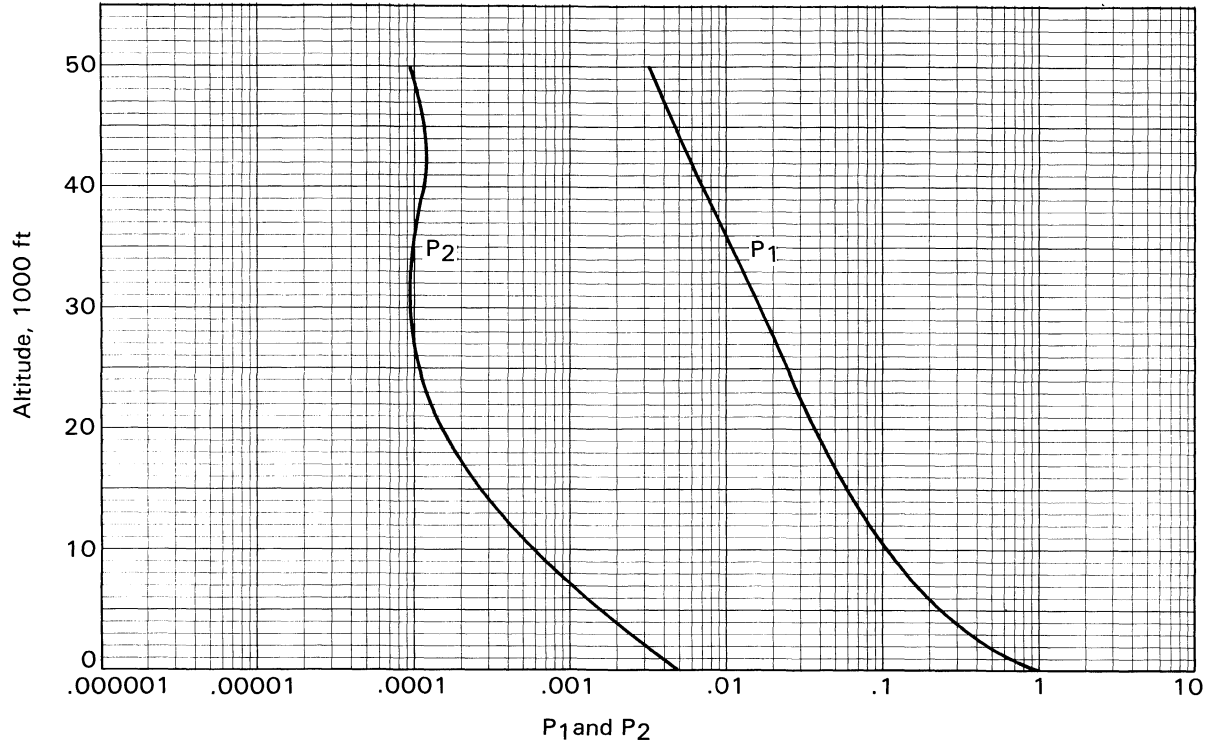


Fig. 4.14 P_1 and P_2 values for use in design.

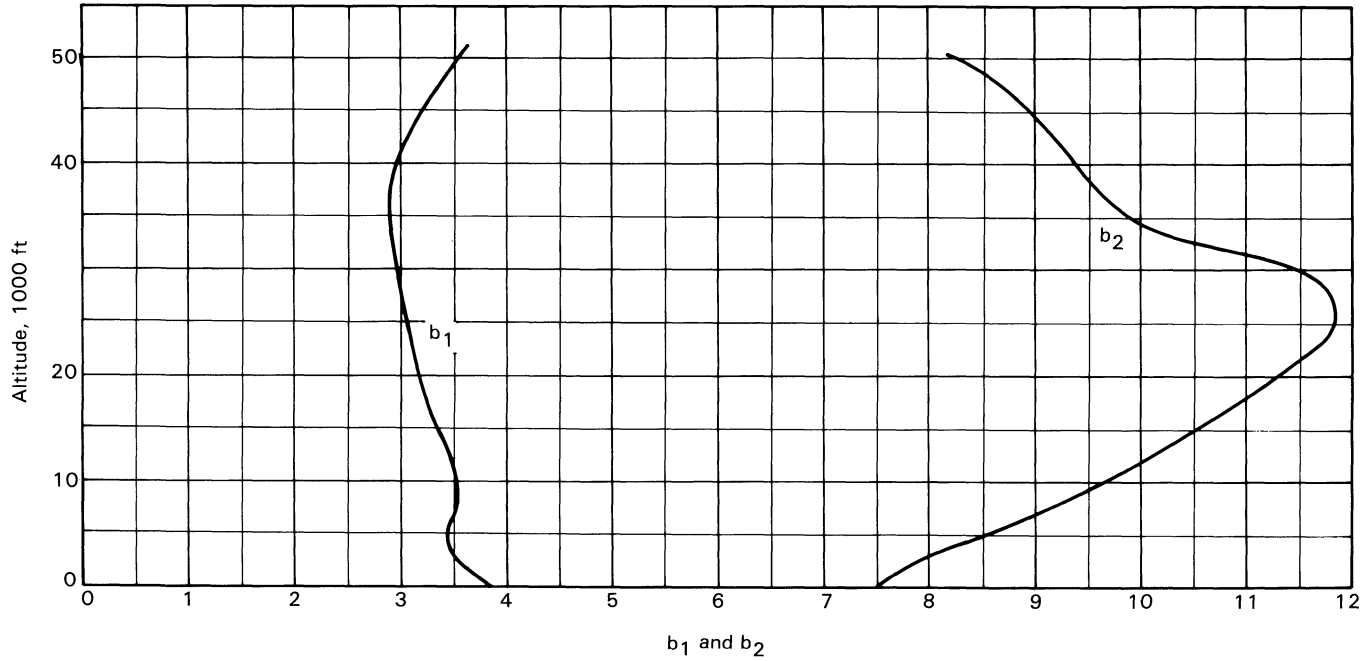


Fig. 4.15 Values of b_1 and b_2 for use in design.

it is now seen that b_1 and b_2 are the rms values of σ_w for the time spent in the respective categories of turbulence.

It may be noted that the area indicated by the signboard in Sketch s is likely to be the largest of the three. This area is given by $1 - P_1 - P_2$, which is greater than 0.90 for all altitudes above about 10,000 ft (as can be seen from the P_1 and P_2 values in Fig. 4.14).

As an aside, it is noted that

$$P\{\sigma_w > \sigma_{w1}\} = 1 - P(\sigma_w) = \int_{\sigma_{w1}}^{\infty} p(\sigma_w) d\sigma_w$$

This integration has been carried out, by utilizing $p(\sigma_w)$ as given by Eq. (4.26), for a series of altitudes. The results are plotted in Appendix F.

4.7.5 Resulting Generalized Exceedance Expression

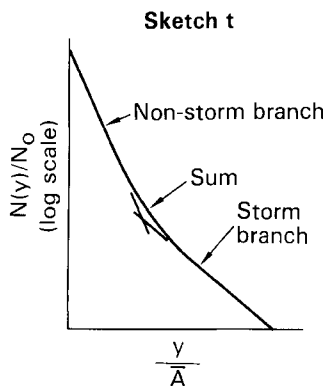
Substituting Eq. (4.26) into Eq. (4.25) gives

$$\frac{N(y)}{N_0} = P_1 \exp\left(-\frac{y/\bar{A}}{b_1}\right) + P_2 \exp\left(-\frac{y/\bar{A}}{b_2}\right) \quad (4.27)$$

The intermediate steps leading from Eqs. (4.25) and (4.26) to Eq. (4.27) are shown in Appendix G.

In Eq. (4.27), y , of course, is any response variable such as, for example, airplane center of gravity acceleration or a particular wing bending moment. \bar{A} and N_0 are obtained by solution of the airplane equations of motion. P_1 , P_2 , b_1 , and b_2 , as noted earlier, are constants describing the probability distribution of σ_w and depend only on altitude.

The two variables are $N(y)/N_0$ and y/\bar{A} . If $N(y)/N_0$ is plotted vs y/\bar{A} (Sketch t) a generalized exceedance curve results. An actual exceedance curve for a particular load quantity on a given airplane then follows by multiplying ordinates by N_0 and abscissas by \bar{A} .



Each of the two terms in Eq. (4.27) is seen to plot as a straight line on the semilog coordinates.

It is seen that the same four parameters, P_1 , P_2 , b_1 , and b_2 , define both the σ_w distributions and the generalized exceedance curves. Thus, the generalized exceedance curves provide an alternative to the probability density as a means of describing the statistical distribution of σ_w . This alternate form of presentation is generally preferred, because of its closer relation to the way in which the σ_w distributions are used in loads determination and the way in which the σ_w distributions are determined from operational data (Sec. 4.8).

Generalized exceedance curves based on the P 's and b 's of Figs. 4.14 and 4.15 are shown in Fig. 4.16. This figure is taken from FAA-ADS-53.¹³ For

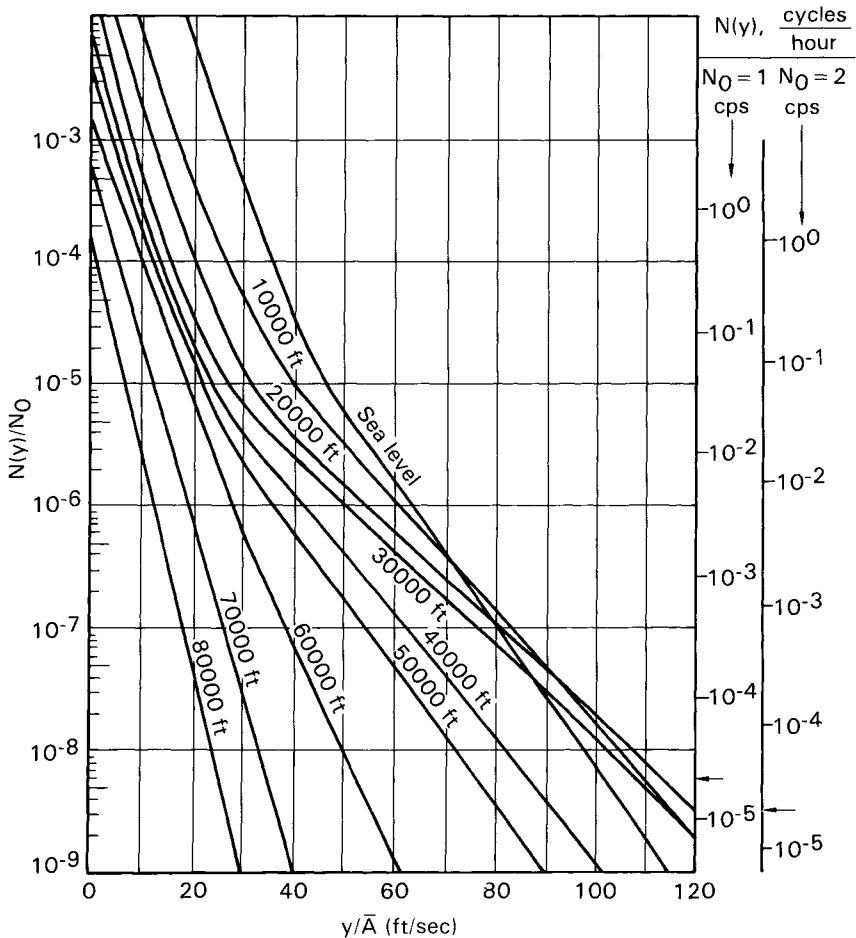


Fig. 4.16 Generalized exceedance curves.

BASIC PSD CONCEPTS

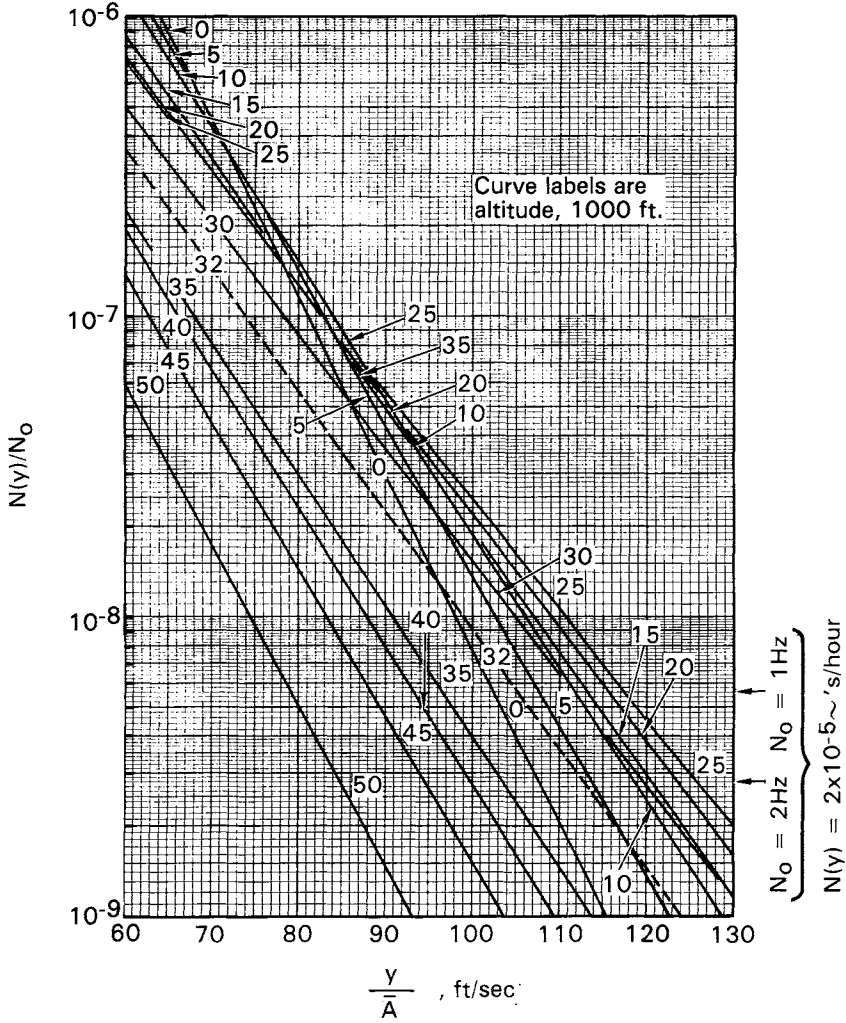


Fig. 4.17 Generalized exceedance curves; expanded scales.

perspective, frequency of exceedance scales in c/h have been added for two representative values of N_0 , 1.0 and 2.0 Hz. It is seen that y/\bar{A} has the units of gust velocity. It is sometimes designated U_σ (Sec. 5.3.2). A portion of Fig. 4.16 to expanded scale and with curves included for intermediate altitudes is shown in Fig. 4.17.

4.7.6 Superposition of Mission Segments

For a mission composed of a number of segments, the exceedances contributed by the individual segments, as given by Eq. (4.27), are superimposed:

$$N(y) = \sum_i t_i N_0 \left[P_1 \exp\left(-\frac{y/\bar{A}}{b_1}\right) + P_2 \exp\left(-\frac{y/\bar{A}}{b_2}\right) \right] \quad (4.28)$$

\uparrow
 Fraction of time in segment i
 [not the same as t_i in Eq. (4.24)]

Values of P_1 , P_2 , b_1 , b_2 , N_0 , and \bar{A} differ from segment to segment. These quantities, therefore, like t_i should properly carry the subscript i ; this subscript has been omitted in Eq. (4.28), for simplicity.

Inasmuch as \bar{A} and N_0 differ from segment to segment, the variables must be considered to be $N(y)$ and y instead of $N(y)/N_0$ and y/\bar{A} .

4.7.7 Effect of 1-g Load

When exceedance curves are to be used for limit load determination, the pertinent load is the net load, including the 1-g load as well as the gust increment. If we let y denote the net load and note that the 1-g load will, in general, vary from segment to segment, Eq. (28) now becomes

$$N(y) = \sum_i t_i N_0 \left[P_1 \exp\left(-\frac{|y - y_{1-g}|/\bar{A}}{b_1}\right) + P_2 \exp\left(-\frac{|y - y_{1-g}|/\bar{A}}{b_2}\right) \right] \quad (4.29)$$

Again, the variables are considered to be $N(y)$ and y .

4.8 DETERMINATION OF P 's AND b 's FROM FLIGHT DATA

4.8.1 What to Measure: Gust Velocity vs C.G. Acceleration

There have been a number of flight-test programs in which actual gust velocities have been measured by techniques described briefly in Sec. 4.5.6. Both the instrumentation and the data reduction involved in such measurements, however, are far too complex to be practical when it is desired to collect the thousands of hours of data needed to define σ_w distributions for routine airline (or military) operations. Instead, for collection of operational

data, the airplane c.g. normal acceleration is measured. Sufficiently accurate values of \bar{A} can be obtained from simple formulas and curves (Chapter 8) to permit conversion of c.g. acceleration data to gust velocity data. Either *rms values* of c.g. acceleration or c.g. acceleration *peak count data* can be converted to the corresponding gust velocity data in this way.

4.8.2 RMS vs Peak Count Approach

Values of P 's and b 's can be obtained, in principle, from either rms data or peak count data. A major problem in using rms data, however, is that turbulence is almost never sufficiently stationary to yield meaningful rms values. Suppose, for example, that a typical four-minute flight-test "burst" is processed to give both the rms value of the c.g. acceleration and the c.g. acceleration exceedance data [$N(y)$ vs y]. The highest measured peaks are almost certain to be higher than predicted using the measured rms value in Rice's equation. Good agreement with the measured peak count data can almost always be obtained, however, by considering the burst to consist of two or more portions having different rms values.*

Moreover, a good deal of turbulence is a lot less stationary than the typical flight test burst, selected in the first place for its apparent stationarity. Indeed, it is hard to see how an rms approach could be applied at all to the occasional relatively isolated gusts that do exist. For these reasons, a peak count approach is much to be preferred. In addition, it is probably much easier, for either a human being or a computer, to read and count peaks or level crossings than to calculate rms values.†

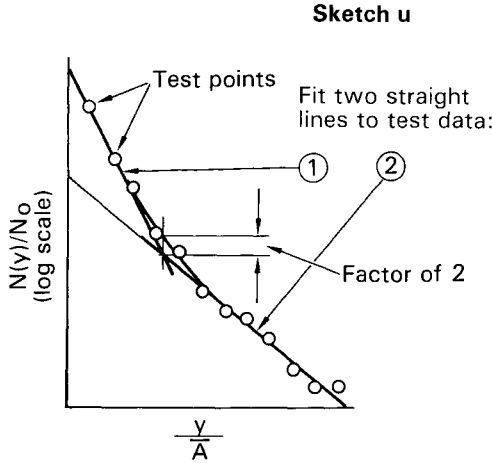
4.8.3 Procedure: Peak Count Approach

The peak count (or level-crossing) data are collected by an altitude band. For each c.g. acceleration peak (or level crossing), the corresponding \bar{A} and N_0 values are computed utilizing recorded speed, altitude, and airplane weight; $N(y)/N_0$ and y/\bar{A} are then obtained. Points are then plotted and fitted

*For a more detailed discussion, with theoretical and experimental examples, the section on stationarity on pp. 99–109 of AAFDL TR-68-127 is highly recommended. See also Sec. 12.2 herein.

†It is interesting to note that the first determinations of σ_w distributions from operational data did use the peak count approach. These are reported in Refs. 17 and 18. These determinations utilized data already processed on a discrete-gust basis; in fact, only the peak count data were available. Thus, whether by intent or fortunate accident, the "right" approach was used. Only later, when σ_w 's were extensively calculated in major flight test programs, starting with the B-66B low-level gust study,¹⁹ were σ_w distributions obtained directly from rms values of measured data. Only later still did it become apparent how misleading such data would be.

by straight lines as indicated in Sketch u. Line 1 defines the nonstorm term in Eq. (4.27), and line 2 the storm term, as indicated.



The intercepts of the two lines give P_1 and P_2 .^{*} The slopes give b_1 and b_2 ; $b = 0.4343 [\Delta(y/A) \text{ per decade}]$.^{*}

^{*}For a single term in Eq. (4.27),

$$\frac{N(y)}{N_0} = P e^{-\frac{y/\bar{A}}{b}}$$

$$\log_e \frac{N(y)}{N_0} = \log_e P - \frac{y/\bar{A}}{b}$$

$$\log_{10} \frac{N(y)}{N_0} = \log_{10} P - 0.4343 \frac{y/\bar{A}}{b}$$

1) When $y/\bar{A} = 0$, $\log_{10} \frac{N(y)}{N_0} = \log_{10} P$

2) When $\Delta \left[\log_{10} \frac{N(y)}{N_0} \right] = 1$ (i.e., one decade)

$$-0.4343 \frac{\Delta(y/\bar{A})}{b} = 1$$

whence $b = -0.4343 \Delta(y/\bar{A})$

4.8.4 Dependence of b 's on L

It should be emphasized that the values obtained for the b 's using the procedure of Sec. 4.8.3 depend on the value of L used in computing the \bar{A} 's. Consequently, these b 's apply only in conjunction with a particular value of L . See Sec. 4.5.6.

4.8.5 Sources of Data

Values of P 's and b 's for use in design (such as given by Figs. 4.14 and 4.15) may utilize various sources of data in their determination. The primary sources to date are the old NASA VGH program and similar military programs. More recently, programs have been instituted to utilize the AIDS systems on the newer airplanes. These include the NASA digital VGH program, Lockheed-California's Airline Usage Data program, and the CAA's CAADRP program. The CAADRP program concentrates on the higher load levels. Data are also available from programs in which the primary emphasis is psd data, such as the B-66 low-level gust program. Inferences have also been made from airplane incidents and accidents; b_2 values used by the USAF for high-speed low-altitude flight were obtained in this way, as discussed in SEG TR-65-4.²⁰

It should be emphasized that each source of P 's and b 's provides a description of the atmosphere as sampled in that particular program. Airline operational data, for example, will reflect whatever gust avoidance techniques were utilized in the particular operations. The sampling, therefore, should be consistent with the use to which the data will be put.

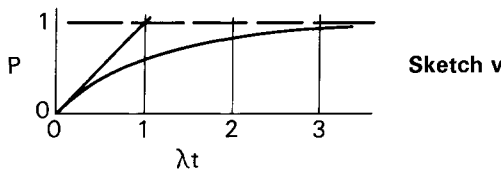
4.9 RELATION BETWEEN FREQUENCY OF EXCEEDANCE AND PROBABILITY OF EXCEEDANCE

When one speaks of a *frequency of exceedance* of y of, for example, $10^{-4}/h$, it is intuitively obvious that the *probability* that this same value of y will be exceeded in one hour of flight is likewise 10^{-4} . Similarly, the probability of exceeding this value in a three-hour flight is 3×10^{-4} .

However, suppose the frequency of exceedance of some very much lower value of y is 3/h. Clearly, the probability of exceedance of this new value of y in one hour of flight cannot be 3, since no probability can exceed unity. The equation relating frequency of exceedance and probability is

$$P = 1 - e^{-\lambda t}$$

where t is the period to which the probability applies and λ is the frequency of exceedance (Ref. 21, pp. 110-118).



Downloaded by RMIT UNIV BUNDOORA on June 4, 2013 | http://arc.aiaa.org | DOI: 10.2514/4.861888

It can be seen from the sketch, or by expressing $e^{-\lambda t}$ as a power series in λt (Peirce, Eq. 759, Ref. 22), that for small t , $P \approx \lambda t$. It is also evident from the sketch that, at large λt , $P < \lambda t$, and it is evident from the equation that, no matter how large λt becomes, P does not exceed unity.

Problems

In these problems, use the following airplane and gust data as needed:

$GW = 116,000$ lb c.g. 25% MAC

$V = 261$ knots equivalent airspeed (KEAS)

$h = 20,000$ ft

Gust psd and transfer function for wing root bending moment are as tabulated

Frequency Hz	Gust psd* (fps) ² /Hz	$ H ^2$ (in. lb/fps) ²
0.2	0.835	0.027×10^{12}
0.4	0.274	0.247
0.6	0.138	0.493
0.8	0.087	0.466
1.0	0.060	0.452
1.2	0.044	0.515
1.4	0.034	0.575
1.6	0.027	0.493
1.8	0.022	0.274
2.0	0.019	0.137
2.2	0.016	0.068
2.4	0.01	0.044
2.6	0.012	0.027

*von Kármán spectrum with $\sigma_w = 1.00$.

Note: 1-g level flight value of root bending moment is 11.0×10^6 in. lb.

4.1 Compute and plot the psd of wing root bending moment for the given airplane and flight condition. Do not use log or semilog graph paper.

4.2 Roughly estimate \bar{A} and N_0 ($\bar{A} \pm 10\%$, $N_0 \pm 20\%$). (*Hint:* Draw a triangle on your graph having about the same area as under the psd curve. Be careful of units when obtaining the “area” of the triangle.) (1 min.)

4.3 Repeat Problem 4.2, assuming rigid airplane. (*Hint:* Identify the small bump in the psd curve due to the first elastic mode resonance and sketch what the curve would look like without the bump.)

BASIC PSD CONCEPTS

67

- 4.4** Calculate \bar{A} and N_0 to within about 5%. (10 min.)
- 4.5** Given that $\sigma_w = 30$ fps, compute and plot $N(y)$ vs y (where y is root-bending moment) over the range from $y = 0$ to the value expected to be exceeded about once an hour. Show frequency scales in cps, c/min, and c/h. Use \bar{A} and N_0 values from Problem 4.4 (or 4.3). (*Hint*: Use Rice's equation.)
- 4.6** Still taking $\sigma_w = 30$ fps, determine and plot the fraction of time the upbending gust incremental bending moment is in excess of various values. Cover the range from $y = 0$ to the value expected to be exceeded 0.1% of the time. (*Hint*: Assume the process to be Gaussian and use Fig. 4.2.)
- 4.7** Does the curve of Problem 4.6 give the probability that the airplane will experience a load in excess of a given value? (Requires thought!) Why?
- 4.8** Using the results of Problem 4.4 (or 4.3), plot the exceedance curve for root-bending moment for flight in this flight condition, considering the actual mix of σ_w values to be expected at this altitude. Plot as exceedances in c/h vs net bending moment (not gust increment) in units of 10^6 in. lb. Use semilog paper. (*Suggestion*: Use the generalized exceedance curves of Fig. 4.16.)
- 4.9** What is the value of P_2 in Problem 4.8? Of P_1 ? Obtain by extrapolating the generalized exceedance curve and check by reading from Fig. 4.14.
- 4.10** What is the bending moment exceeded (on the average) once in 10,000 hours of flying in this flight condition?
- 4.11** What is σ_w likely to be for the patch of turbulence in which this bending moment is reached? (*Suggestion*: Assume that a typical patch of turbulence will be of such duration that the peak-to-rms ratio is about 3.)
- 4.12** Check any one point on the curves of Fig. 4.16, using the b and P values of Figs. 4.14 and 4.15.
- 4.13** For the point you picked in Problem 4.12, which contributed more, storm or nonstorm turbulence? Is this what you would have expected looking at where your point lies on the curve?

This page intentionally left blank

5

CONTINUOUS TURBULENCE GUST LOADS CRITERIA

Chapter 4 introduced some concepts, facts, and tools related to the power-spectral determination of gust loads. The present chapter discusses how these concepts, facts, and tools are utilized to assure that a new airplane will have sufficient strength to provide a satisfactory level of safety. FAA-ADS-53¹³ and the *Journal of Aircraft* paper by Stauffer and Hoblit²³ also cover much the same material, each from its own somewhat different point of view. The pertinent portions of Ref. 23 are the Introduction and the “Criteria and General Approach” section under “Gust Criteria and Loads.” The presentation is in terms of design load determination for the L-1011-1. FAA-ADS-53¹³ provides a much more detailed treatment, emphasizing how the criteria were originally developed. The pertinent portions are the Introduction and Secs. 4, 15, and 17. The Introduction is especially recommended as it provides historical background. Suggested formal criteria are presented in Secs. 15.1.6, 15.2.7, and 15.3.3.

5.1 FAR REQUIREMENTS

Surprisingly, until as recently as September 1980, the only reference to power-spectral gust loads criteria in FAR 25² was the following brief statement:

“25.305 Strength and deformation. . . .

(d) The dynamic response of the airplane to vertical and lateral continuous turbulence must be taken into account.”

This does not mean that the FAA has been uninterested in power-spectral criteria. Indeed, incorporation of more explicit criteria into Appendix G to FAR 25² (finally issued in September 1980) had been in process at least since 1974. The FAA has also worked closely with manufacturers in developing power-spectral gust loads criteria for specific airplanes at least since the early 1960's.

What was probably the first concerted attempt to develop a comprehensive set of power-spectral gust loads criteria of general applicability was undertaken by the Lockheed-California Company in 1964–1966, under contract with the FAA. This resulted in Report FAA-ADS-53, “Development of a Power-Spectral Gust Design Procedure for Civil Aircraft.”¹³ This has since become, in effect, a worldwide basic reference. The criteria formulated in FAA-ADS-53¹³ have been recognized by the FAA, since their issuance, as

constituting an “acceptable means of compliance” with FAR 25.305(d). They also formed the basis for the current Appendix G to FAR 25, which differs primarily in the prescribed design gust velocities and their variation with altitude.

5.2 MILITARY REQUIREMENTS

USAF requirements for power-spectral determination of limit design gust loads appear in MIL-A-008861A(USAF).¹⁴ This document, as distinguished from the corresponding Navy document, MIL-A-8861(ASG),²⁵ was first issued in 1971 and has not been revised. The power-spectral gust load criteria contained therein are essentially those of FAA-ADS-53,¹³ with reduced values of L and correspondingly adjusted values of the b 's at altitudes below 2500 ft, and with provision for evaluating mission analysis loads on an ultimate as well as a limit basis. Actually, virtually the same criteria were first published in 1967 in SEG-TR-67-28²⁴ and presumably constituted unofficial Air Force policy during the interim period.

The U.S. Navy, as of September 1981, does not require power-spectral determination of limit design gust loads. Since at least as early as 1960, however, it has required, through MIL-A-8866(ASG),²⁵ power-spectral determination of repeated loads spectra. The “turbulence field parameters” (P 's, b 's, and L 's) are defined on the basis of a Dryden psd with $L = 1000$ ft ($L = 500$ ft for altitudes less than 1000 ft). The Navy is now amenable, however, to substitution of the FAA-ADS-53¹³ turbulence model in applications to particular airplanes.

5.3 BASIC FORMS OF CRITERION

Power-spectral gust loads criteria can be of two basic types: mission analysis and design envelope. In actual practice, provision is usually made for some combination of the two.

5.3.1 Mission Analysis Criterion

The mission analysis criterion is based on the use of the frequency of exceedance equation, Eq. (4.29) of Chapter 4. This equation is

$$N(y) = \sum_i t_i N_0 \left[P_1 \exp\left(-\frac{|y - y_{1-g}|/\bar{A}}{b_1}\right) + P_2 \exp\left(-\frac{|y - y_{1-g}|/\bar{A}}{b_2}\right) \right] \quad (5.1)$$

Under this criterion, a set of typical mission profiles* is first established, together with the fraction of flights represented by each. If there is uncertainty as to the usage of the airplane, as there usually is, it may be desirable to establish two different profile “mixes,” in order to be reasonably sure of

*The terms “mission profile” and “flight profile” are used synonymously; the latter has sometimes been preferred in commercial airplane work to avoid the connotation of a military application.

CONTINUOUS TURBULENCE GUST LOADS CRITERIA 71

bracketing the actual operation. Considerations involved in establishing the flight profiles are discussed in more detail in Sec. 5.5.

These profiles are then divided into segments for analysis. Enough segments must be used so that speed, altitude, and weight can be assumed constant over each segment without introducing undue error. For a typical subsonic transport, it has been considered sufficient to define four segments each for climb and descent (in addition to any segments that may be needed for flaps-extended flight, usually omitted in wing loads determination because of the negligible contribution to total exceedances) and from one to four segments for cruise, depending on the flight duration.

Values of the P 's and b 's in Eq. (5.1) reflect a standard set of gust statistics, ordinarily those defined by Figs. 4.14 and 4.15. Values of N_0 and A are obtained by appropriate dynamic analysis for as many load quantities y (shears, bending moments, torsions, etc.) as may be desired. The dynamic analysis must utilize a gust psd shape consistent with the b 's; the von Kármán shape with $L = 2500$ ft is now almost universally accepted for this purpose. In military applications, modifications to L , b_1 , and b_2 are usual at altitudes below 2500 ft.

The actual computation, for each load quantity y , involves selecting a series of values of y , computing $N(y)$ for each segment, and adding. Subtotals for each profile can also be obtained. Typical exceedance curves obtained by this procedure are shown in Figs. 5.1 and 5.2. Values of the various load quantities at the design frequency of exceedance are then read from the curves, or obtained by equivalent computations. The limit design frequency of exceedance recommended in FAA-ADS-53¹³ is 2×10^{-5} c/h. This is a generally accepted value. Its basis is discussed in Sec. 5.4.

Hours vs miles. At the time FAA-ADS-53¹³ was written, frequencies of exceedance were often expressed on a *per-mile* instead of a *per-hour* basis. This practice was the natural result of thinking in terms of isolated gusts instead of continuous turbulence. Reasons for the selection of a per-hour criterion are discussed in FAA-ADS-53, Sec. 4.1. In brief, they relate to the likelihood that flight crews for sure, and probably passengers as well, will tend to fly the same number of *hours* (say per year), as airplanes become faster, rather than the same number of *miles*.

Limit vs ultimate. The decision to define design loads on a limit instead of an ultimate basis is also discussed in FAA-ADS-53¹³ (Sec. 15.1.1). In the end, it was based on various practical considerations. Despite this decision, it must be emphasized that airplanes do encounter gust loads approaching ultimate, and that if the strength associated with the 1.5 factor of safety were not there, the airplanes would not survive. Consequently, there should be at least qualitative assurance that for a new airplane, as for existing designs, the structural deformation and damage as the ultimate load level is approached are not so great as to prevent the safe return of the airplane. Similarly, under conditions of turbulence for which loads approach the ultimate level, functioning of all vital systems, (including the pilot!) should remain such as not to jeopardize the safe return of the airplane.

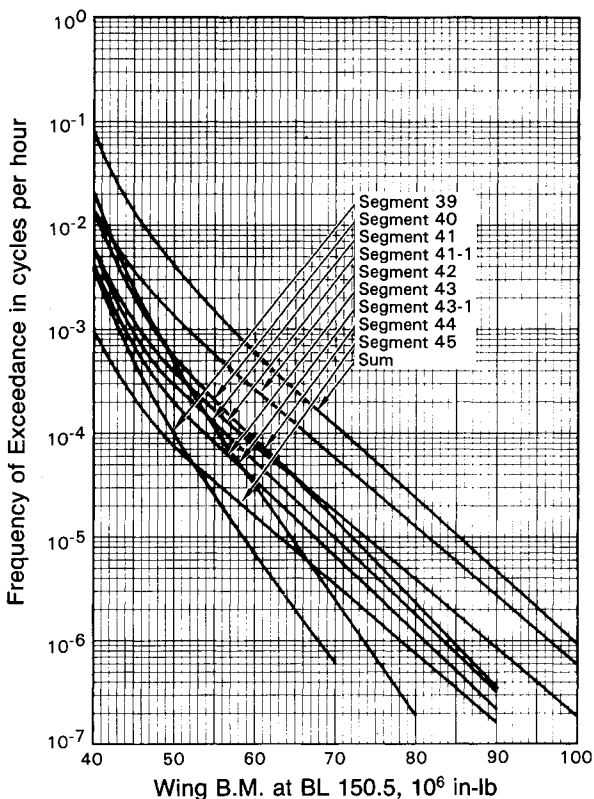


Fig. 5.1 Typical frequency of exceedance curves. Single profile of early L-1011 version; profile 5, low wing weight mix.

If an explicitly stated ultimate frequency of exceedance should be needed, a value of about 1×10^{-8} c/h is reasonable (at least for wing loads in up-bending). This value is obtained by extrapolating calculated exceedance curves for typical airplanes and load quantities, to a load of 1.5 times limit. Ultimate frequencies of exceedance are discussed further in Appendix H.

5.3.2 Design Envelope Criterion

Under the design envelope criterion, all considerations of actual operational usage are ignored. Instead, design is to the specified design envelope of speed, altitude, gross weight, fuel weight, zero-fuel weight, and c.g. position. In this respect, the criterion is similar to the past discrete-gust criteria, as well as to the existing limit design maneuver loads criteria.

Under this form of criterion, a shape of gust psd is again selected; as in the

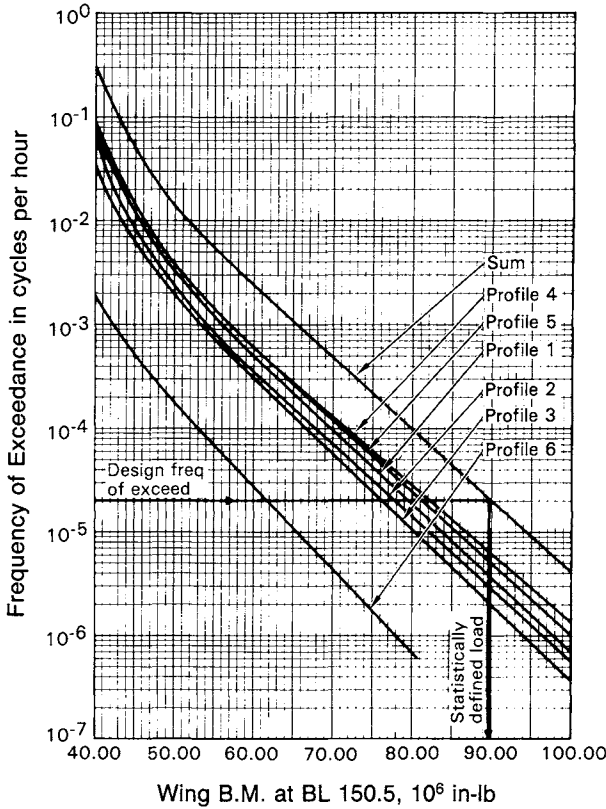


Fig. 5.2 Typical frequency of exceedance curves. Sum of profiles of early L-1011 version; low wing weight mix.

mission analysis criterion, this is ordinarily taken as the von Kármán shape with $L = 2500$ ft. \bar{A} is then obtained by dynamic analysis for as many load quantities y as are of interest. The limit design values of y is then given by

$$y_{\text{design}} = \sigma_y \eta_d = \left(\frac{\sigma_y}{\sigma_w} \sigma_w \right) \eta_d = (\bar{A} \sigma_w) \eta_d = \bar{A} (\sigma_w \eta_d) \quad (5.2)$$

Design rms value of y

Design ratio of peak to rms values

From dynamic analysis

Design gust velocity U_σ

$$y_{\text{design}} = \bar{A} \cdot U_\sigma$$

(5.3)

Downloaded by RMIT UNIV BUNDOORA on June 4, 2013 | http://arc.aiaa.org | DOI: 10.2514/4.861888

(The quantity y_{design} given by Eq. (5.2) or Eq. (5.3) is, of course, only the incremental load due to the turbulence. To this must be added the load associated with 1-g level flight.)

It is seen that the quantity U_σ is the product of a design rms gust velocity σ_w and a design ratio of peak to rms values, η_d . U_σ has the units of gust velocity and can be thought of as a *continuous turbulence design gust velocity*. The breakdown between the two factors, σ_w and η_d , is ordinarily not of consequence, except as an aid in visualizing the significance of the criterion; only the product is specified.

The quantity $\sigma_w \eta_d$, or U_σ , can also be thought of as a design value of y/\bar{A} . Dividing both sides of Eq. (5.3) by \bar{A} , we obtain

$$\left(\frac{y}{\bar{A}}\right)_{\text{design}} = U_\sigma \tag{5.4}$$

Design values of the continuous turbulence gust velocity U_σ , like design values of the discrete-gust velocity U_{de} , are specified as a function of altitude. (Note that U_σ is a *true* gust velocity, whereas U_{de} is an *equivalent* gust velocity.)

The variation of U_σ with altitude can be established rationally on the basis of constant frequency of exceedance of y/\bar{A} .

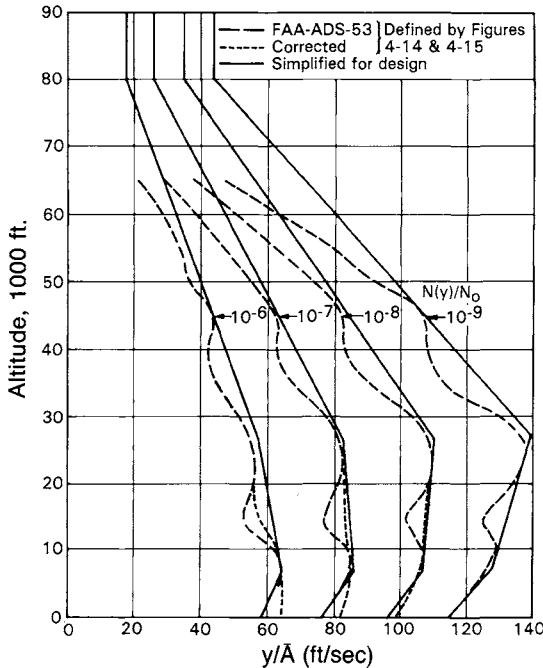


Fig. 5.3 Basic variation y/\bar{A} or U with altitude.

CONTINUOUS TURBULENCE GUST LOADS CRITERIA 75

The dash lines in Fig 5.3, taken from Fig. 5-6 of FAA-ADS-53,¹³ indicate the variation of y/\bar{A} with altitude for several constant values of $N(y)/N_0$. These are, in effect, cross plots of Fig. 4.16 (Sec. 4.7.5), although, actually, in plotting Fig. 5.3, points were taken at 5000-ft altitude intervals instead of the 10,000-ft intervals of Fig. 4.16.

In Fig. 5.3, the long dash lines are as shown in FAA-ADS-53.¹³ The dotted lines are the result of correcting an error in the plotted points at 15,000 ft and reairing the data (more carefully) at 500 and 5000 ft. The dash lines are then simplified for design use as indicated by the solid lines. To facilitate interpolating, these solid lines are repeated in Fig. 5.4 with intermediate curves added.

Once an appropriate design value of U_σ is selected at any given altitude, the curve in Fig. 5.4 that passes through that point provides the rational variation with altitude. Design values of U_σ and their basis are discussed in Sec. 5.4.

The design envelope criterion as discussed here, and as ordinarily used, does not account for the effect of variations in N_0 on load. How this effect might be accounted for is discussed in Sec. 5.6.

5.3.3 Choice Between Mission Analysis and Design Envelope Forms of Criterion

Prior to the introduction of power-spectral methods, structural design criteria were almost universally of the design envelope type. However, whenever there has been any real question of the adequacy of a given airplane to withstand the gust loads to which it may be exposed, or of the adequacy of existing criteria for application to new vehicles operating on vastly different flight profiles, a mission analysis type of evaluation has been performed. Only the mission analysis approach will provide loads that are adequate for a new airplane that operates most of the time close to its design envelope, without penalizing the many airplanes that generally operate rather far within their design envelopes. For these reasons, at the Lockheed-California Company the mission analysis format for a gust loads criterion has been considered a necessity. Furthermore, only the mission analysis criterion provides a convenient means of evaluating the effects of changes in operating practices during the life of a fleet.

On the other hand, the design envelope criterion offers advantages that many manufacturers consider compelling. In the mission analysis approach, flight profiles must be established to reflect expected typical operation. Judgment obviously is required in defining these profiles, and the loads obtained will vary to greater or lesser extent depending on the multitude of decisions that are made. As a result, one can never be sure that the loads obtained are exactly the "right" loads; and in the administration of the criterion, differences of opinion may arise and be difficult to reconcile. All of this uncertainty is avoided in the use of the design envelope criterion.

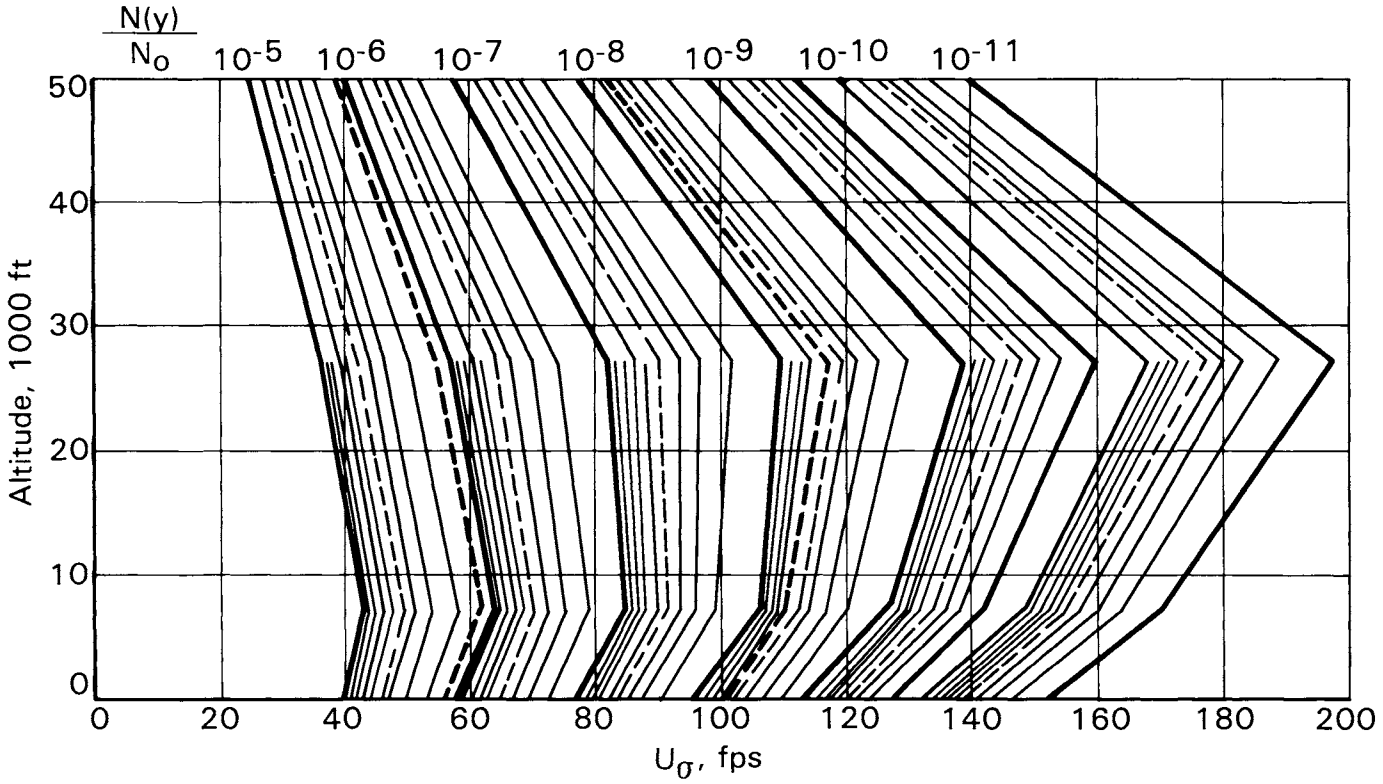


Fig. 5.4 Variation of U_g with altitude, family of constant $N(y)/N_0$ curves.

Furthermore, under a design envelope criterion, gust loads can be defined in the early stages of design for a very limited number of flight conditions considered most likely to be critical; additional flight conditions can then be added in due course as the design progresses. Under a mission analysis criterion, on the other hand, the analysis must include all flight conditions, plus the generation of exceedance data, before a single load is available.

It should be remarked that one *apparent* advantage of the design envelope criterion is entirely illusory. It is sometimes felt that the use of a design envelope criterion assures that the airplane can be safely operated at any point within or on the design envelope — that the criterion assures a conservative design. *This is not true!* As discussed in Sec. 5.4, design gust velocities are based on experience; the design gust velocities that are selected are adequate *only* when the new airplane, like its predecessors, operates normally *well within* its design envelope.

5.3.4 Combined Criterion

In an attempt to retain as far as possible the advantages of both the mission analysis and design envelope forms of criterion, while minimizing their respective disadvantages, a criterion combining both forms was developed in FAA-ADS-53.¹³ This combined form of criterion is utilized in the Aerospace Industries Association (AIA) recommendation to the FAA (Aerospace Technical Council Technical Report No. 104, August 1970)²⁶ and in Appendix G to FAR 25; it is also utilized in MIL-A-008861A (USAF),¹⁴ although without option 1 as given next .

This criterion provides for a choice between the following, in any given application:

- 1) A design envelope analysis alone, with gust velocities set sufficiently high to make a mission analysis unnecessary.
- 2) A mission analysis in combination with a design envelope analysis at reduced gust velocities; the highest loads from either analysis are to be used for design. The design envelope analysis provides a “floor” below which the loads must not drop; it thus provides insurance against a rapid increase in loads as the design envelope is approached or an unconservative definition of the design missions.

5.4 DESIGN LEVELS

Theme: Design levels are based on the strength of past satisfactory airplanes.

This section discusses the establishment of a *design frequency of exceedance* (mission analysis criterion) and *design gust velocities* (design envelope criterion).

It should be emphasized that gusts are statistical in nature and that it is not possible, therefore, simply to define a “worst possible” gust and design for this gust.

One obvious approach, especially if one thinks in terms of a mission analysis criterion, is to establish design levels on an absolute basis, starting with agreement as to an acceptable loss rate. It has been found, however, that this approach simply is not practical, for a variety of reasons. The first is the difficulty of securing agreement on a loss rate, or even that *any* loss rate is acceptable. A second reason is the difficulty of predicting, with sufficient accuracy for this purpose, the real loads to be experienced and the real strength available to withstand these loads.

A much sounder approach, and one that is generally accepted, is to base design levels on the strength of existing satisfactory airplanes. This concept will be recognized as identical to that underlying the comparative tuned discrete-gust analysis developed earlier and described in Sec. 3.5.3. Indeed, the first applications of power-spectral methods to design loads substantiation was on a similar comparative basis (see FAA-ADS-53, pp. 2-4).¹³

Thus, the limited design frequency of exceedance is set at a value such that if loads are determined for the existing airplanes in accordance with the proposed criterion, these loads will correspond to the limit strength (2/3 of ultimate strength) of these airplanes.

Similarly, limit design gust velocities U_o are set at values such that loads given by the design criterion will also correspond to the limit strength of these existing airplanes.

With the design levels set in this way, the strength is certain to be adequate, inasmuch as criteria of any greater severity would indicate the existing airplanes to be unsatisfactory, a result contradicted by their satisfactory service records. Criteria of less severity might be adequate, but calculations of frequencies of exceedance of ultimate strength for these and other airplanes (e.g., FAA-ADS-53, p. 213) result in values of roughly 10^{-8} , or once in 2000 50,000-h lifetimes. This is frequent enough to discourage any thoughts that less strength might be acceptable.

5.4.1 Mission Analysis: Design Frequency of Exceedance

Limit strength frequencies of exceedance were determined in FAA-ADS-53¹³ for three airplanes: the Lockheed Model 749 Constellation, Lockheed Model 188 Electra, and the Boeing Model 720B, a variant of the Model 707. The values for all three airplanes fell in the narrow range from 1.1×10^{-5} to 2.1×10^{-5} c/h. Inasmuch as the service experience for all three airplanes was satisfactory, the least severe value is the rational choice. A value

$$N(y) = 2 \times 10^{-5} \text{ c/h}$$

was selected for design.

5.4.2 Design Envelope Criterion: Design Gust Velocity at V_C

Limit strength values of U_σ for the same three airplanes at design cruise speed V_C covered a much wider range

Model 188	$U_\sigma = 62$ fps
Model 749	$U_\sigma = 88$ fps
Model 720B	$U_\sigma = 108$ fps

These values are each read from Fig. 5.4 at an altitude of 7000 ft, after moving along a constant $N(y)/N_0$ line from the critical altitude at which originally plotted. All are based on wing strength.

More recent information on two newer airplanes, the L-1011 and the DC-10, indicates limit strength U_σ values in the range 76–80 fps. These, too, are based on wing strength. [The DC-10 and L-1011 values are only approximately comparable to the 188, 749, and 720B values, in that critical altitudes were determined on the basis of the slightly different ATC TR 104²⁶ variation of U_σ with altitude (Fig. 5.5) instead of the FAA-ADS-53¹³ variation (Fig. 5.4).]

For the design envelope floor for use in conjunction with the mission analysis criterion: A value $U_\sigma = 62$ fps at 7000 ft was proposed in FAA-ADS-53. The variation with altitude is indicated by the first heavy dotted line in Fig. 5.4, corresponding to $N(y)/N_0 = 1.2 \times 10^{-6}$. This curve is repeated in Fig. 5.5 as the left-most solid line. Two more recent proposals agree fairly closely, as indicated by the two other curves in Fig. 5.5 also labeled “Design envelope floor for use *with* mission analysis.”

For the design envelope criterion to be used alone: A wide range of curves has been proposed. These are shown in Fig. 5.5, labeled “for use *without* mission analysis.”

The FAA-ADS-53¹³ curve is based on application of the mission analysis criterion under the assumption that 100% of the flight time is at each design envelope point in turn. The resulting curve depends somewhat on N_0 . From the three vertical scales accompanying the generalized exceedance curves in Fig. 4.16, reading across from the design frequency of exceedance of 2×10^{-5} c/h on the right-hand scales, we can see that the appropriate $N(y)/N_0$ is about 4×10^{-9} . This corresponds to U_σ of about 114 fps at 7000 ft. The value selected was 6×10^{-9} , giving a U_σ of 110 fps at 7000 ft. This value of $N(y)/N_0$ identifies the particular curve in Fig. 5.4 that defines the variation of U_σ with altitude, which is then repeated in Fig. 5.5.

The assumption of 100% of flight time in a critical flight condition appears excessively conservative, even though the computed 720B capability of 108 fps is almost this high. (The reason for the high U_σ capability of the 720B relative to its mission analysis capability is not known; one has to suspect some inconsistency in the analysis, perhaps use of excessively severe mission profiles.)

The AIA proposal²⁶ (still referring to Fig. 5.5) appears to be fairly realistic

for current midrange to long-range transports, such as the L-1011, the DC-9 and DC-10, and the Boeing 727, 737, 747, 757, and 767. The U_o values indicated by this curve are permissible under FAR Appendix G for this type of transport. For short-range or commuter operations, however, with cruise altitudes typically at around 20,000 ft vs 30,000–35,000 ft for the mid- to long-range airplanes, higher U_o 's are clearly appropriate.* The higher U_o values identified by the curve labeled "FAR 25 Appendix G" are intended to provide for such more severe types of operation. They are required to be used unless "the design is comparable to a similar design with extensive satisfactory service experience," in which case, lower values will be acceptable, down to the values indicated by the AIA curve. More specifically, FAR 25 Appendix G requires the following factors to "be taken into account when assessing comparability to a similar design: (1) The transfer function of the new design should exhibit no unusual characteristics as compared to the similar design which will significantly affect response to turbulence; e.g., coalescence of modal responses in the frequency regime which can result in a significant increase in loads. (2) The typical mission of the new airplane is substantially equivalent to that of the similar design. (3) The similar design should demonstrate the adequacy of the U_o selected."

In light of the foregoing discussion, one would expect the AIA values to be acceptable to the FAA for any airplane comparable to the present medium- to long-range transports. Of the three factors noted, (2) and (3) should be the crucial ones. In taking into account these two factors, it would appear logical to consider the current large transports, collectively, to constitute a "similar design," for which the adequacy of the AIA values has been demonstrated. Factor (1) should be of less importance, inasmuch as it refers to differences that, it can be argued, are adequately accounted

*From the generalized exceedance curves, Fig. 4.16, it is seen that y/\bar{A} (i.e., U_o) is about 10% higher at 20,000 ft than at 32,000 ft. In addition, \bar{A} 's will be higher, varying roughly linearly with both the equivalent airspeed and the square root of the density ratio

$$\Delta n \propto \frac{\rho \sigma_w V_T C_{L_\alpha} S}{W} \propto \frac{\rho}{\rho_0} \sigma_w V_T$$

$$\propto \sqrt{\frac{\rho}{\rho_0}} \sigma_w V_e$$

For the L-1011, cruising at 20,000 ft instead of 32,000 ft would result in a probable increase in equivalent airspeed in the ratio $330/293 = 1.13$ and an increase in $\sqrt{\rho/\rho_0}$ in the ratio 1.24. The potential for an increase in loads is significant. There will, however, be partially offsetting secondary effects, such as the decrease in C_{L_α} with decreasing Mach number ($1.05/1.25 = 0.84$, loads decrease in the ratio $0.84^{2/3} = 0.89$) and increased damping in the short period and elastic modes (in the ratio of the air density, 1.54, with the loads affected by some much smaller percentage).

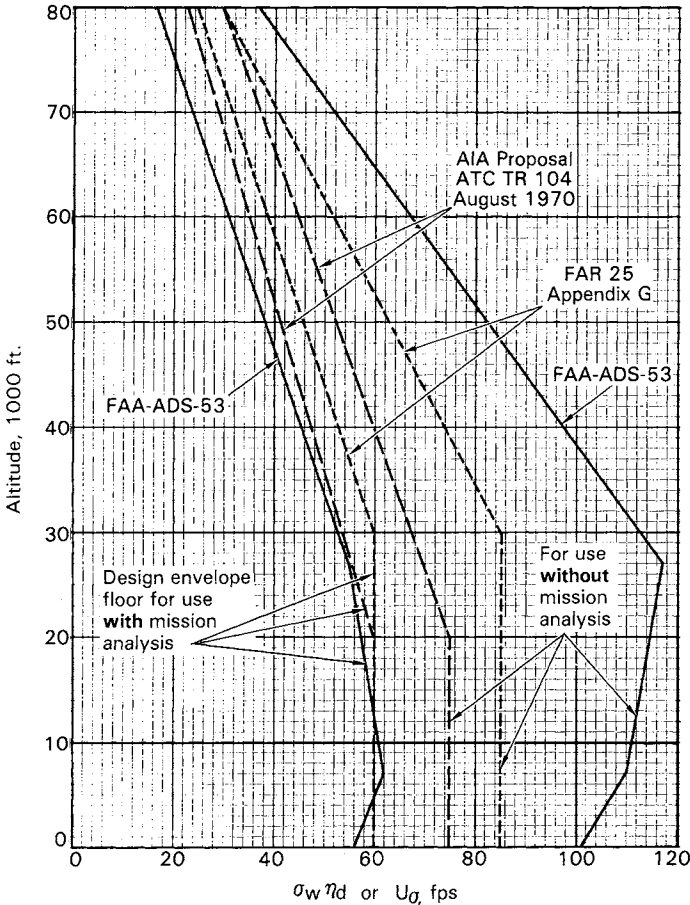


Fig. 5.5 Various proposals for variation of design U_σ with altitude.

for by the dynamic analysis; the gust velocities should not, logically, be a consideration.

5.4.3 Design Envelope Criterion: Design Gust Velocities at V_B and V_D

Reflecting the philosophy of the older discrete-gust criteria (Sec. 2.3), design U_σ values are normally taken as 1.32 times the V_C values at speed V_B and 0.50 times the V_C values at speed V_D . These factors are the same as the corresponding ratios of U_{de} values.

5.5 FLIGHT PROFILE GENERATION

This section contains some practical suggestions on generating flight profiles for use in applying the mission analysis criterion. Although it is intended primarily for application to commercial transport aircraft, portions will be found to be applicable to various military types as well. No rigid procedure can be spelled out for this task. It is to be expected that generating realistic profiles will require ingenuity, judgment, and the tapping of various resources outside the loads organization, perhaps even outside the manufacturer's company. Examples of flight profile generation, with discussion, are available in FAA-ADS-53¹³ and in FAA-ADS-54.²⁷ The L-1011 generation is summarized very briefly in Ref. 23.

5.5.1 *Typical vs Maximum Values*

It is to be emphasized that the profiles generated are to reflect typical operation. This implies use of average values of flight parameters such as speed, altitude, payload, flight duration, etc. Or, it may involve using a spectrum of values if the variation is over a wide range and significantly affects the loads. Care should be taken not to use "maximum" or "design" values. It may be desirable to introduce some small conservatism to account for real uncertainties as to utilization of a new airplane, but this should be kept to a minimum. (An example is the use of both a "high-weight" and a "low-weight" mix of profiles in the L-1011 mission analysis.)

Moreover, when utilization by one airline customer is moderately more severe than by another, the flight profiles should still reflect the composite of all operations, rather than the single most severe. This is not to deny, of course, that, when an exceedance of limit or ultimate load does occur, it is more likely to involve one of the more severely utilized airplanes.

A corollary is that design loads ordinarily should not be increased when airplanes are sold to a new operator whose utilization is moderately more severe than any contemplated in the original mission analysis. When such a situation occurs, it is prudent to determine quantitatively how much the loads would increase if determined on the basis of this operator's utilization alone. Ordinarily, however, the effect on frequency of exceedance of limit or ultimate load for the fleet as a whole (all operators) will be small enough so that no action will be needed.

The advantages of the mission analysis criterion are too great to jeopardize its acceptance by interpreting all of its results too literally!

5.5.2 *Flight Duration*

Usually, several profiles are generated to reflect a range of flight distances or durations, although there is some question about how much the loads change due to changes in flight duration, especially if the cruise altitude does not change. At the Lockheed-California Company, data on fractions of

CONTINUOUS TURBULENCE GUST LOADS CRITERIA 83

flights at various distances for a new airplane can be obtained from the marketing organization. Such data will be based on analysis of the route structures of actual or potential customer airlines.

5.5.3 Cruise Altitude

A best-average cruise altitude should be selected for each profile. Experts in the aerodynamics and flight test organizations should be consulted.

5.5.4 Speed

Cruise Mach number will be heavily influenced by economic factors and should be predictable within a fairly narrow range. For climb and descent speeds, guidance is available from NASA VGH data on actual operational usage of similar airplanes. A key parameter is the spread between actual and placard speeds; pilots never fly, on the average, within 10 or 15 knots of the placard speed, and the gap is often much wider. Within the U.S., airspeeds are limited by FAA regulation to 250 knots EAS at altitudes below 10,000 ft. Such a limitation is not common outside the U.S., however.

5.5.5 Weight Empty

This should, of course, include “operating items”—that is, it is an operating weight empty. An effort should be made, through consultation with the weight organization, to include typical customer options and provide for weight growth.

5.5.6 Payload

Projected passenger load factors are sometimes available from the marketing organization. For the L-1011-1, such projections showed an average passenger load factor of 0.65 on initiation of service, decreasing to 0.53 after eight years. A variation with flight distance was also projected, peaking at 0.65 for a 400-n.-mi. flight and decreasing to 0.44 for flights of more than about 1700 n.mi. Passenger load factors for “inclusive tour” operations apparently are much higher, perhaps 0.95. For the L-1011-1, this higher payload was partially offset by the absence of operation over the shorter flight distances involving lower cruise altitudes. There is some concern that, with deregulation of airline routes and fares, the passenger load factors may increase significantly. Current data are published from time to time in extensive tables in *Aviation Week*.

Cargo is much more difficult to estimate, inasmuch as cargo capacities are many times the cargo amounts usually carried. Passenger baggage, incidentally, should be treated independently of cargo and linked with the number of passengers aboard.

A good reasonableness check for total payload utilizes the parameter

$$\frac{\text{Operational payload}}{\text{Weight-limited payload}}$$

For various L-1011 models, projected values of this parameter have ranged from about 0.50 (L-1011-1) to 0.68 (L-1011-250). The Electra weights used in the FAA-ADS-53 mission analysis gave a value of 0.52. The Model 749 weights gave 0.53.

Data on total payload are also available from the NASA Digital VGH program.

5.5.7 Fuel

Trip fuel and its rate of usage are normally calculated by Aerodynamics for the specific profiles defined by Loads. Reserves, however, require judgment. Normal reserves may be somewhat greater than FAA minimums, which, in turn, are greater than the structural reserve fuel defined in FAR 25, Para. 25.343. In addition, a significant fraction of flights will involve landing with fuel onboard greater than normal reserves, in order to permit taking off on the next leg without refueling. This is referred to as “fuel-through” operation. “Fuel freighting,” when extra fuel is carried to take advantage of price differentials, has also been common. Lockheed-California practice has been to establish separate profiles for normal reserves and for fuel-through/fuel-freighting operation.

5.5.8 Check Flights

Pilot training and check flights are of wide variety and are difficult to consolidate into a single “typical” profile. Also, the number of such flights differs widely from airline to airline, or has in the past. Fortunately, such flights are becoming less frequent, because of increasingly sophisticated maintenance procedures and the growing use of flight simulators for training. The gust loads generally are not very much affected by these flights, partly because of their infrequency and partly because payload is not carried.

5.5.9 Sample Profile Plots: Segmentation

Plots of a representative flight profile (for the L-1011) are shown in Figs. 5.6 and 5.7. Typical segmentation, for the same profile, is shown in Table 5.1.

5.5.10 Flaps-Extended Segments

Because of the relatively low airspeeds with flaps extended, flaps-extended segments do not contribute significantly to wing-load exceedances at the limit load level. Consequently, flaps-extended segments are often not included and are not shown in Figs. 5.6, 5.7, and Table 5.1.

960 Nautical Mile Flight Profile
High Weight

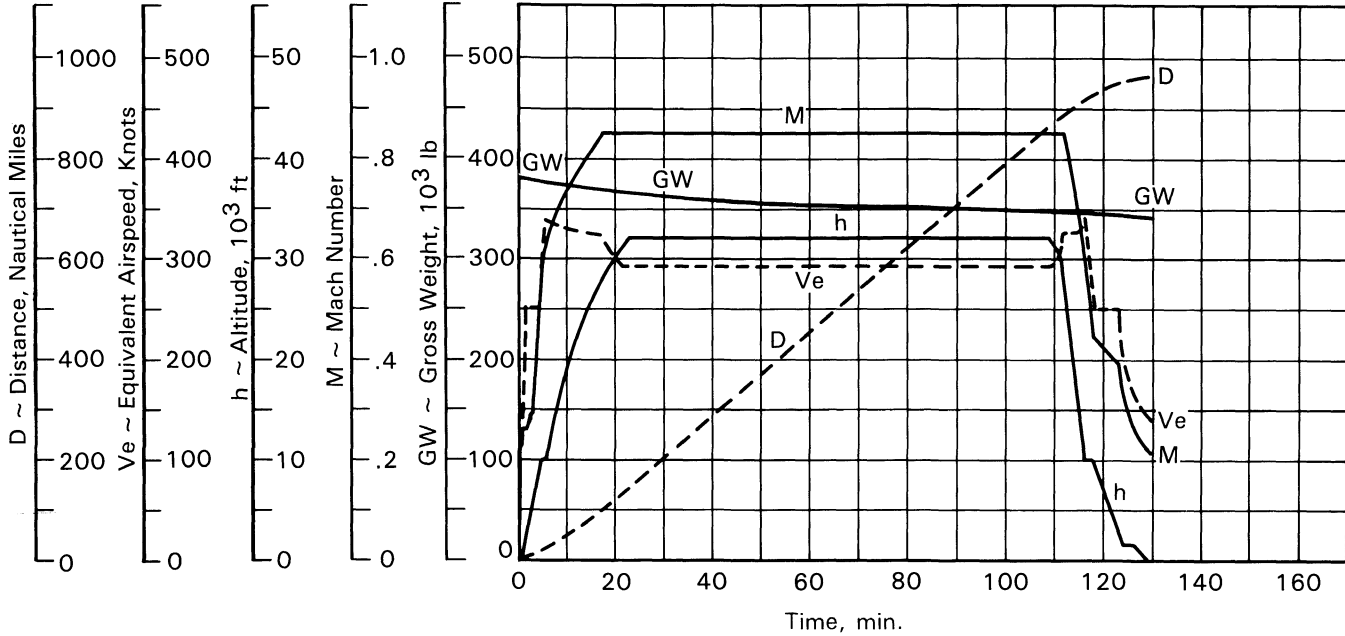


Fig. 5.6 Typical flight profile for the L-1011-1.

Table 5.1 Typical flight profile segmentation, L-1001-1: 960-n.mi.—profile high weight

Case number	Gross weight, lb	h /ft	Mach number	V_{KEAS}	Engine power setting	t_i minutes	t_i/t_T	t_i/t_T Low-wing weight composite	t_i/t_T High-wing weight composite
12A	380,000	2,000	0.353	225	Takeoff	2.5	0.01930	0.00249	0.00249
12	379,000	5,000	0.415	250	Maximum cruise	1.5	0.01158	0.00150	0.00150
13	377,000	12,000	0.635	335	Maximum cruise	3.5	0.02703	0.00349	0.00349
14	375,000	18,000	0.709	331	Maximum cruise	4.0	0.03089	0.00398	0.00398
15	372,000	26,000	0.822	324	Maximum cruise	10.5	0.08108	0.01046	0.01046
16	363,000	32,000	0.850	293	PLF	43.5	0.33591	0.04333	0.04333
17	350,000	32,000	0.850	293	PLF	43.5	0.33591	0.04333	0.04333
18	345,000	26,000	0.822	324	Flight idle	4.0	0.00398	0.00398	0.00398
19	344,000	18,000	0.709	331	Flight idle	2.0	0.01544	0.00199	0.00199
20	343,000	12,000	0.635	335	Flight idle	3.5	0.02703	0.00349	0.00349
21	343,000	5,000	0.415	250	Flight idle	5.3	0.04093	0.00528	0.00528
21B	342,640	1,500	0.303	195	AP	5.7	0.04401	0.00568	0.00568

Note: Zero fuel weight (ZFW) = 271,840 lb; cargo weight = 5000 lb; passenger load factor = 0.070. For $h = 0$ to 21,800 ft, cabin altitude = sea level; for $h > 21,800$ ft, cabin pressure differential = 8.44 psi, t_i = time in segment i ; t_i/t_T = fraction of time in segment i , for this mission or for total mission mix. Total time for this mission is 129.5 minutes.

CONTINUOUS TURBULENCE GUST LOADS CRITERIA 87

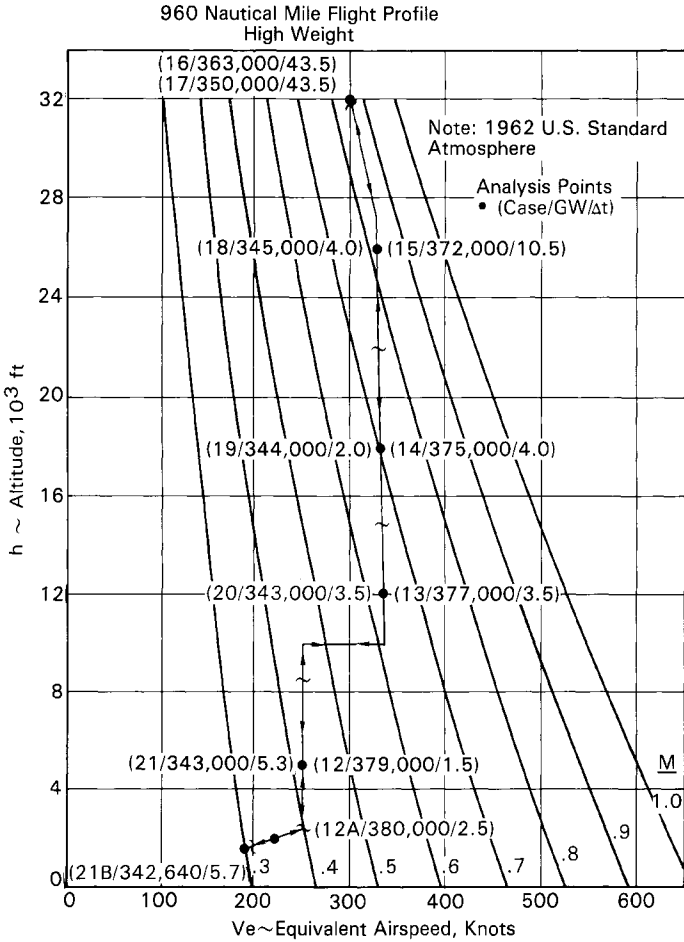


Fig. 5.7 Typical flight profile on speed-altitude coordinates for the L-1011-1.

The flaps-extended segments may, however, affect design loads on the horizontal tail, because of the large down-balancing tail load in 1-g flight. They also may contribute to wing fatigue, through the ground-air-ground cycle. With flaps extended, the 1-g flight wing loads are substantially increased as a result of the large down tail load; consequently, the “air” side of the ground-air-ground cycle is likely to be governed by flaps-down flight, even though the gust increment, a small fraction of the total, is smaller than at higher speeds. The flaps-extended segments also have a major influence, of course, on fatigue of the flap structure itself, although primarily through dynamic pressure in 1-g flight rather than as a result of gust loading.

Downloaded by RMIT UNIV BUNDOORA on June 4, 2013 | http://arc.aiaa.org | DOI: 10.2514/4.861888

Data on flap-operating practices are difficult to obtain. Some ingenuity will be required to identify helpful sources, and judicious estimates may be necessary.

5.5.11 Average Value of a Parameter vs Weighted Average vs Spectrum of Values

Two samples of operational airspeed data for the L-1011 are shown in Fig. 5.8. In a), there is no problem in using simply the average speed of 290 knots. In b), however, the range is great enough that use of a simple average would not be realistic. For example, consider the effect on a frequency of exceedance curve for gust loads if the given speed distribution were to be divided into a high-speed and low-speed part, with the average speed in each part used for analysis. The low-speed band would contribute negligibly to the exceedance curve. The high-speed portion would contribute only half as

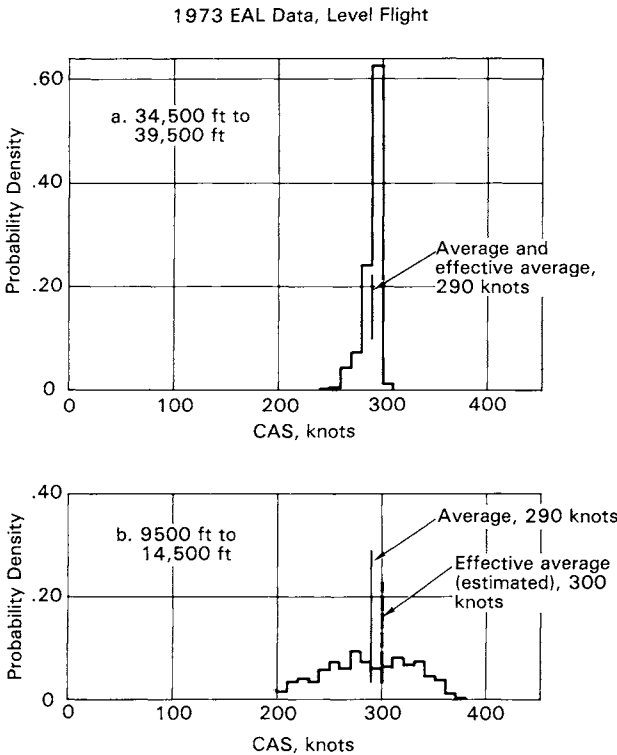


Fig. 5.8 Typical airspeed distributions for the L-1011-1.

CONTINUOUS TURBULENCE GUST LOADS CRITERIA 89

many cycles as the total distribution, but its average speed would be appreciably higher. The increase in load due to the higher speed would have a considerably greater effect on the exceedance curve than the reduction in cycles. In order to approximate this effect, an effective speed can be estimated, somewhat greater than the average speed.

To assist in making such estimates, the actual effective value has been determined theoretically for four special cases. The results are shown in Fig. 5.9 as a function of the range of variation of the parameter and the shape of the exceedance curve. These results are predicated on a direct proportionality of the load to the value of the parameter. The airspeed, to a fair approximation, is such a parameter; a pair of L-1011-3(ACS) runs, for example, indicated wing bending moment to vary as $V^{0.6}$ to $V^{0.9}$ as speed was reduced from $M = 0.85$ to $M = 0.78$ at $h = 32,000$ ft. The extrapolation of the curves in Fig. 5.9 to $a/b = 0.5$ at $b/L = 0$ is believed to be valid. The indicated exceedance curve shape (sketch, Fig. 5.9), with $\log E_0/E_r = 4$ to 4.5, is believed to be a very good approximation at the limit load level; at the ultimate load level, the value would be 7.5 to 8.

In the event that such estimation methods are not considered adequate, a spectrum of values of the parameter can be used, with the number of flight segments increased accordingly. It is unlikely, however, that such refinement will ever be necessary for a simple variable such as airspeed, payload, etc. It might be necessary if loads vary drastically, uncertainly, or nonlinearly with variations in the parameter.

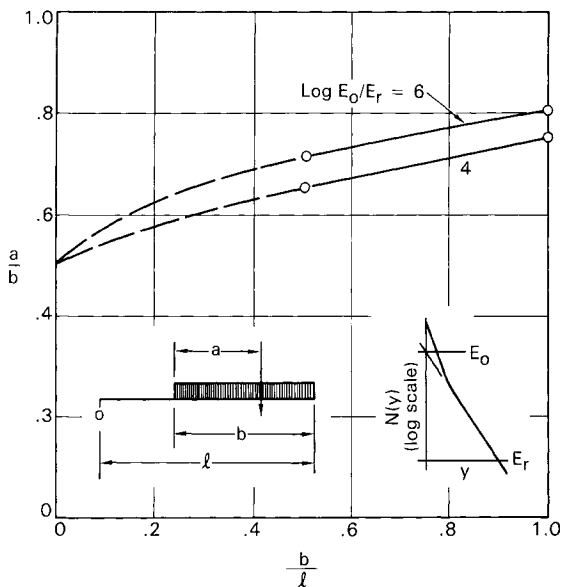


Fig. 5.9 Effective average value of a parameter.

5.6 MODIFICATION OF DESIGN ENVELOPE CRITERION TO ACCOUNT FOR N_0

It is clear from Eq. (5.1) and Figs. 4.16 and 4.17 that, under a mission analysis criterion, an increase in N_0 results in an increase in design load. The exceedance curve moves up; and, therefore, at a given (design) frequency of exceedance the load increases.

Rationally and realistically, design envelope loads should also vary with N_0 . This can be seen qualitatively by reference to Fig. 5.10. Increasing N_0 compresses a given sample of record into a shorter time, making room for the possible occurrence of a higher peak elsewhere in the given time span.

Quantitatively, the effect of N_0 can be accounted for by modifying Eq. (5.3), Sec. 5.3.2,

$$y_{\text{design}} = \bar{A} \cdot U_{\sigma}$$

to give

$$y_{\text{design}} = \bar{A} U_{\sigma} \left(1 + \frac{2.306 b_2}{U_{\sigma}} \log_{10} \frac{N_0}{N_{0_{\text{ref}}}} \right) \quad (5.5)$$

In this equation, $N_{0_{\text{ref}}}$ is the N_0 value at which the design U_{σ} 's apply. The relatively simple form of Eq. (5.5) results from the assumption that the nonstorm term in the exceedance equation [Equation (4.27), Sec. 4.7.5] has a negligible effect at the limit load level.*

*The full derivation follows. From Eq. (4.27), dropping the nonstorm term, we obtain

$$N(y) = N_0 P_2 e^{-\frac{y/\bar{A}}{b_2}} \quad (4.27a)$$

Taking logarithms of both sides yields

$$\log_e N(y) = \log_e N_0 + \log_e P_2 - \frac{y/\bar{A}}{b_2} \quad (4.27b)$$

If we consider $N(y)$ now to be the design value, it and P_2 will remain constant as N_0 varies, so that

$$\frac{y_d/\bar{A}}{b_2} = \log_e N_0 + \underbrace{\log_e P_2 - \log_e N(y)}_{\text{Constant, } C} \quad (4.27c)$$

And if we consider U_{σ} to be the design value of y_d/\bar{A} , established with N_0 implicitly assumed to have a particular reference value $N_{0_{\text{ref}}}$, Eq. (4.27c) becomes

$$\frac{U_{\sigma}}{b_2} = \log_e N_{0_{\text{ref}}} + C \quad (4.27d)$$

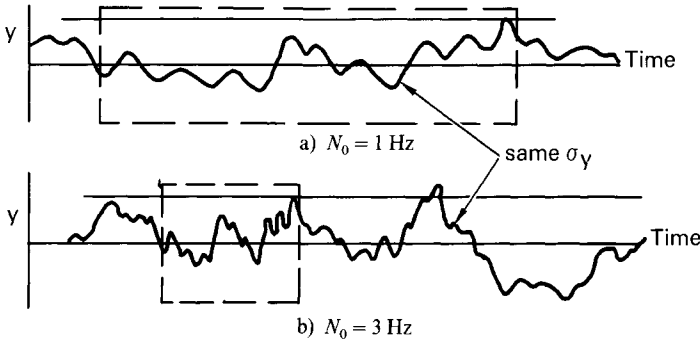


Fig. 5.10 Effect of N_0 on probable load.

The correction factor in brackets in Eq. (5.5) is plotted vs N_0/N_{0ref} in Fig. 5.11 for three values of b_2/U_σ . It is interesting to see that N_0 has a somewhat greater effect on design envelope loads than on mission analysis loads. This comparison may be somewhat misleading, however, in that design envelope V_B loads are sometimes critical, with $U_\sigma = 1.32 \times 75 = 99$ fps, and mission analysis loads may actually be governed as much by climb segments as cruise segments, with their higher \bar{A} 's and therefore lower U_σ 's.

For various reasons, some of which are noted in Sec. 15.2.3 of FAA-ADS-53,¹³ it is general practice not to include adjustments for N_0 in design envelope criteria.

Solving Eq. (4.27d) for C and substituting into Eq. (4.27c) gives

$$\frac{y_d/\bar{A}}{b_2} = \log_e N_0 + \frac{U_\sigma}{b_2} - \log_e N_{0ref} \tag{4.27e}$$

whence

$$y_d = b_2 \bar{A} \left(\frac{U_\sigma}{b_2} + \log_e \frac{N_0}{N_{0ref}} \right) \tag{4.27f}$$

and multiplying and dividing by U_σ/b_2 , we get

$$\begin{aligned} y_d &= \bar{A} U_\sigma \left(1 + \frac{b_2}{U_\sigma} \log_e \frac{N_0}{N_{0ref}} \right) \\ &= \bar{A} U_\sigma \left(1 + \frac{2.306 b_2}{U_\sigma} \log_{10} \frac{N_0}{N_{0ref}} \right) \end{aligned} \tag{4.27g}$$

which agrees with Eq. (5.5) as stated earlier.

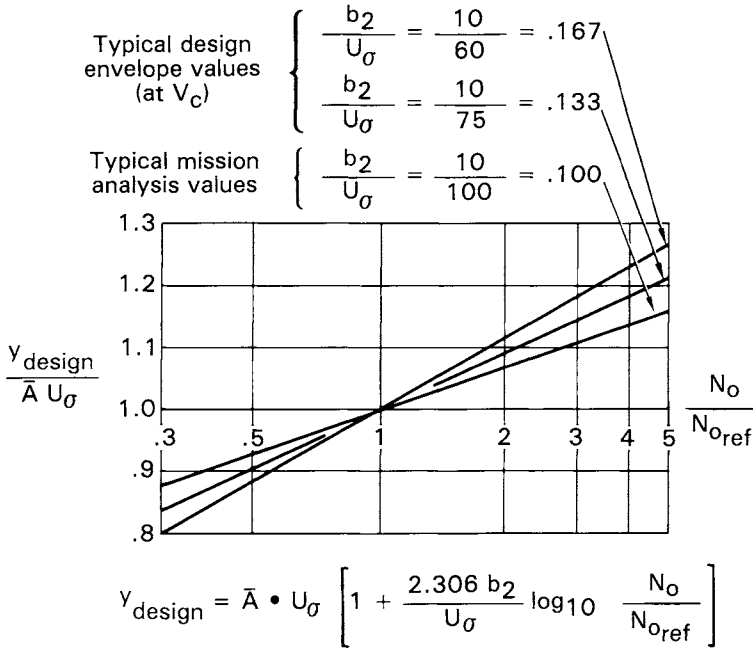


Fig. 5.11 Effect of N_0 on design load.

5.7 COMBINED VERTICAL AND LATERAL GUST LOADS

5.7.1 How to Combine

If the vertical and lateral components of turbulence are both stationary Gaussian random processes, the stresses (or loads) due to each can be determined separately and combined according to the theoretical relationship

$$f = \sqrt{f_v^2 + f_L^2} \tag{5.6}$$

5.7.2 When to Combine

The following examples indicate that the combined stress is always less than if the stresses are added directly:

f_v	f_L	f
1.00	1.00	1.41
1.00	0.70	1.22
1.00	0.50	1.12
1.00	0.30	1.04

CONTINUOUS TURBULENCE GUST LOADS CRITERIA 93

It is also seen that if a second stress is less than, say 30% of the first, it can well be ignored altogether.

Accordingly, for most airplane components, loads can be based on vertical gust or lateral gust alone. This, of course, has been the usual practice for many years. Exceptions are as follows:

1) *Engine loads.* Vertical and lateral gust engine loads tend to be of comparable criticality; and there are likely to be structural members both in the engines themselves and in the engine support structure that are significantly stressed by both vertical and lateral gust loadings. On the L-1011, design loads for all three engines reflect the combination of vertical and lateral gust inputs, in accordance with Eq. (5.6).

2) *Horizontal tail loads.* On the L-1011, for certain flight conditions, both theory and test indicate that the induced load on the horizontal tail due to lateral gust on the fin can be as great as the load due to vertical gust. The load quantity most affected is root shear. For the L-1011-3, mission analysis net loads increased in the following ratios:

	S_z		M_x	
	Positive	Negative	Positive	Negative
BL ^a 74	1.19	1.26	1.09	1.12
BL ^a 202	1.06	1.09	1.07	1.08
BL ^a 370	1.05	1.05	1.06	1.06

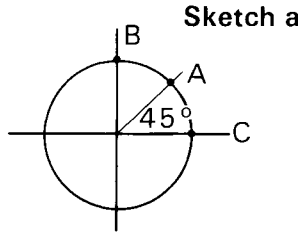
^aBL; Buttock or Butt line (i.e. in. laterally from airplane centerline).

On the basis that this effect should not be considered until the net load increases, by, say, 7%, an appropriate design practice would be to divide the above ratios by 1.07; resulting values, when greater than unity, should be applied to the vertical-gust-only loads as multiplying factors. The 7% value is an estimate of how much wing loads might sometimes increase if lateral gust affects were included; reasonable engineering practice has been to ignore this increase.

T-tail designs have generally been considered sensitive to combined vertical and lateral gusts.

The BCAA requires the consideration of “round-the-clock” discrete gusts—that is, the application of a discrete gust of design gust velocity in any direction in the $y-z$ plane. The results are the same as given by Eq. (5.6).

3) *Fuselage loads.* Fuselage loads are potentially critical for combined vertical and lateral gust. However, for the L-1011, it was found that design to vertical and lateral gusts individually resulted inherently in sufficient strength to withstand stresses given by Eq. (5.6). The plausibility of this result is indicated by a highly idealized example.



If the stresses at B due to vertical gust and at C due to lateral gust are equal, and if the allowable axial stress is the same at all points around the circumference of the fuselage cross section, then the applied stresses at B and C are equal, and the applied stress at A , as given by Eq. (5.6), is

$$\begin{aligned}
 f_A &= \sqrt{(0.707 f_B)^2 + (0.707 f_C)^2} \\
 &= \sqrt{(0.707 f_B)^2 + (0.707 f_B)^2} = f_B = f_C
 \end{aligned}$$

5.7.3 Mission Analysis Application

Equation (5.6) applies to any single flight condition. In a mission analysis, it may be that one segment predominates for vertical gust and a different segment for lateral gust. In this situation, Eq. (5.6) is conservative. This conservatism can be eliminated by running a mission analysis in which for each segment

$$\bar{A} = \sqrt{\bar{A}_V^2 + \bar{A}_L^2} \tag{5.7}$$

$$N_0 = \frac{\sqrt{N_{0V}^2 \bar{A}_V^2 + N_{0L}^2 \bar{A}_L^2}}{\sqrt{\bar{A}_V^2 + \bar{A}_L^2}} \tag{5.8}$$

\bar{A} and N_0 as thus computed must, of course, be for a particular load or stress quantity that “feels” both vertical and lateral gust excitation. A horizontal tail shear or bending moment would be such a quantity. So would an internal fuselage stress, such as A in sketch a.

5.7.4 Additional Conservatism

Equation (5.6) is valid for design use only if the turbulence is isotropic. But real turbulence is not necessarily truly isotropic. Even for a single flight condition, therefore, Eq. (5.6) may be slightly conservative relative to real turbulence.

Unpublished Lockheed analyses of data generated from Ref. 19 indicate that, based on 4-min averages at low altitudes, rms vertical and lateral gust velocities differ from each other half the time by more than about 12–15%.

5.8 STABILITY AUGMENTATION OR ACTIVE CONTROL SYSTEM (ACS)

When loads are decreased as a result of the presence of any kind of active control system (ACS) such as a load alleviation system, or stability augmentation system, it is appropriate to include such reductions in the design loads. The percent reduction in the design loads is less than indicated by linear theory, however, because of *unavailability* (as affected by reliability) and *saturation*.

5.8.1 Unavailability

An ACS failure can be either *active* or *passive*. An active failure is a failure such as a hardover or an oscillation that produces loads by itself. These loads are ordinarily treated independently of the gust loads. A passive failure simply results in the unavailability of the active control system to perform its function some fraction of the total flight time. An estimate of this fraction is necessary to determine the effect of unavailability on loads.

Mission analysis criterion. Under this criterion one simply includes in the flight profiles a certain fraction of time with active controls off. If the ratios between shear, bending, and torsion are substantially different ACS-off and ACS-on, an “allocation” approach comparable to that discussed next for design envelope loads should be used.

Design envelope criterion. Figure 5.4 is used to relate frequencies of exceedance, in terms of $N(y)/N_0$, to design U_σ values. Limit loads are determined separately, system-on and system-off. The respective U_σ values are defined by a pair of $N(y)/N_0$ values meeting the condition that

$$p \left[\frac{N(y)}{N_0} \right]_{\text{system-off}} + (1-p) \left[\frac{N(y)}{N_0} \right]_{\text{system-on}} = \left[\frac{N(y)}{N_0} \right]_{\text{basic criterion}} \quad (5.9)$$

where p is the fraction of time system-off.

Any pair of values of $N(y)/N_0$ that satisfy Eq. (5.9) may be used. The selection of these two values simply involves an arbitrary choice of how the total allowable exceedances will be allocated between system-on and system-off operation. The choice will ordinarily be such that system-on and system-off loads are about equally critical.

In applying this criterion, it will be found that U_σ system-on will have to be slightly higher than the basic value (no active control system, Sec. 5.4.2), in order to balance the much lower U_σ system-off.

This subject is discussed much more fully in AGARDograph No. 175²⁸ (pp. 8–9). It is also discussed, but less adequately, in Sec. 15.2.4 of FAA-ADS-53.¹³ Application of the same concept to maneuver loads is discussed in an AIAA paper by Ramsey and Lewolt.²⁹

5.8.2 Saturation

There are always practical limits to the control surface displacements and rates that can be achieved. Consequently, an active control system will be less effective at high load levels than when operating in the linear range.

To evaluate this reduction in effectiveness, time-history analyses are performed. In these analyses, control system nonlinearities, such as displacement and rate limits, are represented. A continuous-turbulence gust velocity time history is used as input, at various σ_w levels. The outputs are analyzed statistically.

This approach is discussed in more detail in Chapter 10, in AGARD-ograph No. 175²⁸ (pp. 5–7), and by Gould, describing the L-1011 work in Ref. 30.

6

LOAD COMBINATIONS AND DESIGN CONDITIONS

This section provides an elementary introduction to material that is covered, for the most part, in much greater depth in Secs. 10, 11, and 12 of FAA-ADS-53¹³ and in the paper by Stauffer and Hoblit.²⁴ These references offer somewhat different points of view as well as additional information. The present discussion also, in certain areas, goes well beyond the treatment provided by the other two sources—in particular, in Secs. 6.1.5, 6.2.2, and 6.2.4.

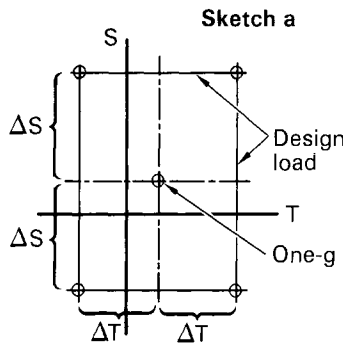
6.1 THE PHASING PROBLEM

With the information presented in Chapters 4 and 5, it is possible to establish limit design values of shear, bending moment, and torsion at a series of locations along the wing, or on any other major airplane component. A problem remains, however. The design values of these various quantities are values that generally occur at different times. Stresses in the structure cannot be determined until appropriate combinations of these loads are defined.

Let us consider as an example shear and torsion at a particular wing station.

6.1.1 Signs Undefined

First, a continuous turbulence gust load increment is inherently without sign. Positive and negative values are equally likely, and both must be considered in establishing design loads. Under a mission analysis criterion, separate exceedance curves are obtained for positive and negative values of the increment.



At this point, there is no indication whether maximum upshear, for example, combines with maximum leading-edge-up torsion or maximum leading-edge-down torsion, or some intermediate value. And the combination of signs does make a difference.

Sketch b

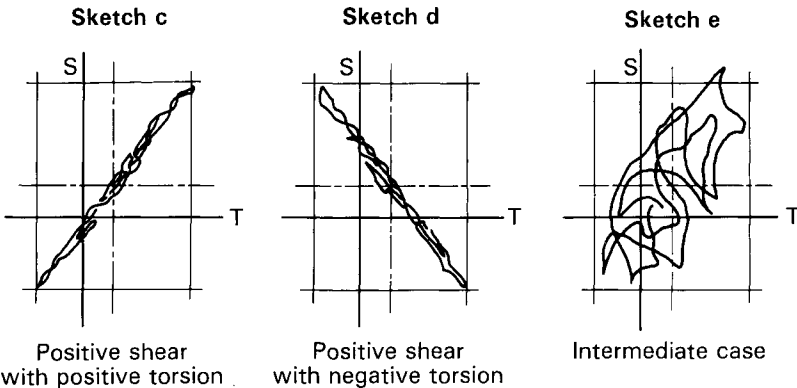


An obvious example is indicated by Sketch b. The outer arrows show shear flow on a wing box section due to transverse (vertical) shear and the inner arrows due to torsion.

For positive shear and torsion, as shown, the shear flows *add* in the *front* beam and *subtract* in the *rear* beam. If the sign of either shear or torsion is reversed, then the shear flows will add in the rear beam and subtract in the front beam.

6.1.2 How Sign Combinations Might Be Determined from Airplane Tests

If in actual flight through turbulence, shear and torsion were to be measured simultaneously and plotted vs each other, any of several results might be obtained as shown in Sketches c-e:

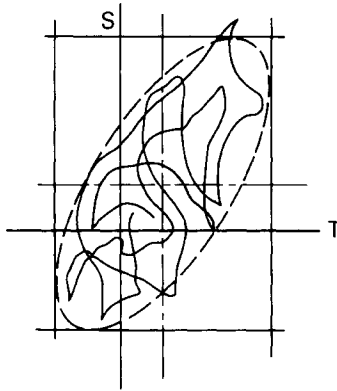


Downloaded by RMIT UNIV BUNDOORA on June 4, 2013 | http://arc.aiaa.org | DOI: 10.2514/4.861888

6.1.3 Design to Circumscribing Ellipse

The general appearance of Sketch e suggests, and theory will confirm, that it would be appropriate, in the general case illustrated in Sketch e, to design to an ellipse drawn to circumscribe the test data as shown in Sketch f. This ellipse then defines design combinations of shear and torsion. It is also spoken of as defining the design “phasing” of shear and torsion.

Sketch f

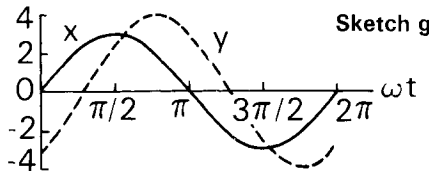


This use of the term phasing, it might be noted, is not in accordance with its usual exact definition. The terms phase and phasing are usually used to denote the angle by which a pure sinusoid leads or lags another sinusoid of the same frequency. The phase angle also, however, establishes pairs of simultaneously occurring values of the two variables. For example, if

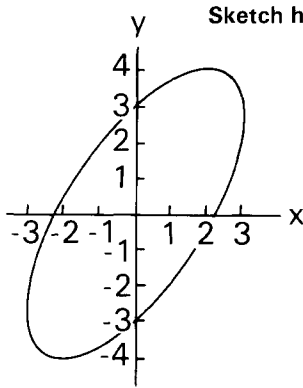
$$x = 3 \sin \omega t$$

and

$$y = 4 \sin(\omega t - 50^\circ)$$



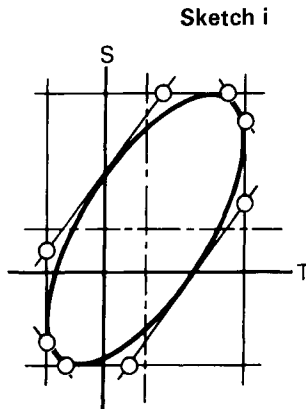
then simultaneously occurring combinations of x and y are given by the ellipse shown in Sketch h.



It is seen that, as a result of the 50-deg phase difference between the two variables, the maximum value of y occurs only in combination with a reduced value of x ; similarly, the maximum value of x occurs only with a reduced value of y .

If x and y are now random variables, such as wing shear and torsion in turbulence, the above definition of phase has no meaning, as the two variables are no longer pure sinusoids. There will still be a tendency, however, as illustrated in Sketch f, for the maximum, or design-level, or equal probability values of the two variables not to occur simultaneously. Appropriate combinations, as in the case of the pure sinusoids, are again defined by an ellipse. The term phasing, as used in this context, refers to this tendency. Thus, the term “unphased” loads would apply to the design levels of shear, bending moment, and torsion individually. “Phased” loads would be those values modified by the application of appropriate phasing factors to provide statistically appropriate combinations.

With these statistically appropriate combinations defined by an ellipse, actual design points can be conveniently defined, with only a small conservatism, at the corners of a circumscribing octagon, as shown in Sketch i.



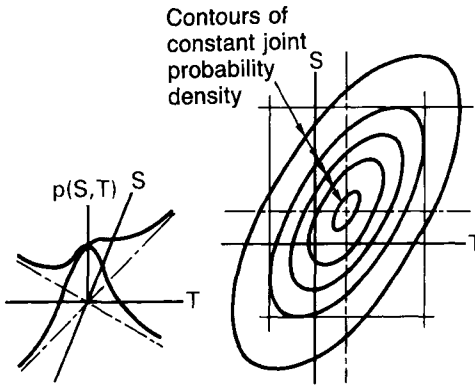
6.1.4 Analytical Determination of Equal Probability Ellipse

If a stationary Gaussian random input is applied to a linear system, then the *joint* probability density of any two outputs is Gaussian.

Contours of constant probability density for such a distribution are ellipses defined analytically by the correlation coefficient ρ (Sketch j). The correlation coefficient, like \bar{A} and N_0 , is calculated from the input psd and the frequency-response function:

$$\rho_{xy} = \frac{1}{\bar{A}_x \bar{A}_y} \int_0^\infty \Phi_w(\omega) \left[H_{x_{real}}(\omega)H_{y_{real}}(\omega) + H_{x_{imag}}(\omega)H_{y_{imag}}(\omega) \right] d\omega \quad (6.1)$$

Sketch j



Equation (6.1) follows from equations given in Appendix B of FAA-ADS-54 (Ref. 27).

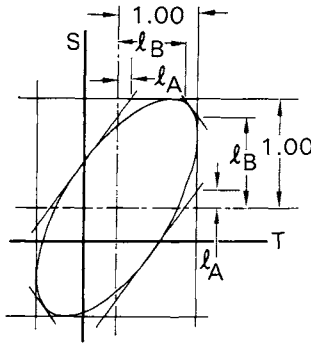
With ρ known, a constant probability ellipse can be defined, in terms of a circumscribing octagon, by means of the ratios

$$\left. \begin{aligned} \ell_A &= 1 - \sqrt{2(1 - \rho)} \\ \ell_B &= -1 + \sqrt{2(1 + \rho)} \end{aligned} \right\} \quad (6.2)$$

where ℓ_A and ℓ_B are defined by means of Sketch k.

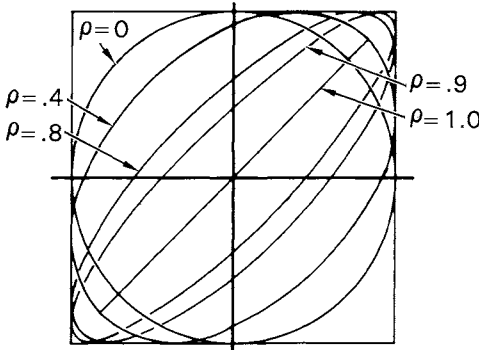
Values of ρ range from -1.00 to $+1.00$. Values close to $+1.00$ correspond to a slender ellipse oriented as in Sketch c. Values close to -1.00 indicate an orientation as in Sketch d. A value of zero indicates an ellipse with axes vertical and horizontal, a fat symmetrical ellipse. The actual equation of the ellipse is essentially Eq. (4.5) Sec. 4.3.4 with $p(x, y)$ a constant.

Sketch k



The general appearance of ellipses defined by various values of ρ is indicated by Sketch l.

Sketch l



It might be remarked that basing design load combinations on an ellipse that represents constant probability density can be justified at this point only intuitively. To be rigorous, design load combinations should be based not on constancy of the probability density but of the cumulative probability, for example,

$$\int_y^\infty p(y) dy$$

Probability density

Even formulating this problem is difficult; but some helpful insight that buttresses the intuitive conclusion is offered in Sec. 6.1.5 following.

6.1.5 Fictitious Structural Element Concept

Before it was recognized that design combinations of shear and torsion could be obtained easily and cleanly by means of the equal probability ellipse, a rather different approach was developed. This alternate approach provides further insight into the meaning of the equal-probability ellipse; it also has a potential for practical application where the equal probability ellipse does not provide a complete answer. (This section is not necessary to an understanding of the material that follows and may be omitted during the first reading of the book with no loss of continuity.)

As an alternative to defining design combinations of shears, bending moments, and torsions, it is possible to determine design-level values of internal loads and stresses directly. For example, by expressing front beam shear flow as

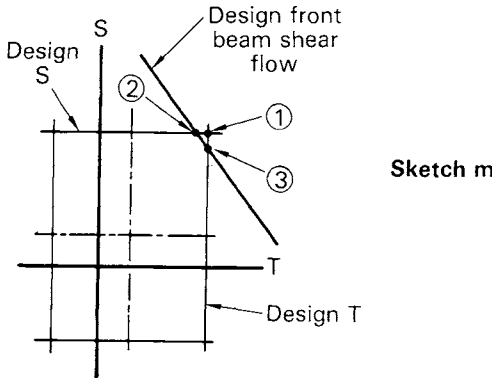
$$q = a_1S + a_2M + a_3T \tag{6.3}$$

its frequency-response function can be determined readily from the frequency-response functions of S , M , and T . Its psd can then be determined, and from its psd, \bar{A} , N_0 , and its design value.

Let us now assume for simplicity that shear flow is affected solely by shear and torsion.* Equation (6.3) then becomes

$$q = a_1S + a_3T \tag{6.4}$$

This equation is used first to obtain the design value of q , as just discussed in connection with Eq. (6.3). With the design value of q determined, Eq. (6.4) then defines a diagonal straight line on shear-torsion coordinates as shown in Sketch m.

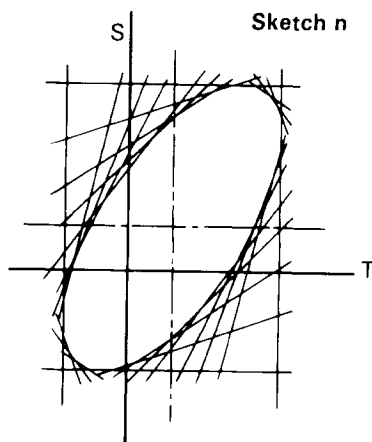


*Actually the contribution of bending moment is also significant, because of the tapered-beam effect. In the extreme case in which the upper and lower beam caps intersect at the wing tip and a concentrated load is applied at that point, the entire load is carried by truss action; the shear in the beam web then is zero.

This line represents the various combinations of shear and torsion that result in the design magnitude of front-beam shear flow. No point beyond this line can represent a valid combination of S and T , because the front-beam shear flow would exceed its design value. Points (2) and (3), therefore, might be taken as realistic design points; point (1) would obviously be conservative. Thus, determination of design load or stress in a particular structural element provides quantitative information about appropriate design combinations of the external shear and torsion.

There is no need, however, for Eq. (6.4) to relate to an *actual* front beam. The values of the coefficients a_1 and a_3 used in the analysis could just as well have been selected arbitrarily. Moreover, by systematically varying the values of a_1 and a_3 , a whole family of diagonal lines can be obtained (Sketch n), each representing design load or stress in some *fictitious* structural element. An appropriate family might be defined by

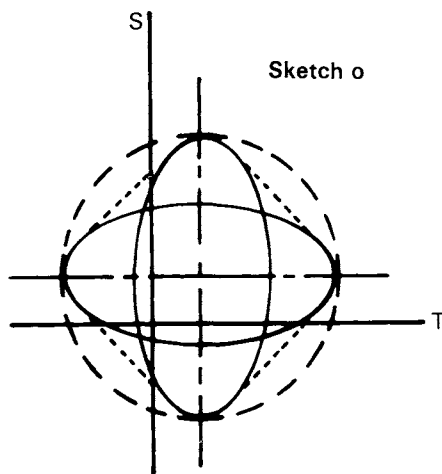
$$\frac{a_3}{a_1} = \pm 0.2 \frac{\bar{A}_S}{\bar{A}_T}, \quad \pm 0.5 \frac{\bar{A}_S}{\bar{A}_T}, \quad \pm 1.0 \frac{\bar{A}_S}{\bar{A}_T}, \quad \pm 2 \frac{\bar{A}_S}{\bar{A}_T}, \quad \pm 5 \frac{\bar{A}_S}{\bar{A}_T}$$



In Sketch n, the figure defined by this family of diagonals is seen to be at least approximately elliptical in shape. It is believed that the shape is *exactly* elliptical when the design load in each fictitious (or real) structural element is obtained as a constant times the rms value, as in the standard design envelope criterion (Eq. (5.3), Sec. 5.3.2). The family of diagonals might alternately be determined on the basis of a constant $N(y)$, but still for a single flight condition, for example, by using Eq. (5.5), Sec. 5.6. The figure

defined in this way probably is not exactly an ellipse. If the figure is determined on a mission analysis basis, it may be rather far from an ellipse.

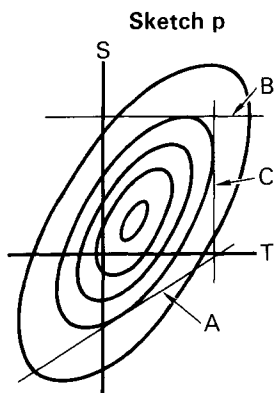
It is in the mission analysis application that the fictitious structural element approach may have its greatest potential for practical application. Suppose that mission segment *A* contributes predominantly to shear exceedances and segment *B* to torsion exceedances. Suppose also that for both segments, $\rho = 0$. Then, the equal probability ellipses for these two segments might be as indicated by the solid lines in Sketch o. The "equal probability ellipse," drawn in the usual way using the available value of ρ , would then be as indicated by the dash line. Fictitious structural elements carried through the entire mission analysis might well justify the less severe envelope indicated by the heavy dotted line.



Another potential application is to the time-history determination of loads (Sec. 5.7.2, Chapter 10). Here it may be either easier or more realistic, or both, to use one or more fictitious structural elements than to determine correlation coefficients. At the Lockheed-California Company, for example, it has been traditional to use the fictitious structural element concept in the determination of design taxi loads.

The expectation that the fictitious structural element approach defines figures that are exact ellipses (when the loads are defined as constant multiples of the rms values) is based on the following line of reasoning:

1) Consider the design-level equal probability density ellipse. With each point on this ellipse, associate a tangent, such as line *A* in Sketch p. One line of this family, labeled *B*, corresponds to the design value of shear, treated as a single-load variable. Another, labeled *C*, corresponds to the design value of torsion.



2) For all such lines, the volume beyond the line is the same. The volume referred to here is the volume under the probability density surface, where the probability density is considered to be plotted normal to the plane of the paper. This follows from the fact that as the figure is uniformly stretched or compressed in the x and y directions, respectively, until the ellipses become circles, the fraction of the total volume beyond any given line remains the same. Once the ellipses become circles, all of the beyond-the-line volumes are obviously the same.

3) Therefore, the cumulative probability associated with each such line is the same, and is the same as for S or T alone.

4) For every fictitious structural element, Sketch n, the volume beyond the line is also the same.

This follows from the fact that for any given element, the region on the S - T plot beyond the line is the region for which combinations of S and T give a stress in the element greater than design. The corresponding volume is, therefore, the probability that the design load is exceeded in the element. This is the design probability, the same for all elements. If $y_d = \sigma_y \eta_d$, a fixed value of η_d corresponds to a fixed probability given by Fig. 4.2, with $\eta_d = y/\sigma$.

5) Therefore, the fictitious structural element lines must coincide with the tangents to the equal probability density ellipse.

It is therefore concluded that:

1) The fictitious structural element lines do indeed define an ellipse.

2) The equal-probability-density contour does indeed define points of equal cumulative probability, in that each single point is associated with a tangent at that point, which, in turn, is associated with a fictitious structural element, for which the probability of exceeding design load is the same as for S or T alone.

6.2 LOADS FOR STRESS ANALYSIS

Normal stress analysis practice utilizes “design conditions.” Each design condition consists of a set of forces in equilibrium, defined over a major airplane component, such as the left wing or the fuselage forebody or the vertical tail, or even over the entire airplane. Under such a set of forces, the stresses in every minute element of the structure can be determined; and the same set of forces can be applied in a static test.

Power-spectral methods, on the other hand, do not result in this sort of design condition. They lead, instead, to individual design levels of load such as shear, bending moment, and torsion at various points in the structure. These are defined statistically and generally do not occur simultaneously. We have seen in Sec. 6.1 how design combinations of shear and torsion, for example, can be established. However, redundant-structure stress analysis methods are gradually replacing the older, simpler, and less accurate methods. These newer methods reflect the fact that the stresses at a given wing station, for example, depend not only on the shear, bending moment, and torsion at that station but also on where the individual loads are applied inboard and outboard of that station. As a result, it becomes necessary to know not only the loadings on a given wing transverse section, but also the loads acting simultaneously over the entire wing.

The following sections describe various ways of bridging the gap between statistically defined external loads and the needs of stress analysis.

6.2.1 Traditional Beam Stress Analysis

Given properly phased shear, bending moment, and torsion at a particular wing section, axial and shear stresses at any given point on the section can be calculated by traditional methods

$$f_t = \frac{My}{I} \quad f_s = \frac{1}{t} \left[\frac{SQ}{I} + \frac{T}{2A} \right]$$

Note that S must be the “beam” shear, obtained by subtracting from the total shear that part carried by truss action of the beam caps.

With this simple type of stress analysis, the problem almost goes away. One simply defines conditions at each corner of the octagon in Sketch 1. Shear and bending moment will be assumed to be “in phase.” This is often, but not always, a fairly good assumption.

This elementary beam analysis, however, often is not adequate, so other approaches are needed.

6.2.2 Deferring the Phasing Problem: Internal Loads or Stresses

The phasing problem can be deferred by obtaining psd’s, A ’s, and ρ ’s for internal loads or stresses:

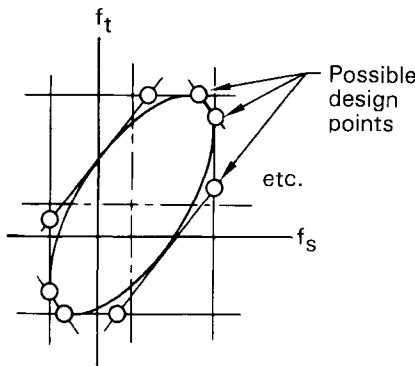
{ Axial loads in stringers
 { Shear flows in skin

or

{ Axial stress f_t
 { Shear stress f_s

It is still necessary to obtain phasing, but now the phasing to be determined is between f_t and f_s . For every panel, design combinations of f_t and f_s are defined at each corner of their octagon (Sketch q). The key advantage of this approach is that ordinarily only two internal load or stress quantities are involved; the phasings among the three external load quantities, S , M , and T , are automatically and correctly taken into account. Nevertheless, there are an astronomical number of psd's to be computed, two for every structural panel, and they have to be recomputed every time the structure changes.

Sketch q



This approach requires much closer coordination between the loads and stress operations than is usually the practice. It may even require combining these two operations. This approach does offer the potential, however, for automated preliminary design. The computer determines design combinations of f_t and f_s on all panels, determines the margin of safety for each, and resizes the structure accordingly in preparation for the next pass.

6.2.3 Matching Condition Technique

Background. Although the method described in the preceding section has considerable potential, it has not been used, as far as the author knows, as a production tool in the design of airplanes. Instead, at the Lockheed-California Company in particular, emphasis has been placed on the actual

generation of design conditions that match, in realistic combinations, the statistically defined loads resulting from the power-spectral analysis.

The concept of a design condition has long permeated the entire art of structural analysis. Inasmuch as the various design loading conditions are relatively uninfluenced by changes in the structure (short of major changes in the overall stiffness), it has been possible to keep the loads determination function entirely distinct from the stress analysis and structural design functions. Design and optimization of the structure are thus facilitated. The usual refinements in the stress analysis methods as the design progresses are easily accommodated. Refinements in the loads determination can proceed independently of those in the stress analysis.

To meet this need for "design conditions," the matching condition technique was developed at the Lockheed-California Company starting in the early 1960's. With continuing improvements, it has been used routinely ever since. The techniques developed at the Lockheed-California Company for generating matching conditions are described in some detail by Moon,³¹ by Stauffer and Hoblit,²³ and in Sec. 11 and Appendix C of FAA-ADS-53.¹³ A brief qualitative description is provided in the following paragraphs.

The basic concept employed in matching condition generation is suggested by the fact that, in flying through turbulent air, an airplane responds statically to the low-frequency components of the turbulence (long gradient gusts), and it responds dynamically in its various elastic modes to the higher-frequency components of the turbulence. The two types of response, the static and the dynamic, generally have quite different distributions of load throughout the structure. Moreover, each elastic mode will have its own distinctive load distribution. In flight through typical turbulence, there is a random interplay among these various distributions. As a result, no single distribution that might be applied can be expected to reproduce simultaneously the correct stress histories at all points in the structure.

Elementary distributions. Accordingly, in generating matching conditions, the approach is to start with a number of elementary distributions. Each of these consists of a set of forces in equilibrium, representing the static response of the airplane or the dynamic response in a particular elastic mode. In particular, two static response distributions might be included. One would consist of the aerodynamic forces and reacting pitch and plunge inertia forces due to a unit angle of attack. The other would consist of the aerodynamic forces and reacting pitch and plunge inertia forces due to a unit pitch velocity. The elastic mode distributions would each consist of three sets of forces: the inertia forces associated with free vibrations at the natural frequency of the mode, the aerodynamic forces produced by the oscillating motion, and the pitch and plunge inertia forces needed to balance the aerodynamic forces.

Superposition of elementary distributions. These elementary distributions, as building blocks, are then superimposed in various proportions to

give a number of design conditions that, collectively, envelope the statistically defined shears, bending moments, and torsions. Further, this enveloping takes proper account of phasing of the various load quantities, such as shear and torsion at each wing station. It thus provides, for example, the proper amount of torsion in combination with the maximum shear and the proper shear with the maximum torsion. The procedure is essentially one of trial and error. The work can be systematized, however, to permit homing in fairly rapidly on each desired condition. Moreover, a computer program has been developed³¹ that utilizes “linear-optimization” theory to vastly reduce the amount of trial and error required. The result is almost a batch-processing computer operation.

Taking as an example the generation of wing load conditions for a conventional subsonic transport, one would first obtain shear-torsion and bending-torsion ellipses and their circumscribing octagons, as shown in Sketch k, at some eight or ten wing stations. At a given station, separate load conditions would be defined matching each of the eight corners of the octagon. Inasmuch as shear and bending tend to be highly correlated—that is, their ellipse would be slender—often a single condition can match the corresponding corners of both the shear-torsion and bending-torsion octagons at a given station. Although in general all eight corners of each octagon would be matched, it is usually possible to eliminate several of the eight points as obviously not critical, thus reducing the number of conditions that must be generated.

Spanwise, it is desirable for a single condition to match at several adjacent stations; however, it is not to be expected that a single condition will match over the entire span. It is, of course, necessary that, at those stations where a given condition does not match, it fall within rather than outside of the design octagons.

Mission analysis considerations. When the statistically defined loads are obtained using a mission analysis criterion, it is customary to select a single predominant mission segment as representative. One-*g* loads for this segment are subtracted from the net loads read from the exceedance curves, to give incremental loads. [When the design envelope floor (Sec. 5.3.4) exceeds the mission analysis load, the design envelope load, including its 1-*g* value, is substituted for the exceedance-curve value.] Correlation coefficients ρ for this same predominant segment are used to define equal probability ellipses. The elementary distributions also, at least initially, are based on this segment.

A possible source of either conservatism or unconservatism in this approach is the variation of ρ from segment to segment. Another possible source of conservatism is the variation of the ratio of torsion to shear, or torsion to bending, from segment to segment; see Sec. 6.1.5. If these potential inaccuracies are of concern, one or more fictitious structural elements can be defined, as described in Sec. 6.1.5, and carried through the mission analysis. A more usual approach, however, is to make an approximate adjustment, perhaps based on estimated weighted averages.

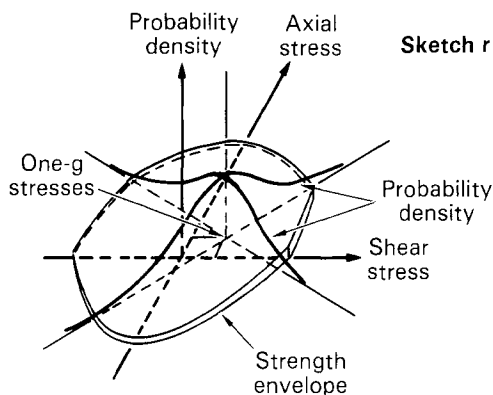
Design envelope considerations. When loads are obtained on a design envelope basis, the shear-torsion ellipses or octagons—and separately the bending-torsion ellipses or octagons—for all conditions should be superimposed. The result will be a single shear-torsion envelope and a single bending-torsion envelope at each station. Elementary distributions should be based on whichever flight condition defines the particular point being matched. In other words, use of more than one set of elementary distributions will usually be advantageous.

6.2.4 Joint Probability Technique

The generation of matching conditions does require a certain degree of skill, ingenuity, and judgment. Also, at best it involves at least some small degree of approximation. As a result, it has sometimes been felt that a more “scientific” approach, which would concentrate on local stresses, would be preferable. These considerations led The Boeing Company to develop what has generally been referred to as the joint probability technique. (Apparently, no consideration was given at that time, 1964, to the much simpler internal loads and stresses approach described in Sec. 6.2.2; or perhaps nobody had yet thought of it.) The joint probability technique is based on a concept suggested in NASA TR R-199¹⁰ (pp. 51 and 52). Its development is reported in FAA-ADS-54²⁷, a companion report to FAA-ADS-53.¹³

In the joint probability approach, it is assumed that any potentially critical element of structure is subjected to a combination of shear and axial stresses (as in Sec. 6.2.2). This clearly is an appropriate assumption for most skin-stringer structures; and where the stress pattern is more complex, suitable approximations can probably be made.

Design envelope criterion. Under the design envelope form of criterion, the single quantity $U_\sigma = \sigma_w \eta_d$ is replaced by design values of σ_w and η_d individually. For each potentially critical point in the structure, the joint probability density of applied axial and shear stresses is determined analytically for the specified σ_w . A typical result is shown in Sketch r.



The strength envelope, or allowable stress interaction curve, also shown in Sketch r, is determined separately, based on the actual structure.

The volume under the joint probability density surface outside the strength envelope, the part cut away in the sketch, is then the probability that the design strength is exceeded at any instant of time. A design value of this probability P is specified.

Determination of design σ_w and P . The design value of σ_w is determined from the design value of $U_\sigma = \sigma_w \eta_d$ (Sec. 5.4.2) and an appropriately selected value of η_d :

$$\sigma_w = \frac{\sigma_w \eta_d}{\eta_d} \tag{6.5}$$

The rational selection of η_d is discussed in Appendix I, where it is shown that the appropriate value of η_d is a function of U_σ/b_2 (b_2 as in Eq. (4.27), Sec. 4.7.5), as given by Fig. 6.1. Actually, the selection can be somewhat arbitrary, inasmuch as any error in σ_w will be largely offset by a corresponding error in P . In FAA-ADS-53, a value

$$\eta_d = 3.5$$

was selected. It would now appear that a better value, based on Fig. 6.1 with

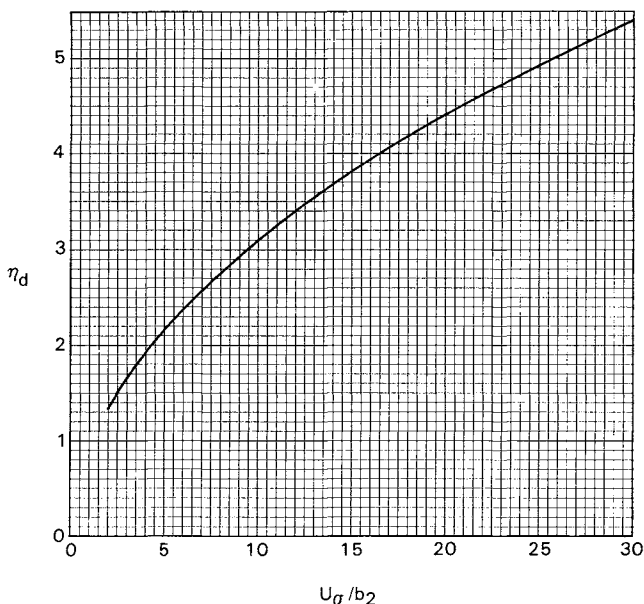


Fig. 6.1 Variation of η_d with U_σ/b_2 .

$U_\sigma = 75$ fps at 20,000 ft, would be about 2.5; this follows from a b_2 value, read from Fig. 4.15, of 11.3.

Corresponding to $\eta_d = 3.5$, a value of P is read from Fig. 4.2, entering with $y/\sigma = 3.5$. The value is 2.3×10^{-4} . Actually, this value corresponds to a strength envelope that is a single straight line, such as line B (or A or C) in Sketch p. For any actual strength envelope, the probability will be greater. For consistency of required strength with that given by the “single-variable” philosophy illustrated by Sketch p, some higher design value of P is appropriate. For this reason, the design value of P recommended in FAA-ADS-53¹³ is

$$P = 3 \times 10^{-4}$$

Further remarks on joint probability techniques. From the discussion in Sec. 6.1.5, it can be seen that the *matching condition technique* can be characterized as a “single-variable” approach; each of the many lines in sketch n that collectively define the ellipse represents a single load variable. Similarly, the *internal loads and stresses* approach of Sec. 6.2.3 is a single-variable approach.

At least superficially, the *joint probability technique* appears to be more “accurate” than any single-variable technique. For example, if the strength envelope of a critical panel were actually to coincide with an equal probability ellipse, the gust velocity capability would be only about 80% of that for the case in which the strength envelope is (in effect) a single straight line tangent to the same ellipse. On the other hand, the probability of having a strength envelope that hugs the equal probability ellipse this closely is extremely low. In practice, variations in shape of strength envelope are unlikely to affect the gust velocity capability by more than a few percent. Further, the greater rationality of the joint probability technique is somewhat illusory in that it fails to consider the joint probability of reaching design strength at various different locations in the airplane. This subject is a very complex one, so much so that gust loads engineers seem to have chosen unanimously not to become involved in it. For further understanding, the reader is referred to the thorough discussion available in Secs. 12.2–12.4 of FAA-ADS-53.¹³

Mission analysis criterion. Use is again made of the strength envelope relating axial and shear stresses at each of many locations in the structure. $N(y)$ is redefined as the number of outward-directed crossings of the strength envelope per hour, rather than as the number of positive-slope crossings per hour of a series of given values of a single load quantity. Procedures for computing this quantity are developed in Appendix B of FAA-ADS-54.²⁷

This page intentionally left blank

7

GUST RESPONSE EQUATIONS OF MOTION: FORMULATION AND SOLUTION

Determination of \bar{A} and N_0 values requires formulation and solution of the airplane equations of motion.

The purpose of this chapter is to provide a very brief overview of this subject, largely for completeness. Also included, however, are some notes of a more detailed nature that may add a helpful perspective. A full discussion of the gust response equations of motion and their solution would be long and involved and beyond the intended scope of this book. Although expertise in this area is rather widespread, the writer is unaware of any really satisfactory comprehensive treatise. The discussion throughout this section will be recognized as drawing heavily on L-1011 experience; it should, however, be applicable fairly generally.

7.1 GENERALIZED COORDINATES

The generalized coordinates used in formulating the gust response equations of motion ordinarily consist of the natural modes of the airplane. These consist of the free-airplane vibration modes together with the pertinent rigid-body modes. These modes normally include:

Vertical Gust	Lateral Gust
Plunge	Sideslip } Yaw } Customarily in a Roll } moving axis system
Pitch	
Elastic modes that respond dynamically	
Elastic modes having static response that affects aerodynamic force distribution	Elastic modes that respond dynamically Elastic modes having static response that affects aerodynamic force distribution

For the L-1011, 20 elastic modes have ordinarily been used in the vertical gust analysis, and 30 in the lateral gust analysis. In the lateral gust analysis, it was found necessary to use more than 20 modes in order to represent static

aeroelastic twist of the fin, inasmuch as the fin is relatively light, and consequently, the lowest fin-twist mode is of relatively high frequency. Sometimes generalized coordinates other than rigid-airplane or free-vibration modes are useful. The motion of a control surface about its hinge line is such an example.

7.2 GRID SYSTEMS

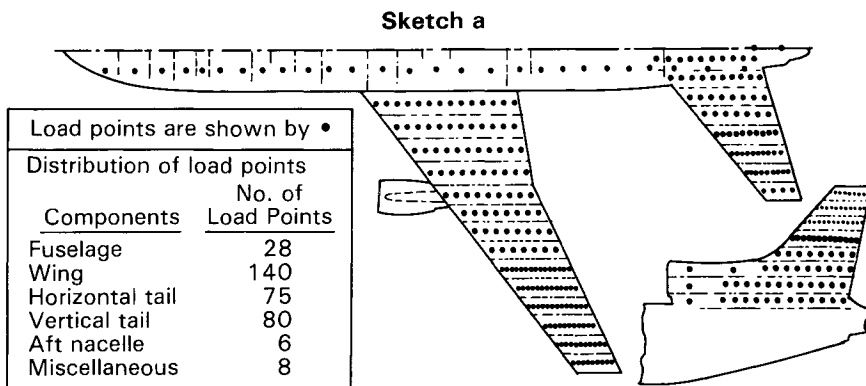
Both input and output data are in effect “lumped” at discrete points on the structure. These points are ordinarily defined at the Lockheed-California Company by three-dimensional grids. Usually, it is found expedient to use several different grids for different purposes.

Input data needed for static and dynamic loads determination include: mass data; stiffness data; and aerodynamic data.

Output data consist basically of forces. These forces may be applied directly to the structure to determine stresses; or they may be integrated to give shears, bending moments, and torsions. These integrated loads provide visibility for the loads and facilitate comparisons of various conditions.

The various grids used might include the following.

Basic loads grid. This is a relatively fine grid. Basically, it is the grid on which output forces are lumped. Thus, it is the grid on which design-condition panel loads will be defined prior to transfer to the structural (deflection) influence coefficient grid for use in stress analysis. Inasmuch as inertia forces follow directly from masses, this grid may also be used in providing the input mass data; it is, in fact, used for this purpose on the L-1011. The specific form of the basic loads grid will ordinarily be dictated by the form of the lifting surface aerodynamic theory used; it is imperative that the airloads given by the theory be defined on this grid. For the L-1011, for example, use of kernel function aerodynamics required that panel boundaries be laid out streamwise and at constant fractions of chord, so that pressures given by the theory could be integrated in closed form to give panel airloads. Lump points were taken roughly at the midpoints of the panels thus defined.



Mass grid. In general, it may be advantageous to define a separate mass grid for convenience in preparing mass data. Masses, or the associated inertia forces, would then be transferred to the basic loads grid.

SIC grid. This is the structural (deflection) influence coefficient grid, used in representing the stiffness characteristics of the structure. It is laid out by the stress organization to be compatible with the structural arrangement. It tends to be somewhat coarser than the basic loads grid. It is also the grid to which loads are transferred for stress analysis.

Aerodynamic control point grid. A separate aerodynamic control point grid may or may not be necessary. The kernel function theory used on the L-1011 did require such a grid; the theoretical airloads over the airplane were expressed as functions of angle of attack at these points. The kernel function theory required this grid to be laid out at prescribed constant fractions of chord and semispan.

Dynamic analysis grid. This grid is somewhat coarser than the SIC grid; it uses points selected from there.

In the analysis of an airplane with a very low aspect ratio wing, shears, bending moments and torsions have little meaning. It may be desirable in this case to lump forces, and masses, directly on the SIC grid. A basic loads grid must still be used in the initial determination of aerodynamic forces, but these are immediately transferred to the SIC grid. Critical conditions are then identified by scanning internal loads (stringer loads, shear flows, etc.) after a structural model run has been made.

7.3 BASIC DATA

7.3.1 Mass Data

Panel weights are provided by the weight organization, reflecting payload and fuel quantities specified by the loads organization.

7.3.2 Stiffness Data

The stiffness data are provided in the form of SIC's, that is, as deflections per unit load. These SIC's are determined by the stress organization by means of redundant-structure analysis.

For the purpose of dynamic loads determination, these SIC's should be determined on the basis of unbuckled skin—or at least on the basis of buckling corresponding to a fairly low load level. Stress analysis and static loads determination properly utilize a structural idealization in which the buckled state of the skin at the limit load level is accounted for, yielding a reduced stiffness. Motion in the elastic modes, however, is governed largely by motions at lower load levels; consequently, the stiffness used should

correspond to these lower load levels. A further practical advantage of basing the SIC's on unbuckled structure is that test data, both from ground vibration tests and flight in turbulence, will be at low-load levels; correlation with theory is much more direct when the low-load SIC's are used.

The biggest effect of buckled vs unbuckled skin is on the fuselage stiffness. Wing structure is generally robust enough so that there is little buckling at the limit-load level. On the L-1011, actual fuselage stiffness was greater than derived from the limit-load modeling by some 40%, corresponding to an increase in frequency of the fuselage-bending mode of nearly 20%. Part of this increase was due to inclusion of the circumferential fail-safe straps, which did not affect strength but did increase the average stiffness.

Sometimes, a simpler determination of SIC's is desirable than by redundant analysis of the three-dimensional structure. For this purpose, the structure can be represented by a "stick model," in which the wing, fuselage, and tail surfaces are represented by "sticks" or "wires" located at the appropriate elastic axes and with stiffness defined by EI and GJ values that vary along the axes. Such models may be available at an earlier stage of design and they may also facilitate investigations of the effects of stiffness variations; for example, in matching natural frequencies observed in ground vibration tests and flight tests.

7.3.3 Aerodynamic Data

Aerodynamic data are usually generated in the form of aerodynamic influence coefficients (AIC's). These give airloads at lump points on a loads grid as a function of angles of attack of points on a control-point grid.

The AIC's are determined basically by means of unsteady lifting surface theory; accordingly, the AIC's are a function of frequency. For gust loads determination, AIC's would be computed at from 7–10 frequencies; they might then be interpolated to other frequencies if required. For the L-1011, kernel function theory was used, as presented in NASA TR-R-48.³² Currently, the trend is toward use of double-lattice theory as presented by Albano and Rodden³³ and Giesing, Kalman, and Rodden in AFFDL TR-71-5.³⁴

Adjustments are made to the theoretical AIC's as necessary to provide reasonable agreement with wind-tunnel force and pressure data at zero frequency. The zero-frequency adjustments can be applied at all frequencies, or they can be used only at low frequencies and tapered down to zero at some appropriate frequency, perhaps 1 or 2 Hz.

It is believed that such adjustments will be much smaller when doublet-lattice instead of kernel-function theory is used. One of the major adjustments required in the L-1011 data resulted from determining wing AIC's on the basis of a wing continuous through the fuselage with the fuselage not present. This resulted, as might be expected, in a somewhat unconservative spanwise lift distribution. The doublet-lattice theory can take account of the absence of the wing in the region of the fuselage.

7.4 USE OF MATRICES AND MATRIX ALGEBRA

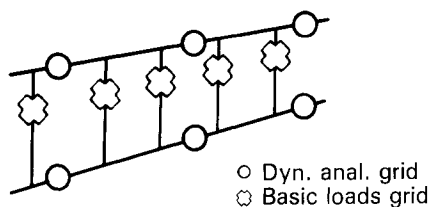
Closely related to the grid-system representation of the airplane is the extensive use of matrices and matrix algebra. With a grid-system representation, large amounts of data must be handled, so that the use of matrices and matrix algebra to manipulate and store the data is virtually a necessity. SIC and AIC data, for example, are inherently in matrix form—deflection at point i due to force at point j , or aerodynamic force at i due to angle of attack at j . The manipulation of data involves the use not only of formal matrix algebra but also other very useful operations not consistent with formal matrix algebra, such as element-by-element multiplication and division.

Matrix algebra is used, of course, to facilitate the actual solution of the equations of motion. It is also used, however, to systematize a multitude of simple computations. A typical example (see Appendix J.1) is the computation of generalized masses of free-vibration and rigid-body modes, according to the expression

$$m = \sum_{\text{structure}} \phi^2 \Delta M$$

A frequently used matrix manipulation in loads work is the transfer of data from one grid to another. A common example involves the transfer of *mass* or *force* data from a relatively fine basic loads grid to a coarser dynamic analysis grid. Adjacent points on the dynamic analysis grid are considered to be joined by simply supported beams in such a pattern that reactions on the dynamic analysis grid to forces on the basic loads grid can readily be determined (Sketch b). The mechanism involved in this “beaming” of forces is reflected in a transformation matrix that, when multiplied by forces on the basic loads grid, yields the equivalent forces on the dynamic analysis grid.

Sketch b



Such a matrix can be generated either point by point and beam by beam, or by computer programs that utilize the coordinates of the points to generate their own beam networks. It is interesting to note that the *transpose* of the beaming matrix is an interpolation matrix. Multiplication of displacements on the dynamic analysis grid by the interpolation matrix yields displacements on the basic loads grid.

Combining these two matrices with the diagonal matrix of masses on the basic loads grid yields a matrix of masses on the dynamic analysis grid. This matrix is not a diagonal matrix. But it has the neat property that, when premultiplied by accelerations on the dynamic analysis grid, it gives inertia forces on the dynamic analysis grid, consistent with the actual (interpolated) accelerations on the basic loads grid and the associated basic-loads-grid inertia forces.

All of the foregoing applies to transformations by “splining” as well as by beaming, although, of course, the generation of the transformation matrix then becomes more complicated.

A word of caution is in order: Matrix operations are valid only when each individual operation that they define is physically valid. It is often all too easy to skip the hard thinking that may be required to assure this validity.

7.5 LOADS AS FUNCTIONS OF GENERALIZED COORDINATE RESPONSE

The equations of motion, as noted earlier, are written in generalized coordinates, and the solutions yield generalized coordinate responses. These responses are to inputs consisting of steady-state sinusoidally varying gust velocities of unit amplitude. The output responses, therefore, are frequency-response functions as discussed in Secs. 4.4.5 and 4.4.6.

Load responses are then computed from these generalized coordinate responses. Panel inertia forces follow from panel accelerations, which in turn follow from generalized coordinate accelerations. Panel airloads follow from panel angles of attack in conjunction with the AIC's; the angles of attack follow from the gust velocities, the panel angular displacements, and the panel velocities. Panel loads, inertia plus aerodynamic, are then integrated to give shears, bending moments, and torsions.

These operations can be performed in various sequences. In the Lockheed-California Company VGA and LGA programs, the net panel motions are determined first, by superimposing the motions in the various modes. Net panel loads are then determined and integrated. In the Lockheed-California Company GLP programs, developed later, panel forces and integrated loads are obtained for each mode as functions of the generalized coordinate response.* The net values of the panel forces and integrated loads are then obtained directly by superposition of the contributions of the various generalized coordinates.

7.6 SOLUTION FOR FREQUENCY-RESPONSE FUNCTIONS

Some of the basic concepts involved in the actual formulation and solution of the differential equations of motion are suggested in Appendix J.2.

*Inasmuch as the relation of panel forces and integrated loads to generalized coordinate response is defined as a function of frequency, the effects of generalized acceleration and velocity as well as of generalized displacement are accounted for.

An example of the specific content of these equations is shown in Sec. J.3. These two appendices are included to provide the newcomer with some indication of what is really contained in the much more complicated equations that will be encountered in practice. Solution of the differential equations yields frequency-response functions for both generalized coordinate response (Appendices J.2 and J.3) and integrated load response (Sec. 7.5).

7.7 INCLUSION OF AN ACTIVE CONTROL SYSTEM

Inclusion of an active control system, autopilot, stability augmentation system, or whatever is no great problem. Ordinarily, each pertinent control surface displacement will be introduced as an additional generalized coordinate. Equations will then be included that define the displacement of each control surface as a function of motions in the generalized coordinates. These additional equations reflect the contribution of each generalized coordinate to the sensed accelerations or rates to which the control system responds, together with the control laws governing the control surface motions in response to the sensed quantities.

7.8 COMPUTATION OF \bar{A} , N_0 , and ρ

These computations, for both generalized coordinate response and integrated load response, follow directly from the following equations:

$$\bar{A} \text{—Eq. (4.7), Sec. 4.4.2}$$

$$N_0 \text{—Eq. (4.20), Sec. 4.6.3}$$

$$\rho \text{—Eq. (6.1), Sec. 6.1.4.}$$

One should be aware, however, that values of N_0 may be somewhat sensitive to the upper limit of integration. See the discussion of this in Appendix E.

7.9 CHECKS FOR ERROR

Because of the great complexity of the gust response calculations, one should be alert for opportunities for checks. Types of checking are discussed in the following sections.

7.9.1 Routine Checks

These might include:

- 1) Orthogonality check of vibration modes (Appendix J.1)
- 2) Comparison of W , I_{yy} , and c.g. location as computed from rigid-body mode data, with known values

$$[\phi_R]^T [M] [\phi_R] = \begin{bmatrix} a_{11} & a_{12} \\ a_{21} & a_{22} \end{bmatrix}$$

$$a_{11} = W \quad a_{22} = I_{yy} \quad \frac{a_{12}}{a_{11}} = \text{c.g. location}$$

3) Comparison of C_{L_α} , C_{L_q} , C_{m_α} , C_{m_q} as computed from rigid-body mode data, with known values

$$[\phi_R]^T [AIC] [\phi_R] = \begin{bmatrix} b_{11} & b_{12} \\ b_{21} & b_{22} \end{bmatrix}$$

$$b_{11} = C_{L_\alpha} \quad b_{12} = C_{L_q} \quad b_{21} = C_{M_\alpha} \quad b_{22} = C_{M_q}$$

7.9.2 Reasonableness Checks

These include examination of mode shapes and psd's.

7.9.3 Checks Using Simplified Response Curves

C.g. acceleration \bar{A} 's can be checked against values given by simplified response curves (Chapter 8).

7.9.4 Static Loads Check

This is an important check to make at an early stage in the development of a new airplane. It is accomplished by applying as a forcing function a very low-frequency elevator oscillation (instead of a gust) and comparing load-per-g ratios with static loads results for the same flight condition.

7.9.5 Flutter Check

This also has value at an early stage of design. The gust input is set equal to zero in the gust-response equations, and stability solutions are obtained. These are then compared with results for comparable flight conditions obtained from analyses formulated independently for flutter evaluation. The flutter check complements the static loads check by providing information on the adequacy of the elastic-mode representation, including the aerodynamics at elastic-mode frequencies.

8

SHORT-CUT METHODS

The preceding chapter gave some idea of the vast effort required to set up and solve the airplane equations of motion when a full state-of-the-art dynamic analysis is needed. There are also, however, situations in which much less elaborate analyses are appropriate. Such analyses can be useful for preliminary design loads determination or even to provide qualitative understanding of the effects of certain parameter variations. Such analyses always involve the assumption, initially, of a rigid airplane. The effects of static aeroelastic deformation and elastic-mode dynamic response can then be incorporated, if needed, by means of empirical factors.

The various shortcut methods discussed here are all directed toward determination of c.g. load factor—or more specifically \bar{A} , and in some cases N_0 , of c.g. load factor. Actual loads are then determined, if needed, by static loads methods. In all of these methods, few enough airplane parameters are involved so that the approach is to *presolve* the equations of motion, and integrate to give \bar{A} and N_0 , for a matrix of values of these airplane parameters. The many solutions thus obtained are then plotted as a function of the various parameters.

8.1 PLUNGE-ONLY CURVES

8.1.1 \bar{A} from Curves in FAA-ADS-53

Figure 8.1, taken from Fig. 5.2a of FAA-ADS-53,¹³ gives values of the coefficient K_σ as a function of the parameters $\bar{\mu}$ and \bar{c}/L . The quantity $\bar{\mu}$ is identical to the mass parameter μ_g used with the FAR gust loads formula, Eq. (2.3) of Sec. 2.3. L is the scale of turbulence and \bar{c} the mean geometric chord.

The airplane is considered to be rigid and free to plunge only. \bar{A} is obtained as

$$\bar{A} = K_\sigma \frac{\rho V_T C_{L\alpha}}{2(W/S)} \quad (8.1)$$

The curves in Fig. 8.1 are based on the von Kármán shape of gust psd.

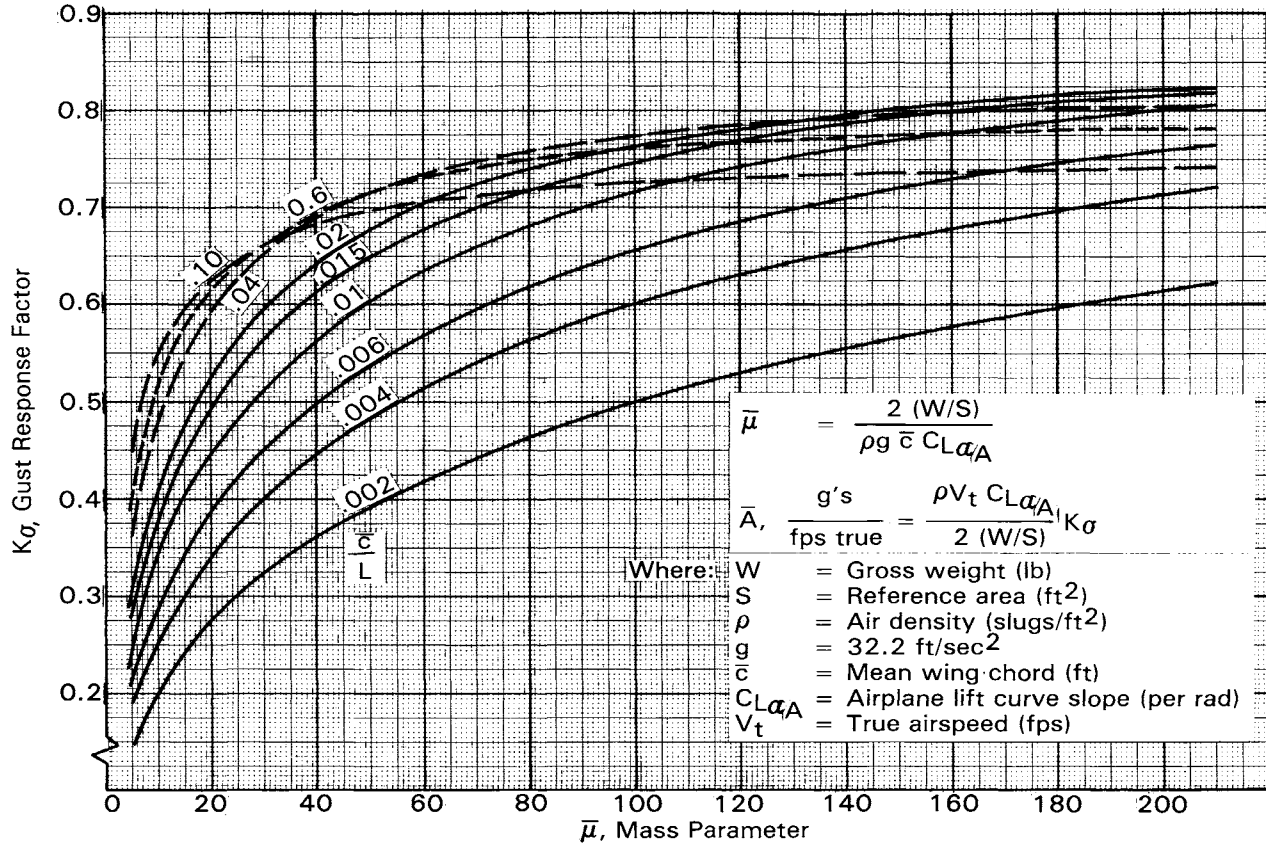


Fig. 8.1 Gust response factor; plunge only, von Kármán gust spectrum. From FAA-ADS-53.¹³

Unsteady lift growth assumptions are as follows:

1) Because of gust penetration (“Kussner” effect*), the gust (or response) psd is multiplied by a factor

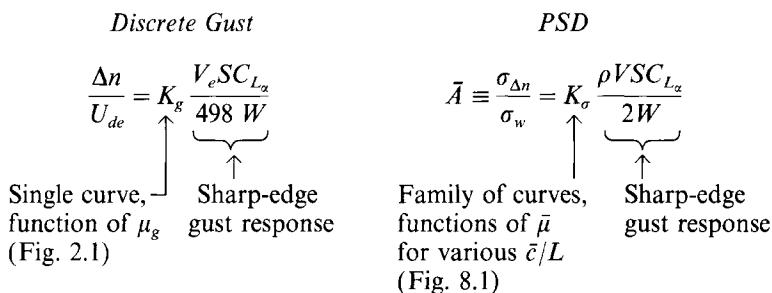
$$\frac{1}{1 + 2\pi k}$$

where $k = \omega c/2V$. This factor was proposed by Liepmann in his 1952 paper.¹²

2) Because of airplane motion (“Wagner” effect*), lift growth is assumed to be instantaneous.

Inclusion of the Kussner effect while ignoring the Wagner effect would appear to be inherently unconservative, in that the lift due to the gust is reduced, whereas the alleviating lift due to the airplane motion is not reduced.† Also, the aforementioned factor for the Kussner effect is unconservative in itself, as pointed out in Sec. 8.4.

8.1.2 Relation to Discrete-Gust Formula



It is seen that the use of Fig. 8.1 is virtually identical to the use of the FAR discrete-gust formula. In using the discrete-gust formula, K_g is given by Fig. 2.1 or by an empirical equation [Eq. (2.2), Sec. 2.3] as a function of μ_g ; in the use of Fig. 8.1 K_σ is given by the figure as a function of $\bar{\mu}$ and \bar{c}/L . The discrete-gust formula gives $\Delta n/U_{de}$; use of Fig. 8.1 gives $\Delta n/U_\sigma$ (Secs. 5.3.2, 5.4.2, and 5.4.3).

*The Kussner function is the indicial response to penetration of a sharp-edge gust, $K_g(t)$ in Sketch a in Appendix A. The Wagner function is the indicial response to a sudden change in angle of attack, $K_w(t)$ in this sketch.

†Curves of the type presented in Fig. 8.1 were first presented in Report 1272¹⁸ where they were based on the Dryden shape of gust psd. The curves in Report 1272,¹⁸ like those shown in Fig. 8.1, were obtained from equations developed by Fung.³⁵ Accordingly, curves of this type have traditionally been referred to at the Lockheed-California Company as “Fung curves.” Other less significant differences between the Fig. 8.1 curves and those in Ref. 18 are that in Report 1272¹⁸ the coefficient K_σ is designated $\sqrt{I(K, s)}/\pi$ and the mass parameter is designated K and is four times $\bar{\mu}$, and in the definition of the mass parameter $C_{L\alpha}$ is replaced by 2π .

The static discrete-gust formula could be replaced by a static psd formula, and, as far as the work is concerned, nobody would know the difference! The result, however, would be more realistic loads. It would be necessary, however, to establish realistic design U_σ values, giving proper consideration to the fact that elastic-mode dynamic effects are not accounted for.

8.1.3 N_0 from Curves in AFFDL-TR-70-106

It is not clear to the writer that simple theory can give values of N_0 that are as good, even, as guesses guided by results of analysis of other airplanes. The problem is the sensitivity of N_0 to the response at higher frequencies. This is influenced by a variety of factors ignored in the simple analysis, as discussed in Appendix E. For what they may be worth, however, curves based on simple plunge-only theory are provided in Fig. 8.2. These are taken from Fig. 18 of AFFDL-TR-70-106.³⁶

The curves give a coefficient k_0 as a function of a mass parameter μ , the same as $\bar{\mu}$ in Fig. 8.1, and $2L/c$. N_0 is then given by

$$N_0 = \frac{V}{\pi \bar{c}} k_0 \quad (8.2)$$

8.1.4 \bar{A} from Curves in Houbolt³⁶

Curves comparable to those of Fig. 8.1 are also available in Fig. 16 (or 17) of AFFDL-TR-70-106.³⁶ These are reproduced here as Fig. 8.3. Like the curves in Fig. 8.1, they are based on the von Kármán spectral shape. The lift growth treatment, however, is apparently much improved, with respect to both Kussner and Wagner functions.

8.1.5 Hall Formula

Taylor in his *Manual on Aircraft Loads*³⁷ quotes and discusses a formula presented by J. Hall in an unpublished paper in 1962. This formula gives the frequency-response function for an airplane free to plunge only. It appears to include a realistic representation of the Kussner function, but it is not clear that the Wagner function is accounted for. Taylor shows the resulting curves of K_σ plotted vs a parameter $c\mu_g/L$, for various values of c/L . Hall's parameter $c\mu_g/L$ is identical to the highly advantageous parameter δ/L introduced in Sec. 8.2.1, but which the author has never seen used elsewhere. The Hall formula is currently being used by G. Coupry of ONERA in studies correlating c.g. accelerations measured in transport operations.

8.1.6 Plunge-Only Curves as Special Case of Pitch-Plunge Curves

Plunge-only curves are also available as a special case of the pitch-plunge curves discussed in Sec. 8.2. These utilize the same lift growth treatment as

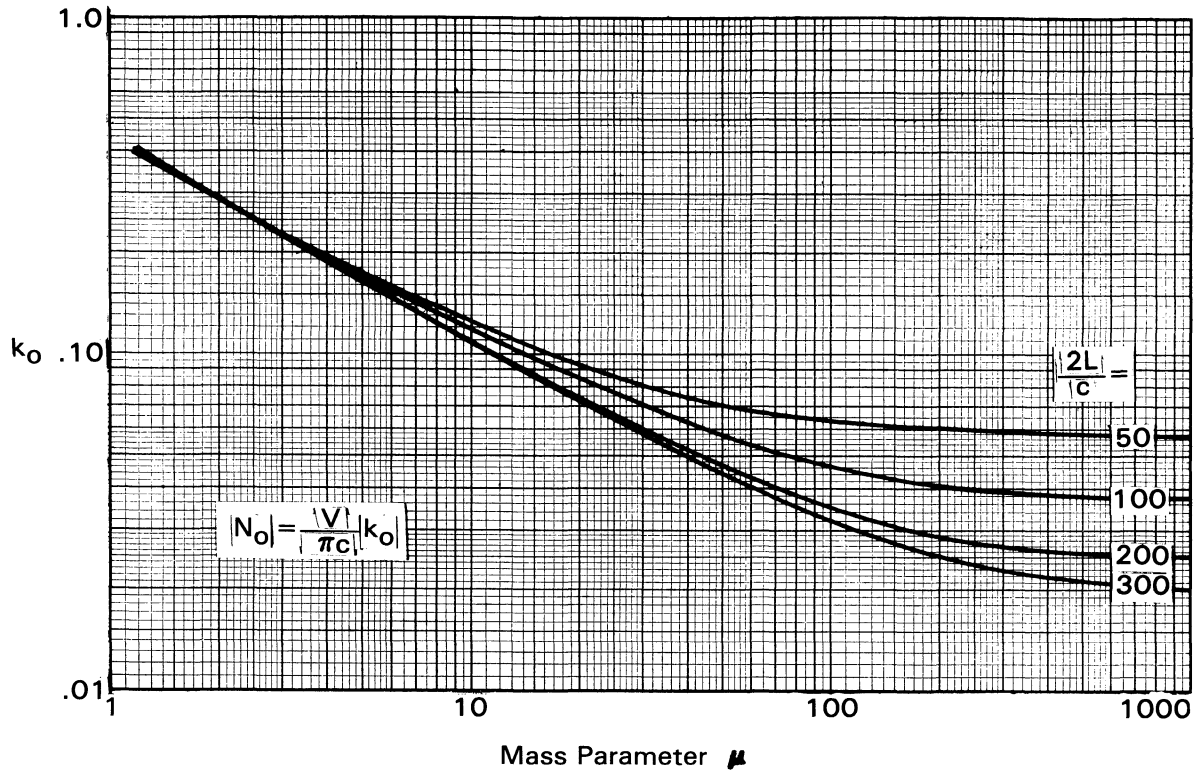


Fig. 8.2 Gust response N_0 values; plunge only, von Kármán spectrum. From AFFDL-TR-70-106.³⁶

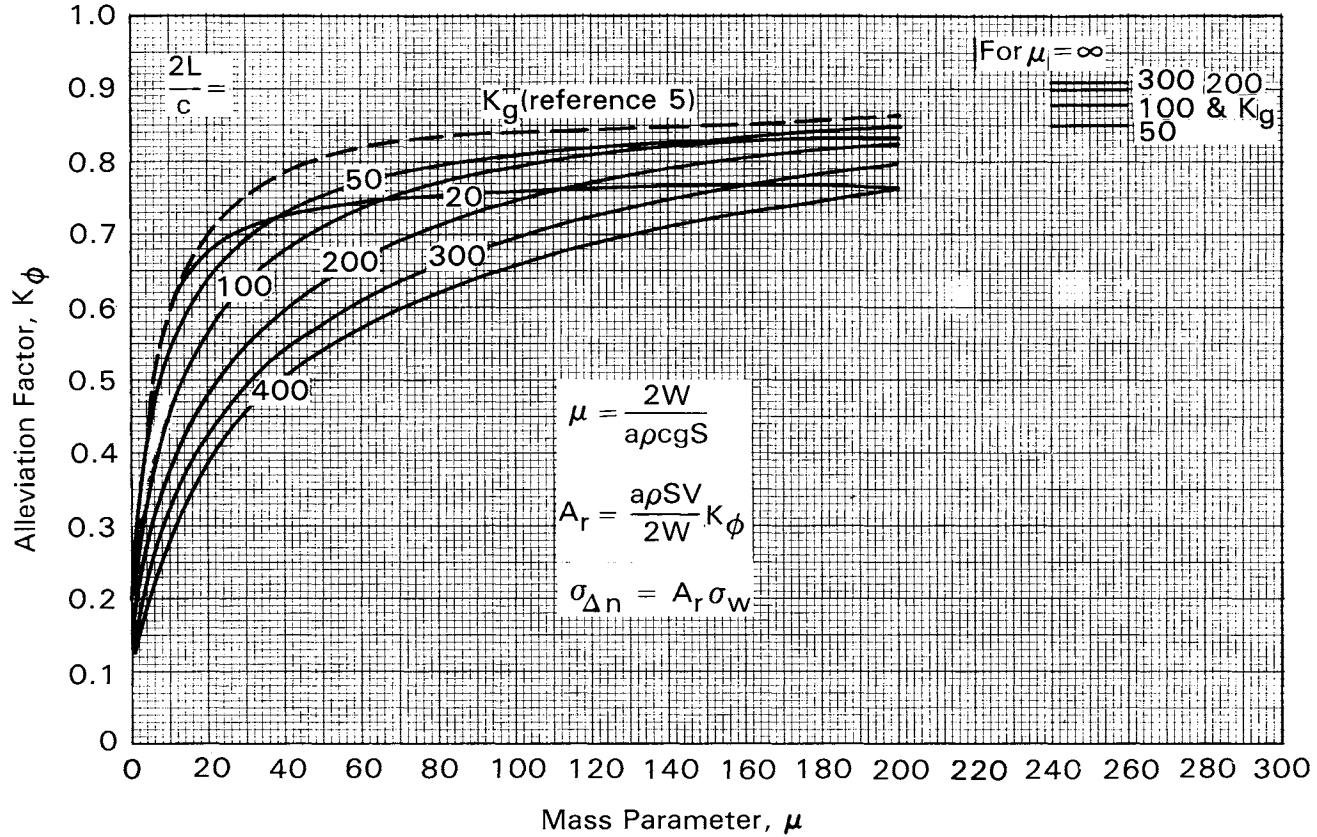


Fig. 8.3 Gust response factor; plunge only, von Kármán spectrum. From AFFDL-TR-70-106.³⁶

Fig. 8.1, but offer several advantages that will be apparent later. For further discussion of this special case, see Sec. 8.5.

8.2 PLUNGE-PITCH CURVES: HOBLIT PARAMETERS

For the plunge-only case, it is seen from Fig. 8.1 that K_σ is defined by two parameters, $\bar{\mu}$ and \bar{c}/L . When a pitch freedom is added, two additional dimensionless parameters are required, in order to account for the natural frequency and damping of the airplane short-period mode.

A comprehensive set of curves giving K_σ (and also other nondimensionalized responses) as functions of four such parameters was published in NACA TN 3992³⁸ in 1957. These curves were based on the Dryden spectral shape, however; and the choice of nondimensional parameters left much to be desired.

In 1964, therefore, the K_σ curves were recomputed at the Lockheed-California Company in terms of a much more convenient and illuminating set of parameters, for three different spectral shapes including the von Kármán shape. The resulting curves were published for Lockheed use in LR 18382, an internal Lockheed report. The development of these curves is summarized in this section and samples of the curves are shown.

8.2.1 Selection of Parameters

Nondimensional response ratio K_σ . The obvious nondimensionalization of the response is the same as in Sec. 8.1, as a ratio to the sharp-edge gust response

$$\begin{aligned}
 K_\sigma &= \frac{\Delta n}{\text{sharp-edge gust } \Delta n} \\
 &= \frac{\bar{A}}{[\rho V_T S C_{L_\alpha} / (2W)]} \quad (8.3)
 \end{aligned}$$

Plunge-only parameters, δ/L and \bar{c}/δ . In selecting the remaining four dimensionless parameters, those on which the response parameter K_σ will be considered to depend, attention was first directed toward the traditional mass parameter variously designated μ or $\bar{\mu}$ or μ_g . This mass parameter has been widely used, first in conjunction with the FAR discrete-gust formula, Sec. 2.3, and later in the various psd plunge-only analyses, where it appears, for example, in Figs. 8.1 and 8.3.

This mass parameter, however, is not a very good one. The problem is that it contains the mean chord \bar{c} .

The mean chord is indeed a significant quantity in defining the pitch characteristics of an isolated airfoil. It is even a convenient reference in defining the pitch characteristics of a given entire airplane. Furthermore, in

current discrete-gust design criteria, it has acquired an artificial importance in that the length of the design gust is rather arbitrarily taken as a given multiple of the wing chord (Sec. 2.3).

In a given patch of continuous turbulence, however, all lengths of gusts are present, in proportions defined by the gust psd. In this situation as long as "everything else" is held constant, the *only effect of the chord* on the gust response is through its influence on the *unsteady lift growth*; this is a relatively secondary effect. The "everything else" that is considered to be held constant includes, of course, the airplane mass W/g and also the quantity $\rho SC_{L\alpha}$, which measures the capability of developing lift. For some background on how the wing chord effects the unsteady lift growth, see Appendix A.

The unfortunate effect of including \bar{c} in the mass parameter can be seen by reference to Fig. 8.4. The curves shown there are those of Fig. 8.1. Suppose, now, that a point is marked on the figure corresponding to $\mu = 200$ and $\bar{c}/L = 0.002$ (small circle). Then, consider \bar{c} to be varied, with $2W/\rho g SC_{L\alpha}$ and L held constant. If \bar{c} is doubled, μ decreases to 100 and \bar{c}/L increases to 0.004, giving a second circled point. The other circled points are obtained similarly. The resulting trace is seen to be almost flat; it begins to bend down

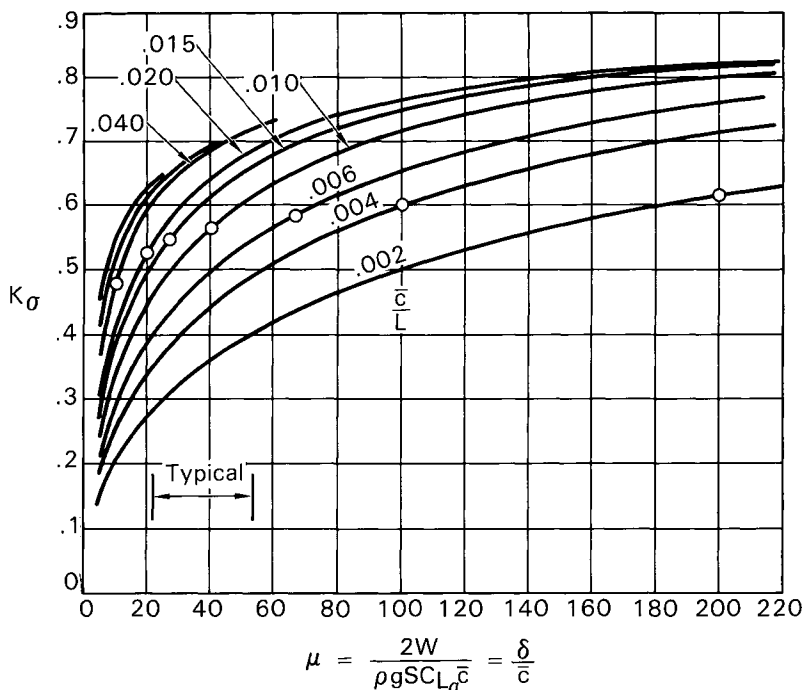
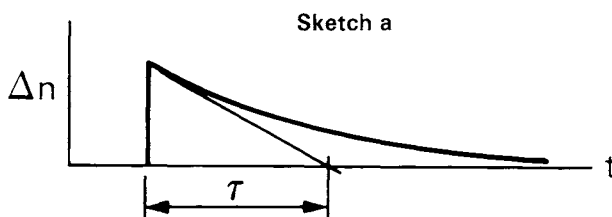


Fig. 8.4 Effect on gust response factor of varying \bar{c} only. Curves from FAA-ADS-53.¹³

significantly only at the lower values of μ , where \bar{c} is large and consequently unsteady lift effects are more substantial.

So instead of K_σ being fairly sensitive to \bar{c} , as one would infer from the curves, noting that μ is proportioned to $1/\bar{c}$, K_σ is actually quite insensitive to \bar{c} when account is taken of the fact that \bar{c}/L also changes.

In order to eliminate \bar{c} as a fundamental parameter, it is noted that a reference length can also be defined in terms of the response characteristics of the airplane. If the plunge-only response is considered to be fundamental, the reference length, or characteristic length, can be defined as follows. Consider the airplane to be free to plunge only and to encounter a sharp-edge (step) gust. The acceleration time history is then as shown in Sketch a.



The time τ is defined by the initial tangent to the curve and would be designated the "time constant" of the system. If τ is then multiplied by the true airspeed, it becomes a distance δ , which is correspondingly designated the "distance constant" of the system. If lift-lag effects are disregarded, the curve in the sketch can readily be shown [by solving the appropriate differential equation, Eq. (A.1) of Appendix A] to be an exponential function, with δ given by the simple expression

$$\delta = 2W/\rho g S C_{L\alpha} \quad (8.4)$$

The quantity δ is considered to be the fundamental characteristic length of the airplane.

The three lengths that influence the gust response are

$$\delta, \bar{c}, L$$

The only dimensionless ratio that can be formed from these three quantities *without* including \bar{c} is δ/L (or, if one should prefer, its reciprocal). δ/L will be considered the fundamental plunge-only parameter.

The second dimensionless ratio, reflecting unsteady lift effects, could be taken as either \bar{c}/δ or \bar{c}/L . Each has its advantages. The ratio \bar{c}/δ was selected as representing a ratio of strictly airplane and flight condition parameters, allowing the turbulence to enter in only through the first parameter, δ/L .

It will be observed that μ is simply δ/\bar{c} , the reciprocal of the parameter \bar{c}/δ , chosen for use here to reflect unsteady lift growth effects.

With K_σ plotted now vs δ/L instead of vs $\mu = \delta/\bar{c}$, for various values of \bar{c}/δ , the curves of Fig. 8.4 collapse to the more closely clustered group shown in Fig. 8.5. Two curves of constant \bar{c}/L are also shown in Fig. 8.5 by the dashed lines. These curves, for $\bar{c}/L = 0.002$ and $\bar{c}/L = 0.02$, largely bound the data shown in Fig. 8.4 and thus clarify the extent to which the data of Fig. 8.4 collapse to a narrower range in Fig. 8.5.

Pitch parameters, $f_0\tau$ and ζ . Traditionally, frequencies are nondimensionalized in terms of V_T and \bar{c} to give reduced frequencies such as

$$\frac{\omega\bar{c}}{2V_T} \quad \text{or} \quad \frac{f\bar{c}}{V_T}$$

Now that we are replacing \bar{c} with δ as a more useful reference length, the short-period undamped natural frequency f_0 is nondimensionalized as

$$\frac{f_0\delta}{V_T}$$

or more simply, because $\tau = \delta/V_T$, as

$$f_0\tau$$

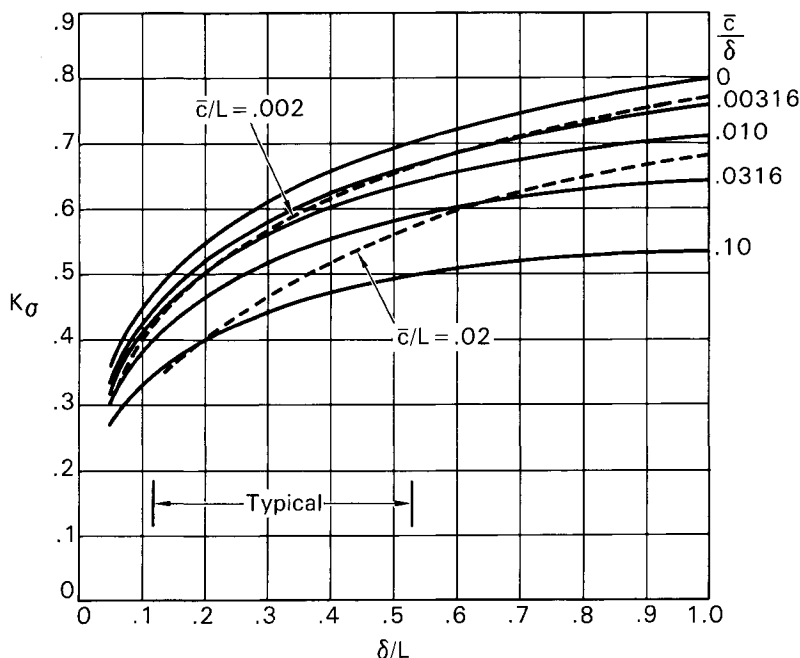


Fig. 8.5 Gust response factor; plunge only as a function of δ/L and \bar{c}/δ .

This parameter can be thought of, in an inverse sense, as the ratio of the plunge-only time constant τ to the short-period natural period, $T = 1/f_0$. The remaining dimensionless parameter is taken as the short-period damping ratio ζ , the ratio of actual to dead-beat damping constants.

Summary. The five dimensionless parameters in terms of which the curves of LR 18382 were prepared are

Dependent variable:

$$k_\sigma = \frac{\bar{A}}{(\rho V_T SC_{L_\alpha} / 2W)} = \frac{\bar{A}}{(V_T / g \delta)}$$

Independent variables:

$$\frac{\delta}{L}; \quad \frac{\bar{c}}{\delta}; \quad f_0 \tau; \quad \zeta$$

where

$$\delta = 2W / \rho g SC_{L_\alpha}$$

and

$$\tau = \delta / V_T$$

It should be emphasized that the gust sensitivity is influenced by three factors or groups of factors. These are

1) The sharp-edge gust response ratio (g/fps),

$$(\rho V_T SC_{L_\alpha}) / (2W)$$

2) The plunge-only response characteristics, defined by the parameters δ/L and \bar{c}/δ .

3) The short-period stability characteristics, defined by the parameters $f_0 \tau$ and ζ .

8.2.2 Lift Growth Assumptions

The curves presented in LR 18382 were based on the same lift growth assumptions utilized in the preparation of Fig. 8.1. The Kussner effect (gust penetration) was accounted for by multiplying the gust (or response) psd by $1/(1 + 2\pi k)$, and the Wagner effect (airplane motion) was ignored.

In Sec. 8.4 it is pointed out that the $1/(1 + 2\pi k)$ assumption is not a very good one and that the exact Kussner effect can be much better approximated by use of a readily determined effective \bar{c} in this expression, and thus in the parameter \bar{c}/δ , in place of the actual \bar{c} .

8.2.3 Charts

The curves in LR 18382 were plotted separately for each of three gust spectral shapes. Each of the three sets consisted of 96 11 × 17 in. sheets. Only the set based on the von Kármán spectrum is likely to be of use currently. This set was identified in the report as based on the “isotropic turbulence spectrum” and is contained in pp. 114–211 there. Six sample pages from this set, reduced in size, are included here as Figs. 8.6a–f. The selection of these samples is such that they should be of considerable use for actual quantitative checks of gust load factor as well as for indicating general trends.

The curves were plotted in two separate formats. The first emphasizes the effect of the short-period characteristics. On each sheet, δ/L and \bar{c}/δ are held constant and curves of K_σ vs $f_0\tau$ are shown for various values of ζ . The 48 sheets represent a matrix of eight δ/L values and six \bar{c}/δ values

$$\begin{array}{cccccccc} \delta/L = & 0.01 & 0.0316 & 0.10 & 0.316 & 1.0 & 3.16 & 10 & 31.6 \\ \bar{c}/\delta = & 0 & 0.00316 & 0.01 & 0.0316 & 0.10 & 0.316 & & \end{array}$$

Examples of this format are shown in Figs. 8.6a and b.

The second format emphasizes the effect of the plunge-only characteristics. On each sheet, $f_0\tau$ and ζ are held constant and curves of K_σ vs δ/L are shown for various values of \bar{c}/δ . The 48 sheets in this format represent a matrix of eight $f_0\tau$ values and six ζ values

$$\begin{array}{ccccccccc} f_0\tau = & 0.10 & 0.159 & 0.178 & 0.316 & 0.56 & 1.0 & 1.78 & 3.16 \\ \zeta = & 0.10 & 0.178 & 0.316 & 0.56 & 1.0 & 1.78 & & \end{array}$$

Examples of this format are shown in Figs. 8.6c–f.

As an aid to interpolation, it might be pointed out that adjacent values of the various parameters differ in the ratio either $\sqrt[3]{10}$ or $\sqrt[4]{10}$ —that is, by constant increments in the logarithm.

Vertical vs lateral gust. Although these charts were intended for use in determining vertical gust response, they can also be used to obtain a very good approximation of the lateral gust response.* In Fig. 8.6, a note is included on each sheet indicating whether the parameter values associated with that sheet are more typical of vertical or lateral gust response.

*This application was suggested in NASA TN D-6273 (Ref. 39), which provides the basis for Sec. 8.3. In the lateral gust application, the airplane is constrained against roll. Despite the fact that typical Dutch roll motions involve roll angles of several times the yaw angles, this constraint seems to have little effect on the lateral gust loads. In other words, with respect to lateral gust loads, the Dutch roll mode is, in effect, a yaw mode. For some confirming Electra results, see FAA-ADS-53¹³ (p. 105).

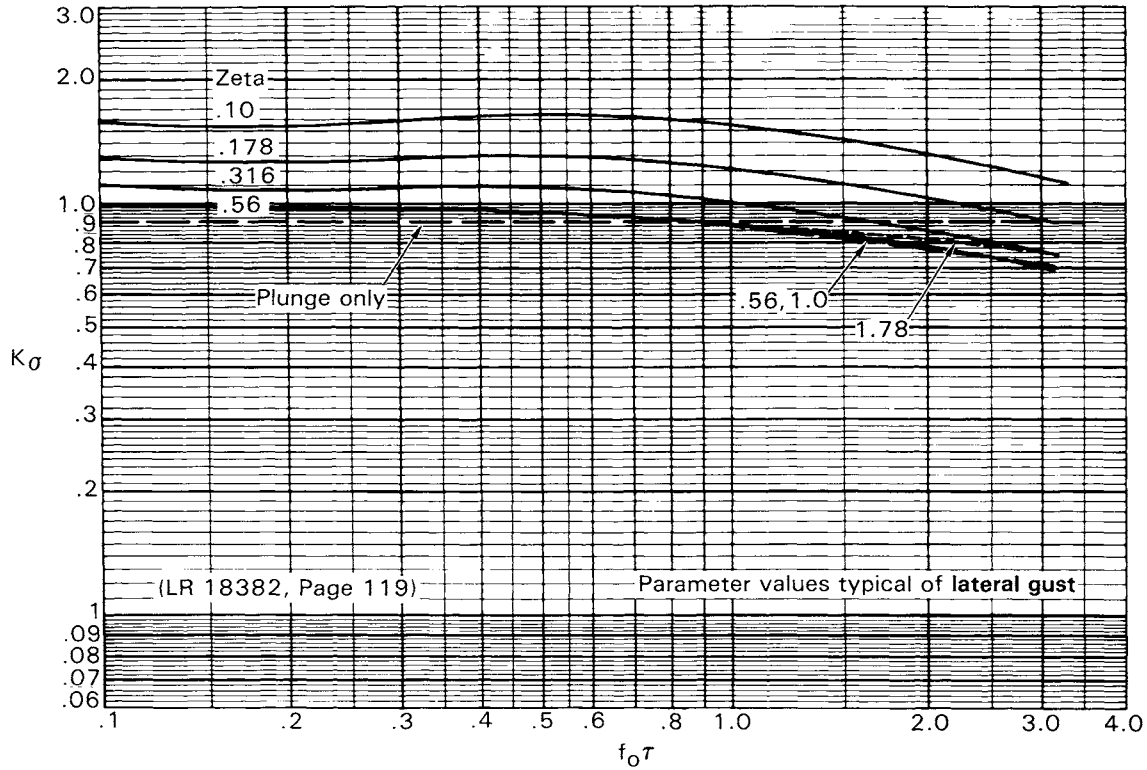


Fig. 8.6a Variation of gust-induced vertical load factor with $f_0 \tau$ and ζ : $\bar{c}/\delta = 0.0$, $\delta/L = 3.16$.

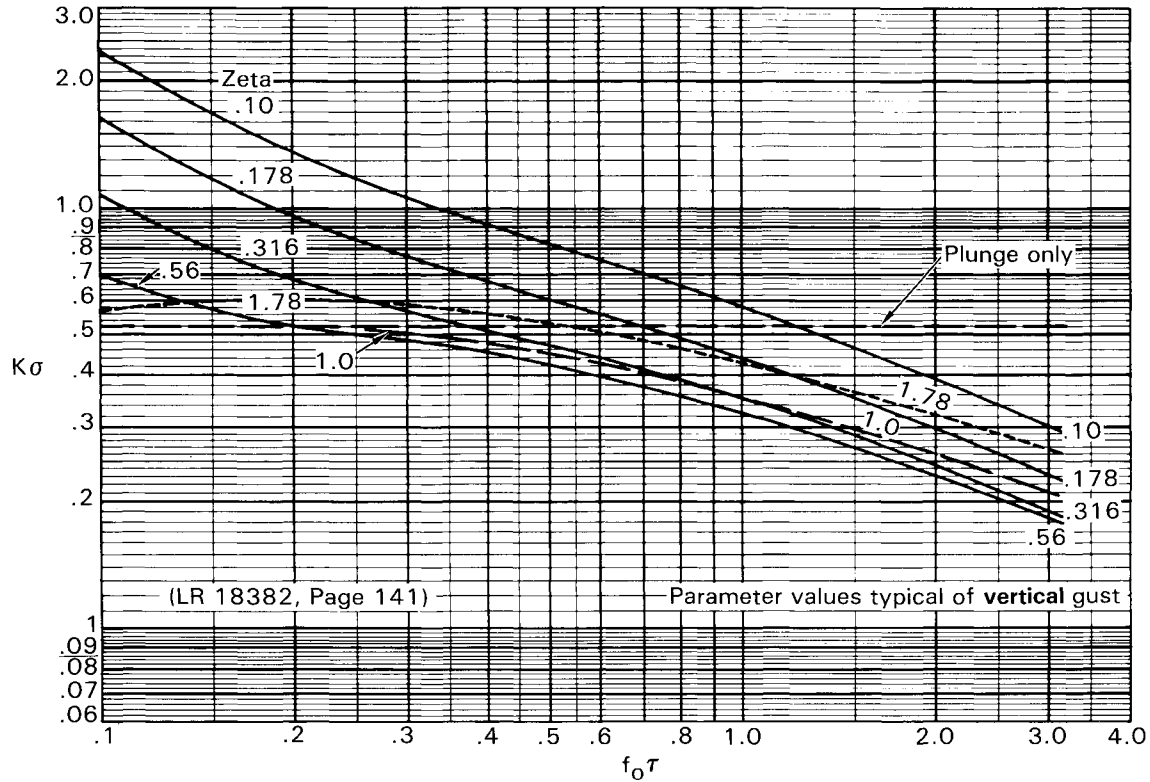


Fig. 8.6b Variation of gust-induced vertical load factor with $f_0\tau$ and ζ : $\bar{c}/\delta = 0.0316$, $\delta/L = 0.316$.

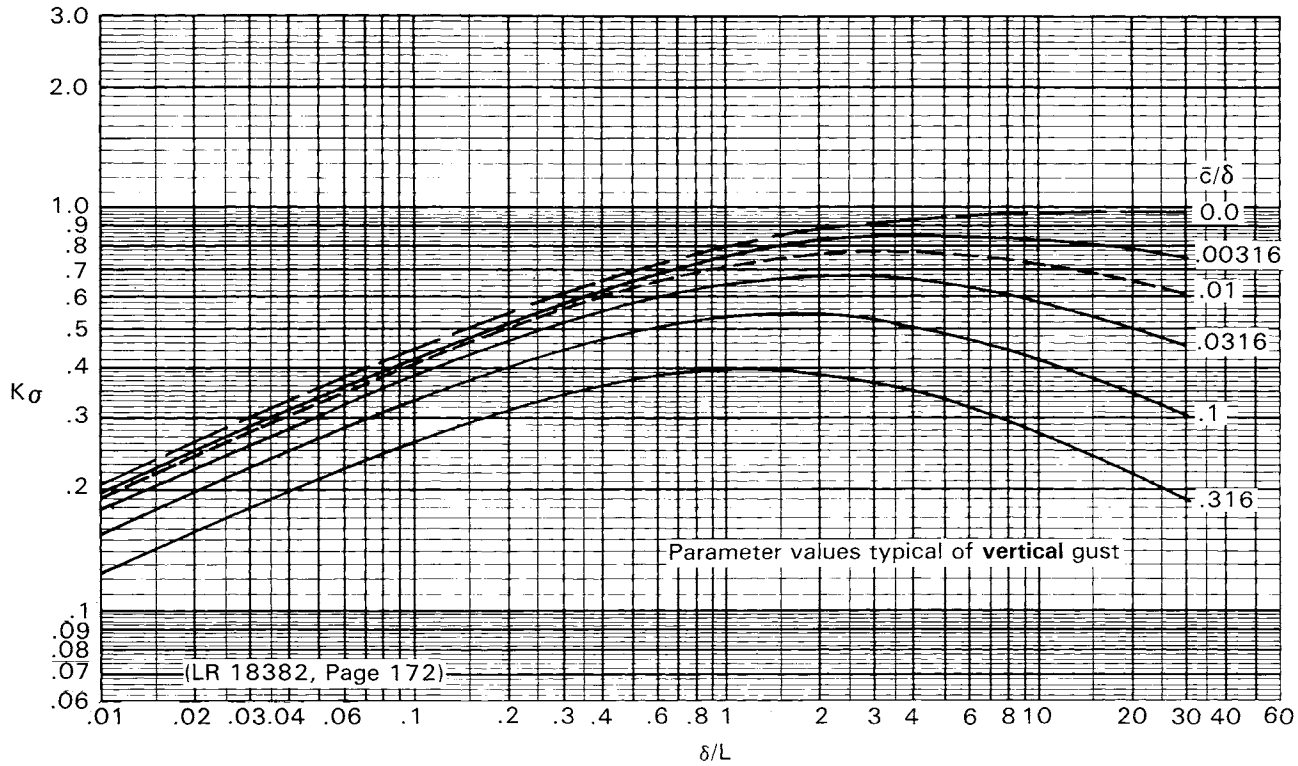


Fig. 8.6c Variation of gust-induced vertical load factor with δ/L and \bar{c}/δ : $f_0\tau = 0.159$, $\zeta = 1.00$ (same as plunge only).

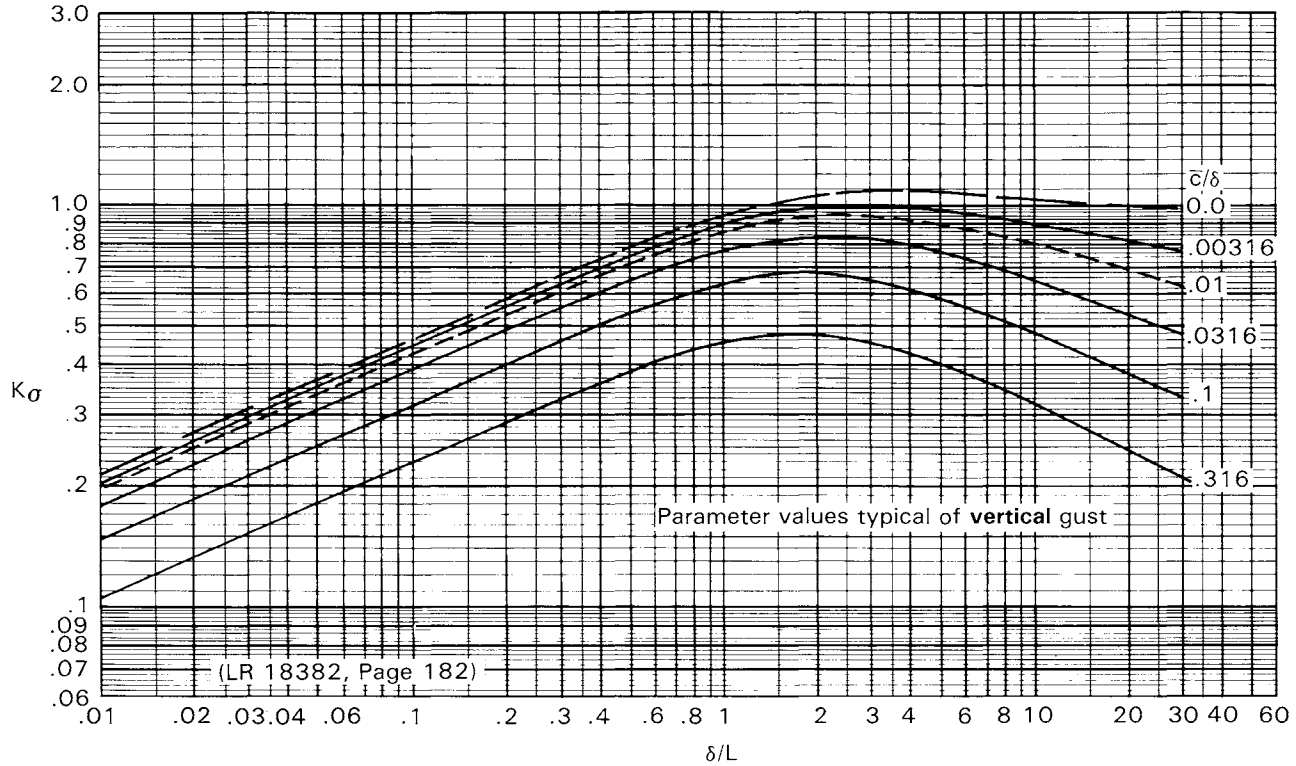


Fig. 8.6d Variation of gust-induced vertical load factor with δ/L and \bar{c}/δ : $f_0\tau = 0.316$, $\zeta = 0.316$.

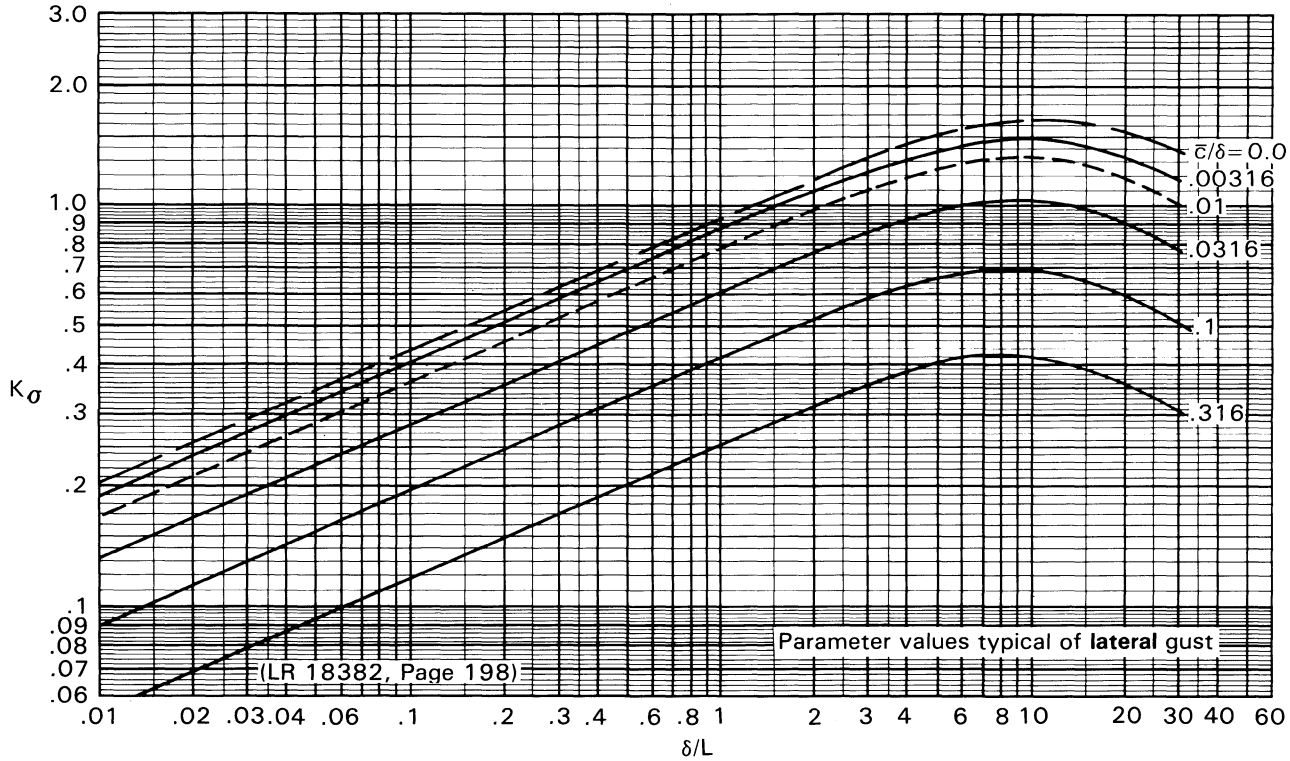


Fig. 8.6e Variation of gust-induced vertical load factor with δ/L and $\bar{c}/\delta: f_0\tau = 1.78, \zeta = 0.100$.

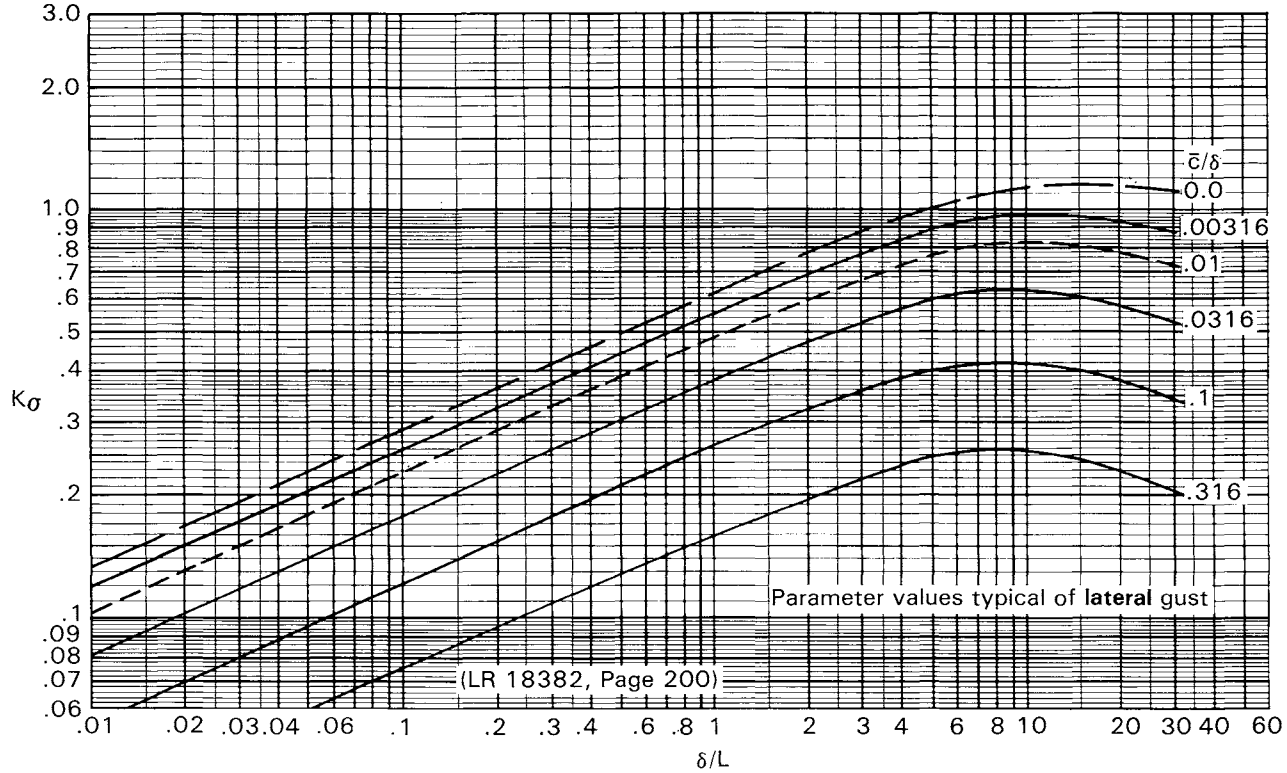


Fig. 8.6f Variation of gust-induced vertical load factor with δ/L and $\bar{c}/\delta: f_0\tau = 1.78, \zeta = 0.316$.

Plunge-only case. It is pointed out in NACA TN 3992³⁸ that for a certain combination of pitch parameters, K_o is the same as for plunge-only. This combination is defined by

$$f_0\tau = 1/2\pi = 0.159$$

$$\zeta = 1.00$$

The plunge-only case is included as a horizontal line on each of the first-format charts and as a separate sheet of the second-format set, Fig. 8.6c.

Typical values of parameters. Values of the parameters δ , τ , δ/L , c/δ , $f_0\tau$, and ζ for a number of representative airplanes and flight conditions are shown in Tables 8.1 and 8.2 for vertical and lateral gust, respectively.

PSD Shapes. The effects of parameter variations on the c.g. acceleration psd shapes are shown by the plots of Appendix K. A striking feature is the consistency of the curves between the plunge-only and free-to-pitch cases.

8.2.4 Procedure for Use of the Charts

The detailed procedure for use of the charts (Figs. 8.6a–f) can be summarized as follows:

- 1) Obtain the plunge-only distance constant,

$$\delta = \frac{2W}{\rho g S C_{L_\alpha}}$$

where

W = airplane weight, lb

ρ = air density, slug/ft³

g = acceleration due to gravity, 32.2 ft/s²

S = reference wing area, ft²

C_{L_α} = airplane lift-curve slope per rad [for lateral gust, substitute ($-C_{y\beta}$)]

The units of δ will be in ft.

- 2) Obtain the plunge-only time constant

$$\tau = \delta/V_T$$

where

$$V_T = \text{true airspeed, ft/s}$$

The units of τ will be seconds.

3) Obtain from any available source the short-period undamped natural frequency, f_0 , (cps) and relative damping ζ . For many purposes, estimates will suffice. These can be based on values for previous similar airplanes,

Table 8.1 Values of Parameters for Particular Airplanes: Vertical Gust

Airplane and flight regime	Flight condition		Airplane and condition data						Dimensional parameters				Nondimensional parameters				
	h , 1000 ft	V_e , knots	W , 1000 lb	S , ft ²	\bar{c} , ft	$C_{L\alpha}$ / rad	ρ , slug/ft ³	$\sqrt{\rho/\rho_0}$	$W/C_{L\alpha}S$	δ , ft ^a	τ , s ^b	f_0	ζ	$f_0\tau$	\bar{c}/δ	δ/L^c	\bar{c}/L^c
749 Cruise	15	200	89	1650	13.4	5.65	0.001496	0.793	9.55	400	0.94	0.38	0.76	0.36	0.034	0.16	0.0054
749 Descent	6	209	89	1650	13.4	5.65	0.001988	0.914	9.55	300	0.78	0.43	0.81	0.33	0.045	0.12	0.0054
188 Cruise	15	272	89	1300	14.0	5.60	0.001496	0.793	12.02	510	0.88	0.31	0.76	0.28	0.027	0.20	0.0056
L-1011 Cruise	28	320	302	3456	24.5	6.55	0.000958	0.635	13.33	865	1.017	0.27	0.58	0.27	0.028	0.35	0.0098
L-1011 Landing	0	133	302	3456	24.5	5.15	0.002378	1.000	16.97	443	1.972	0.124	0.58	0.25	0.055	0.18	0.0098
L-1011-3 (ACS) ^d	32	293	409	3456	24.5	6.85	0.000828	0.590	17.28	1296	1.545	0.23	0.50	0.36	0.0189	0.52	0.0098
U-2 ^e	62.5	116	15	600	8.4	6.8	0.000199	0.290	3.68	1149	1.701				0.0073	0.46	0.0034
Peele example	16.2	367	17.3	342	8.5	5.17	0.00143	0.775	9.78	425	0.531	0.523	0.29	0.28	0.0200	0.170	0.0034

^a $[2(W/C_{L\alpha}S)]/32.2\rho$ ^b $\sqrt{\rho/\rho_0}\delta/1.689V_e$ ^c $L = 2500$. ^dFlight condition DA-10 (cruise). ^eTypical of HICAT flights.

Note: c/δ and c/L are based on actual c . Use effective values 1/6 to 1/3 of actual value.

Table 8.2 Values of Parameters for Particular Airplanes: Lateral Gust

Airplane and flight regime	Flight condition			Airplane and condition data					Dimensional parameters					Nondimensional parameters			
	h , 1000 ft	V_e , knots	W , 1000 lb	S , ft ²	\bar{c} , ft	$C_{y\beta}$ / rad	ρ , slug/ft ³	$\sqrt{\rho/\rho_0}$	$W/C_y^\beta S$	δ , ft ^a	τ , s ^b	f_0	ζ	$f_0\tau$	$1\bar{c}/6\delta$	δ/L^c	$1c/6L$
L-1011 Cruise	28	320	302	3456	24.5	0.974	0.000958	0.635	89.7	5820	6.84	0.204	0.097	1.40	0.0007	2.33	0.0016
L-1011 Cruise ^d	28	320	302	3456	24.5	0.974	0.000958	0.635	89.7	5820	6.84	0.204	0.5	1.40	0.0007	2.33	0.0016

^a $[2(W/C_{L\alpha}S)]/32.2\rho$. ^b $\sqrt{\rho/\rho_0} \delta/1.689V_e$. ^c $L = 2500$. ^dWith yaw damper.

Note: Values for f_0 , ζ , and $f_0\tau$ are approximate.

possibly coupled with knowledge about required handling qualities. If computed values are required, they can be obtained from the expressions

$$f_0 = \frac{V_T \bar{c}}{\pi \bar{c} r} \sqrt{-\frac{\bar{c}}{4\delta C_{L\alpha}} \left(C_{m_z} + \frac{\bar{c}}{2\delta} C_{m_q} \right)} \quad (8.5)$$

$$\zeta = \frac{V_T}{4\pi\delta f_0} \left(1 - \frac{\bar{c}^2}{2r^2} \frac{C_{m_q} + C_{m_{\dot{z}}}}{C_{L\alpha}} \right) \quad (8.6)$$

where, in addition to the nomenclature previously introduced,

- C_m = pitching-moment coefficient, $M/qS\bar{c}$
- C_{m_α} = longitudinal static stability derivative, $\partial C_m/\partial\alpha$
- $C_{m_{\dot{\alpha}}}$ = pitching-moment coefficient per nondimensional unit rate of change of angle of attack

$$\partial C_m/\partial \left(\frac{\bar{c}\dot{\alpha}}{2V_T} \right)$$

C_{m_q} = pitch damping derivative

$$\partial C_m/\partial \left(\frac{\bar{c}\dot{\theta}}{2V_T} \right)$$

r = radius of gyration in pitch, ft

\bar{c} = mean aerodynamic chord, ft

The foregoing expressions are for vertical gust; for lateral gust, see Table 8.4, Sec. 8.3.

The evaluation of these stability derivatives should include the effect of stability augmentation devices or systems, if present.

- 4) Select a value of the effective chord \bar{c} . See Sec. 8.4.
- 5) Select a value of L , the scale of turbulence. Ordinarily, $L = 2500$ ft (except in military applications at altitudes below 2500 ft).
- 6) Evaluate the following quantities:

$$\delta/L \quad \bar{c}/\delta \quad f_0\tau$$

- 7) Enter the charts with δ/L , \bar{c}/δ , $f_0\tau$, and ζ and read K_σ .

Note that a two-dimensional interpolation between charts will be necessary. It is suggested that the first-format set of charts be used, and that in

interpolating on δ/L the dependent variable be converted to

$$\frac{K_\sigma}{(\delta/L)^{0.333}}$$

reflecting the slope of the curves in Figs. 8.6c and d at typical δ/L values of 0.2–0.5. (At the higher δ/L values within this range, the exponent might be reduced somewhat, e.g., to 0.25.)

8) Compute the gust sensitivity \bar{A}

$$\bar{A} = K_\sigma \frac{\rho V_T S C_{L_\alpha}}{2W} \quad (8.7)$$

or in shorter form

$$\bar{A} = K_\sigma \frac{V_T}{g\delta} \quad (8.8)$$

8.3 PLUNGE-PITCH CURVES: PEELE PARAMETERS

In NASA TN D-6273³⁹ Peele presents curves that are used in a somewhat different way than those of Fig. 8.6. Instead of reading K_σ directly as a function of four parameters, one reads two intermediate quantities, R_2 and R_4 , each as a function of three parameters only (the same three in each case). R_2 and R_4 are then combined in a simple formula to give K_σ . Inasmuch as R_2 and R_4 are insensitive to one of the three parameters, the lift growth parameter, R_2 and R_4 can each be read from a single sheet of curves. Thus, the computations may be facilitated—at least the interpolations should be easier—but the trends are obscured.

Peele gives curves not only for R_2 and R_4 but also R_0 and R_6 . With these four values he obtains not only \bar{A} but also N_0 , and not only for Δn but also for pitch angle, pitch rate, and pitch acceleration. The N_0 values should be more realistic than the values given by Fig. 8.2.

8.3.1 Procedure

The procedure for use of the Peele³⁹ curves is summarized in Table 8.3. This table references Table 8.4 and Fig. 8.7 for calculation of the parameters needed for use with the curves. The curves are shown in Figs. 8.8a–d. Table 8.3 then references Table 8.5 for the formulas used to combine R_1 , R_2 , R_3 , and R_4 to give the various \bar{A} 's and N_0 's.

The computational procedure defined in TN D-6273³⁹ has been modified in Tables 8.3–8.5, so that the computations are in terms of the parameters introduced in Sec. 8.2. The numerical results will be identical; but it is believed that mistakes are less likely because the various quantities have a more obvious physical significance.

Table 8.3 Steps in Obtaining \bar{A} and N_0 Using Peele Curves

Step	Vertical gust	Lateral gust
1) Collect airplane data	S = Reference wing area c = Reference wing <i>chord</i> r = Radius of gyration in <i>pitch</i> ^a W = Gross weight h = Altitude ρ = Density V_T = True airspeed M = Mach number L = Scale of turbulence $C_{L\alpha}, C_{m\alpha}, C_{m\dot{\alpha}}, C_{m\ddot{\alpha}}$ ^a	S = Reference wing area c = Reference wing <i>span</i> r = Radius of gyration in <i>yaw</i> ^a W = Gross weight h = Altitude ρ = Density V_T = True airspeed M = Mach number L = Scale of turbulence $C_{y\beta}, C_{n\beta}, C_{nr}$ ^a
2) Calculate ^b	δ f_0 ζ $\tau = \delta/V$ $f_0\tau$ δ/L sk_0 $\ddot{\alpha}k_0$ $V_T/g\delta$ B_1 B_2	δ f_0 ζ $\tau = \delta/V$ $f_0\tau$ δ/L sk_0 $\ddot{\alpha}k_0$ $V_T/g\delta$ B_1 B_2
3) Read	R_0, R_2, R_4, R_6 as required, Fig. 8.8	R_0, R_2, R_4, R_6 as required, Fig. 8.8
4) Calculate	\bar{A} and N_0 as required, Table 8.5	\bar{A} and N_0 as required, Table 8.5

^aNeeded only if f_0 and ζ not available from other sources.

^bNumerical values will be different for vertical and lateral gust.

 □ = Quantities needed for reading R values from Fig. 8.8.

 ○ or ○ = Quantities needed, in addition to R , for calculating \bar{A} and N_0 values using formulas of Table 8.5.

Table 8.4 Formulas for Stability Characteristics and Other Constants Needed for Use with Peele Curves

Quantity	Longitudinal, vertical gust	Lateral, lateral gust
δ Translational response distance constant	$\frac{2W}{\rho g S C_{L_x}}$	$\frac{2W}{\rho g S (-C_{y\beta})}$
τ Translational response time constant	δ/V_T	δ/V_T
f_0 Undamped natural frequency	$\frac{V_T \bar{c}}{\pi \bar{c} r} \sqrt{-\frac{\bar{c}}{4\delta C_{L_x}} \left(C_{m_x} + \frac{\bar{c}}{2\delta} C_{m_q} \right)}$	$\frac{V_T b}{\pi b r} \sqrt{-\frac{b}{4\delta (-C_{y\beta})} \left(-C_{n_\beta} + \frac{b}{2\delta} C_{n_r} \right)}$
ζ Relative damping constant	$\frac{V_T}{4\pi \delta f_0} \left(1 - \frac{\bar{c}^2}{2r^2} \frac{C_{m_q} + C_{m_z}}{C_{L_x}} \right)$	$\frac{V_T}{4\pi \delta f_0} \left[1 - \frac{b^2}{2r^2} (-C_{y\beta}) \right]$
B_1^a	$4 \left(\zeta - \frac{1}{4\pi f_0 \tau} \right)^2$	$4 \left(\zeta - \frac{1}{4\pi f_0 \tau} \right)^2$
B_2^b	$\frac{2\zeta}{2\pi f_0 \tau} - \frac{1}{(2\pi f_0 \tau)^2} - 1$	$\frac{2\zeta}{2\pi f_0 \tau} - \frac{1}{(2\pi f_0 \tau)^2} - 1$
sk_0	$2\pi \frac{f_0 \tau}{\delta/L}$	$2\pi \frac{f_0 \tau}{\delta/L}$

^aFor the plunge-only case, $B_1 = 1$ and $B_2 = 0$.

^bThe expression given here for B_2 may be in error. Both it and the expression in Ref. 39 from which it was derived give negative values of \bar{A} when reasonable airplane data are used as input.

Note: All quantities will have different numerical values for vertical and lateral gust response.

Note: The stability derivatives will normally have the following signs:

$$C_{L_x} \text{ pos} \quad C_{y\beta} \text{ neg}, \quad C_{m_x} \text{ neg} \quad C_{n_\beta} \text{ pos}, \quad C_{m_q} \text{ neg} \quad C_{n_r} \text{ neg}, \quad C_{m_z} \text{ neg.}$$

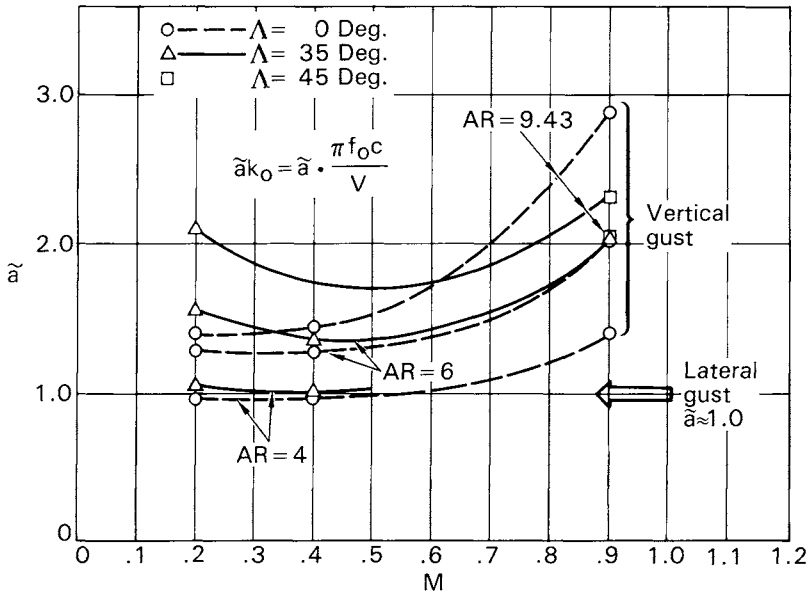


Fig. 8.7 Values of Kussner parameter \tilde{a} .

Table 8.5 Response Formulas for Use with Peele Curves

Quantity	\bar{A}	N_0
C.g. Load factor	$\bar{A}_{\Delta n} = V/g\delta\sqrt{R_4 + B_1R_2}$	$N_{0\Delta n} = f_0\sqrt{\frac{R_6 + B_1R_4}{R_4 + B_1R_2}}$
Pitch or yaw angle	$\bar{A}_{\theta,\psi} = (1/V)B_2\sqrt{R_0}$	$N_{0\theta,\psi} = f_0\sqrt{R_2/R_0}$
Pitch or yaw rate	$\bar{A}_{\dot{\theta},\dot{\psi}} = (2\pi f_0/V)B_2\sqrt{R_2}$	$N_{0\dot{\theta},\dot{\psi}} = f_0\sqrt{R_4/R_2}$
Pitch or yaw acceleration	$\bar{A}_{\ddot{\theta},\ddot{\psi}} = (2\pi f_0)^2/V\sqrt{R_4}$	$N_{0\ddot{\theta},\ddot{\psi}} = f_0\sqrt{R_6/R_4}$

Note: $V/g\delta$ is the sharp-edge gust response, which is also given by $\rho V_7 SC_{L\alpha}/2W$.

$R_0, R_2, R_4,$ and R_6 are integrals read from Fig. 8.8. B_1 and B_2 are constants given by the formulas of Table 8.4.

$R_0, R_2, R_4, R_6, B_1, B_2, \delta,$ and f_0 will have different numerical values for vertical and lateral gust response.

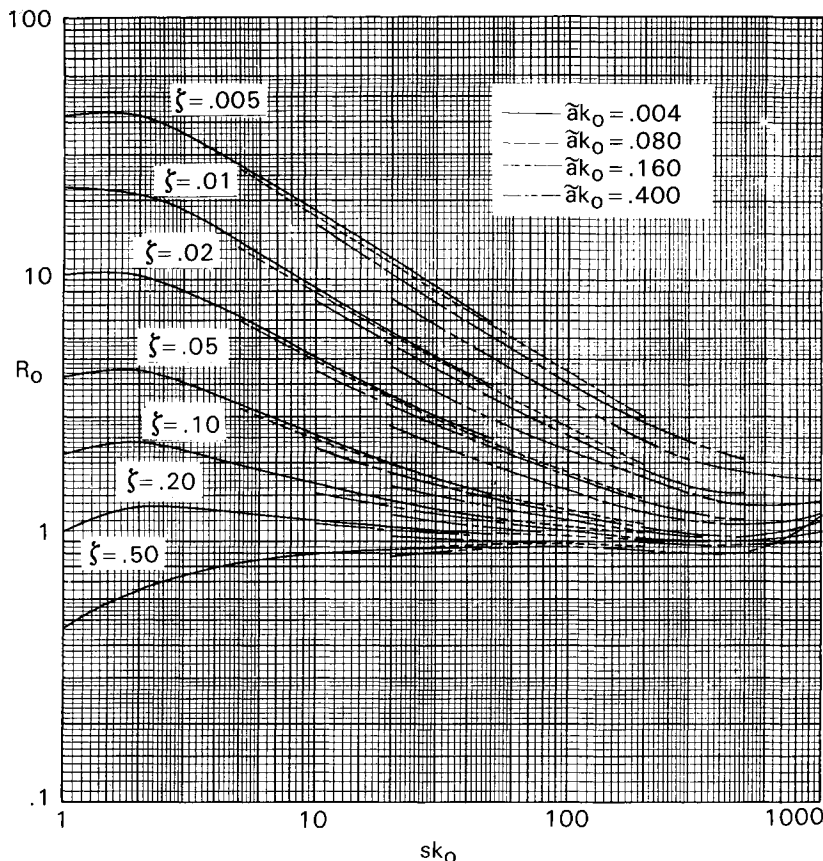


Fig. 8.8a Peele response integrals: R_0 (TN D-6273³⁹, Fig. 1).

8.3.2 Lift Growth Assumptions

Although Peele still neglects the Wagner effect—that is, the lag in the buildup of lift due to airplane motions—his treatment of the Kussner effect is much more realistic than that reflected in the FAA-ADS-53¹³ plunge-only curves (Fig. 8.1) and the LR 18382 curves (Fig. 8.6).

This treatment is shown in Fig. 8.9. The factor $|\phi(k)|^2$ by which the psd is reduced by the unsteady lift effect is calculated theoretically for several planforms and Mach numbers, and the curves are approximated by exponential functions. The coefficient of k in the exponent required to give a match for each case is tabulated in TN D-6273³⁹; these tabulated values are plotted in Fig. 8.7.

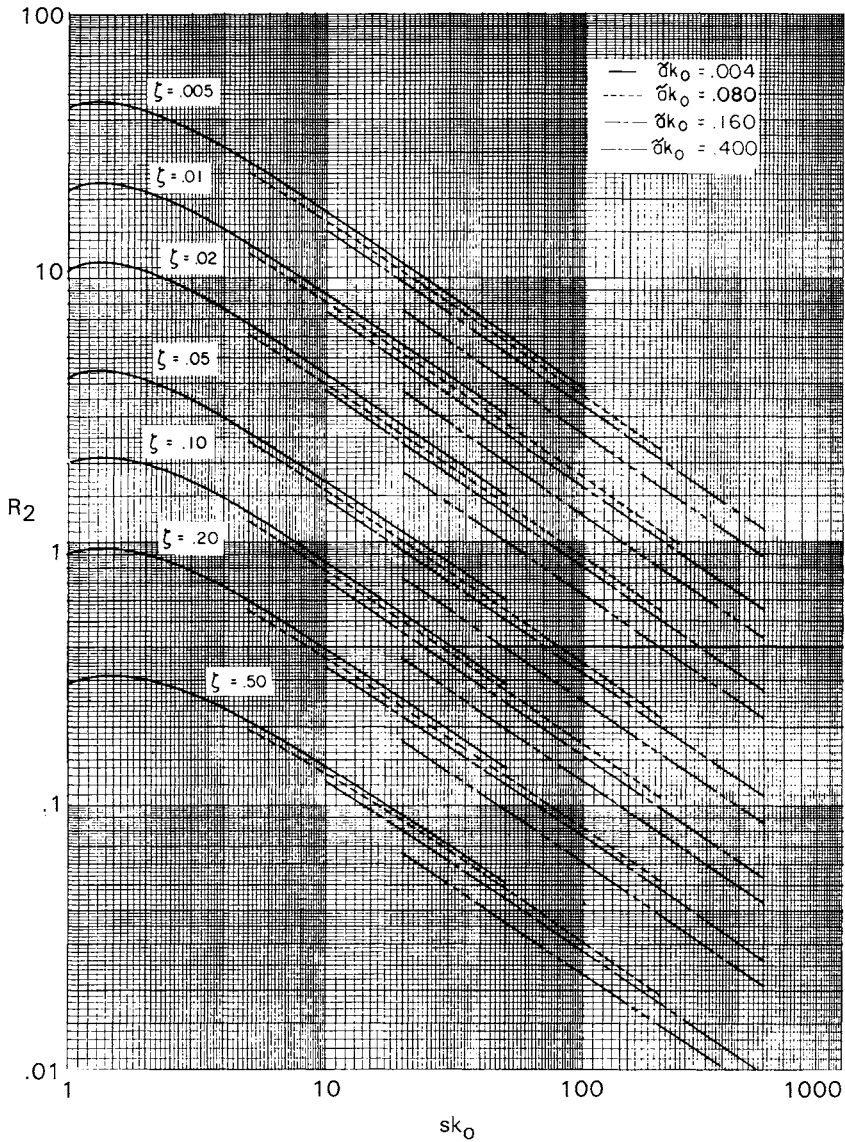


Fig. 8.8b Peeler response integrals: R_2 (TN D-6273³⁹, Fig. 2).

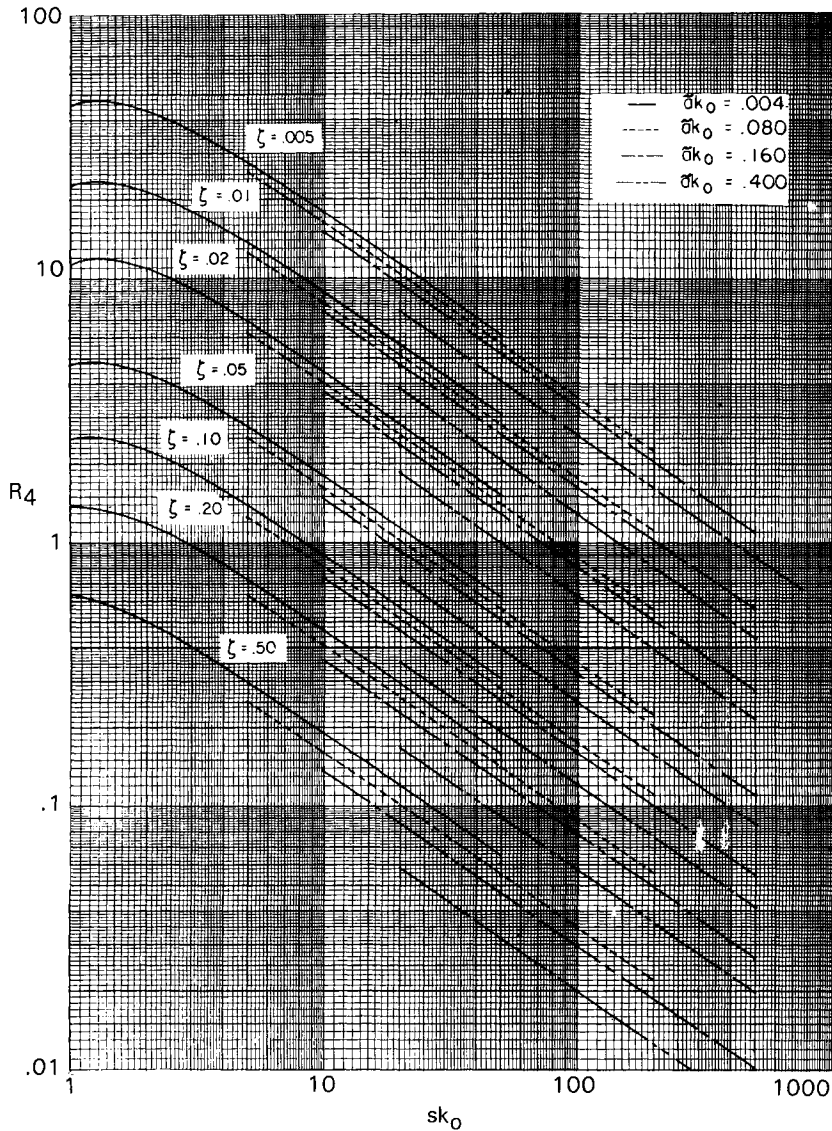


Fig. 8.8c Peelle response integrals: R_4 (TN D-6273³⁹, Fig. 3).

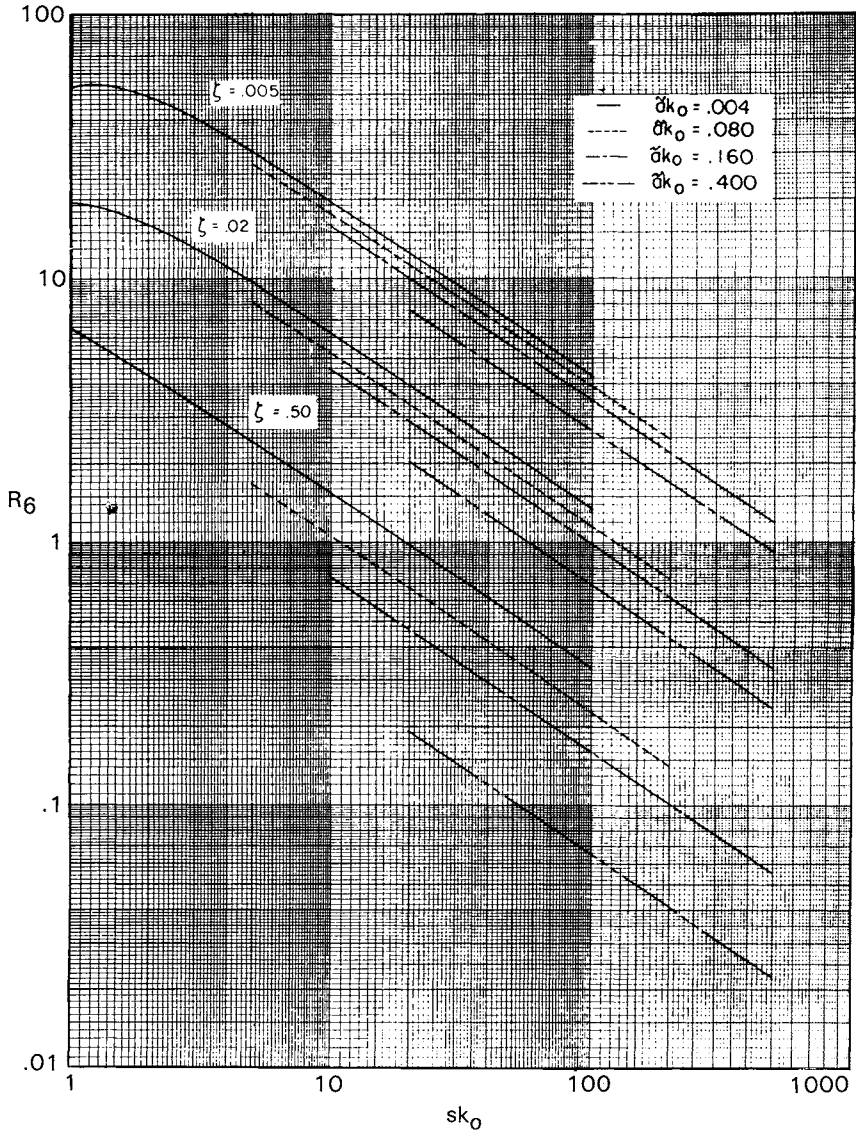


Fig. 8.8d Pelee response integrals: R_6 (TN D-6273³⁹, Fig. 4).

Downloaded by RMIT UNIV BUNDOORA on June 4, 2013 | http://arc.aiaa.org | DOI: 10.2514/4.861888

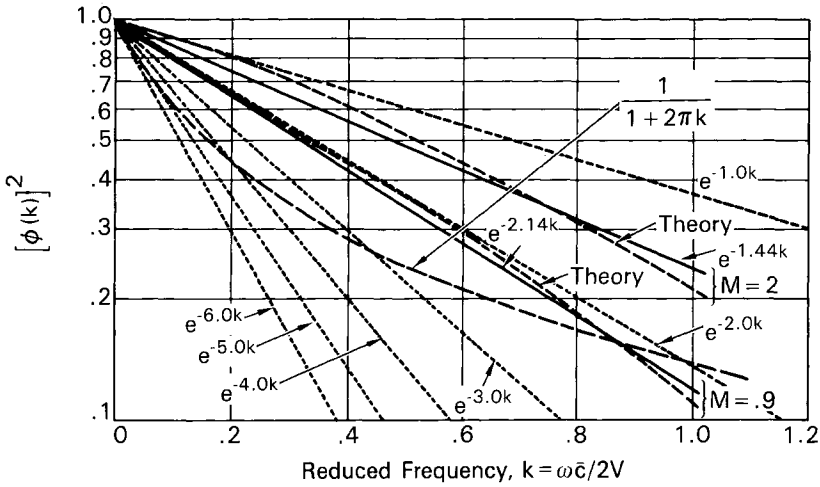


Fig. 8.9 Comparison of approximations for $|\phi(k)|^2$.

8.3.3 Relation of Peele Parameters to Hoblit Parameters

For reference, the various parameters appearing in TN D-6273³⁹ are defined in terms of the Hoblit parameters:

$$k_0 = \frac{\pi f_0 \bar{c}}{V_T} = \pi f_0 \tau (\bar{c} / \delta) \quad (8.9a)$$

$$\gamma = 4\pi f_0 \tau \zeta \quad (8.9b)$$

$$s = \frac{2}{\bar{c}/L} = 2[(\delta/L)(\bar{c}/\delta)] \quad (8.9c)$$

$$sk_0 = 2\pi \frac{f_0 \tau}{\delta/L} \quad (8.9d)$$

$$\tilde{a}k_0 = \tilde{a} \frac{\pi f_0 \bar{c}}{V_T} = \tilde{a} \pi f_0 \tau (\bar{c} / \delta) \quad (8.9e)$$

$$\kappa = 4\mu = 4\delta / \bar{c} \quad (8.9f)$$

8.4 QUALITATIVE RELATIONS BETWEEN PEELE AND $1/(1 + 2\pi k)$ LIFT GROWTH ASSUMPTIONS AND DEFINITION OF AN EFFECTIVE \bar{c} FOR USE IN SECS. 8.1.1 AND 8.2

In order to compare the Peele factor for lift growth due to gust penetration (Fig. 8.9) with the $1/(1 + 2\pi k)$ factor used in generating Figs. 8.1 and 8.6, the $1/(1 + 2\pi k)$ factor has been added to Fig. 8.9. In this figure, the Peele assumption is shown by the family of short-dashed lines. The quantity \bar{a} used in the Peele approach is the coefficient of k in the exponent. The $1/(1 + 2\pi k)$ assumption, used widely in the past and, in particular, in computing the curves of Figs. 8.1 and 8.6, is given by the long-dash line.

First, to gain perspective, the following two observations can be made:

- 1) Typical values of \bar{a} are seen from Fig. 8.7 to lie in the range 1.0–2.0.
- 2) The most important frequencies are those in the vicinity of the airplane longitudinal short-period natural frequency, typically at about 0.25–0.50 Hz. This corresponds roughly to a k of 0.02–0.05 in Fig. 8.9. For example, with $\bar{c} = 25$ ft, $V = 800$ fps, and $f_0 = 0.25$ Hz,

$$k = \frac{\omega \bar{c}}{2V} = \frac{2\pi(0.25)(25)}{2(800)} = 0.025$$

With $\bar{c} = 15$ ft, $V = 600$ fps, and $f_0 = 0.50$ Hz,

$$k = \frac{\omega \bar{c}}{2V} = \frac{2\pi(0.50)(15)}{2(600)} = 0.04$$

It is seen that in this frequency range, even with $\bar{a} = 2.0$, the long-dash line overpredicts the reduction in lift relative to the short-dash line by something like a factor of 3. Conversely, to produce agreement would require a factor of 3 increase in \bar{a} for the short-dash lines or a factor of 3 shift to the right of the long-dash line. This shift to the right of the long-dash line would be equivalent to an effective \bar{c} of $1/3$ of the actual.

More specifically, to obtain the value of \bar{a} that corresponds to the $1/(1 + 2\pi k)$ lift growth assumption: 1) Select the value of k at which agreement is desired; 2) Find the short-dash line that intersects the long-dash line at this value of k ; and 3) The coefficient of k in the exponent is the desired \bar{a} ; this will be designated \bar{a}' .

Example: $f = 0.5$ Hz, $V = 600$ fps, $\bar{c} = 15$ ft

$$k = \frac{\omega \bar{c}}{2V} = \frac{2\pi(0.5)(15)}{2(600)} = 0.04$$

$$\bar{a}' \approx 6$$

To obtain the *effective chord* for use with the $1/(1 + 2\pi k)$ lift growth assumption to match a desired value of \tilde{a}' as read from Fig. 8.7: 1) Select k at which agreement is desired; 2) Enter the curves (Fig. 8.9) with this k and obtain \tilde{a}' as described; and 3) Obtain effective \tilde{c} as

$$\tilde{c}_{\text{eff}} = \tilde{c} \frac{\tilde{a}}{\tilde{a}'}$$

Example:

$$k = 0.04, \quad \tilde{a} = 2$$

Entering Fig. 8.9 with

$$k = 0.04, \quad \tilde{a}' \approx 6,$$

we obtain

$$\tilde{c}_{\text{eff}} = \tilde{c} \frac{\tilde{a}}{\tilde{a}'} = \frac{2}{6} \tilde{c} = \frac{1}{3} \tilde{c}$$

Inasmuch as the value of k at which agreement is desired is usually very small—for example, 0.02–0.05—the long-dash curve can be approximated by its initial tangent

$$|\phi(k)|^2 = \frac{1}{1 + 2\pi k}$$

$$\frac{d}{dk} |\phi(k)|^2 = \frac{(-1)(2\pi)}{(1 + 2\pi k)^2}$$

$$\text{At } k = 0, \quad \frac{d}{dk} |\phi(k)|^2 = -2\pi$$

The initial slope of the curve

$$|\phi(k)|^2 = e^{-\tilde{a}k}$$

is $-\tilde{a}$.

Therefore, the short-dash line with the same initial tangent as the long-dash line is given by

$$\tilde{a} = 2\pi$$

As a result, \tilde{a} can be taken as 6.28 or rounded off to 6. Thus,

$$\bar{c}_{\text{eff}} = \bar{c} \frac{\tilde{a}}{6.28} \quad (8.10a)$$

or
$$\bar{c}_{\text{eff}} = \bar{c} \frac{\tilde{a}}{6} \quad (8.10b)$$

With the effective and actual \bar{c} 's differing by a factor of 3 or more, one might wonder why the original $1/(1 + 2\pi k)$ expression is so much in error. Much of the answer lies in the fact that, in Liepmann's 1952 paper,¹² the comparison of the approximate expression with the available theoretical curve is plotted (in Fig. 1, Ref. 12) over a linear scale from $k = 0$ to $k = 8$. The fit is indeed fairly good over the range $k = 0.3$ to $k = 8$. But over the important range $k = 0.02$ to $k = 0.05$, the curves are so steep that all accuracy in reading the curves is lost. The approximate curve, however, is clearly lower than the theoretical curve. It could conceivably be enough lower to fully explain the discrepancy.

8.5 USE OF PLUNGE-PITCH CURVES TO GIVE PLUNGE-ONLY DATA

The choice of parameters utilized for the plunge-pitch curves in Sec. 8.2 is equally advantageous when the simplicity of a plunge-only analysis is desired.* In this case, $f_0\tau$ and ζ are dropped, leaving as parameters δ/L and \bar{c}/δ . Figure 8.6c by itself then provides the necessary data. The same data, on expanded linear coordinates (but less accurately plotted), are shown in Fig. 8.5.

If a chart such as Fig. 8.5 or Fig. 8.6c is to be used for a single airplane, then \bar{c} and L are both constant and the family of curves shown can be replaced by a single curve, giving K_σ as a function only of δ . This approach has been used at the Lockheed-California Company to infer rms gust velocities from c.g. accelerations measured in operational flight.

8.6 USE OF SIMPLIFIED EQUATIONS OF MOTION

The curves presented in Secs. 8.2 and 8.3 are based on what Houbolt refers to in AFFDL TR-75-121⁴⁰ as a stability derivative approach. He contends that this approach may be excessively inaccurate as a result of ignoring effects such as the following: 1) The time lag associated with the tail encountering the gust at a later time than the wing; 2) Unsteady lift due to airplane

*Determination of probability distributions of σ_w from operational data on c.g. acceleration exceedances (Sec. 4.8) might be such an application.

motion as well as gust penetration; 3) Unsteady downwash on the tail; and 4) Finite span effects on unsteady lift.

With these effects included, too many parameters are involved to permit presolving the equations to construct charts such as those of Figs. 8.6 and 8.8. Instead, Houbolt develops the equations of motion in a form that can readily be solved with a minimum of both human effort and computer cost. An unswept wing is assumed. These equations are presented in AFFDL TR-75-121.⁴⁰ They have been programmed at NASA and we understand that the program is available to others on request.*

8.7 EMPIRICAL ADJUSTMENTS

In using the charts of Secs. 8.1, 8.2, or 8.3 for loads estimation, empirical factors can be applied to the resulting accelerations or loads to account for effects known not to have been included in the theory.

8.7.1 Gust Penetration

Experience indicates that for a conventional swept-wing subsonic transport, the gust penetration effect increases the loads approximately in the ratio 1:10. It is not known how much of this increase is due to the wing sweep, how much is due to the lift on the nose, and how much is due to the lag between wing and tail. Only the last of these three effects is accounted for in the method of Sec. 8.6.

8.7.2 Wagner Effect

The factor of increase needed to account for the assumption of instantaneous lift buildup due to airplane motions (Secs. 8.1.1, 8.2, 8.3) is not known. At one time, it was thought that to account for the combined effect of the $1/(1 + 2\pi k)$ Kussner treatment and omission of a Wagner effect would require an increase in the loads of roughly 8%, but the source of this number is no longer available. The Wagner effect alone might be half of this or less.

8.7.3 Elastic-Mode Dynamic Effects

Dynamic factors for various airplanes, components, and load quantities are shown in Fig. 8.10. These, together with similar data from other sources, may provide a useful guide.

It might be remarked that if the material in Chapter 8 is to be used to obtain airplane *loads* rather than just *load factors*, the loads will be determined from the load factors by conventional static loads methods. The actual procedure should be one that is appropriate to gust load rather than maneuver load determination; for the same load factor, the wing shears and

*The user of Houbolt's equations should be cautioned that considerable care may be required to properly convert between the nondimensional forms used in the equations and the dimensional forms that have meaning for real airplanes in real turbulence.

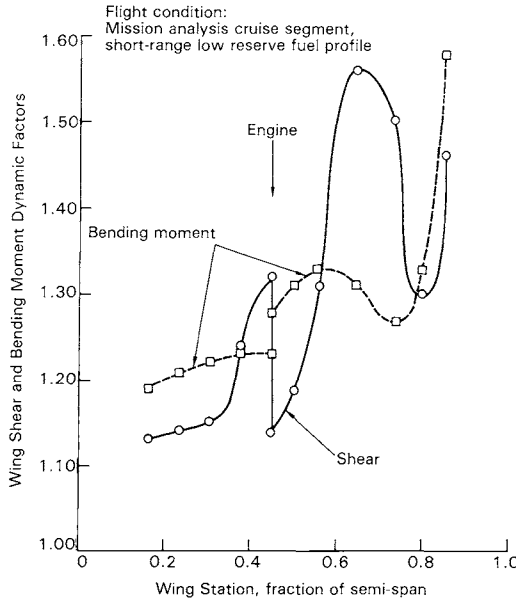


Fig. 8.10a Sample dynamic factors for gust loads: L-1011 wing.

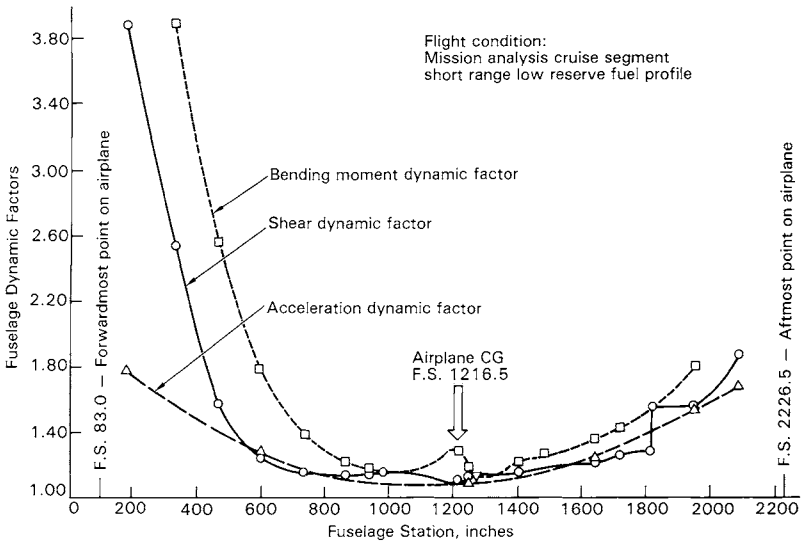


Fig. 8.10b Sample dynamic factors for gust loads: L-1011 fuselage.

SHORT-CUT METHODS

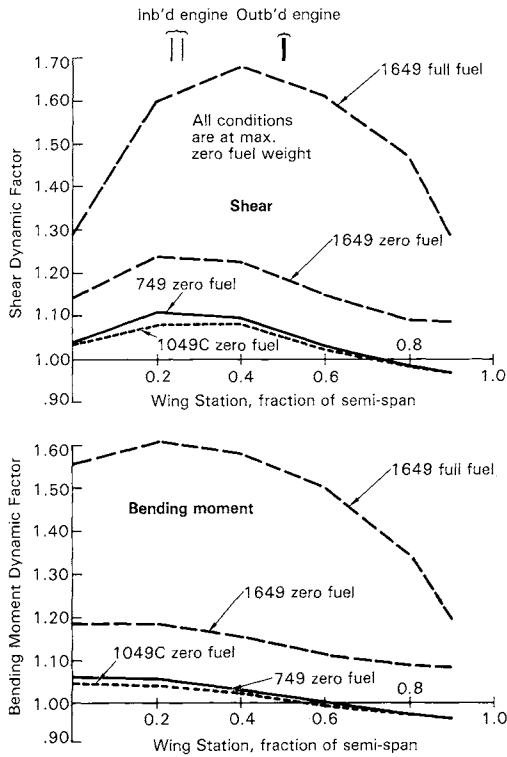


Fig. 8.10c Sample dynamic factors for gust loads: Constellation wing.

bending moments may be 10–15% lower for gust than for maneuver, as a result of differences in tail load.

Problems

In these problems, use the following airplane and gust data as needed.

Airplane geometry:

$S = 1850 \text{ ft}^2$

$MAC = 13.3 \text{ ft}$

$b = 150 \text{ ft}$

Flight condition:

$GW = 116,000 \text{ lb, c.g. } 25\% \text{ MAC}$

$V = 261 \text{ KEAS}$

$h = 20,000 \text{ ft}$

Derived Data:

$$M = 0.58$$

$$V_T = (261)(1.689) \frac{1}{0.730} = 604 \text{ fps}$$

$$\mathcal{R} = b^2/S = 150^2/1850 = 12.2$$

$$\rho = 0.001267 \text{ lb s}^2/\text{ft}^4$$

$$q = \frac{261^2}{295} = 231 \text{ lb/ft}^2$$

$$C_L = \frac{W}{qS} = \frac{116,000}{(231)(1850)} = 0.271$$

Moments of inertia:

$$I_{xx} = 7.4 \times 10^9 \text{ lb in.}^2$$

$$I_{yy} = 7.3 \times 10^9 \text{ lb in.}^2$$

$$I_{zz} = 13.9 \times 10^9 \text{ lb in.}^2$$

Aero data:

$$C_{L_\alpha} = 0.115/\text{deg} = 6.56/\text{rad}$$

$$C_{m_\alpha} = -1.75$$

$$C_{m_q} = -41.9$$

$$C_{m_{\dot{\alpha}}} = -12.9$$

$$C_{y_\beta} = -0.562/\text{rad}$$

$$C_{n_\beta} = 0.0860/\text{rad}$$

$$C_{n_r} = -0.116$$

8.1 Determine \bar{A} and N_0 for the given airplane and flight condition, assuming the airplane free to plunge only. Use the curves of Figs. 8.1 and 8.2. Take $L = 2500$ ft.

8.2 Determine \bar{A} for the given airplane and flight condition using the plunge-pitch curves of Fig. 8.6. Take $L = 2500$ ft. If you need guidance, see the complete solution given below for Problem 8.3. (If you have trouble calculating f_0 and ζ , take $f_0 = 0.463$ Hz and $\zeta = 0.60$.)

8.3 Determine \bar{A} for c.g. n_y (lateral gust) for the given airplane and flight condition using the curves of Fig. 8.6. Take $L = 2500$ ft. Repeat, assuming that a yaw damper is installed that increases ζ from 0.153–0.56.

Solution:

$$\begin{aligned} \delta &= \frac{2W}{\rho g S (-C_{y_\beta})} = \frac{(2)(116,000)}{(0.001267)(32.2)(1850)(0.562)} \\ &= 5470 \text{ ft} \end{aligned}$$

Downloaded by RMIT UNIV BUNDOORA on June 4, 2013 | http://arc.aiaa.org | DOI: 10.2514/4.861888

SHORT-CUT METHODS

$$\tau = \delta / V_T = 5470 / 604 = 9.06 \text{ s}$$

$$r = \sqrt{\frac{I_{zz}}{W}} = \sqrt{\frac{13.9 \times 10^9}{116,000}} = 346 \text{ in.} = 28.8 \text{ ft}$$

$$f_0 = \frac{V_T b}{\pi b r} \sqrt{-\frac{b}{4\delta(-C_{y\beta})} \left(-C_{n\beta} + \frac{b}{2\delta} C_{nr}\right)}$$

$$= \frac{604}{\pi(150)} \frac{150}{28.8} \sqrt{-\frac{150}{(4)(5470)(0.562)} \left[-0.0860 + \frac{150}{(2)(5470)} (-0.116)\right]}$$

$$= 0.218 \text{ Hz}$$

$$\zeta = \frac{V_T}{4\pi\delta f_0} \left[1 - \frac{b^2}{2r^2} \frac{C_{nr}}{(-C_{y\beta})}\right]$$

$$= \frac{604}{4\pi(5470)(0.218)} \left[1 - \frac{1}{2} \left(\frac{150}{28.8}\right)^2 \left(\frac{-0.116}{0.562}\right)\right]$$

$$= 0.153 \quad \leftarrow$$

$$f_0\tau = (0.218)(9.06) = 1.97 \quad \leftarrow$$

$$\bar{c}/\delta = 13.3/5470 = 0.00243 \quad \leftarrow$$

$$\delta/L = 5470/2500 = 2.19 \quad \leftarrow$$

We now use the curves of Fig. 8.6 to find K_σ . The numbers identified by arrows are those needed for entering Fig. 8.6.

First, from Fig. 8.6e for which $f_0\tau = 1.78$ and $\zeta = 0.10$, enter with the given values of \bar{c}/δ and δ/L and read

$$K_\sigma = 1.15$$

Then ratio to the actual values of $f_0\tau$ and ζ by using Fig. 8.6a, for which $\bar{c}/\delta = 0$ and $\delta/L = 3.16$. Going from

$$\left\{ \begin{array}{l} f_0\tau = 1.78 \\ \zeta = 0.10 \end{array} \right\} \quad \text{to} \quad \left\{ \begin{array}{l} f_0\tau = 1.97 \\ \zeta = 0.153 \end{array} \right\}$$

K_σ goes from 1.36 to 1.10; that is, decreases in the ratio 1.10/1.36. The final value of K_σ is then (approximately)

$$K_\sigma = 1.15 \frac{1.10}{1.36} = 0.93$$

Now, compute \bar{A}

$$\begin{aligned}\bar{A} &= \frac{V_T}{g\delta} K_\sigma = \frac{604}{(32.2)(5470)} (0.93) = (0.00343)(0.93) \\ &= 0.00319 \text{ g/fps}\end{aligned}$$

If ζ increases from 0.153–0.56 as the result of adding a yaw damper, the factor of decrease in K_σ can be determined approximately from Fig. 8.6a, entering with $f_0\tau = 1.97$.

K_σ is seen to decrease in the ratio $0.78/1.10 = 0.71$, or from 0.93 to 0.66. \bar{A} decreases in the same ratio, from 0.00319 to 0.00226 g/fps. If Fig. 8.6b were used instead of Fig. 8.6a, the ratio of decrease would have been $0.23/0.32 = 0.72$, surprisingly close to the value 0.71 obtained using the more appropriate figure.

8.4 Determine \bar{A} and N_0 for c.g. n_z for the given airplane and flight condition using the Peele curves. Take $L = 2500$ ft. (If you need guidance, see the complete solution given below for Problem 8.5. If you have trouble calculating f_0 and ζ , take $f_0 = 0.463$ Hz and $\zeta = 0.60$.)

8.5 Determine \bar{A} and N_0 for c.g. n_y (lateral gust) for the given airplane and flight condition using the Peele curves. Take $L = 2500$ ft.

Solution:

Follow the procedure outlined in Table 8.3

$$S = 1850$$

$$b = 150$$

$$r = \sqrt{\frac{I_{zz}}{W}} = \sqrt{\frac{13.9 \times 10^9}{116,000}} = 346 \text{ in.} = 28.8 \text{ ft}$$

$$W = 116,000 \text{ lb}$$

$$h = 20,000 \text{ ft}$$

$$\rho = 0.001267 \text{ lbs}^2/\text{ft}^4$$

$$V_T = 604 \text{ fps}$$

$$M = 0.58$$

$$L = 2500 \text{ ft}$$

$$C_{y\beta} = -0.562 \quad C_{n\beta} = 0.0860 \quad C_{n_r} = -0.116$$

SHORT-CUT METHODS

Calculate using formulas given in Table 8.4:

$$\delta = \frac{2W}{\rho g S (-C_{y\beta})} = \frac{2(116,000)}{(0.001267)(32.2)(1850)(0.562)}$$

$$= 5470 \text{ ft}$$

$$f_0 = \frac{V_T b}{\pi b r} \sqrt{-\frac{b}{4\delta(-C_{y\beta})} \left(-C_{n\beta} + \frac{b}{2\delta} C_{nr}\right)}$$

$$= \frac{604}{\pi(150)} \frac{150}{28.8}$$

$$\times \sqrt{-\frac{150}{(4)(5470)(0.562)} \left[-0.0860 + \frac{150}{(2)(5470)} (-0.116)\right]}$$

$$= 0.218 \text{ Hz}$$

$$\zeta = \frac{V_T}{4\pi\delta f_0} \left[1 - \frac{b^2}{2r^2} \frac{C_{nr}}{(-C_{y\beta})}\right]$$

$$= \frac{604}{4\pi(5470)(0.218)} \left[1 - \frac{1}{2} \left(\frac{150}{28.8}\right)^2 \left(\frac{-0.116}{0.562}\right)\right]$$

$$= 0.153 \quad \leftarrow$$

$$\tau = \delta/V_T = 5470/604 = 9.06$$

$$f_0\tau = (0.218)(9.06) = 1.97$$

$$\delta/L = 5470/2500 = 2.19$$

$$sk_0 = 2\pi \frac{f_0\tau}{\delta/L} = 2\pi \frac{1.97}{2.19} = 5.66 \quad \leftarrow$$

$$\tilde{a} = 1.0 \quad (\text{Fig. 8.7})$$

$$\tilde{a}k_0 = \tilde{a} \frac{\pi f_0 \tilde{c}}{V_T} = 1.0 \frac{\pi(0.218)(13.3)}{604} = 0.0151 \quad \leftarrow$$

$$V_T/g\delta = 604/(32.2)(5470) = 0.00343$$

$$B_1 = 4 \left(\zeta - \frac{1}{4\pi f_0 \tau} \right)^2 = 4 \left(0.153 - \frac{1}{4\pi(1.97)} \right)^2$$

$$= 0.0507$$

B_2 —not needed

Read from the curves

$R_2 = 0.76$ } Interpolate by marking a strip of paper with the same log
 $R_4 = 0.83$ } scale used on the graph and inverting top to bottom.

$R_6 = 2.7$ Interpolate by means of cross plot. Use the figure
 itself for graph paper. Keep the same vertical scale;
 change the horizontal coordinate to ζ and move the
 decimal point in the numbers.

Calculate using the formulas given in Table 8.5

$$\begin{aligned}
 A_{\Delta n} &= \frac{V_T}{g\delta} \sqrt{R_4 + B_1 R_2} \\
 &= 0.00343 \sqrt{0.83 + (0.0507)(0.76)} \\
 &= (0.00343)(0.932) = 0.00320
 \end{aligned}$$

$$\begin{aligned}
 N_{0\Delta n} &= f_0 \sqrt{\frac{R_6 + B_1 R_4}{R_4 + B_1 R_2}} \\
 &= 0.218 \sqrt{\frac{2.7 + (0.0507)(0.83)}{0.83 + (0.0507)(0.76)}} \\
 &= (0.218)(1.78) = 0.387
 \end{aligned}$$

9

SPANWISE VARIATION OF VERTICAL GUST VELOCITY

9.1 INTRODUCTION

To this point, the gust velocity has been considered to vary along the flight path, but not to vary laterally or vertically. In other words, the gust structure has been considered to be “one-dimensional.” However, if the turbulence is considered to be isotropic, then the gust velocity will, in fact, vary laterally. This lateral, or “spanwise,” variation will be identical statistically to the variation along the flight path.

Over the past decade, analytical procedures for determining dynamic gust loads with the effects of spanwise variation included have become generally available. Some of these procedures account only for the spanwise variation of vertical gust velocity. Others are more general—including, for example,

- 1) The *vertical* variation of *lateral* gust velocity, which is analogous on the fin to the spanwise variation of vertical gust velocity on the wing.

- 2) The *vertical* variation of *vertical* gust velocity, which results in a difference between the gust velocity profiles encountered, in a T-tail configuration, by the wing and the horizontal tail.

- 3) The *lateral* variation of *lateral* gust velocity, which results in a difference between the gust velocity profiles encountered by the fin, the left and right wing-mounted engines, and left and right wing-tip fins (if present).

At both the Lockheed-California and Lockheed-Georgia companies, the more general approach has been taken, resulting in what is referred to as a “three-dimensional” (3-D) gust analysis. The term three-dimensional as applied to the turbulence description refers to the number of position coordinates, such as fore-aft, lateral, and vertical, on which the gust velocity is assumed to depend.

In both the Lockheed-California and Lockheed-Georgia analyses, the 3-D aspects follow very closely work done by Frederick D. Eichenbaum of the Lockheed-Georgia Company.⁴¹⁻⁴³

9.2 APPLICATIONS OF THREE-DIMENSIONAL GUST ANALYSIS

As of this writing (1988) 3-D gust analysis has not yet come into use for routine gust loads determination at the Lockheed-California Company—or, as far as is known, elsewhere in the industry. One reason is the somewhat greater computer cost, although this may not be as great as previously

expected.* A second reason is the need to establish modified design U_o 's and a modified design frequency of exceedance to reflect the effect on \bar{A} 's of the 3-D analysis. Major use was made of the three-dimensional analysis, however, in determining the effect of corrective roll control on gust loads for the L-1011-3 (ACS) airplane; and it may not be long before the three-dimensional analysis replaces 1-D analysis in routine loads determination.

One well-established use of three-dimensional gust analysis is in the comparison of flight measured with theoretical gust loads. In determining transfer functions from flight data (more precisely, frequency-response functions), there are advantages in using the "cross-spectrum method." The resulting transfer function corresponds to a theoretical "cross-transfer function" that can be determined only by means of a three-dimensional analysis. This subject is discussed at length in Sec. 5.7.3 of Ref. 9.

9.3 EFFECT OF THREE-DIMENSIONAL GUST ANALYSIS ON LOADS

Extensive comparisons of wing load psd's and \bar{A} 's as given by 1-D and 3-D analyses have been conducted at the Lockheed-California Company for the L-1011 airplane. Some of the key results can be summarized briefly as follows.

The effect of the three-dimensional analysis on the short-period peak in the bending-moment psd, somewhat surprisingly, can be either an increase or a decrease. The effect on c.g. acceleration short-period peak, however, is always a decrease, as would be expected.

At the first bending-mode frequency, the effect of the three-dimensional analysis is to reduce the elastic-mode response by about 15% (as measured by the transfer function modulus, before squaring). This is comparable to the 19% value shown by Coupry⁴⁴ for the Concorde. A much earlier, much cruder analysis in Ref. 45 indicates the possibility of either an increase or a decrease, depending on the ratio of wing to fuselage masses.

For L-1011 wing shear and bending moment \bar{A} 's, the overall effect of the three-dimensional analysis is a reduction of about 6%. For torsion just inboard of the engine, increases of as much as 76% have been found, due to excitation of the first antisymmetric bending mode by the spanwise variation of gust velocity. The spanwise variation of vertical gust velocity contributes somewhat to airplane rolling moment in turbulence, although the predominant contributor is the lateral gust velocity. The 3-D analysis inherently accounts for both effects.

9.4 EFFECT OF L ON THREE-DIMENSIONAL GUST RESPONSE

In Sec. 4.5.6 it was emphasized, in a one-dimensional context, that the scale of turbulence L usually does not affect gust loads significantly as long

*Currently, it is estimated that to perform a combined vertical and lateral gust three-dimensional analysis would cost very roughly 40-50% more than to conduct the two separate one-dimensional analyses. If different flight conditions were needed for vertical and lateral gust loads, however, this percentage would, of course, increase.

SPANWISE VARIATION OF VERTICAL GUST VELOCITY 167

as σ_ω is adjusted appropriately as L varies. This variation must be such that the high-frequency asymptote to the gust psd remains constant.

Similarly, L usually has an insignificant effect on the difference between one-dimensional and three-dimensional gust-response psd's. The pertinent parameter controlling the difference between one-dimensional and three-dimensional psd's does not involve L ; instead, it is λ/b , where λ is the gust wavelength (equal to $2\pi/\Omega$) and b is the wing span. It is obvious, for example, that the spanwise variation of gust velocity will have a negligible effect when $\lambda/b \gg 1.00$.

That L has a negligible effect is illustrated, for the rigid-airplane case, by Fig. 9.1. The analytical results were first plotted in (R & M 3665⁴⁶) vs ΩL for various values of b/L ; but if ΩL is replaced by Ωb as the abscissa, the four curves collapse almost perfectly to the single curve indicated by the tick marks.

A similar concept applies in determining flexible-airplane loads due to three-dimensional turbulence. In such determinations, it is necessary to obtain the coherences (nondimensionalized cross-spectral densities) between gust velocity profiles separated by various spanwise distances, p . Eichenbaum⁴³ is careful to plot these coherences vs Ωp , not ΩL , for various values of p/L . He is also able to go a step further and define the coherences as simple closed-form single-variable functions of ΩL and of two additional variables, each independent of L .

The point to be made is that despite the common practice of expressing three-dimensional gust effects in terms of parameters involving L , it is rare that, in the end, L has a significant effect; one should take care not to be misled by appearances to the contrary.

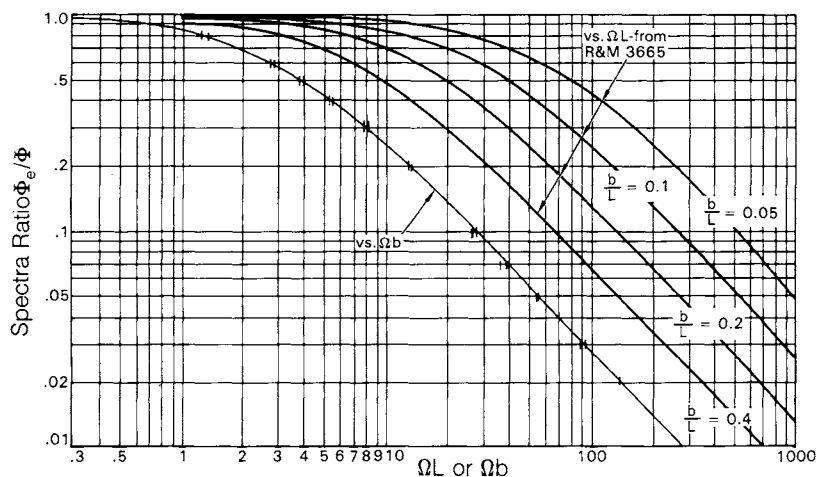


Fig. 9.1 Ratio of von Kármán spectra with and without span-averaging effects for constant loading. Based on data from R&M 3665.

This page intentionally left blank

10

TREATMENT OF NONLINEAR SYSTEMS

In Chapters 4–9 of this book, the determination of airplane response to a given continuous turbulence gust input has invariably utilized, as basic relations, Eqs. (4.7) and (4.15):

$$\sigma_y = \sqrt{\int_0^\infty \Phi(f) df} \tag{10.1}$$

$$\Phi_0(f) = \Phi_i(f) |H(f)|^2 \tag{10.2}$$

These equations inherently involve *superposition* of the responses to an infinite number of infinitesimal sine wave inputs, as discussed in Sec. 4.4.1. Consequently, they have meaning only when the system represented by $H(f)$ is linear. In fact, $H(f)$ itself has meaning only when the system is linear. When the system is not linear, other techniques must be used.

10.1 SOURCES OF NONLINEARITIES

The most important nonlinearities affecting airplane response to turbulence are those introduced by an active control system; that is, a load alleviation system, a stability augmentation system, or an autopilot. The key control system nonlinearities, from a loads standpoint, are displacement limiting and rate limiting. Displacement limiting often takes the form of hinge-moment limiting; that is, the limiting displacement is governed by the hydraulic force available to deflect the surface. The combined effect of displacement and rate limiting is referred to as “saturation.” As a result of saturation, an active control system will be less effective at high-load levels than when operating in the linear range.

Actually, the limiting action is more complex than just indicated, in that hinge moment and rate limiting act in combination. Even for quantitative analysis, however, it may sometimes be acceptable to approximate the saturation phenomenon in terms of distinct displacement and rate limits.

Aerodynamic nonlinearities can probably also be important. To date, however, as far as is known to the writer, no attempts have been made to include these explicitly in gust loads determination.

10.2 USE OF TIME-HISTORY ANALYSIS

The accepted procedure for determining the effect on loads of control system saturation involves *time-history analysis*, in which the major nonlinearities of the control system are included in the airplane representation. A continuous-turbulence gust velocity time history of several minutes duration is used as an input. Runs at several σ_w levels are made. (Appendix I provides information that may be helpful in selecting appropriate σ_w levels.) Time histories of one or more load quantities are included as outputs; these are then analyzed statistically by some form of peak counting.

No attempt is made to include the nonlinearities in the full dynamic gust analysis. The inclusion of the nonlinearities and the time-history treatment make the analysis so complex and cumbersome that such an approach would be completely impractical. Instead, the percentage effect of saturation is determined from the time-history analysis and applied to the results of the full linear analysis.

10.3 SIMPLIFICATIONS MADE

The following major simplifications are ordinarily made in performing the time-history analysis:

1) *Unsteady aerodynamics*. In the large-order linear dynamic gust loads analysis, the unsteady aerodynamic forces are defined in the frequency domain. Unsteady aerodynamic influence coefficient (AIC) matrices are used for this purpose. Currently, at the Lockheed-California Company, time-domain approximations to the frequency-domain AIC's are used in the time-history analysis.

2) *Reduced-order elastic-airplane representation*. The challenges here are: first, to reduce the number of elastic modes while preserving an adequate representation of the static-aeroelastic effects; and second, to eliminate as far as possible the complexities arising from the introduction of higher-order derivatives in representing the unsteady aerodynamics. The approach used in the saturation time-history analysis of the L-1011-3(ACS) active control system is summarized briefly by Gould.³⁰

3) *Single representative flight condition*. Ordinarily, the time-history analysis will be for a very limited number of flight conditions, perhaps only one. Critical or representative flight conditions will be selected.

4) *Limited number of load outputs*. In the L-1011-3(ACS) analysis, the only loads for which time histories were obtained were two bending moments and one torsion, all in the critical region of the wing. This was considered adequate.

10.4 GUST VELOCITY TIME HISTORY

The gust velocity time history is obtained by first generating a stationary Gaussian "white-noise" time history (white noise is characterized by a psd that is constant over the frequency range of interest). This is then passed through a filter that gives the desired Dryden or von Kármán psd.

The Dryden psd shape can be matched exactly by a fairly simple filter. This is given in Laplace Transform form, by

$$\frac{w_g}{\eta} = \frac{\sigma_w}{\sqrt{\Phi_\eta}} \sqrt{\frac{\tau}{\eta}} \frac{1 + \sqrt{3}\tau s}{(1 + \tau s)^2}$$

where

$$\begin{aligned} w_g &= \text{gust velocity} \\ \eta &= \text{white-noise gust velocity} \\ \Phi_\eta &= \text{psd of white-noise gust velocity} \\ \tau &= L/V \end{aligned}$$

The von Kármán shape can only be approximated. However, excellent approximations are available with fairly simple filters. One such filter, for use over the range $L\Omega = 0$ to $L\Omega = 200$ (corresponding to a range of $\Omega/2\pi$ of 0–0.013 c/ft with $L = 2500$ ft) is

$$\frac{w_g}{\eta} = \frac{\sigma_w}{\sqrt{\Phi_\eta}} \frac{\sqrt{\tau}}{\pi} \frac{(1 + 2.187\tau s)(1 + 0.1833\tau s)(1 + 0.021\tau s)}{(1 + 1.339\tau s)(1 + 1.118\tau s)(1 + 0.1277\tau s)(1 + 0.0146\tau s)}$$

10.5 INTERPRETATION OF RESULTS

Some thought will be required in determining what sort of response peak count data to obtain from the response-time histories and how to interpret the peak count data to give percentage increases in loads. Several approaches are described and compared by Gould.³⁰

This page intentionally left blank

11

ANALYSIS OF GUST-RESPONSE FLIGHT-TEST DATA

11.1 PURPOSE OF GUST-RESPONSE FLIGHT TESTING

The essential purpose of gust-response flight testing is to confirm the validity of the airplane representation and especially to make sure that no major characteristics have been overlooked. Gust-response flight testing is not intended to determine actual loads, or even response characteristics, for a multitude of specific flight conditions—the theory, once validated, does this. Nor is it intended to provide any measure of the absolute severity of the loads to be expected in service, inasmuch as the loads experienced in the tests depend on the severity of whatever turbulence happens to be encountered. The gust-response flight testing is not even intended, ordinarily, to provide a precise indication of the accuracy of the analysis.

Three major gust-response flight test programs have been conducted over the years by the Lockheed-California Company. These have been the Electra structural review, 1960; the L-1011 development flight testing, 1971; and the L-1011 active controls evaluation, 1977–1978. All three of these programs have illustrated, by intent or otherwise, the Lockheed-California philosophy of gust-response flight testing as stated above.

The Electra tests disclosed that elastic-mode dynamic overtravel had a major effect on *wing torsions*; prior to that time, it had been customary to look at dynamic effects only in terms of dynamic magnification factors on *wing shears* and *bending moments*. It was assumed that torsions went along in proportion.

The L-1011 development flight tests showed that the airplane representation was generally fairly adequate. They did disclose, however, that wing torsions at certain locations were higher than indicated by the 1-D gust theory because of inputs not accounted for in the theory; the most important of these inputs appeared to be corrective roll control by the pilot. As a result, empirical wing torsion increments have been included in the design loads of all later L-1011 airplanes. (The strength of the original L-1011-1 wing was found adequate to withstand the higher torsions.)

The L-1011 active control gust-response flight testing was intended primarily to confirm that existing theory, when extended to airplanes with active controls, would accurately predict the load reductions due to the active controls. By far the most important consequence of this program, however, was that it called attention to the importance of pilot corrective roll control

as an additional source of load in turbulence. Without active controls, the percent increase in load due to roll control is small enough to ignore—except for its effect on torsions, discovered in the earlier development flight-test program. But with the loads due to vertical gust substantially reduced by the active controls, the loads due to corrective roll control—shears and bending moments as well as torsions—become percentagewise much greater. It became clear, therefore, that they now had to be included in the design loads.

11.2 BASIC APPROACH

The basic approach in gust-response flight testing is to 1) Fly through continuous turbulence; 2) Measure time histories of various loads and other responses; 3) Simultaneously measure the gust velocity time history (vertical and lateral) by means of vanes or a differential pressure probe mounted on a boom ahead of the nose; 4) From the recorded time histories, compute frequency-response functions using power-spectral techniques; 5) Compare with analytically determined frequency-response functions for the same flight condition.

Conceivably, the same information could be obtained by flying through discrete gusts instead of continuous turbulence. The frequency response functions would then be determined from the Fourier transforms of input and response. The reasons for choosing continuous turbulence are 1) that it is easier to find sufficiently stationary continuous turbulence than sufficiently isolated discrete gusts; 2) it is more likely that all frequency components of interest will be present in continuous turbulence than in a single discrete gust; and 3) inasmuch as the design loads are determined on a continuous-turbulence basis, it is advantageous to make the flight-test comparisons on a continuous-turbulence basis as well.

The determination of frequency-response functions from the flight-test data and the comparison of these with theory is a vast subject, which will be covered here largely by reference to other sources. Reference 9, the Lockheed-prepared report of the L-1011 active controls flight testing, and Ref. 10 (pp. 4-6 and 26-27 and Appendices D and E) are suggested as basic references.

11.3 SELECTION OF SAMPLES FOR ANALYSIS

Experience has indicated that, to secure adequate statistical reliability, “bursts,” or turbulence samples, should total roughly 3-5 min for each flight condition. Individual bursts must be at least as long as one FFT block (see Sec. 11.6), on the order of 30 s. Each burst must be reasonably stationary, as judged by looking at a c.g. acceleration “strip-chart” trace. In other words, it should look like a stationary Gaussian random process.

Each burst also should reflect turbulence of at least moderate intensity, as indicated by the presence of several c.g. acceleration peaks in the vicinity of 0.5 g or higher.

11.4 GUST VELOCITY DETERMINATION

Gust probe outputs are essentially angle-of-attack measurements; these are influenced not only by the gust velocities but also by motions of the airplane, especially at the lower frequencies. The effects of the airplane motions must therefore be removed from the probe data.

A simple equation for removing the airplane motions, shown on page 5 of NASA TR R-199,¹⁰ is

$$w_g = V(\alpha_v - \bar{\alpha}_v) - V(\theta - \bar{\theta}) + \int_0^t (a_z - \bar{a}_z) dt + \ell_x(\theta - \bar{\theta}) \quad (11.1)$$

where

- w_g = vertical gust velocity
- α_v = vane angle
- θ = airplane pitch angle
- a_z = vertical acceleration
- ℓ_x = distance from airplane c.g. to probe

and a bar denotes the mean value.

This equation illustrates the general principles involved, but reflects a multitude of assumptions and approximations that may not be acceptable in practice. Much more complex equations have generally been used at the Lockheed-California Company. These are based on the thorough development by Eichenbaum⁴⁷ of the Lockheed-Georgia Company.

It is important that the gust velocity computations be checked by flying pitch, roll, and yaw maneuvers in still air and computing gust velocities. These should, of course, remain zero throughout the maneuvers. Experience has indicated that considerable difficulty may be encountered in fine-tuning the gust velocity computations to give a satisfactory still-air-maneuver check.

11.5 USE OF PSD'S

The basic processing of the flight data involves determination of power spectra for the measured time histories of the input (gust velocity) and the various outputs (load and other response quantities). These are then used to compute the required frequency-response functions.

Both power spectra and cross spectra are required. The cross spectrum, or cross-spectral density, is exactly analogous to the power spectrum, except that two variables are involved. In particular, Eqs. (4.8), (4.9), and (4.10) of Chapter 4 become

$$\Phi_{xy}(\omega) = \lim_{T \rightarrow \infty} \frac{1}{\pi T} \left[\int_{-T}^T x(t) e^{i\omega t} dt \right] \left[\int_{-T}^T y(t) e^{-i\omega t} dt \right]$$

Downloaded by RMIT UNIV BUNDOORA on June 4, 2013 | http://arc.aiaa.org | DOI: 10.2514/4.861888

$$R_{xy}(\tau) = \overline{x(t)y(t+\tau)} = \lim_{T \rightarrow \infty} \frac{1}{2T} \int_{-T}^T x(t)y(t+\tau) dt$$

$$\Phi_{xy}(\omega) = \frac{1}{\pi} \int_{-\infty}^{\infty} R_{xy}(\tau) e^{-i\omega\tau} dt$$

The cross-spectral density between two variables x and y is a complex quantity and provides information on the phase angle between x and y as well as on their magnitudes.

The frequency-response function can then be determined from the spectral data in either of two ways,

$$\text{Spectrum method: } |H_s| = \sqrt{\Phi_o/\Phi_i} \quad (11.2)$$

$$\text{Cross-spectrum method: } H_c = \Phi_{io}/\Phi_i \quad (11.3)$$

where subscripts i and o denote input and output, respectively.

It is seen from Eq. (11.2) that the spectrum method gives only the modulus of the frequency-response function H . Equation (11.2) follows directly from Eq. (4.15), Sec. 4.4.6. It is seen from Eq. (11.3) that the cross-spectrum method gives both the modulus and phase angle, inasmuch as it utilizes the cross-spectral density Φ_{io} , which is a complex quantity.

A useful quantity that is routinely obtained from the flight-test data is the coherency function (of f). It is given by

$$\gamma^2 = \frac{|\Phi_{io}|^2}{\Phi_i\Phi_o} \quad (11.4)$$

or

$$\gamma^2 = \frac{|H_c|^2}{|H_s|^2} \quad (11.5)$$

It varies between 0 and unity and is a measure of the degree to which the input and the output (or any two quantities) are linearly related. It can be used as a measure of the quality of the data, with values of 0.80 or higher generally indicating good data. It also may indicate the extent to which other inputs are present; for example, pilot-induced control motions. In particular, as suggested by Eq. (11.5), whereas H_s measures the ratio of the *total* output to the *single* measured input (gust-velocity), H_c measures the ratio of *only that part of the output linearly related to (due to) the single measured input*, to that input. Thus, a low value of γ^2 may indicate not that the data are of poor quality but simply that some other major input is present.

The subtleties involved in utilizing H_c , H_s , and γ^2 in comparing measured with theoretical loads are discussed much more fully in Ref. 9 (especially from pp. 5-93 to 5-97).

ANALYSIS OF GUST-RESPONSE FLIGHT-TEST DATA 177

Once frequency-response functions have been obtained, the comparison between theoretical and flight-measured values should be on the basis of plots of *response psd's*. These response psd's are obtained by multiplying the square of the frequency-response function modulus, both measured and theoretical, by the *design* gust psd (the von Kármán psd with $L = 2500$ ft). Inasmuch as the rms value of load, or \bar{A} , is given by the square root of the area under the psd curve, this type of comparison places in proper perspective the differences that occur, varying over the frequency range, between theory and test and between spectrum method and cross-spectrum method of treating the test data. This way of looking at psd's is usually much more productive than trying to draw conclusions on the basis of the flight-measured psd's themselves.

11.6 PSD DETERMINATION: PARAMETER SELECTION

As discussed briefly in Sec. 4.4.3, two procedures have been in wide use to compute psd's from time histories. These are the Blackman–Tukey and FFT procedures. Each of these procedures requires sampling the time histories at some constant sample rate f_s or sample interval Δt , which must be established. It is also necessary to select:

- 1) The maximum frequency at which psd's will be calculated.
- 2) The spacing of frequencies at which psd's will be calculated.
- 3) The number of lags (values of τ) at which the autocovariance function will be computed (Blackman–Tukey) or the length of block (FFT).

Various relations among these quantities are listed for convenient reference in Tables 11.1 and 11.2, for the Blackman–Tukey and FFT techniques, respectively. The actual selection is somewhat a matter of trial and error, but the selections must satisfy the relations indicated. Some explanatory comments follow.

The *Nyquist frequency* f_{\max} is the highest frequency at which information can be obtained from a time history sampled at a given rate. The Nyquist frequency is half the sample rate. Sketch a suggests why data at higher frequencies cannot be obtained. (A wave having twice the frequency shown could go through the same three points.) See also Sec. 11.7.2.

Sketch a

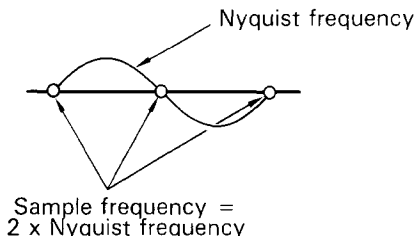


Table 11.1 Notes on Determination of Power Spectra from Test Data Using Blackman–Tukey Procedure.

Let

N = total number of points in sample

Δt = spacing of readings (= 1/sample rate)

Δf = spacing of frequencies

f_{\max} = highest frequency at which psd is determined = Nyquist frequency

τ_{\max} = largest time lag at which autocovariance function is determined [see Sec. 4.4.3, especially Eq. (4.9)]

m = number of lags = $\tau_{\max} / \Delta t$

K = number of statistical degrees of freedom

Then,

$N \Delta t$ = total length of sample

$$f_{\max} = \frac{1}{2 \Delta t} \quad \text{or} \quad \Delta t = \frac{1}{2 f_{\max}}$$

$$\Delta f = \frac{f_{\max}}{m} = \frac{1}{2m \Delta t} \quad \text{or} \quad m = \frac{1}{2 \Delta f \Delta t} = \frac{f_{\max}}{\Delta f} = \text{number of frequencies at which psd is determined}$$

Lowest frequency (other than zero) = Δf

Corresponding wavelength = $\frac{1}{\Delta f} = 2m \Delta t$

$$K = \frac{2N}{m} = \frac{2(N \Delta t)}{m \Delta t} = \frac{2(N \Delta t)}{\frac{1}{2 \Delta f}} = \frac{4(N \Delta t)}{\lambda_{\max}} = 4 \frac{\text{length of sample}}{\text{longest wavelength}}$$

Values of K and corresponding errors in psd at 90% confidence limits are

K	$\frac{\text{Length of sample}}{\text{Longest wavelength}}$	Error in psd at 90% confidence
13	3.25	65%
20	5	52%
40	10	37%
80	20	26%
160	40	18%

Note: Confidence limits are given by

$$\phi_{90\%} = \frac{\Phi_{\text{measured}}}{1 \pm \frac{\% \text{ error}}{100}}$$

Downloaded by RMIT UNIV BUNDOORA on June 4, 2013 | http://arc.aiaa.org | DOI: 10.2514/4.861888

ANALYSIS OF GUST-RESPONSE FLIGHT-TEST DATA 179

Table 11.2 Notes on Determination of Power Spectra from Test Data Using FFT Procedure

Let

N = total number of points in sample; must be an integer multiple of L

L = number of points in a time block; must be an integer power of 2, that is, 32, 64, 128, 256, 512,...

Δt = spacing of readings (= 1/sample rate)

Δf = spacing of frequencies

f_{\max} = highest frequency at which psd is determined = Nyquist frequency

K = number of statistical degrees of freedom

Then,

$N \Delta t$ = total length of sample

$$\frac{N}{L} = \text{number of blocks}$$

$$f_{\max} = \frac{1}{2 \Delta t} \quad \text{or} \quad \Delta t = \frac{1}{2f_{\max}}$$

$$\Delta f = \frac{1}{L \Delta t} = \frac{2f_{\max}}{L} \quad \text{or} \quad \Delta f = \frac{1}{\text{length of block in seconds}}$$

or

$$L = \frac{1}{\Delta f \Delta t} = \frac{2f_{\max}}{\Delta t}$$

= 2 times number of frequencies at which psd is determined

(Accordingly, L corresponds to $2m$ in the Blackman–Tukey procedure.) Note that Δf is limited to values given by the sample rate divided by an integer power of 2.

Lowest frequency (other than zero) = Δf

Corresponding wavelength = $\frac{1}{\Delta f} = L \Delta t$ = length of block in seconds

$$K = \frac{4N}{L} = 4 \text{ times number of blocks}$$

$$= \frac{4(N \Delta t)}{L \Delta t} = \frac{4(N \Delta t)}{\frac{1}{\Delta f \Delta t}} = \frac{4(N \Delta t)}{\lambda_{\max}} = 4 \frac{\text{length of sample}}{\text{longest wavelength}}$$

Again, inasmuch as in Blackman–Tukey

$$K = \frac{2N}{m} = \frac{4N}{2m}$$

L corresponds to $2m$ in Blackman–Tukey. Values of percent error in psd at 90% confidence, for various values of K , are the same as listed in Fig. 11.1.

Selecting a frequency spacing Δf always involves a compromise between *resolution* and *statistical reliability*. Close spacing of frequencies gives high resolution. Wide spacing, in effect, involves averaging over a broader frequency band and thus increases statistical reliability.

The statistical reliability data in Table 11.1 are for individual spectra. They are pertinent, for example, when the objective is simply to study gust velocity spectra. Information on statistical reliability of frequency-response functions, which must be determined from the power spectra of both input and output, is shown in Fig. 11.1.* This figure also includes the corresponding data for individual spectra (dash line), taken from Table 11.1. It is seen that the confidence limits for the frequency-response functions depend on the coherency.

Inasmuch as a typical K value may be on the order of 40 or so, the errors listed in Table 11.1 and plotted in Fig. 11.1 may seem discouragingly high. The situation, however, is not as serious as it appears. Although for individual bursts a value of K of 40 may be typical, it is often possible to average psd's or frequency-response functions from several similar bursts. N , and therefore K , are thus effectively increased. Indeed, it is highly desirable to do this. In processing the 1978 L-1011 active control gust-response flight-test data, for example, it was found that, to achieve adequate stationarity, bursts had to be limited in duration to from one to four 25.6-s FFT blocks. Yet in order to obtain satisfactory statistical reliability, some 300 s of data may be needed. This would require, then, from 3–6 or more bursts, each to be processed separately. Plotting each of the bursts separately would mean from 3–6 times as many plots—to prepare, look at, digest, and store—as if the entire 300 s of data could be obtained in a single burst, or if the separate shorter bursts were averaged. Plotting the individual bursts separately also would mean that to draw conclusions, one would have to look at from 3 to 6 separate plots, all of lower statistical reliability, and mentally average. The lower statistical reliability also means a much less regular plot, making it difficult to isolate the true nature of the curve from the extraneous irregularities.

Provision for such averaging of frequency-response functions is available at the Lockheed-California Company in its merge-and-plot computer program. This is the program that prepares superimposed plots of measured and theoretical frequency-response functions and psd's for easy comparison. Averaging the frequency-response functions requires converting to real and imaginary parts, averaging, and recomputing modulus and phase for the averaged data.

Coherency functions are computed from the averaged frequency-response

*Figure 11.1 is a replot of figures presented on p. 87 of NASA TR R-199.¹⁰ The replot collapses the three curves shown on each of the original figures to a single curve. It thus permits consolidating the four original figures to one figure. Reference 10 also includes similar data on phase angle error; the numerical values seem to be within a few percent of those for the modulus.

ANALYSIS OF GUST-RESPONSE FLIGHT-TEST DATA 181

$$E_1 = \frac{\text{Error}}{\text{Average value}}$$

$$\text{Confidence interval} = \frac{\text{Measured value}}{1 \pm E_1}$$

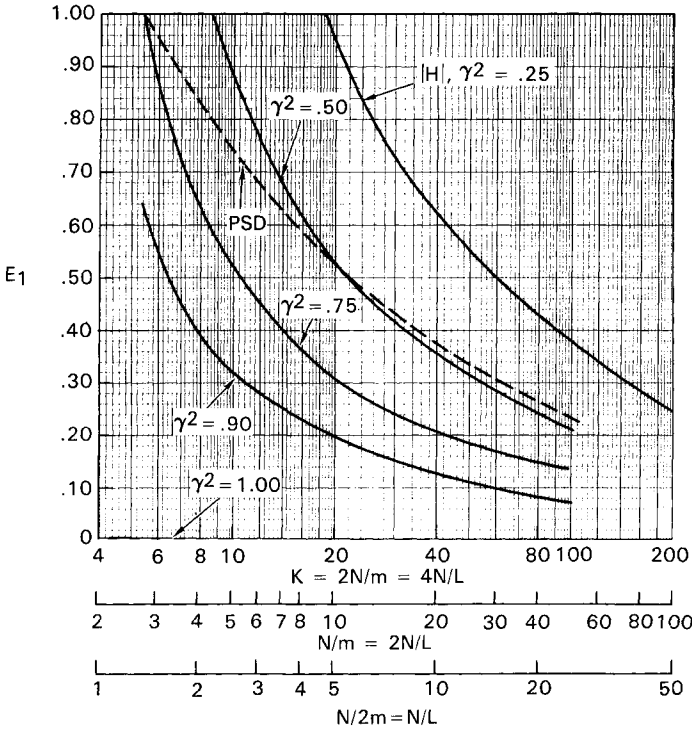


Fig. 11.1 Error in transfer function modulus or in psd at 90% confidence limits.

functions, using Eq. (11.5), Sec. 11.5. Averaging the coherencies directly is not satisfactory. Consider a pair of variables for which the coherency is inherently zero, such as c.g. vertical and lateral accelerations. It has been found that, for a short burst, the computed coherency will vary wildly with frequency, while remaining always positive; but the longer the burst, the closer to zero the computed coherency will remain. Averaging the coherencies from many short bursts will tend to give a coherency that is fairly constant but substantially greater than zero. Data illustrating this phenomenon are shown shown in Fig. 5-102 of Ref. 9. When the coherencies are computed from the averaged frequency-response functions, the coherencies in this situation do indeed approach zero as the length of burst increases.

No provision has been available at the Lockheed-California Company for averaging the flight-measured psd's themselves. This would require a follow-on computer program that would first normalize the various bursts to a

Downloaded by RMIT UNIV BUNDOORA on June 4, 2013 | http://arc.aiaa.org | DOI: 10.2514/4.861888

single rms gust velocity—either a unit value or a weighted-average value, weighting by length of burst. Weighted-average psd's would then be obtained.

So, statistical reliability can indeed be improved by averaging several similar bursts. Moreover, the errors indicated by Fig. 11.1 apply to individual frequencies. To whatever extent the psd or frequency-response curve can be faired over several adjacent frequencies, the expected error decreases. Similarly, the expected percentage error in \bar{A} , where \bar{A} depends on the area under the entire psd curve, is much less than the expected error of a single point. For example, the expected percentage error in the sum of N quantities all having the same average value is $1/\sqrt{N}$ times the expected percentage error in each individual quantity. More generally, the expected percentage error in the sum of N values of Φ —that is, in the area under the psd curve—is given by

$$\left(\begin{array}{c} \text{Expected percentage error} \\ \text{in each } \Phi \text{ value} \end{array} \right) \times \frac{\sqrt{\sum \Phi^2}}{\sum \Phi}$$

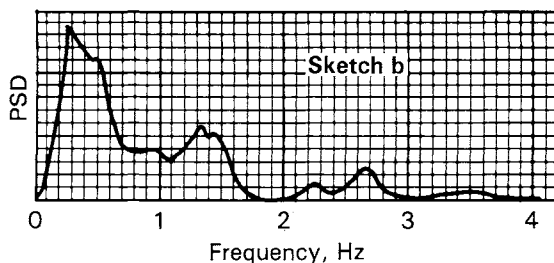
From this it can be shown that the expected percentage error in \bar{A} , as calculated from measured frequency-response data and a design gust psd, is given approximately by

$$\left(\begin{array}{c} \text{Expected percentage error} \\ \text{in frequency-response} \\ \text{modulus, Fig. 11.1} \end{array} \right) \times \frac{\sqrt{\sum \Phi^2}}{\sum \Phi}$$

For the theoretical psd shown in Sketch b and a frequency spacing of 0.05 Hz (one-half the smallest grid interval on the plot), the value of

$$\sqrt{\sum \Phi^2} / \sum \Phi$$

was calculated to be 0.19.



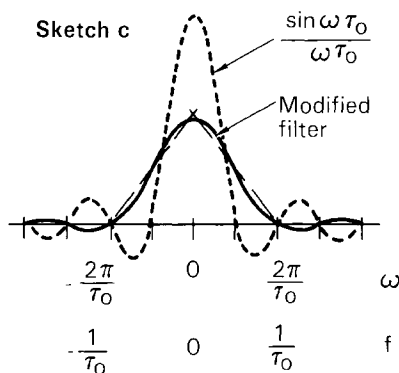
Thus, a 26% error read from Fig. 11.1 would result in an error in \bar{A} of only 26% times 0.19, or 5%.

It might be remarked that a different FFT procedure is sometimes encountered, which appears to be highly inferior to that implied by Table 11.2. The entire record is treated as a single block, leading to a very small Δf and, as a result, a low statistical reliability. The statistical reliability is then restored by very heavy smoothing of the resulting psd's.

11.7 OTHER CONSIDERATIONS IN PSD DETERMINATION

11.7.1 Spectral Window

The numerical procedures used to obtain psd's from time histories inherently produce psd's that are weighted averages over a frequency band comparable in width to the frequency spacing. The actual weighting function, if nothing is done to change it, is as shown by the short-dash line in Sketch c, which is taken from Fig. IVC:5 of the AGARD *Flight Test Manual*. (In this sketch, the ω scale shown in the reference has been corrected and an f scale added. The long-dash straight lines have also been added.) The quantity τ_0 in Sketch c is the same as τ_{\max} in Table 11.1; the frequency spacing, Δf in Table 11.1, is equal to $(1/2)(1/\tau_0)$ in the sketch. The weighting function, which can also be thought of as a filter, is usually referred to as a "spectral window."



The shape of spectral window shown by the short-dash line is undesirable because of the presence of the large side lobes. There are many ways to improve this shape. One of the most widely used, referred to as "Hanning," simply involves smoothing the computed psd's by means of the operation

$$\Phi_{i,\text{smoothed}} = [0.25 \Phi_{i-1} + 0.50 \Phi_i + 0.25 \Phi_{i+1}]$$

The resulting spectral window, labeled "modified filter" in the sketch, is vastly improved. It can be thought of qualitatively as an isosceles triangle as indicated by the long-dash lines in Sketch c.

One effect of the spectral window is to smear out sharp resonance peaks that may occur in a response psd. In order to provide a direct comparison between measured and theoretical psd's, it is advantageous to apply the same filter to the theoretical psd's that is inherently present in the determination of the flight-measured psd's. This adjustment has not been made routinely at the Lockheed-California Company in comparing theoretical with flight-measured psd's. One reason is that \bar{A} 's are negligibly affected. Another is

that one would also like to see what the unadjusted theoretical psd's look like, and computing and showing both is overly expensive.

Another effect of the spectral window is to complicate the computation of damping ratios ζ from response psd curves. ζ is given by

$$\zeta = \frac{\text{bandwidth}}{2 \times \text{resonant frequency}}$$

where the bandwidth is measured at the half-power point; that is, at a psd of one-half the peak value. When the psd's are determined from time histories, ζ 's obtained in this way must be adjusted to remove the spectral window effect. This can be accomplished, for the Hanning spectral window, by means of the curves shown in Fig. 11.2. These are the result of work by Soovere.⁴⁹ Similar curves obtained earlier on the basis of the triangular spectral window shown in Sketch c agreed very closely with those in Fig. 11.2.

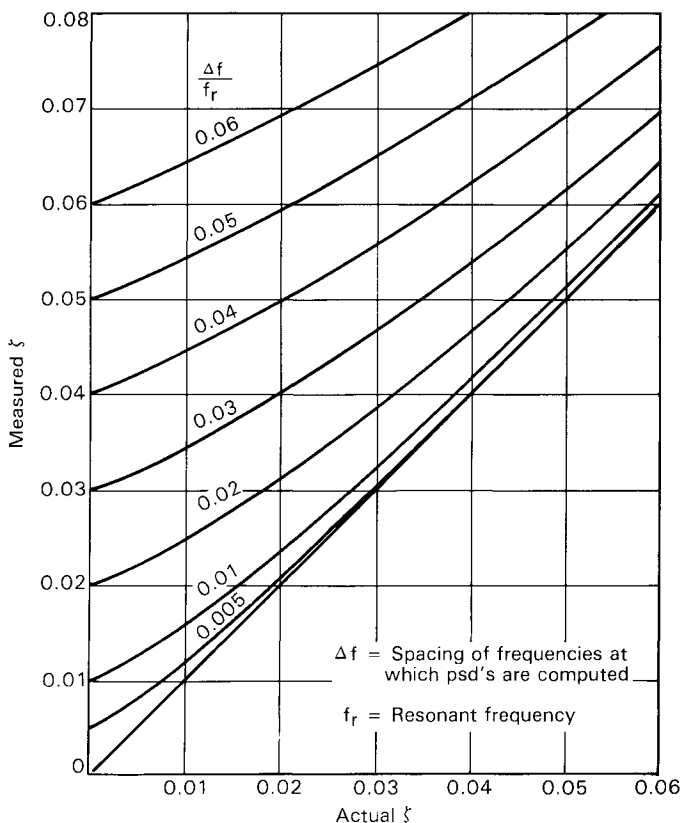


Fig. 11.2 Relation of ζ given by bandwidth of measured psd to actual ζ .

11.7.2 Aliasing and Its Avoidance by Filtering

It has been mentioned (Sec. 11.6) that the Nyquist frequency is the highest frequency at which information on frequency content can be obtained from a time history. Actually, any “power” at frequencies *above* the Nyquist frequency will show up in the calculated psd’s *below* the Nyquist frequency. This phenomenon is known as “aliasing.” To prevent aliasing, it is important that any power that may be present above the Nyquist frequency be filtered out before psd’s are computed. An analog filter can be used before the initial analog-to-digital conversion; or if the initial sampling rate is higher than will be used in the psd calculations, digital filtering can be used. It should be recognized that perfectly sharp filters, either analog or digital, cannot be achieved. Accordingly, if *all* the signal is removed at and above the Nyquist frequency, then the signal will also be attenuated over some range below the Nyquist frequency, perhaps down to 0.50 or 0.75 thereof. Characteristics of a practical family of digital filters are shown in AFFDL-TR-68-127¹⁵ (App. ID). A more thorough discussion of aliasing is available in NASA TR R-199.¹⁰

11.7.3 Prewhitening and Postdarkening

In determining the psd of a quantity that decreases, for example, as the -2 power of frequency, the presence of a spectral window of finite width tends to distort the computed psd, as indicated by the following example:

<i>f</i> , Hz	2	3	4
psd	2.25	1.00	0.56
window coefficient	0.25	0.50	0.25
psd × coefficient	0.56	0.50	0.14
adjusted psd, Σ of psd × coefficient		1.20	

Gust velocity, which tends to vary as the $-5/3$ power of frequency, is a comparable quantity.

To minimize this distortion, it has become customary to form a time history of the *differences* between successive sampled values of the gust velocity. This is essentially a time history of the derivative of the gust velocity. The psd of this quantity is then determined. It will vary much less with frequency, actually as

$$f^{-5/3} \times f^2 = f^{+1/3}$$

Thus, the distortion is greatly reduced. Inasmuch as the resulting psd approximates white noise (psd constant with frequency), the process is referred to as prewhitening. The psd of the gust velocity itself is then obtained from

Downloaded by RMIT UNIV BUNDOORA on June 4, 2013 | http://arc.aiaa.org | DOI: 10.2514/4.861888

the psd of its derivative, essentially by dividing by the square of the frequency; this step is known as postdarkening.*

Actually, there is some question whether prewhitening really does much good. For example, it has a significant effect only at the first few frequencies (as can be seen by changing the numbers in the numerical example). And at these low frequencies, the psd may have started to flatten out so that there is less need for prewhitening anyway. Also, there is some question whether prewhitening should be used in obtaining *response* psd's, even when it is used in obtaining gust velocity psd's.

Further discussion and data on prewhitening are contained in Ref. 50. This reference provides a thorough evaluation of prewhitening as applied to gust psd determination. It does not discuss the effect on frequency-response function determination.

11.8 EFFECTS OF COMPUTING OPTIONS ON PSD'S AND FREQUENCY-RESPONSE FUNCTIONS

In summary, it is seen that computing psd's from measured time histories involves the following choices, all of which can affect the resulting psd's:

- 1) FFT vs Blackman-Tukey.
- 2) Sample rate.
- 3) Frequency spacing.
- 4) Spectral window (psd smoothing, etc.).
- 5) Prewhitening.
- 6) Filtering.

*Actually, because of the finite sampling interval, the prewhitened time history may not be *exactly* the derivative. Accordingly, the postdarkening operation may be a little more complex than indicated. Expressions given in Ref. 10, for example, are

$$\text{Prewhitening:} \quad \hat{w}_i = w_i - w_{i-1} \quad \hat{y}_i = y_i$$

$$\text{Postdarkening:} \quad \Phi_w(\omega) = \frac{\Phi_{\hat{w}}(\omega)}{2(1 - \cos \omega \Delta t)} \quad \Phi_{wy}(\omega) = \frac{\Phi_{\hat{w}y}(\omega)}{1 - e^{i\omega \Delta t}}$$

12

ADEQUACY OF THE STATIONARY-GAUSSIAN IDEALIZATION OF THE GUST STRUCTURE

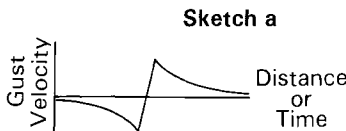
12.1 EVIDENCE OF POSSIBLE INADEQUACIES IN THE STATIONARY-GAUSSIAN MODEL

As indicated in Sec. 4.1.3, there is every reason to consider the stationary-Gaussian idealization of the gust structure to be vastly more realistic than any of the discrete-gust idealizations formerly used as a basis for design load determination. Nevertheless, there is accumulating evidence that actual turbulence is not really stationary and Gaussian. In particular,

1) Pilots in flight simulators complain that stationary-Gaussian turbulence, the usual simulator input, does not feel like real turbulence; it lacks the “intermittency” or “patchiness” that characterizes real turbulence.

2) Gust velocity profiles measured in flight, say of 4 or 5 min duration, although they may appear continuous, often on close examination are seen to be incompatible with the concept of random superposition of sine waves. (See discussion and examples on pp. 14–19 of NASA CR-2913.⁵⁹)

3) As a particular example, gust velocity profiles obtained over storm tops near Oklahoma City in May 1965, although generally continuous in appearance, were seen on close examination to contain a number of occurrences of a pattern clearly indicating a strong vortex pattern (see Burns⁵²).



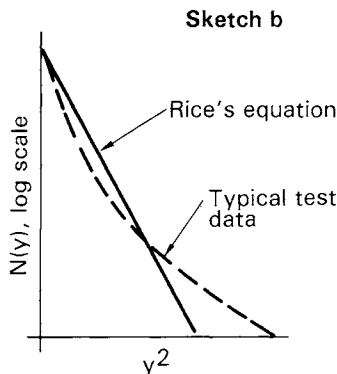
Similar vortex patterns, occurring as relatively isolated gusts, were recorded at low altitudes in the Sangre De Cristo Mountains of Colorado and New Mexico in March and April of 1964.⁵³

4) Even when turbulence samples of several minutes duration appear fairly stationary, to obtain agreement with Rice’s equation usually requires breaking the samples into much shorter subsamples. Each subsample will be of constant σ_w , but the σ_w ’s will vary substantially among the various subsamples. This phenomenon is discussed in detail in Sec. 12.2. NASA CR-2639⁵⁴

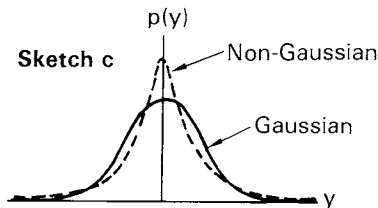
(pp. 39–41) discusses data appearing in a Canadian report,⁵⁵ that seem to show that the more severe (and therefore more important) turbulence patches are only 10–15 s long. This would seem to be too short for statistical equilibrium to be reached, at least for low-frequency, lightly damped modes.

To the extent that discrete gusts actually occur, either in isolation or in a background of continuous turbulence, the duration of the “patch,” of course, is even less—simply the duration of the gust itself, on the order of a second or so.

5) Ratios of peak-to-rms response (e.g., c.g. acceleration) measured in typical 4 or 5 min samples of apparently continuous turbulence sometimes are as high as 5 or 6, whereas Rice’s equation would indicate a value in the range 3–3.5. Moreover, if Rice’s equation is plotted in the form $\log N(y)$ vs y^2 , it appears as a straight line; measured level-crossing data, however, from typical 4 or 5 min samples of apparently continuous turbulence almost invariably display the concave-upward shape indicated by the dash line in Sketch b.



6) Similarly, probability densities of 4–5 min samples typically show a higher than Gaussian probability at large values of y .



7) Even for samples for which the probability distribution of the gust velocity itself is very nearly Gaussian, the probability distribution of the derivative of the gust velocity, or of gust velocity differences over some small

σ = rms gust velocity, m/sec

K = kurtosis coefficient, equal to 3 for the Gaussian case

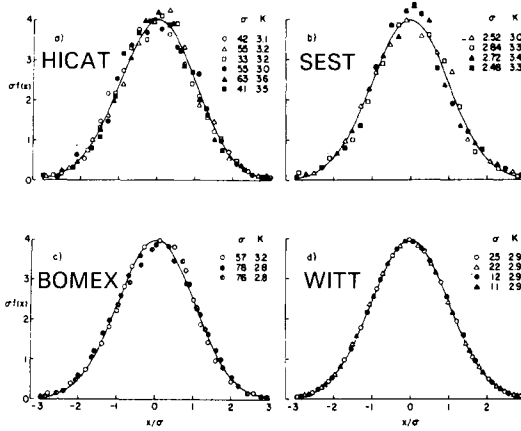


Fig. 1 Normalized probability density functions of X compared with Gaussian law: a) HICAT; b) severe storm turbulence; c) BOMEX; d) wind-tunnel turbulence. Circles are for streamwise components; triangles for lateral; squares for vertical. Open symbols are for first run; closed for second run; semiclosed for third run. The unit of σ is m/sec.

ρ = correlation coefficient between $X(t)$ and $X(t + \tau)$; ρ close to unity indicates small τ

K_z = kurtosis coefficient, equal to 3 for the Gaussian case

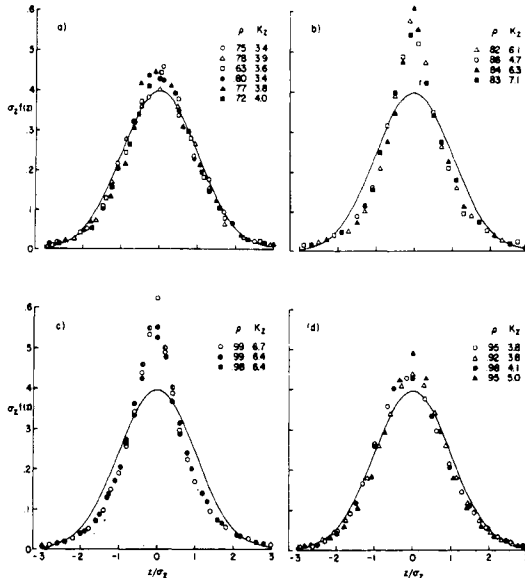


Fig. 2 Normalized probability density functions of Z compared with Gaussian law, where $Z = X(t + \tau) - X(t)$. All notes and symbols are the same as for Fig. 1.

Fig. 12.1 Probability densities of measured gust velocities and gust velocity differences. (From Chen.⁸)

constant time interval (equivalent to a distance increment along the profile), depart substantially from the Gaussian distribution. (See discussion in Sec. 4.3.4.) Examples are shown by Chen⁸ from four different programs, including both atmospheric and wind-tunnel turbulence. (The three atmospheric turbulence cases are shown also in Fig. 9 of Ref. 54.) Chen's data are reproduced in Fig. 12.1. Similar data are shown by Burns⁵² for data obtained over storm tops in Oklahoma.

Clearly, a lot of turbulence is not accurately described, in its detailed characteristics, by the stationary-Gaussian model. The two key questions are: 1) Is there a better model? and 2) Despite the various departures of real turbulence from the stationary-Gaussian model, does this model nevertheless do a good job of predicting loads?

Before addressing these questions explicitly, however, it is important to consider the relationship between non-Gaussian and nonstationary turbulence.

12.2 NON-GAUSSIAN TURBULENCE VS NONSTATIONARY TURBULENCE

This subject is thoroughly discussed in AFFDL-TR-68-127¹⁵ (pp. 99–109). The essentials are as follows.

First, it is noted that the prediction of load or acceleration peaks due to turbulence, under a continuous turbulence concept, is invariably based on Rice's equation (Sec. 4.6.3). This equation can be derived theoretically, under the assumption that the turbulence is stationary and Gaussian. As indicated in Sketch b (Sec. 12.1), Rice's equation plots as a straight line on coordinates of $\log N(y)$ vs y^2 . Consequently, if a given turbulence sample is stationary and Gaussian, a plot of level crossings on these coordinates will approximate a straight line. The most meaningful test of whether a sample is stationary and Gaussian, therefore, is given by such a plot of the test data. Indeed, such a plot addresses directly the real question: Is Rice's equation valid?

There seems to be a tendency in evaluating turbulence samples to assume implicitly that a sample is stationary and then to evaluate whether it is Gaussian. This tendency perhaps results from the absence of any definite way to evaluate stationarity, whereas it is a simple matter to compute the probability density and compare it with a Gaussian curve.

It is entirely possible, however, for a given sample to be *locally* Gaussian, but nonstationary overall. If, for example, two Gaussian samples having different rms values are joined to form a single sample, the *combined* sample will indeed be non-Gaussian. This can be illustrated on a frequency-of-exceedance basis by the following example.

Consider a patch of turbulence to consist of two portions, each stationary and Gaussian, but of different rms levels:

First 90%	$\sigma_w = 1.75 \text{ fps}$
Last 10%	$\sigma_w = 3.50 \text{ fps}$

Then, for the sample as a whole,

$$\sigma_w = \sqrt{(0.90)(1.75)^2 + (0.10)(3.50)^2} = 2.00 \text{ fps}$$

The expected exceedance curve for such a patch can be obtained by adding together the two parts, taking account of the relative time in each, as shown in Fig. 12.2.

The significant result shown in this figure is that the expected highest peak for the actual nonstationary sample is 40% higher than obtained by application of Rice's equation to the sample as a whole ($\sqrt{114/55} = 1.44$). Both this result, with its obvious effect on the peak-to-rms ratio, and the concave-upward shape of the resulting level-crossing curve are generally consistent with flight-test data.

It might be remarked that in this example, the 10% of time at the high σ_w level need not be at either the beginning or end of the run. It could equally well have occurred in the middle, or in still smaller portions distributed throughout the run. In all cases, the exceedance curve would be the same. The only requirement, from the standpoint of application of the theory to loads prediction, is that the individual stationary portions be long enough, or the rms level vary gradually enough, so that the theoretical input-output relations for a stationary-Gaussian process apply.

Exceedance curves from nine HICAT runs are shown in AFFDL-TR-68-127,¹⁵ plotted on the Sketch b coordinates. The runs varied in duration from 1.83–16 min and reflected various degrees of stationarity as indicated by the appearance of the time histories. In all cases, an excellent fit of the test data was obtained by adding only two straight-line components. Ratios of the peak value given by the fitted curve to the peak value indicated by Rice's equation ranged from 1.16–2.58.

It seems much more plausible, therefore, to consider turbulence to be Gaussian and nonstationary than stationary and non-Gaussian. Indeed, the

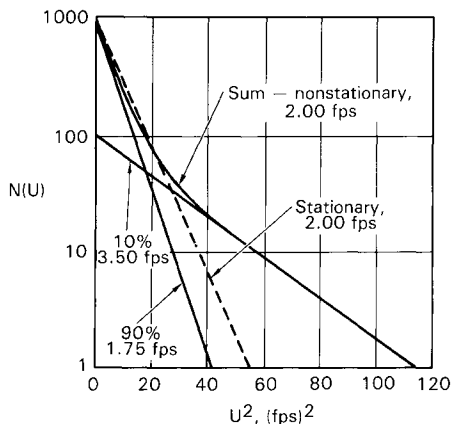


Fig. 12.2 Theoretical effect of non-stationarity on exceedance curve.

whole concept of building up generalized exceedance curves by superimposing turbulence patches of different rms levels, as discussed in Sec. 4.7, reflects the fact that turbulence, over long periods of flying, can in no way be considered stationary. Further, the concept that turbulence is Gaussian but nonstationary is inherent in the determination of σ_w distributions (P 's and b 's) from operational c.g. acceleration peak count data; see the discussion in Sec. 4.8.2. In such a determination, the question of stationarity within individual samples never arises.

12.3 EVALUATION OF THE ADEQUACY OF THE STATIONARY-GAUSSIAN MODEL

12.3.1 *Reasons for Questioning the Stationary-Gaussian Model*

From a scientific standpoint, there seems to remain two reasonable bases for questioning the validity of the stationary-Gaussian model. One is the evidence by Chen,⁸ mentioned in Sec. 12.1, that even when the probability density of the gust velocity itself is Gaussian, the probability density of gust velocity *differences* is typically not Gaussian.* The other, also mentioned in Sec. 12.1, is uncertainty as to whether the rms gust velocity varies slowly enough, or remains constant over long enough periods of time, so that the theoretical input-output relations apply. In this context, an individual gust would represent the limiting case of a short period of time.

12.3.2 *Current Position*

Despite the rather disquieting thoughts brought out in the preceding paragraphs, the stationary-Gaussian model may still do a good job of predicting loads.

First, it should be pointed out that much severe turbulence, although perhaps not strictly stationary Gaussian, does indeed have the appearance of continuous turbulence. Time histories of gust velocity obtained during passes through thunderstorms in the NB-66B high-altitude gust survey program⁵⁶ certainly did not look like single updrafts. Once the airplane was in the storm, the time histories showed a very continuous pattern. In the F-106 study⁵³ of turbulence close to the ground in the Sangre De Cristo mountains of Colorado and New Mexico, in which true gust velocities as high as 175 fps

*Reeves⁵⁴ points out that a similar test can be conducted using a sample that is nonstationary and for which, therefore, the overall probability density of the gust velocity is non-Gaussian. If for each stationary region of the sample, the process is Gaussian, then, for the sample as a whole, the probability density of the gust velocity differences (for any constant lag τ) will be identical to the probability density of the gust velocity itself, even though neither is Gaussian.

were measured, “invariably the maximum gusts occurred in areas of continuous turbulence.”⁵³

Second, and more important, the response of an airplane as a whole to vertical gusts is usually heavily damped. Such a system has a short memory; the response is governed very predominantly by the particular gust the airplane is encountering right now, with very little carry-over from preceding gusts. In other words, it should make little difference whether the airplane encounters a particular stationary-Gaussian profile or isolated gusts extracted from that profile. Of course, other airplane motions, such as elastic-mode response and the Dutch-roll response to lateral gusts, may be much more lightly damped.

It is reasonable to believe, therefore, that even if the turbulence were to consist primarily of discrete gusts, the stationary-Gaussian assumption, leading to what might be called an equivalent stationary-Gaussian model, would provide a realistic means of accounting for the actual mix of gradient distances and gust shapes. The stationary-Gaussian model should be expected to account

1) *Realistically* for the presence of *highly damped* modes to *either* discrete or continuous turbulence.

2) *Realistically* for the response of *lightly damped* modes to continuous turbulence.

3) *Conservatively* for the response of *lightly damped* modes to discrete gusts.

Actually, the stationary-Gaussian model is probably *slightly conservative* for the response of lightly damped modes to continuous turbulence, in that continuous turbulence tends not to be of long enough duration in any one patch for statistical equilibrium to be reached.

Also, if indeed the most severe gusts occur essentially as discrete gusts, then the design levels for continuous turbulence, having been set to provide for these discrete gusts, will be unrealistically high for continuous turbulence as such.

Finally, it is reasonable to believe that any error introduced by the non-Gaussian nature of the gust velocity differences (Figs. 12.1 and 12.2) is largely self-compensating, in that the same theory is used in deriving the generalized exceedance curves from operational data and in applying them to the design of a new airplane.

12.3.3 Quantitative Evaluation

It should be possible to determine whether the optimistic, largely intuitive evaluation just enunciated is valid by means of a practical quantitative study. The procedure would be

1) Collect a number of not very stationary gust velocity time histories, totaling perhaps 50 min duration.

2) Establish several highly simplified airplane models. These would include, first, a plunge-only model with perhaps four δ values (Sec. 8.2.1) and,

second, a second-order elastic-mode and Dutch-roll model with perhaps two natural frequencies and three ζ 's. Kussner lift-lag effects should be accounted for.

3) Establish a gust velocity psd, probably von Kármán, with additional attenuation beyond, for example, 3 Hz to assure finite N_0 .

4) For each airplane model, determine analytically the c.g. acceleration \bar{A} and N_0 values.

5) Run time histories for each airplane model over individual or pieced-together turbulence samples, recording c.g. acceleration.

6) Count peaks (level crossings); convert to $N(y)/N_0$ and y/\bar{A} .

7) Plot. Use a separate plot for each profile, but superimpose on each plot the exceedance curves for all airplane models.

The degree to which the curves for all airplane models coincide indicates the validity of the stationary-Gaussian model.

A comparable investigation* has been carried out by British Aircraft Corporation and is reported in Ref. 57 (BAC Report VTO/D/M/257, November 1976). Results are somewhat inconclusive. The various exceedance curves do not coincide to the degree one might like, but neither is the agreement really bad. One source of the disagreement appears to be an inconsistency in the treatment of N_0 ; further work in this area could be quite fruitful.

A related study by Houbolt is reported in AFFDL-TR-74-148 (Ref. 58). This treats stationarity only; the gust samples are generated by piecing together patches of stationary-Gaussian turbulence of widely varying σ_w levels. The measured level-crossing curves generally agree excellently with the theoretical curves. At the highest σ_w levels, durations of the individual patches were, for example, only 0.7, 4.1, and 18.2 s. Unfortunately, at the lower levels, the individual patches were so long as to obscure any effect of the nonstationarity.

12.4 OTHER MODELS

Attempts to develop alternate gust models have taken two directions. In work pioneered by Reeves et al.,^{54,59,60} the approach has been to start with the stationary-Gaussian model and modify it in some way—for example, by modulating the stationary-Gaussian time history according to a much lower-frequency random time history. Later work along this line appears in NASA CR-2913.⁵¹

Of far greater importance from a loads standpoint is the “statistical discrete-gust” approach developed by Jones at the RAE, starting about 1968. The British manufacturers and CAA have been extremely uneasy about the use of power-spectral methods for establishing design gust loads; they have felt strongly that the gusts that produce limit and ultimate loads are essentially

*No plunge-only model included; natural frequencies only in elastic-mode range; no high-frequency attenuation of gust velocity; and less gust velocity time-history data.

discrete in nature, and they have felt compelled to develop a discrete-gust model for design loads determination. Jones' work as of 1973 is summarized in RAE TR 73167.⁷ His approach utilizes basically a one-minus-cosine ramp shape, with provision for alternating positive and negative ramps of variable magnitude. The gust velocity varies as the one-third power of the ramp length. Provision is made for both design envelope and mission analysis treatments.

Both the Reeves and Jones approaches may be practical for simulator use, although it is believed that neither is yet in wide use. Reeves' work, in fact, was first directed toward this application. A variation of the Jones model has been developed for simulator application in AGARD CP-198⁶¹ by Tomlinson, also of the RAE. This model has been used at Northrop in a simulator study of fighter aircraft ride quality.

The application of either of these two types of models to loads is much more difficult. The application of the Reeves approach to loads determination appears to be still at an early stage of development. Trial applications have been made of the Jones model (e.g., by Hawker-Siddeley, reported in Ref. 62, and by BAC, reported in Ref. 57) but the Jones model has not yet found a place in loads specifications.

The Lockheed-California view, probably shared generally throughout the U.S., is that the Jones approach is hopelessly cumbersome to use, is far from straightforward in its derivation, provides a good deal less information than current psd methods, and is probably no more realistic. It does, at least, improve vastly on older discrete-gust methods by establishing a plausible variation of gust velocity with gradient distance. Noback⁶³ concludes that the tuned discrete-gust and psd methods will give approximately the same results, for simple airplane models, as long as the gust velocity in the discrete-gust analysis varies as the gust length to the one-third power. The Lockheed-California views on the Jones approach are pretty much in parallel to those elucidated in considerable detail by Coupry,⁶⁴ although Lockheed is not in full agreement with one or two of Coupry's several points.

The psd and statistical discrete-gust (Jones) methods were also compared in a 1975 report by Noback.⁶⁵ His conclusion was that "the Statistical Discrete Gust Method has no advantages and a number of disadvantages compared to the Power Spectral Density method and is not suitable as an airworthiness requirement for the calculation of design loads."

The FAA, through its National Resource Specialist Terence J. Barnes, is currently (1988) urging the development of the Jones approach as an alternate to the psd approach, for two reasons. First, it should produce loads that can be used directly for stress analysis; it thus avoids, for example, the need to generate matching conditions, which can be quite discouraging to a small manufacturer. Second, it should facilitate accounting for control system nonlinearities, since a separate analysis (Sec. 10.2) should no longer be necessary for this purpose. It might be remarked that one of the key challenges to adoption of the Jones approach for large flexible airplanes is likely to be in generating unsteady aerodynamic data in the time domain.

This page intentionally left blank

13

PRESENT PLACE OF DISCRETE-GUST LOAD REQUIREMENTS

Chapter 12 considered the adequacy of the continuous turbulence methods of gust loads determination. It then explored the potential for development of an advanced discrete-gust method that would reflect more closely the properties of real atmospheric turbulence than do either the present discrete-gust methods or the continuous turbulence methods. But what do we do right now? Given that continuous turbulence methods are to be used in any event, is there a benefit to be gained from continued use of the present discrete-gust methods, methods which have remained essentially unchanged over the past 30 years? Chapter 13 addresses this question.*

As the continuous turbulence concept gradually gained acceptance during the late 1950's and the early 1960's, good engineering judgment dictated use of the old and new concepts in conjunction until sufficient experience could be gained to assure that the newer approach would be adequate by itself. It seems to have become quite clear, however, that the discrete-gust criteria are no longer necessary to assure safe design. Some of the factors leading to such a conclusion are indicated in the following sections.

13.1 NATURE OF ATMOSPHERIC TURBULENCE

As noted in Secs. 12.1 and 12.3.1, one can find considerable evidence to indicate that the most severe gusts occur more or less as individual gusts. Nevertheless, as noted in Sec. 12.3.2, there is also a lot of very severe turbulence that looks pretty continuous. One cannot avoid a strong intuitive feeling that although neither the stationary-Gaussian nor discrete-gust idealization is perfect, the stationary-Gaussian is much more like real turbulence than the pure one-minus-cosine discrete gust of fixed gradient distance and fixed gust velocity.

13.2 TUNED DISCRETE-GUST ANALYSIS

From a tuned discrete-gust standpoint, it is clear that there is no real alternative to treating elastic-mode dynamic effects on a power-spectral basis. The elastic-mode effects, in a discrete-gust analysis, are highly sensitive

*Chapter 13 draws heavily from Ref. 13, Sec. 17.

to the gust gradient distance. Yet, at least as of the mid-1960's, there simply were no data available on how the gust velocity should vary with gradient distance, or on the joint probability of gust velocity and gradient distance, or on how to provide for the possibility of successive gusts building up a resonant response in a lightly damped mode. Even today, it is not clear how close we are to achieving a practical solution to this problem on a discrete-gust basis. Certainly, the constant-gust-velocity tuned discrete-gust analysis of that period (as described in Chapter 3) did not provide an adequate solution.

As the power-spectral techniques became available, however, they offered for the first time a practical way of bypassing these knotty problems. One cannot but feel that the relation of gust velocity to gradient distance inherent in the power-spectral description of atmospheric turbulence must be quite representative of discrete gusts as well as continuous turbulence. For lightly damped modes, the continuous turbulence analysis would clearly be necessary regardless of whether a discrete-gust analysis were performed. It is hard to see any benefit in continued use of the tuned discrete-gust analysis *in addition to the clearly more realistic continuous turbulence analysis*.

It might be remarked further that the tuned discrete-gust analysis never became a "tried and true" approach, as did the use of the FAR static discrete-gust formula. Seldom if ever did the tuned discrete-gust dynamic analysis actually put weight into an airplane; instead, it almost invariably showed that the strength already there as a result of other design conditions was adequate.

As a result, on the publication of FAA-ADS-53¹³ in 1966, the FAA accepted the psd methods contained therein as an acceptable means of full compliance with the FAR 25.305(c) requirement that transient effects be accounted for in determining design gust loads. The CAA and BCAR, however, still require the use of the tuned discrete-gust dynamic analysis.

13.3 STATIC DISCRETE-GUST LOADS

From a static loads standpoint, the impression long prevailed that gust loads are not sensitive to the gradient distance—as illustrated, in fact, by Fig. 3.2 here. From this impression, it was then inferred—incorrectly, in fact—that the discrete-gust and power-spectral approaches would give virtually identical loads.

Actually, however, discrete-gust and power-spectral approaches can give results that differ fairly substantially. These differences are illustrated by Table 13.1, which compares the discrete-gust U_{de} that each of a family of airplanes would have to be designed to in order to have the same continuous turbulence U_{σ} capability.

Airplane A in this family is the Table I(a) airplane of NACA TN 4332.¹⁷ It is typical of four-engine piston-powered transports of the early 1950's and is similar to the DC-6. *Airplane B* is the same, except for a 50% increase in wing loading; it is roughly representative of the Lockheed Model 188

PLACE OF DISCRETE-GUST LOAD REQUIREMENTS 199

Table 13.1 U_{de} Values Required to Give Same Strength as $U_{\sigma} = 115$ fps for Various Airplanes; Altitude = 20,000 ft

Airplane	Relative $\frac{W}{C_{L\alpha}S}$	Relative \bar{c}	$W/C_{L\alpha}S$ and \bar{c} comparable to	K_{σ}/K_g	U_{de} required to give same strength as $U_{\sigma} = 115$ fps $83.95(K_{\sigma}/K_g)^a$	Relative U_{de} in preceding column
E	0.5	1	DC-3	0.518	43.5	0.87
A	1.0	1	DC-6	0.596	50.0	1.00
B	1.5	1	L-188	0.656	55.1	1.10
C	2.0	1	—	0.703	59.0	1.18
D	2.0	5	SST	0.780	65.5	1.31

^a83.95 is 115 fps times 0.73, the square root of the density ratio at 20,000 ft.

Electra. *Airplane C* reflects a further 33% increase in wing loading. *Airplane D* represents a large delta wing airplane characteristic of some supersonic transport (SST) configurations; $W/C_{L\alpha}S$ is the same as for Airplane C but the wing chord is increased by a factor of five. *Airplane E* reflects a 50% decrease in wing loading relative to Airplane A and is representative of the DC-3 generation of transports. The actual numbers used in the calculations are listed in Table 13.2.

The key results are shown in the next to last column of Table 13.1, with relative values shown in the last column. The use of a reference value of U_{σ} of 115 fps in the next to last column may seem rather high. This value is consistent, however, with the design U_{σ} value of 85 fps indicated in Sec. 5.4.2 together with an elastic-mode dynamic factor of 1.25 and a factor of 1.08 to account for the estimated unconservatism of the K_{σ} values obtained from Fig. 8.1:

$$(85)(1.25)(1.08) = 115$$

It is seen from Table 13.1 that, for example, if a U_{de} of 50 fps is the “right” value for Airplane A, then Airplane D would have to be designed to a 31% higher U_{de} of 65.5 fps to be equally safe. The fairly substantial differences among the numbers in either of the last two columns indicate that the discrete-gust and power-spectral approaches can give significantly different results, even where resonant buildup in poorly damped modes cannot be a contributing factor. (By “different results” is meant that if U_{de} and U_{σ} are set so that the two methods give equal loads for one airplane, then for other airplanes the two methods will give different loads.)

The reasons for the differences shown in Table 13.1 are not hard to understand.

Table 13.2 Airplane Data Used as Basis for Table 13.1

Airplane	W	S	$C_{L\alpha}$	\bar{c}	$(W/C_{L\alpha}S)$	δ^a	$\mu = \delta/\bar{c}$	$\frac{\bar{c}}{L}^b$	$\frac{\delta}{L}$ ^b	$\frac{\bar{c}}{\delta}$	K_g ^c	K_σ ^d	$\frac{K_\sigma}{K_g}$
E	38500	1463	5.70	13.7	4.61	226.6	16.54	0.0055	0.0906	0.0605	0.666	0.345	0.518
A	77000	1463	5.70	13.7	9.23	453.2	33.08	0.0055	0.1813	0.0302	0.758	0.452	0.596
B	115500	1463	5.70	13.7	13.85	679.8	49.62	0.0055	0.2719	0.0202	0.795	0.522	0.656
C	154000	1463	5.70	13.7	18.47	906.4	66.16	0.0055	0.3626	0.0151	0.815	0.573	0.703
D	385000	7315	2.85	68.5	18.47	906.4	13.23	0.0274	0.3626	0.0755	0.628	0.490	0.780

^a $2(W/C_{L\alpha}S)$ ^b $L = 2500$. ^cSee Eq. 2.2. ^dSee Fig. 8.1.
0.0407

PLACE OF DISCRETE-GUST LOAD REQUIREMENTS 201

Between Airplanes A, B, C, and E, the reason is simply that the psd approach accounts, in effect, for the variation of gust velocity with gradient distance, whereas the discrete gust approach does not. Because of its higher wing loading—or more precisely, its higher value of $W/C_{L\alpha}S$ —Airplane C, for example, acquires vertical velocity less rapidly as it enters any given gust than does Airplane A. This phenomenon is reflected in higher gust factors (K_g and K_σ) on both discrete-gust and power-spectral bases. On encountering gusts of various wavelengths, however, Airplane C will tend to feel the longer wavelength gusts that Airplane A rides over. Accounting for the higher gust velocity of the longer gusts, therefore, will increase the loads for Airplane C more than for Airplane A, and in contrast to the discrete-gust formula, the power-spectral treatment does reflect the mixture of gusts of all wavelengths and, especially, the higher gust velocities associated with the longer wavelengths. Thus, differences in $W/C_{L\alpha}S$ account for the different results for Airplanes A, B, C, and E.

Between Airplanes C and D, the reason for the difference relates to the fact that in the discrete-gust method, the gust length is assumed to be proportional to the wing chord. This assumption simplifies the calculations (as indicated in Sec. 2.3 and Appendix A), and for past airplanes, it may have been fairly realistic. However, the extremely long chord of Airplane D results in a gust so long that the airplane tends to rise with the gust and develop relatively little load. And this alleviating effect of the gust length is not offset by any increase in gust velocity. The power-spectral treatment, of course, provides for a mixture of gusts of all lengths and does reflect the fact that the longer gusts have significantly higher gust velocities.

It seems almost self-evident that the principal reason for the difference between discrete-gust and power-spectral results is that the discrete-gust method does not account for the variation of gust velocity with gust length. Noback,⁶³ in fact, in his excellent paper demonstrates convincingly that if, in the discrete-gust approach, the gust velocity is taken proportional to the one third power of the gradient distance, the two methods do agree very closely. The agreement is close for both plunge-only and pitch-plunge models. Noback, after noting that the Jones SDG method (Sec. 12.4) does use the one-third power variation, states, “The foregoing is not a plea to use this SDG method, but it is intended as a warning against further reliance on the discrete gust method as described in the regulations.”

Thus, it is evident that the relation of gust intensity to gradient distance is important from the standpoint of static as well as dynamic loads determination. And it is evident that the power-spectral approach accounts much more realistically for the actual mix of gust gradient distances in the atmosphere and for the variation of gust velocity with gradient distance than does the present discrete-gust formula. With a comprehensive power-spectral gust loads criterion in use, which is necessary in any event to provide for the possible resonant buildup of response in poorly damped modes, it is clear that the discrete-gust situation is inherently provided for—and more realistically than by the discrete-gust formula specified in current regulations. The

only function of the current static discrete-gust criterion, therefore, is to provide a very simple means of load determination that can serve as insurance against gross blunders in the generally much more complicated psd dynamic analyses.

13.4 COMPUTATIONAL CONSIDERATIONS

For the purpose of providing a check of the more complicated psd analyses, it is pertinent to emphasize that, as discussed in Sec. 8.1.2, a continuous turbulence criterion is not necessarily any more difficult to apply than the static discrete-gust formula. (Such a check, incidentally, may be beneficial from a regulatory standpoint as well as for a manufacturer's use internally.) To replace the existing static gust loads formula with a corresponding psd formula would only require

- 1) Preparation of curves such as those of Fig. 8.1 or Fig. 8.5 in a form permitting accurate reading of numerical values over the practical range of airplane parameters. (In generating these curves, points to be plotted should be recomputed using the best available lift growth data.)
- 2) Agreement on design U_o values, as functions of altitude.

APPENDIX A PLUNGE-ONLY EQUATION OF MOTION FOR AN AIRPLANE ENCOUNTERING A ONE-MINUS-COSINE VERTICAL GUST

If there is no lag in buildup of lift, equilibrium of vertical forces results in the following differential equation:

$$M\ddot{z} + \frac{\rho}{2} V^2 SC_{L\alpha} \dot{z} = \frac{\rho}{2} V^2 SC_{L\alpha} \frac{U(t)}{V}$$

where

- M = mass of airplane
- V = forward speed (true airspeed)
- U = gust velocity (varying with time)
- z = vertical displacement of the airplane

This can be simplified to

$$M\ddot{z} + \frac{\rho}{2} V SC_{L\alpha} \dot{z} = \frac{\rho}{2} V SC_{L\alpha} U(t) \tag{A.1}$$

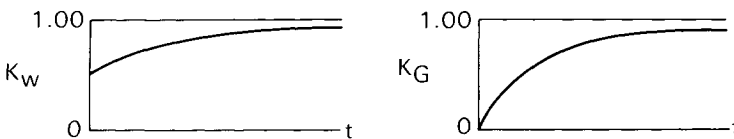
The effect of lag in buildup of lift will now be considered.

Let the buildup of lift due to an instantaneous change in angle of attack be given by an "indicial function" $K_w(t)$, where,

$$K_w(t) = \frac{C_{L\alpha}(t)}{C_{L\alpha}(\infty)}$$

Similarly, let the buildup of lift due to a sharp-edge gust be given by a different indicial function $K_G(t)$. $K_G(t)$ differs from $K_w(t)$ because the angle of attack does not change on the entire wing simultaneously, but gradually as the wing chord enters the gust.

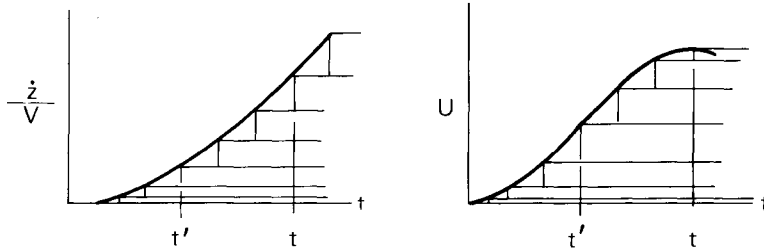
Sketch a



$K_w(t)$ is called the “Wagner function” and $K_G(t)$ the “Kussner function.” They are referred to collectively as lift-growth functions.

To introduce these effects into the differential equation, we consider the changes in angle of attack and gust velocity to occur in infinitesimal increments:

Sketch b



The total lift at time t is then the sum of the lifts resulting from the changes in angle of attack (\dot{z}/V) and gust velocity (U) at all of the various times t' prior to t :

$$d\dot{z} = \ddot{z} dt \quad dU = \dot{U} dt$$

The differential equation thus becomes

$$M\ddot{z} + \frac{\rho}{2} VSC_{L\alpha} \int_0^t K_w(t-t')\ddot{z}(t') dt' = \frac{\rho}{2} VSC_{L\alpha} \int_0^t K_G(t-t')\dot{U}(t') dt' \tag{A.2}$$

For any given airplane, K_w and K_G are functions only of the number of chord lengths traveled. (The specific functions depend on Mach number, aspect ratio, etc., but the theoretical functions derived on the assumption of an infinite-aspect-ratio rectangular wing at $M = 0$ have been considered to provide a good approximation for most conventional subsonic aircraft.) As a result, it is desirable to replace t by a nondimensional time s equal to the number of chord lengths traveled:

$$s = \frac{Vt}{\bar{c}}, \quad t = \frac{\bar{c}s}{V}; \quad \frac{d}{dt} = \frac{V}{\bar{c}} \frac{d}{ds}; \quad \frac{d^2}{dt^2} = \frac{V^2}{\bar{c}^2} \frac{d^2}{ds^2}$$

The differential equation then becomes

$$\begin{aligned} M \frac{V^2}{\bar{c}^2} \frac{d^2 z}{ds^2} + \frac{\rho}{2} VSC_{L\alpha} \int_0^s K_w(s-s') \frac{V^2}{\bar{c}^2} \frac{d^2 z}{ds'^2} \frac{\bar{c}}{V} ds' \\ = \frac{\rho}{2} VSC_{L\alpha} \int_0^s K_G(s-s') \frac{V}{\bar{c}} \frac{dU}{ds'} \frac{\bar{c}}{V} ds' \end{aligned}$$

Multiplying throughout by

$$\frac{1}{M} \frac{\bar{c}^2}{V^2}$$

gives

$$\frac{d^2z}{ds^2} + \frac{\rho}{2} \frac{\bar{c} SC_{L\alpha}}{M} \int_0^s K_w(s-s') \frac{d^2z}{ds'^2} ds' = \frac{\rho}{2} \frac{\bar{c} SC_{L\alpha}}{M} \frac{\bar{c}}{V} \int_0^s K_G(s-s') \frac{dU}{ds'} ds' \quad (\text{A.3})$$

Designating by $1/\mu$ the dimensionless ratio

$$\frac{\rho}{2} \bar{c} SC_{L\alpha} / M$$

the equation becomes

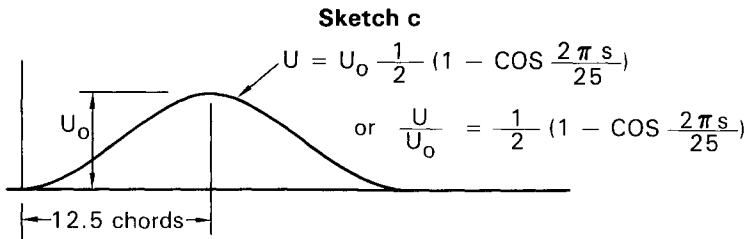
$$\frac{d^2z}{ds^2} + \frac{1}{\mu} \int_0^s K_w(s-s') \frac{d^2z}{ds'^2} ds' = \frac{1}{\mu} \frac{\bar{c}}{V} \int_0^s K_G(s-s') \frac{dU}{ds'} ds' \quad (\text{A.4})$$

The dimensionless parameter

$$\mu = \frac{2M}{\rho \bar{c} SC_{L\alpha}}$$

is generally referred to as the mass parameter.

For design loads determination, the gust profile is considered to be of one-minus-cosine shape, with a "gradient distance" of 12.5 chords:

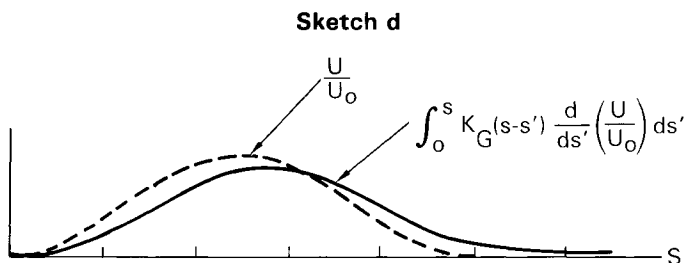


Selection of a fixed gradient distance in chord lengths leads to great simplification of the results and is consistent with experimental data (Fig. 2.1).

This gust profile can now be introduced into the right-hand side of Eq. (A.4) to give

$$\frac{d^2z}{ds^2} + \frac{1}{\mu} \int_0^s K_w(s-s') \frac{d^2z}{ds'^2} ds' = \frac{1}{\mu} \frac{\bar{c} U_0}{V} \int_0^s K_G(s-s') \frac{d}{ds'} \left(\frac{U}{U_0} \right) ds' \quad (\text{A.5})$$

The integral on the right-hand side can be evaluated numerically (step-by-step integration) to give a function of s only:



Equation (A.5) can now be solved numerically (i.e., by step-by-step integration) to give time histories (in nondimensional time s) of d^2z/ds^2 and dz/ds , for each of a series of values of μ . In the numerical solution, the constant factor $\bar{c}U_0/V$ on the right-hand side is carried in literal form; in effect, the solution is performed for $\bar{c}U_0/V = 1$.

For each value of μ , the maximum value of d^2z/ds^2 is noted from the time history. The incremental load factor Δn is then given by

$$\Delta n = \frac{\ddot{z}}{g} = \frac{1}{g} \frac{V^2}{\bar{c}^2} \frac{d^2z}{ds^2} = \frac{1}{g} \frac{V^2}{\bar{c}^2} \frac{\bar{c}U_0}{V} \left(\frac{d^2z}{ds^2} \right)_{\bar{c}U_0/V = 1}$$

In order to put this equation into the form

$$\Delta n = K_g \Delta n_{\text{sharp-edge gust}}^*$$

we multiply and divide by μ

$$\Delta n = \mu \frac{\rho \bar{c} S C_{L_\alpha}}{2M} \frac{1}{g} \frac{V^2}{\bar{c}^2} \frac{\bar{c}U_0}{V} \left(\frac{d^2z}{ds^2} \right)_{\bar{c}U_0/V = 1} = \underbrace{\mu \left(\frac{d^2z}{ds^2} \right)_{\bar{c}U_0/V = 1}}_{K_g} \underbrace{\frac{\rho U_0 V C_{L_\alpha}}{2W/S}}_{\Delta n_{sc}}$$

The coefficient K_g is then plotted as a function of μ . The following empirical equation is found to approximate K_g as thus computed:

$$K_g = \frac{0.88\mu}{5.3 + \mu}$$

* K_g is the gust alleviation factor, not to be confused with $K_G(s)$ used earlier.

The fact that K_g is a function of μ only is due to

1) Consideration of lift growth to be a function only of chord lengths traveled.

2) Selection of a single gust profile, defined by a basic one-minus-cosine shape and a single gradient distance in chords.

It should perhaps be remarked that the particular mass parameter used in the foregoing derivation represents only one of several ways of nondimensionalizing the airplane mass. It appeared in this derivation solely because the lift growth was considered to be a function only of chord lengths traveled. Then, when the gust profile was defined in terms of chord lengths, the mass parameter provided for cancellation of \bar{c} and V from the expression for Δn .

This page intentionally left blank

APPENDIX B ELEMENTARY INTRODUCTION TO SOME CONCEPTS IN PROBABILITY THEORY AND STATISTICS

B.1 PROBABILITY OF A SINGLE EVENT

The “probability of an event E ”—that is, the probability that E will occur in a single trial—is defined as

$$P(E) = \frac{n}{N}$$

where N is the total number of equally probable outcomes, and n is the number of these outcomes that constitute the event E .

If the event E occurs for all N possible outcomes, E clearly is a certainty; in this case, $n = N$ and $P(E) = 1$. On the other hand, if none of the N possible outcomes result in E , E is an impossibility; in this case, $n = 0$ and $P(E) = 0$.

It is evident that, in general,

$$0 \leq P(E) \leq 1$$

As an example, consider an urn that contains 10 balls: 3 black, 5 white, and 2 red. Consider one ball to be drawn at random and let the event E be the drawing of a black ball. We are considering, of course, a mathematical model, in which it is “equally probable” that any one of the 10 balls will be drawn. The probability of event E , the drawing of a black ball, is, in accordance with the aforementioned definition,

$$P(E) = \frac{n}{N} = \frac{3}{10} = 0.3$$

The usefulness of the concept of a probability is that if one conducts a long series of trials, the proportion of occurrences of the event in question tends to come closer and closer to the theoretical value of the probability.

For example, in drawing balls from the urn, a series of 1000 trials (in which the ball is replaced after each drawing) might result in the following outcomes:

Number of trials	10	100	1000
Number of times E occurs (a black ball is drawn)	2	35	315
Ratio of occurrences of E to number of trials	0.200	0.350	0.315
“Expected” number of occurrences of E	3	30	300
Difference between expected and actual number of occurrences of E	-1	5	15

The second line is sometimes called the “absolute frequency of occurrence” of E and the third line, the “relative frequency of occurrence.”

It is seen that as the number of trials increases, the relative frequency of occurrence (line 3) tends to approach the probability. (In fact, an alternate definition of the probability of E is the value toward which the relative frequency tends as the number of trials increases indefinitely.)

The tendency for the relative frequency to approach the probability is a very powerful one, but the expected result does not *have* to happen, of course, in any one sequence of trials. The foregoing example is a typical one, but if one were to repeat the 1000-trial series a great many times, one would expect to obtain an untypical result at least occasionally.

If the numbers of black, white, and red balls in the urn were unknown, one might *experimentally* determine that the probability of drawing a black ball is approximately 0.30. Conversely, knowing the probability to be 0.30, one can expect that, over many trials, roughly 30 percent of the balls drawn will be black.

It is also seen from the previous table that although the *relative* frequency differs from the expected frequency—or probability—by decreasing amounts as the number of trials increases, the *absolute* frequency differs from the expected absolute frequency by *increasing* amounts (1, 5, 15). This result is typical.

B.2 SOME BASIC RULES OF PROBABILITY

For two mutually exclusive events, A and B , the probability that either A or B will occur is

$$P(A \text{ or } B) = P(A) + P(B)$$

Thus, if an urn contains 3 black balls, 5 white balls, and 2 red balls, drawing of a black ball and a white ball in the same trial are mutually exclusive, so that the probability of drawing *either a black or white* ball is

$$\begin{aligned} P(A \text{ or } B) &= P(A) + P(B) \\ &= 0.3 + 0.5 \\ &= 0.8 \end{aligned}$$

For two independent events, the probability of A and B both occurring is

$$P(A \text{ and } B) = P(A) \cdot P(B)$$

Thus, if two urns each contain 3 black balls, 5 white balls, and 2 red balls, and one ball is drawn from each, the probability that *both will be black* is

$$\begin{aligned} P(A \text{ and } B) &= P(A) \cdot P(B) \\ &= (0.3)(0.3) = 0.09 \end{aligned}$$

B.3 PROBABILITY DISTRIBUTION

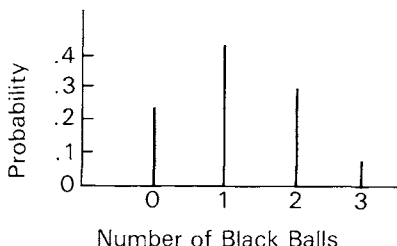
Suppose that three urns each contain 4 black balls and 6 white balls, and that one ball is drawn from each of the three urns. In this situation there are *not* just two possible outcomes, the occurrence or nonoccurrence of the event E , but four possible outcomes:

- 0 black balls
- 1 black ball
- 2 black balls
- 3 black balls

By utilizing the two basic rules of the preceding section, one can readily compute the probabilities of each of these four outcomes in turn.

Number of black balls	Probability	Explanation
0	$(0.6)(0.6)(0.6) = 0.216$	Three independent events, each consisting of drawing a white ball.
1	$(0.4)(0.6)(0.6) + (0.6)(0.4)(0.6) + (0.6)(0.6)(0.4) = 0.432$	Sum of three mutually exclusive events— BWW , WBW , WWB —each of which represents the combined probability of three independent events.
2	$(0.6)(0.4)(0.4) + (0.4)(0.6)(0.4) + (0.4)(0.4)(0.6) = 0.288$	Similar to above.
3	$(0.4)(0.4)(0.4) = 0.064$	Three independent events, each consisting of drawing a black ball.

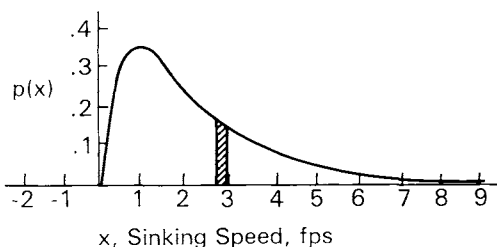
The sum of these four probabilities, is of course, unity. These results can be shown in bar-chart form as follows:



This set of probability numbers is spoken of as the “probability distribution” associated with the various possible outcomes. It describes the way in which the available total probability (1.00) is *distributed* over the various possible outcomes.

If the possible outcomes E are defined by values of a continuous variable x , the number of possible outcomes is, of course, infinite. The probabilities in such a situation are described by a probability density, $p(x)$.

For example, consider the sinking speed of an airplane at landing touch-down. This is not confined to discrete values, such as 1 fps, 2 fps, etc., but can have any value, such as 2.1 fps, 1.78 fps, 3.2713... fps, etc. The probability distribution in this case is defined by a probability density.



The probability density is the quantity such that, in any trial, the probability that x lies between x_1 and $x_1 + dx$ is equal to the area of the element $p(x_1)dx$. Accordingly, the total area under the curve must be unity.

A related quantity that can be used to describe the probability distribution in this case is the probability that x is less than a given value x_1 :

$$P(x < x_1) = \int_{-\infty}^{x_1} p(x) dx$$

Sometimes, the term probability distribution is reserved for this form of describing how the probability is distributed.

A more useful description for use in airplane loads work is the probability that x is *greater* than a given value x_1

Table B.1 Example of Sinking Speed Frequencies of Occurrence

Sinking speed, fps	Number of landings, absolute frequency	Relative frequency ^a	Cumulative relative frequency ^b	Sinking speed ^c
0-1	155	0.236	1.000	0
1-2	243	0.370	0.764	1
2-3	167	0.254	0.394	2
3-4	68	0.104	0.140	3
4-5	19	0.029	0.036	4
5-6	4	0.006	0.007	5
6-7	1	0.001	0.001	6
Over 7	0	0	0	7
		<u>0</u>		
		1.000		

^aRelative Frequency = Number of landings, absolute frequency/657.

^bΣ Relative frequency.

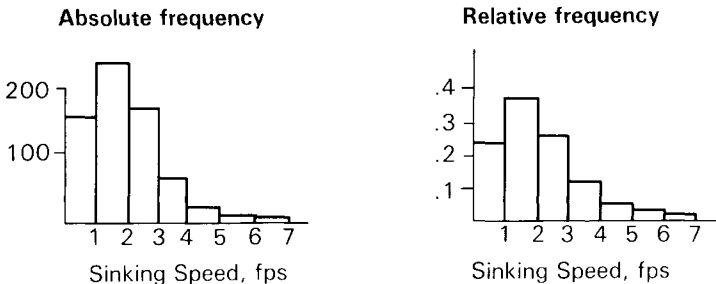
^cSinking speed associated with the cumulative relative frequency.

$$P(x > x_1) = \int_{x_1}^{\infty} p(x) dx$$

This latter description is sometimes referred to as a *cumulative* probability distribution, to distinguish it from a probability density. The various elements $p(x) dx$ are *accumulated* from ∞ back to x_1 .

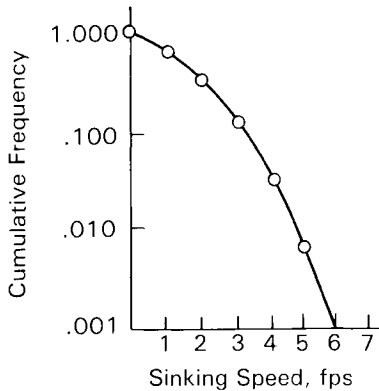
A probability density, like a probability of a discrete event, has a frequency-of-occurrence counterpart. If we consider, in turn, the probability that x lies between 0 and 1, 1 and 2, 2 and 3, etc., sufficient trials can be accumulated within each band to establish a relative frequency of occurrence that tends to approximate the finite probability that x lies in that band. For example, suppose that in 657 landings, the number of landings in each of various sinking speed bands was found to be as given in Table B.1.

Either the absolute or relative frequencies, shown in the second and third columns of Table B.1, can be plotted in histogram form.



Further, if the relative frequencies are divided by the width of the interval (in this case, by coincidence, by unity), then the area within each interval, given by the width times the height, will be the probability associated with that interval. The resulting histogram then approximates the probability density.

The cumulative relative frequency, the fourth column in Table B.1, is usually best plotted on semilog coordinates.



If it were desired to set a limit-design sinking speed corresponding to a cumulative probability of, say, 1/100,000, such a curve could be extrapolated with sufficient confidence to give a rough indication of what this sinking speed should be.

B.4 FREQUENCY OF EXCEEDANCE

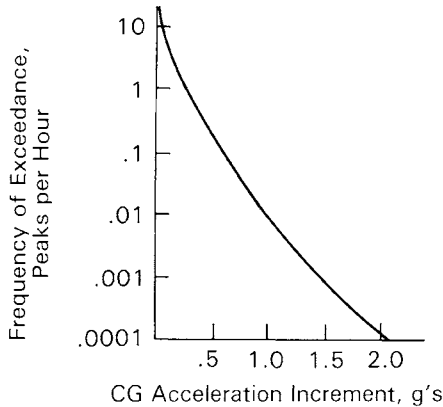
Suppose that a cumulative frequency curve such as shown in the preceding section is prepared not for sinking speed, but for airplane c.g. acceleration “peaks” associated with flight in turbulence. The event is then not a sinking speed but an acceleration peak, and there will be many such peaks, of various magnitudes, in a single flight. The cumulative frequency would then be

$$\frac{\text{number of peaks exceeding a certain value}}{\text{total number of peaks}}$$

This ratio, however, has little significance. (Also, it is ambiguous in that the total number of peaks varies greatly, depending on the selection of a threshold below which it is considered that peaks cannot be reliably identified.) What is significant, instead, is the ratio

$$\frac{\text{number of peaks exceeding a certain value}}{\text{number of hours of flight}}$$

that is, the number of peaks exceeding a given value, on the average, per hour of flight.



A similar and sometimes equally significant quantity is the number of peaks exceeding a given value, on the average, per flight rather than per flight hour.

A frequency of exceedance may describe positive peaks alone, negative peaks alone, the sum of positive and negative peaks, or cycles. A cycle consists of a pair of equal positive and negative peaks; expression of a frequency of exceedance in cycles is appropriate for theoretical exceedance data in which the expected numbers of positive and negative peaks are equal.

It is important to note that a frequency of exceedance (per h) is *not* a probability that an exceedance will occur in a given hour of flight. The distinction is discussed in Sec. 4.9.

This page intentionally left blank

APPENDIX C GAUSSIAN PROBABILITY DISTRIBUTION PLOTS

C.1 PLOTS

Plots of the cumulative Gaussian probability distribution are presented in Fig. C.1a–f. The basic curve on each page is the one labeled “normal.” This curve is a plot of

$$1 - P\left(\frac{y}{\sigma}\right) = \int_{\frac{y_1}{\sigma}}^{\infty} p\left(\frac{y}{\sigma}\right) d\left(\frac{y}{\sigma}\right)$$

rather than the probability distribution itself

$$P\left(\frac{y}{\sigma}\right) = \int_{-\infty}^{\frac{y_1}{\sigma}} p\left(\frac{y}{\sigma}\right) d\left(\frac{y}{\sigma}\right)$$

The quantity $1 - P(y/\sigma)$ is much more meaningful than $P(y/\sigma)$ in loads applications because of the natural interest in the relatively low probabilities of exceeding relatively high loads. A value of $1 - P(y/\sigma)$ of 0.00026 is much more descriptive, for example, than the corresponding value of $P(y/\sigma)$, 0.99974.

Indeed, the reason for preparing and presenting these curves was to make quantitative information available at high y/σ values. All of the widely available tables give values to a fixed number of decimal places, typically 4 or 5. This is obviously far from adequate to describe probabilities of exceedance of 10^{-8} or 10^{-9} !

In Fig. C.1a–c, curves are also given labeled “ $2 \times$ normal” and “circular normal.” The $2 \times$ normal curve is exactly that. It gives the probability that $|y/\sigma|$ will be exceeded—that is, that y/σ will be exceeded without regard to sign. The circular normal curve relates to a joint Gaussian probability distribution of x and y for which $\sigma_x = \sigma_y = \sigma$ and $\rho = 0$, where ρ is the correlation coefficient. For such a distribution, contours of constant probability density are circles. The circular-normal curve in each figure gives the probability that a point x, y lies outside any such circle, where the circle is defined by the ratio of its radius r to $\sigma_x = \sigma_y = \sigma$. In the context of such a joint probability distribution, the three curves are related as indicated by the following

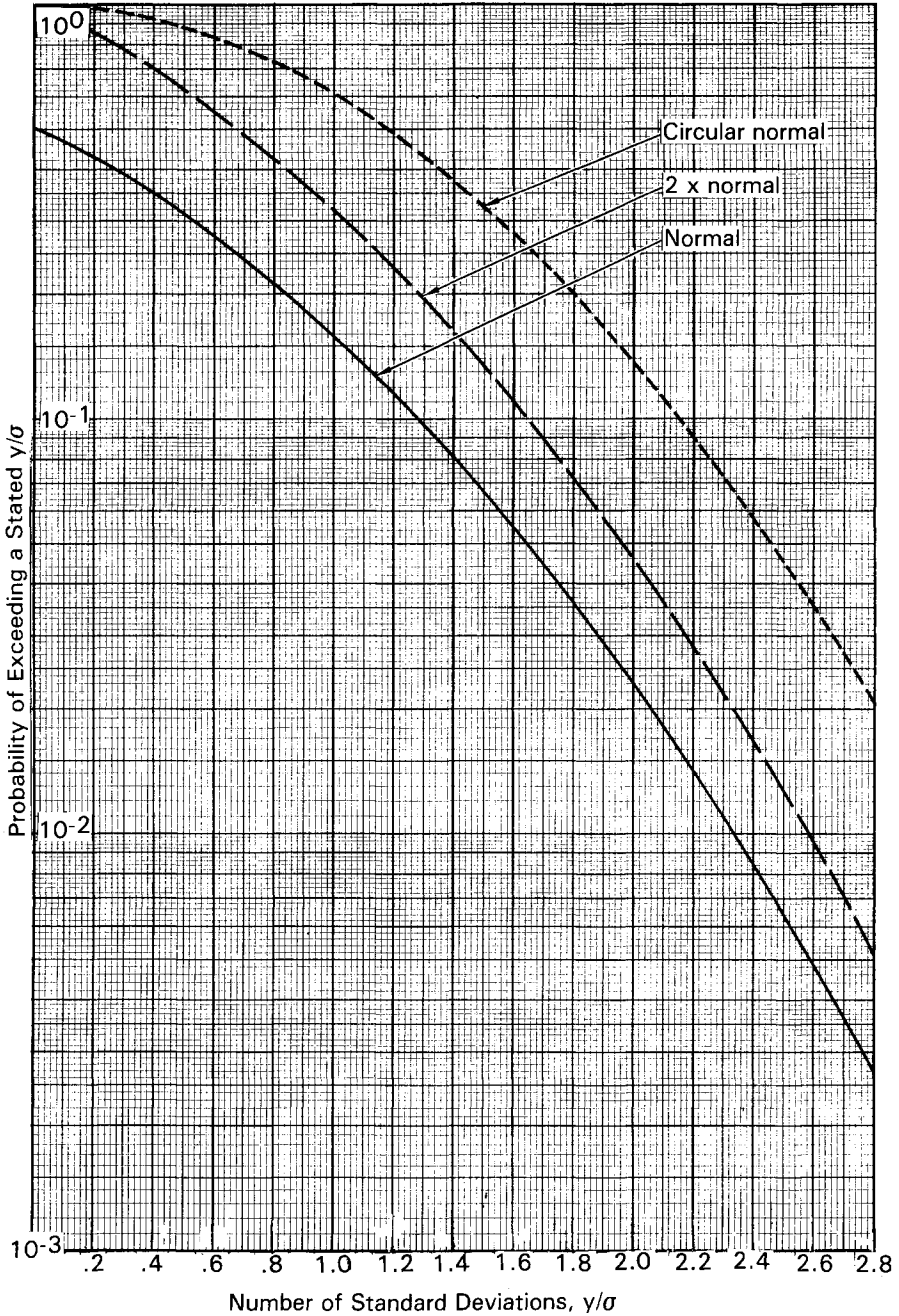


Fig. C.1a Cumulative normal distribution.

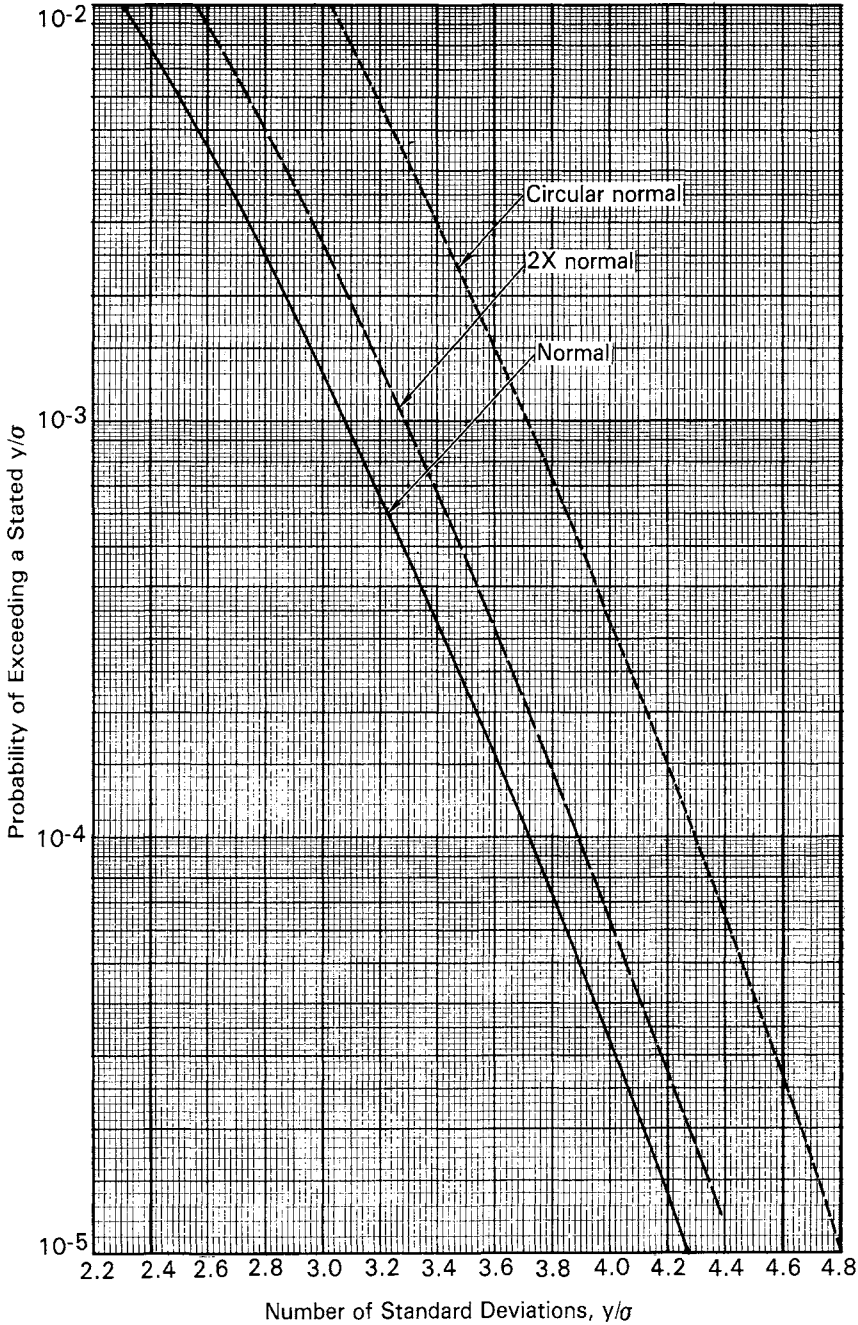


Fig. C.1b Cumulative normal distribution.

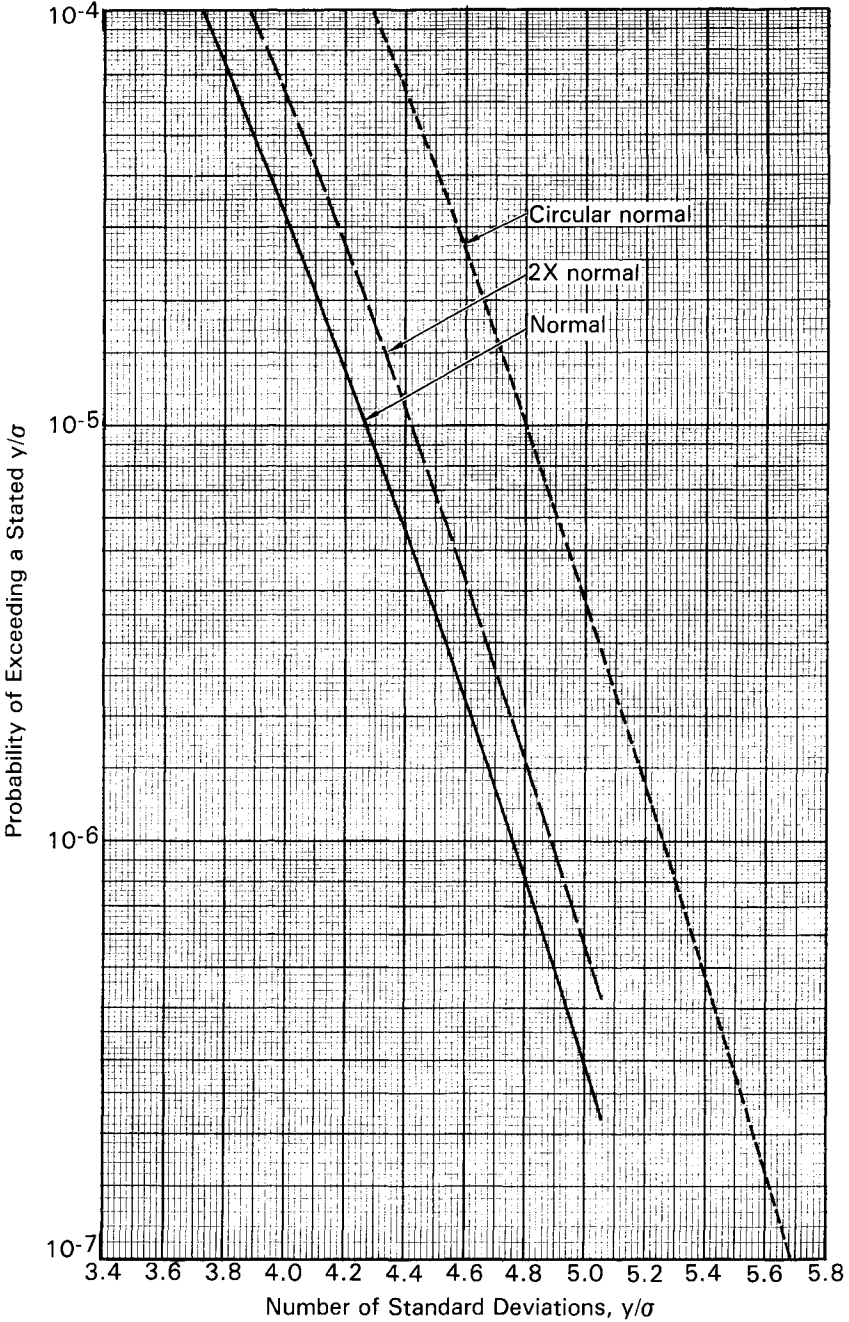


Fig. C.1c Cumulative normal distribution.

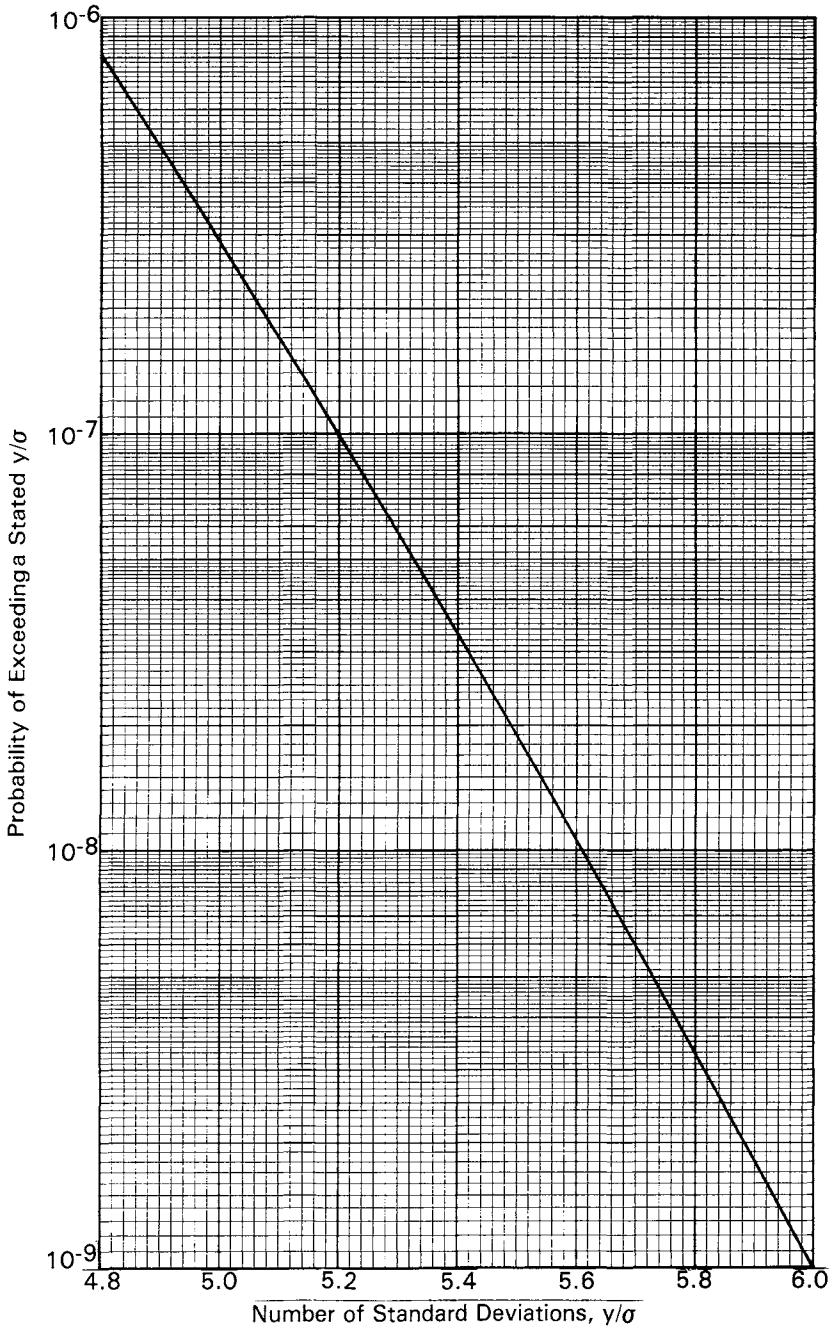


Fig. C.1d Cumulative normal distribution.

Downloaded by RMIT UNIV BUNDOORA on June 4, 2013 | http://arc.aiaa.org | DOI: 10.2514/4.861888

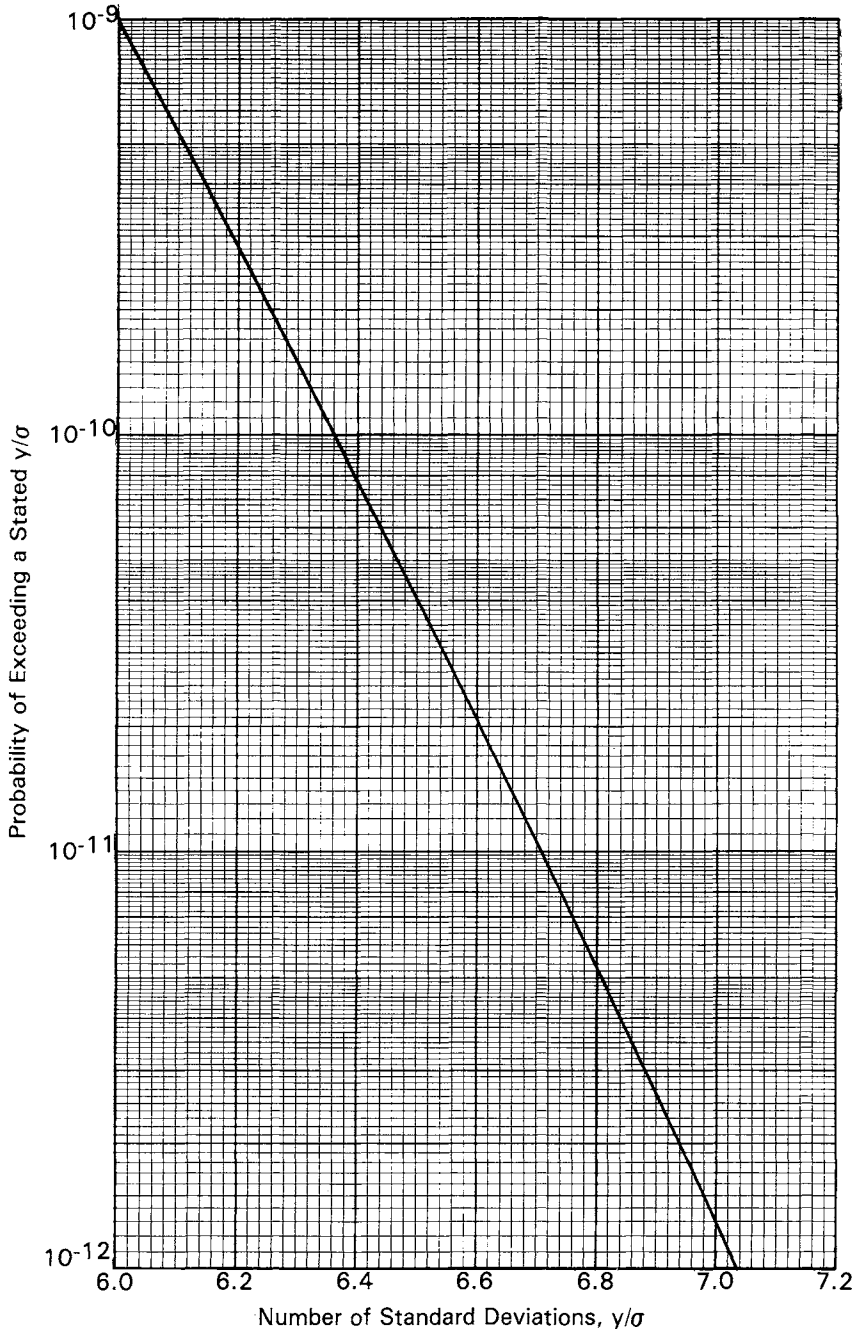


Fig. C.1e Cumulative normal distribution.

Downloaded by RMIT UNIV BUNDOORA on June 4, 2013 | http://arc.aiaa.org | DOI: 10.2514/4.861888

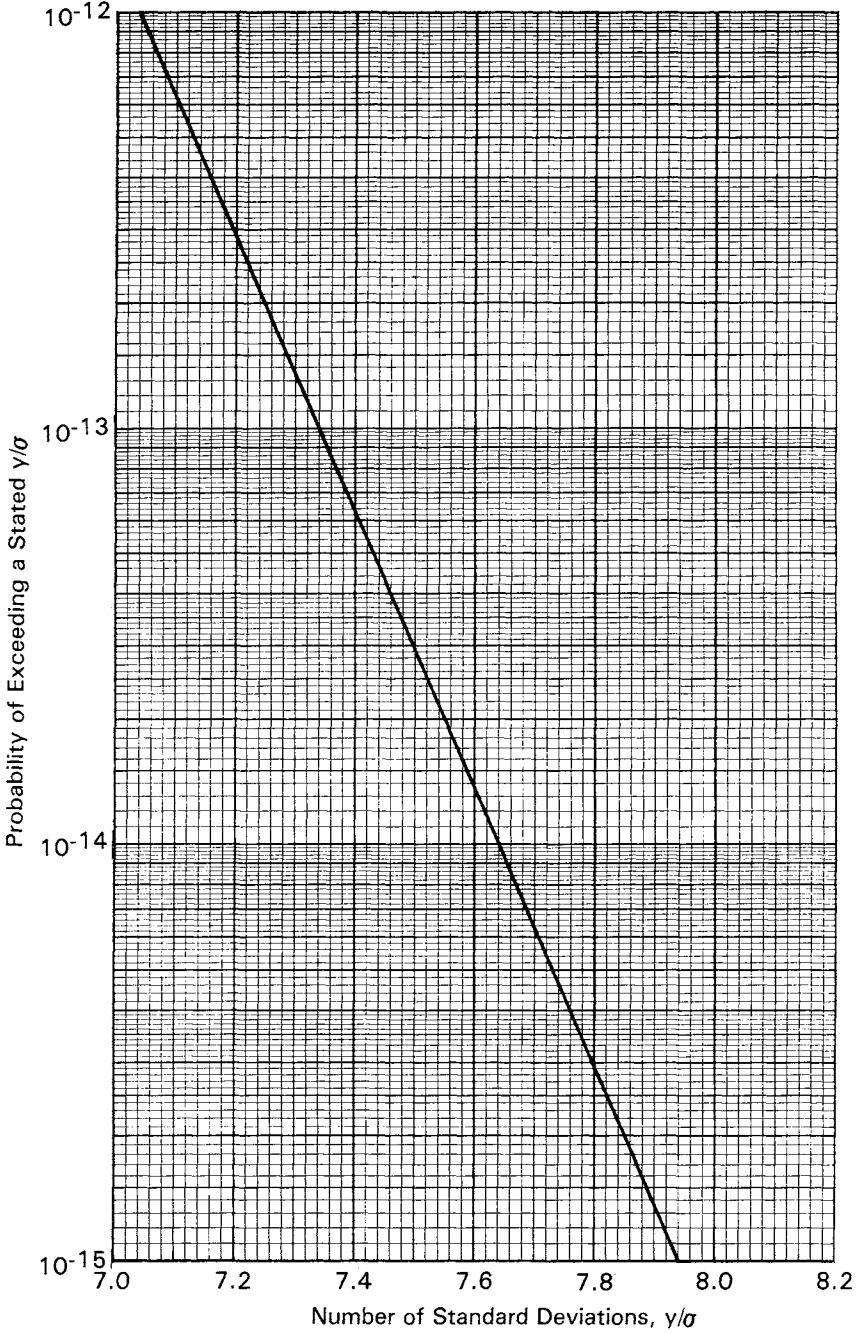
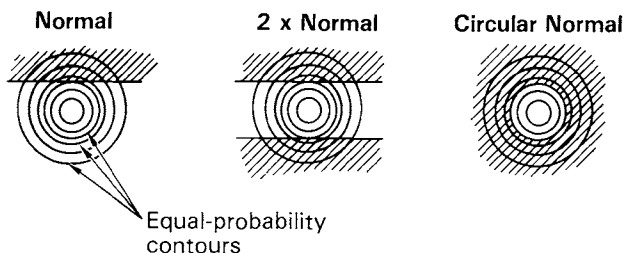


Fig. C.1f Cumulative normal distribution.

sketches, in which the contours are of constant probability density and the shaded area indicates the region over which $\iint p(x, y) dx dy$ is carried out.



C.2 SOURCES OF DATA: y/σ LESS THAN 5.0

For y/σ in the range 0–5.0, the normal curve was plotted from values given in Ref. 66 (Table 26.1, pp. 966–972). Values for the $2 \times$ normal curve followed at once.

Values of the circular normal curve were computed from

$$P\left\{\frac{r}{\sigma} > \frac{r_1}{\sigma}\right\} = e^{-(r_1/\sigma)^2/2}$$

where r is the radius. This formula is given on p.101 of Burington and May.⁶⁷ It can be used for all values of r/σ .

C.3 SOURCE OF DATA: y/σ GREATER THAN 5.0

Only the normal curve is presented for y/σ greater than 5. It was computed using an equation given by Kenney in Ref. 68 (Part Two, pp. 57 and 58). The development follows.

Let y be a random variable with a mean of zero and a Gaussian probability distribution. Its probability density is then

$$p(y) = \frac{1}{\sqrt{2\pi}} \frac{1}{\sigma} e^{-\frac{y^2}{2\sigma^2}} \quad (C.1)$$

To change the variable from y to y/σ , we think in terms of the plot of $p(y)$ vs y ; when abscissas (y) are divided by σ , ordinates [$p(y)$] must be multiplied by σ to maintain unit area under the curve. Thus,

$$p\left(\frac{y}{\sigma}\right) = \frac{1}{\sqrt{2\pi}} e^{-\frac{1}{2}\left(\frac{y}{\sigma}\right)^2} \quad (C.2)$$

The cumulative probability distribution is then

$$P\left(\frac{y_1}{\sigma}\right) = \int_{-\infty}^{\frac{y_1}{\sigma}} p\left(\frac{y}{\sigma}\right) d\left(\frac{y}{\sigma}\right) \quad (C.3)$$

$$= \frac{1}{\sqrt{2\pi}} \int_{-\infty}^{\frac{y_1}{\sigma}} e^{-\frac{1}{2}\left(\frac{y}{\sigma}\right)^2} d\left(\frac{y}{\sigma}\right)$$

$$= 0.5 + \frac{1}{\sqrt{2\pi}} \int_0^{\frac{y_1}{\sigma}} e^{-\frac{1}{2}\left(\frac{y}{\sigma}\right)^2} d\left(\frac{y}{\sigma}\right) \quad (C.4)$$

Now let

$$\frac{y}{\sigma} = \sqrt{2}x \quad \text{or} \quad x = \frac{1}{\sqrt{2}} \frac{y}{\sigma} \quad (C.5)$$

Substituting into Eq. (C.4) gives

$$P\left(\frac{y_1}{\sigma}\right) = 0.5 + \frac{1}{\sqrt{2}} \frac{1}{\sqrt{\pi}} \int_0^{x_1} e^{-x^2} \sqrt{2} dx$$

$$= 0.5 + \frac{1}{\sqrt{\pi}} \int_0^{x_1} e^{-x^2} dx \quad (C.6)$$

In Eq. (C.6), the upper limit becomes x_1 , because when $y/\sigma = y_1/\sigma$, $x = x_1$. This is analogous to the change in upper limit in Eq. (C.3) from y_1 to (y_1/σ) when y was changed to y/σ in Eq. (C.1) to give Eq. (C.2). Alternate reasoning is to note that when

$$\frac{y}{\sigma} = \frac{y_1}{\sigma}, \quad x = \frac{1}{\sqrt{2}} \frac{y_1}{\sigma}$$

so that the upper limit becomes

$$x = \frac{1}{\sqrt{2}} \left(\frac{y_1}{\sigma}\right) = \frac{1}{\sqrt{2}} (\sqrt{2}x_1) = x_1$$

which may or may not be any more rigorous.

To evaluate

$$\int_0^{x_1} e^{-x^2} dx$$

Kenney suggests two different series.

When $x_1 < 1$ (i.e., $\frac{y_1}{\sigma} < \sqrt{2}$):

$$\int_0^{x_1} e^{-x^2} dx = x_1 - \frac{x_1^3}{3} + \frac{x_1^5}{5(2!)} - \frac{x_1^7}{7(3!)} + \frac{x_1^9}{9(4!)} - R \quad (C.7)$$

where

$$R < \frac{x_1^{11}}{11(5!)}$$

This series, if continued, converges for all values of x_1 , but undesirably slowly for values of $x_1 > 1$.

When $x_1 > 1$ (i.e., $\frac{y_1}{\sigma} > \sqrt{2}$):

$$\int_{x_1}^{\infty} e^{-x^2} dx = \frac{e^{-x_1^2}}{2x_1} \left(1 - \frac{1}{2x_1^2} + \frac{3}{4x_1^4} - \frac{3 \cdot 5}{8x_1^6} + \frac{3 \cdot 5 \cdot 7}{16x_1^8} - \dots \right) \quad (C.8)$$

The consecutive terms continue to decrease only as long as $n \leq x_1^2$, where $n + 1$ is the number of the term. Beyond this point, the series diverges.

The plots in Fig. C.1 are of $1 - P(y/\sigma)$ instead of $P(y/\sigma)$. Accordingly, Eq. (C.6) is modified to

$$1 - P\left(\frac{y_1}{\sigma}\right) = \frac{1}{\sqrt{\pi}} \int_{x_1}^{\infty} e^{-x^2} dx \quad (C.9)$$

where

$$x_1 = \frac{1}{\sqrt{2}} \left(\frac{y_1}{\sigma} \right) \quad (C.10)$$

Substituting Eq. (C.8) yields

$$1 - P\left(\frac{y_1}{\sigma}\right) = \frac{1}{\sqrt{\pi}} \frac{e^{-x_1^2}}{2x_1} \left(1 - \frac{1}{2x_1^2} + \frac{3}{4x_1^4} - \frac{3 \cdot 5}{8x_1^6} + \frac{3 \cdot 5 \cdot 7}{16x_1^8} - \dots \right) \quad (C.11)$$

The curve in Fig. C.1d-f was computed from Eqs. (C.10) and (C.11), using the first three terms of the series in Eq. (C.11). The relative error due to dropping the remaining term is, at most, $(3 \cdot 5)/(8 \cdot 3.5355^6) = 0.00096$.

APPENDIX D RATIO OF VON KÁRMÁN TO DRYDEN GUST PSD'S

The ratio of von Kármán to Dryden gust psd's is plotted as a function of frequency in Fig. D.1, for a series of values of true airspeed. The scale of turbulence L is taken as 2500 ft for both spectra. The rms gust velocity is considered to be the same for both spectra.

The plot is actually of the square root of the ratio of psd's, so that the quantity plotted approximates the ratio of the rms responses, when the response is confined to a fairly narrow frequency band.

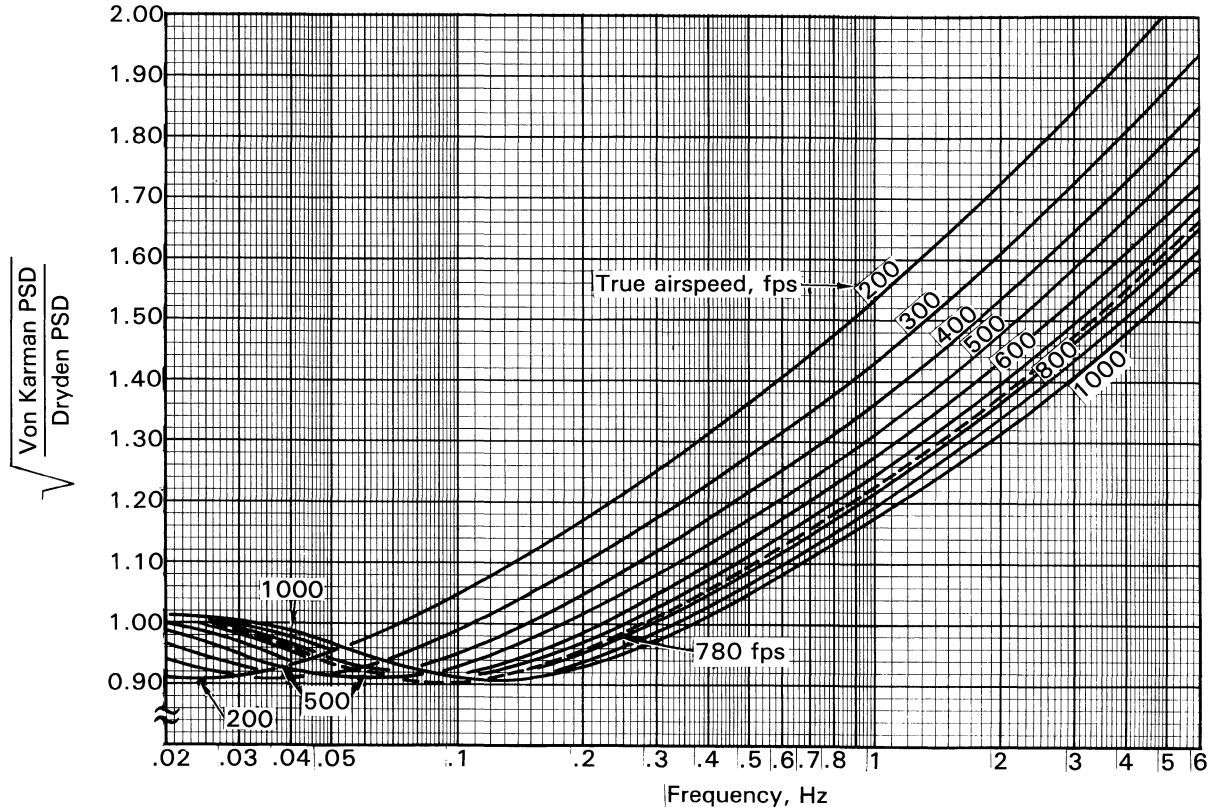


Fig. D.1 Ratio of von Kármán to Dryden gust psd's; $L = 2500$ ft.

APPENDIX E UPPER LIMIT OF INTEGRATION IN COMPUTATION OF \bar{A} , N_0 , AND ρ

E.1 PROBLEM

In the analytical determination of frequency-of-exceedance curves, it is necessary to integrate the response psd's to obtain both \bar{A} and N_0

$$\bar{A} = \sqrt{\int_0^{\infty} \Phi_y(f) \, df}$$

$$N_0 = \sqrt{\frac{\int_0^{\infty} f^2 \Phi_y(f) \, df}{\int_0^{\infty} \Phi_y(f) \, df}}$$

In addition, a similar integration is needed to obtain ρ , the correlation coefficient between any two responses, frequently needed in loads determinations [Eq. (6.1), Sec. 6.1.4].

It is seen that all of these integrals are to be evaluated over the full range of f from 0 to ∞ . In practice, of course, $\Phi_y(f)$ is determined, and the integrals evaluated, only up to some reasonable upper limit, beyond which the contribution to the integral is assumed to be negligible.

For \bar{A} and ρ , computed values are seldom significantly affected by contributions beyond 5 or 10 Hz, but N_0 is a different matter, because of the presence of the f^2 factor. For example, if $\Phi \propto f^{-m}$ beyond some given frequency, then $N_0 = \infty$ (per the calculations) for $m \leq 3$.^{*} Thus, for example,

$$\text{If } \Phi = \frac{\text{const}}{f^{5/3}} \quad N_0 = \infty \text{ (von Kármán gust psd)}$$

^{*}Letting

$$I = \int_a^{\infty} \frac{f^2}{f^m} \, df = \int_a^{\infty} f^{2-m} \, df$$

then, except for the special case of $m = 3$,

$$I = \frac{1}{3-m} f^{3-m} \Big|_a^{\infty} = \frac{1}{3-m} (\infty^{3-m} - a^{3-m})$$

$$\text{If } \Phi = \frac{\text{const}}{f^2} \quad N_0 = \infty \text{ (Dryden gust psd)}$$

$$\text{If } \Phi = \frac{\text{const}}{f^3} \quad N_0 = \infty$$

$$\text{If } \Phi = \frac{\text{const}}{f^{3.01}} \quad N_0 \text{ is finite}$$

For gust velocity, therefore, N_0 is infinite as computed from the generally recognized forms of gust psd. Accordingly, if the integration is performed numerically and carried only to some convenient upper limit, the value of N_0 will be heavily influenced by the selection of the upper limit. Similarly, N_0 and $N(\gamma)$ values obtained from gust velocity time histories can be expected to vary widely depending on the extent to which the high-frequency components are faired out in drawing the curves, removed by the low-pass filter characteristics of the instrumentation, or lost in sampling the analog records at a finite sample interval prior to plotting.

For airplane response, computed N_0 values also depend on the selection of an upper limit. Figure E.1 shows the variation of computed \bar{A} and N_0 values as a function of the upper limit of integration for a typical case. This example, taken from Ref. 36, is for fuselage bending moment on the B-58. It is seen that \bar{A} is well defined with an upper limit of only 6 Hz, whereas N_0 is still increasing at 20 Hz.

E.2 FACTORS TENDING TO MAKE Φ DROP OFF FASTER THAN INDICATED BY SIMPLE THEORY

For several reasons, N_0 for both gust velocity and response may actually be finite. Some of the factors that make both the gust velocity and the

For $m < 3$:

$$I = \frac{1}{|3 - m|} (\infty - a^{3-m}) = \infty$$

For $m > 3$:

$$I = \frac{-1}{|m - 3|} \left(\frac{1}{\infty} - a^{m-3} \right) = \frac{1}{a^{m-3}|m - 3|}$$

For the special case of $m = 3$:

$$\begin{aligned} I &= \left(\int_a^\infty f^{-1} df = \log_e f \right)_a^\infty \\ &= (\log_e \infty - \log_e a) = \infty - \log_e a \\ &= \infty \end{aligned}$$

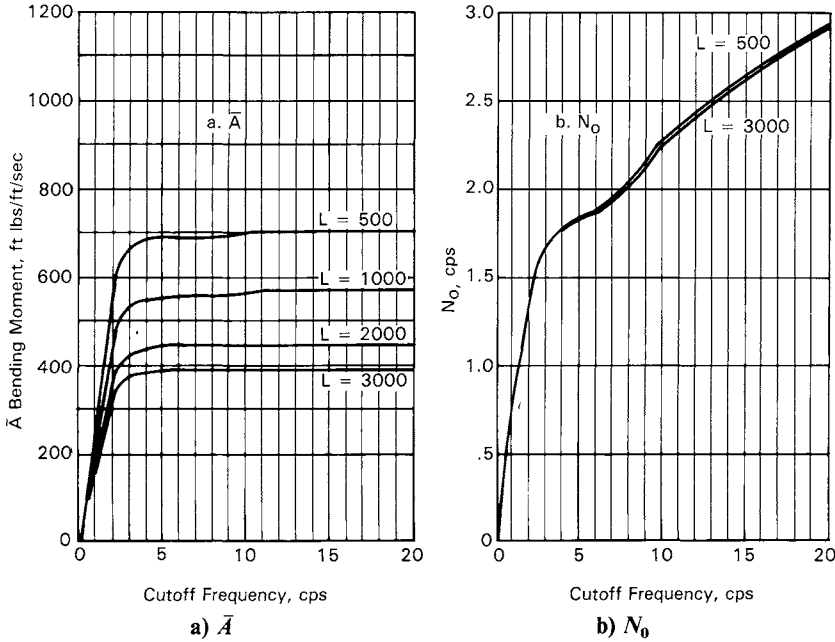


Fig. E.1 Example of variation of \bar{A} and N_0 with upper limit of integration, fuselage bending moment, B-58 airplane, 5% fuel; 50,000 ft.

frequency-response function drop off faster than indicated by theory are the following.

1) *Faster decrease of gust velocity psd with frequency in “viscous sub-range.”* The $-5/3$ power variation of the gust velocity psd with frequency occurs in what is called the “inertia subrange.” At very short wavelengths, viscous effects cause a much faster decrease in psd. Taylor⁶⁹ states that the viscous subrange would be expected to start at a wavelength of “a few centimeters.” Theoretical work by the same author presented in RAE TR 66346⁷⁰ indicates a variation of the psd as the -7 power of frequency in this subrange vs the $-5/3$ power in the inertia subrange.

NACA TN 3920¹¹ quotes an expression for gust psd, based on measurements, that indicates that the viscous subrange starts much earlier, at a wavelength of about 30 ft.*

*This reference suggests the following variation of the Dryden equation, with $c = 50$:

$$\Phi(L\Omega) = \frac{\sigma_w^2}{\pi} \left\{ \frac{1 + 3(L\Omega)^2}{[1 + (L\Omega)^2]^2} + \frac{c^4 + 6c^2(L\Omega)^2 - 3(L\Omega)^4}{[c^2 + (L\Omega)^2]^3} \right\}$$

Frequencies corresponding to the two quoted wavelengths are

$$\lambda = 3 \text{ cm:} \quad f = \frac{V}{\lambda} = \frac{800 \text{ fps}}{0.098 \text{ ft}} = \underline{\underline{8200 \text{ Hz}}}$$

$$\lambda = 30 \text{ ft:} \quad f = \frac{V}{\lambda} = \frac{800 \text{ fps}}{30 \text{ ft}} = \underline{\underline{27 \text{ Hz}}}$$

The first value seems more plausible. It is much too high to do very much good from a practical standpoint.

2) *Averaging of gust velocity over wing chord.* For a typical wing chord of 25 ft, the key frequency is

$$f = \frac{V}{\lambda} = \frac{800 \text{ fps}}{25 \text{ ft}} = \underline{\underline{32 \text{ Hz}}}$$

This is accounted for in current gust loads analyses.

3) *Averaging of gust velocity over wing span.* From Fig. 9.1, the break frequency is given by $\Omega b = 3$. For a typical wing span of 150 ft, this corresponds to a frequency of

$$f = \frac{\omega}{2\pi} = \frac{\Omega V}{2\pi} = \frac{3V}{2\pi b} = \frac{3}{2\pi} \frac{800 \text{ fps}}{150 \text{ ft}} = \underline{\underline{7.5 \text{ Hz}}}$$

Beyond this frequency, the high-frequency exponent decreases from $-5/3$ to $-8/3$, in terms of effectiveness of the gust velocity in producing c.g. acceleration. This effect is accounted for in available 3-D gust loads computer programs, but not currently in routine gust loads determinations.

4) *Lag in buildup of lift.* This apparently is not a significant effect. An old approximate solution,* applicable to two-dimensional incompressible flow,

It can readily be determined that, at high frequency, $\Phi(L\Omega)$ varies as $(L\Omega)^{-4}$. Plotting $\Phi(L\Omega)$ vs $(L\Omega)$ shows that the curve starts to break from the Dryden curve at roughly $L\Omega = 100$ and has established the $(L\Omega)^{-4}$ variation by $L\Omega = 500$.

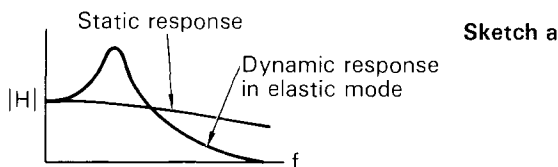
Obviously, this break point must be a function of Ω alone rather than $L\Omega$, so it is necessary to know what value of L was used to nondimensionalize the data on which the value $c = 50$ was based. This is not stated in the reference. However, Ref. 11 was prepared probably a year or two later than Ref. 18, so it is surmised that a value of L of 1000 ft was considered standard. Assuming this value, we obtain

$$\lambda = \frac{2\pi}{\Omega} = \frac{2\pi L}{\Omega L} = \frac{(2\pi)(1000)}{200} = 31.4 \text{ ft}$$

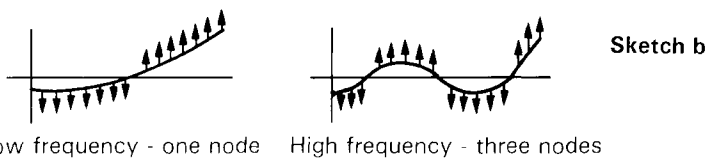
*Utilizing time-domain data from Ref. 5 converted to frequency domain.

indicates that as frequency increases without limit, the lift approaches 0.5 of the zero-frequency value, rather than zero. In any event, this effect is accounted for (for actual planform and Mach number) in current gust loads analyses.

5) *Vibration-isolation effect of elastic-model response.*



6) *Tendency of forces in higher-frequency modes to accumulate over more limited regions of the structure.*



It is seen that, for the same running load, the shear and bending moment will be lower for the higher-frequency model.

7) *Tendency at very high frequencies for local air loads to be reacted by local inertia forces.* At very high frequencies and correspondingly small wavelengths, it would appear that local distributed mass might be great enough, relative to local stiffness (of skin panels, e.g.), so that the gust aerodynamic forces would not be transmitted into the primary structure.

In summary, it appears that the problems of infinite N_0 and sensitivity of computed N_0 to the upper limit of integration are not as serious as might be thought. The reasons are threefold.

1) N_0 is not really infinite even for gust velocity (because of the effects of viscosity).

2) As a result of various phenomena, some of which are accounted for in routine gust loads determination and some of which are not, structural load psd's tend to decrease more rapidly with increasing frequency than does the gust velocity psd.

3) As will be seen in the following section, structural loads are not especially sensitive to N_0 anyway.

E.3 EFFECT OF N_0 ON LOADS

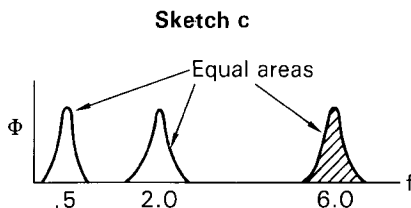
The sensitivity of N_0 to the upper limit of integration (Fig. E.1) is substantially offset by the insensitivity of loads to N_0 . Loads vary directly with \bar{A} ,

but at a given frequency of exceedance, at the limit load level, the incremental load varies only as about the 1/10 power of N_0 .*

$$\text{Load} \propto \sqrt[10]{N_0}$$

Thus, a factor of 2 on N_0 corresponds to approximately a factor of $2^{1/10} = 1.07$ on load.

The following idealized example provides further perspective.



Consider a response psd as indicated by Sketch c. Addition of the 6.0 Hz response (shaded area) increases

$$\bar{A} \text{ in the ratio } \dagger \sqrt{3/2} = \underline{\underline{1.22}}$$

$$N_0 \text{ in the ratio } \dagger \sqrt{\frac{(0.5^2 + 2^2 + 6^2)/3}{(0.5^2 + 2^2)/2}} = 2.51$$

corresponding to a further increase in load
in approximately the ratio $\sqrt[10]{2.51} = \underline{\underline{1.10}}$

E.4 USUAL PRACTICE IN SELECTING UPPER LIMIT

The usual practice is to carry the analyses and the integration to a frequency such that no significant further increase in \bar{A} is to be expected for any load quantity of interest. For current jet transports, this lies in the range 5–15 Hz; 7.5 Hz has been used for much of the L-1011 work. No specific consideration is given to the adequacy of the upper limit thus defined with

*This relation is derived from the generalized exceedance curves of Fig. 4.16. If we enter at the mission analysis limit-design frequency of exceedance of 2×10^{-5} c/h (Sec. 5.4.1) separately for $N_0 = 1$ Hz and $N_0 = 2$ Hz, the y/\bar{A} values at 30,000 ft are 109 and 115.5, respectively. For a factor of 2 increase in N_0 , therefore, the load increases in the ratio $115.5/109 = 1.06$, which is equal to $2^{1/11.9}$.

†For a frequency of exceedance of 2×10^{-3} c/h, corresponding approximately to a design envelope y/\bar{A} of 60, the ratio of loads, at 20,000 ft, is $67.8/61.5 = 1.10$, equal to $2^{1/7.3}$.

Thus, a representative variation is as $N_0^{1/10}$.

‡These ratios follow from Eqs. (4.7) and (4.20), Chapter 4.

respect to N_0 , but in view of the factors noted in Sec. E.2, it would appear that the resulting values of N_0 are fairly realistic.

E.5 HOUBOLT CRITERION

The concept of basing the upper limit of integration only on its effect on \bar{A} has been proposed as a formal criterion, with rational justification, by Houbolt in Ref. 36 and elsewhere. His proposal (p. 21 of Ref. 36) is to plot both \bar{A} and N_0 vs the upper limit of integration, as in Fig. E.1. The top of the knee of the \bar{A} curve is found; N_0 is then obtained by taking the upper limit of integration at the frequency value associated with this knee. For consistency, this frequency might be defined quantitatively as the point where \bar{A} is 98% of its maximum value (p. 29 of Ref. 36).

It is the writer's conviction that Houbolt's rational justification of this procedure is not valid—that the high-frequency content of a time-history record that he discounts as “noise” or “hash,” and that contributes negligibly to the rms value, is *really there* (when predicted by valid theory) and *does* contribute to peak loads if not to rms values. The procedure, therefore, is only an expedient that happens, perhaps, to give fairly good results. If all of the factors noted in Sec. E.2 were properly accounted for in the theory, it might well be that much of the variation of N_0 with upper limit, beyond the \bar{A} knee, would disappear.

This page intentionally left blank

APPENDIX F PLOTS OF σ_w PROBABILITY DISTRIBUTIONS

This appendix presents σ_w probability distribution plots in a particular form, the probability that $\sigma_w > \sigma_{w_1}$ vs σ_{w_1} . These plots appear in Fig. F.1. They are based on P 's and b 's read from Figs. 5-3 and 5-4 of Ref. 13. They are for use with a scale of turbulence L of 2500 ft *at all altitudes*. Military specifications call for reduced L 's at altitudes below 2500 ft, which require modifications to the b 's.

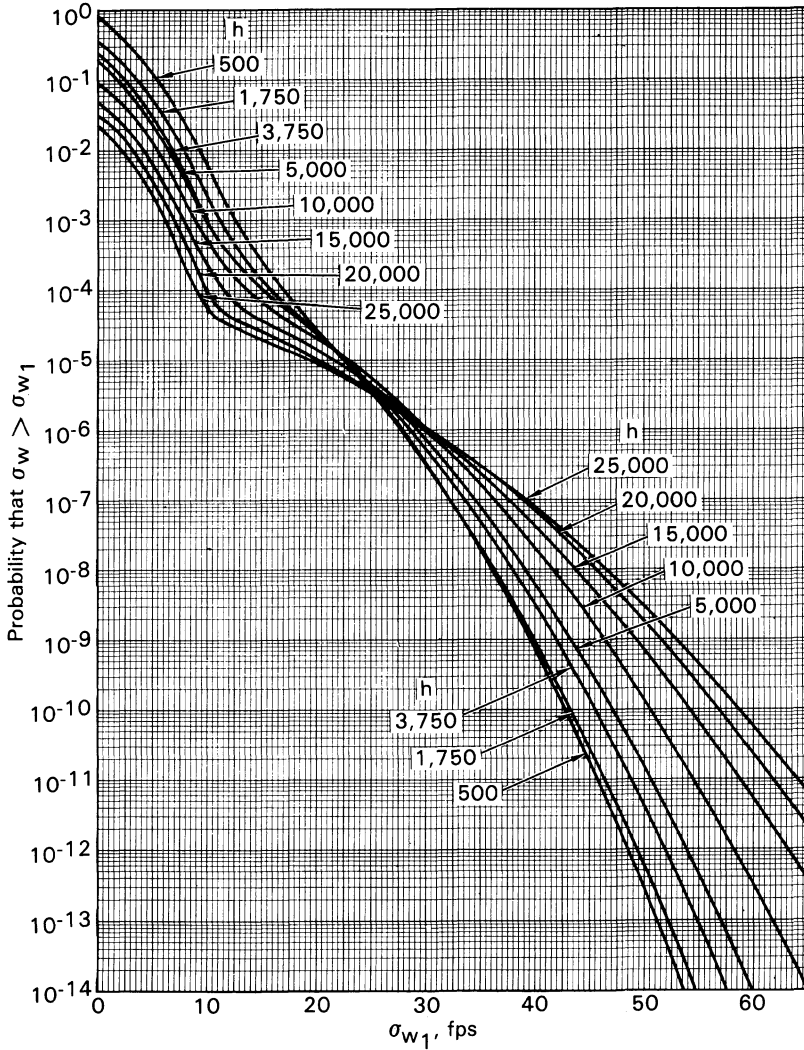
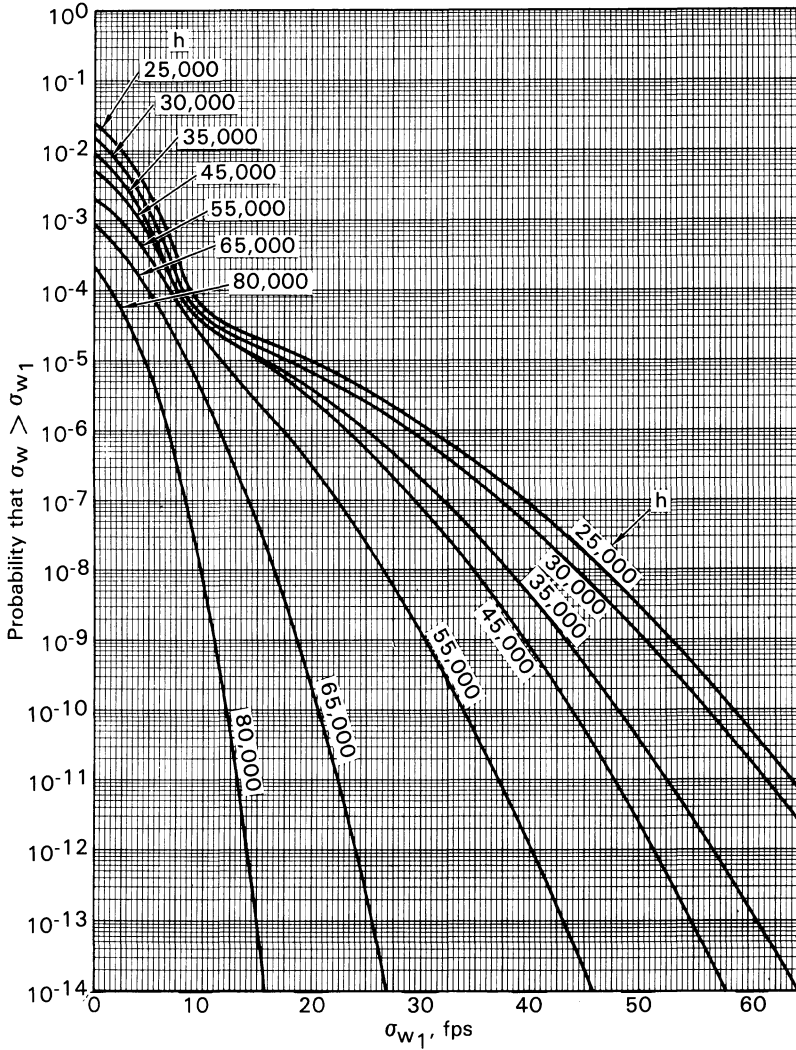


Fig. F.1 Probability distribution of σ_w , P 's, and b 's from Ref. 13.
a) $h = 500\text{--}25,000$ ft.

Downloaded by RMIT UNIV BUNDOORA on June 4, 2013 | http://arc.aiaa.org | DOI: 10.2514/4.861888



**Fig. F.1 (continued) Probability distribution of σ_w , P 's, and b 's from Ref. 13.
b) $h = 25,000\text{--}80,000$ ft.**

Downloaded by RMIT UNIV BUNDOORA on June 4, 2013 | http://arc.aiaa.org | DOI: 10.2514/4.861888

This page intentionally left blank

APPENDIX G DERIVATION OF GENERALIZED FREQUENCY OF EXCEEDANCE EQUATION

Equation (4.27), Sec. 4.7.5, is derived from Eqs. (4.25) and (4.26), Secs. 4.7.3 and 4.7.4, as follows. Substituting Eq. (4.26) into Eq. (4.25) gives

$$\begin{aligned}
 N(y) &= \int_0^\infty N_0 \exp\left[-\frac{1}{2} \frac{(y/\bar{A})^2}{\sigma_w^2}\right] \left\{ P_1 \sqrt{\frac{2}{\pi}} \frac{1}{b_1} \exp\left[-\frac{1}{2} \left(\frac{\sigma_w}{b_1}\right)^2\right] \right. \\
 &\quad \left. + P_2 \sqrt{\frac{2}{\pi}} \frac{1}{b_2} \exp\left[-\frac{1}{2} \left(\frac{\sigma_w}{b_2}\right)^2\right] \right\} d\sigma_w \\
 &= \int_0^\infty N_0 \left\{ \exp\left(-\frac{1}{2} \frac{(y/\bar{A})^2}{\sigma_w^2}\right) \right\} \left\{ P_1 \sqrt{\frac{2}{\pi}} \frac{1}{b_1} \exp\left[-\frac{1}{2} \left(\frac{\sigma_w}{b_1}\right)^2\right] \right\} d\sigma_w \\
 &\quad + \int_0^\infty N_0 \left\{ \exp\left[-\frac{1}{2} \frac{(y/\bar{A})^2}{\sigma_w^2}\right] \right\} \left\{ P_2 \sqrt{\frac{2}{\pi}} \frac{1}{b_2} \exp\left[-\frac{1}{2} \left(\frac{\sigma_w}{b_2}\right)^2\right] \right\} d\sigma_w \\
 &= N_0 P_1 \sqrt{\frac{2}{\pi}} \frac{1}{b_1} \int_0^\infty \exp\left[-\frac{1}{2} \left(\frac{\sigma_w}{b_1}\right)^2\right] \exp\left[-\frac{1}{2} \frac{(y/\bar{A})^2}{\sigma_w^2}\right] d\sigma_w \\
 &\quad + N_0 P_2 \sqrt{\frac{2}{\pi}} \frac{1}{b_2} \int_0^\infty \exp\left[-\frac{1}{2} \left(\frac{\sigma_w}{b_2}\right)^2\right] \exp\left[-\frac{1}{2} \frac{(y/\bar{A})^2}{\sigma_w^2}\right] d\sigma_w \quad (G.1)
 \end{aligned}$$

Each of these two integrals can be put into the form of Peirce's Eq. 495 (Ref. 22)

$$\int_0^\infty e^{-x^2 - \frac{a^2}{x^2}} dx = \frac{\sqrt{\pi}}{2} e^{-2a} \quad (G.2)$$

If we set

$$x = \frac{1}{\sqrt{2}} \frac{\sigma_w}{b_1}$$

it follows that

$$\sigma_w = \sqrt{2b_1}x \quad \text{and} \quad d\sigma_w = \sqrt{2b_1} dx$$

The first integral in Eq. (G.1) thus becomes

$$\begin{aligned} & \int_0^\infty \exp(-x^2) \exp\left[-\frac{1}{2} \frac{(y/\bar{A})^2}{2b_1^2} \frac{1}{x^2}\right] \sqrt{2b_1} dx \\ &= \sqrt{2b_1} \int_0^\infty \exp(-x^2) \exp\left[-\frac{(y/\bar{A})^2}{2^2 b_1^2} \frac{1}{x^2}\right] dx \\ &= \sqrt{2b_1} \int_0^\infty \exp(-x^2) \exp\left(-\frac{a^2}{x^2}\right) dx \\ &= \sqrt{2b_1} \int_0^\infty \exp\left(-x^2 - \frac{a^2}{x^2}\right) dx \end{aligned} \tag{G.3}$$

where

$$a = \frac{y/\bar{A}}{2b_1}$$

The first term in Eq. (G.1) is then, from Eq. (G.2),

$$N_0 P_1 \sqrt{\frac{2}{\pi}} \frac{1}{b_1} \sqrt{2b_1} \frac{\sqrt{\pi}}{2} e^{-2\frac{y/\bar{A}}{2b_1}} = N_0 P_1 e^{-\frac{y/\bar{A}}{b_1}} \tag{G.4}$$

Similarly, the second term is

$$N_0 P_2 e^{-\frac{y/\bar{A}}{b_2}} \tag{G.5}$$

Consequently, Eq. (G.1) becomes

$$N(y) = N_0 P_1 e^{-\frac{y/\bar{A}}{b_1}} + N_0 P_2 e^{-\frac{y/\bar{A}}{b_2}} \tag{G.6}$$

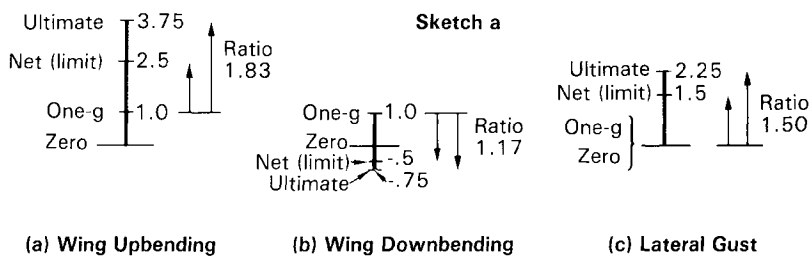
This is Eq. (4.27), Sec. 4.7.5.

Downloaded by RMIT UNIV BUNDOORA on June 4, 2013 | http://arc.aiaa.org | DOI: 10.2514/4.861888

APPENDIX H RELATIVE ULTIMATE GUST CAPABILITIES FOR UPBENDING, DOWNBENDING, AND LATERAL GUST

Gust loads, like most other structural design loads, are customarily defined at the “limit design” level. A factor of safety of 1.50 is then applied to convert to ultimate design loads. As noted in Sec. 5.3.1, however, airplanes do encounter gust loads approaching ultimate, and if the strength resulting from the 1.50 factor of safety were not there, the airplanes would not survive.

Unfortunately, as has often been noted, designing to *limit* loads can be expected to lead to vastly different *ultimate* gust velocity capabilities for upgusts, downgusts, and lateral gusts. (In a continuous turbulence context, it would be more precise to speak of different capabilities for wing upbending, wind downbending, and lateral gust loadings.) This difference is the result of the presence, or absence, of the 1-g steady-flight load, as illustrated by the particular example shown in Sketch a:



Distances vertically along the bar in each case are relative load.

In cases a) and b) in Sketch a, the ratio of gust increment in load to 1-g load is taken as 1.5. This corresponds, in case a), to a ratio of net limit to 1-g load of 2.5. The actual value of this ratio depends on the particular airplane and load quantity. Values for wing-bending moment for various Lockheed transport airplanes at various wing locations range from about 1.75–3.25; the value 2.5 chosen here for the purpose of illustration is fairly typical.

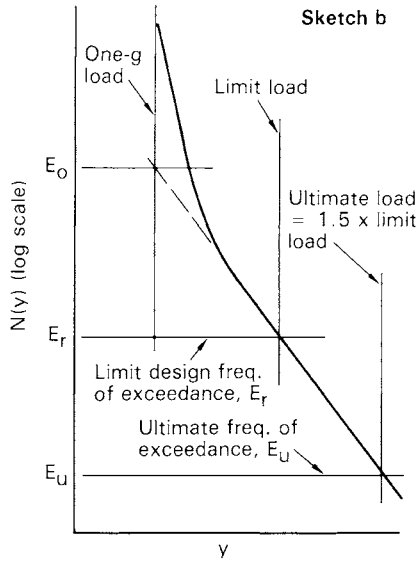
It is seen that the ultimate gust velocity capability for lateral gust is only 82% of that for wing upbending (1.50 vs 1.83 times the limit design gust velocity). For wing downbending, it is only 64% of that for wing upbending (1.17 vs 1.83). In slightly different terms, the additional capability provided by the ultimate factor of safety is only 20% as much for downbending as for upbending (0.17 vs 0.83).

These differences are so great as to suggest that perhaps there is real urgency in establishing ultimate gust load criteria, either in place of or in addition to our present limit load criteria. Indeed, in the design of the L-1011-1, additional wing downbending conditions were defined such as to assure an ultimate frequency of exceedance in downbending comparable to that in upbending.

Nevertheless, there is a line of reasoning that suggests that the historical practice of designing only to limit conditions may yield ultimate strengths that are actually fairly appropriate. This reasoning considers the presence, in actual flight, of maneuvering loads in combination with the gust loads. Loss of control in severe turbulence appears to have been a greater hazard to transport aircraft than high loads due directly to the turbulence. The most likely sequence leading to loss of an airplane would appear to be an upset resulting in a dive and increased airspeed, followed by an attempted recovery by means of a pull-up maneuver. The loads due to the pull-up plus the turbulence then exceed the ultimate strength. The dive might result from either a nose-down upset or an upset in roll. In order to provide for the pull-up maneuver, a larger incremental-load ultimate capability would be necessary for upgusts than for down- or lateral gusts. Such a capability tends to be provided by the current criteria. An airplane in turbulence is, of course, subject to other types of upset than that postulated. A nose-up upset, however, would tend to result in a decrease in airspeed and an increase in altitude; one would expect the ensuing pushover maneuver to be much less severe than a pull-up following a dive. The consequences of an upset in yaw are entirely a matter of speculation.

How this reasoning might work out quantitatively is illustrated in Figs. H.1a-j. These figures all show hypothetical exceedance curves. As indicated earlier (Sec. 4.7.5, Sketch t and Sec. 4.8.3, Sketch u), generalized exceedance curves are usually considered to have a shape given by the sum of two straight lines on a semilog plot (Sketch b). This shape is also a good approximation to dimensional exceedance curves, $N(y)$ vs y , even after the curves for the various mission segments have been added together. Inasmuch as limit load occurs well to the right of the bend in the curve, the storm-turbulence straight line gives a useful approximation in the region between the limit and ultimate levels.

The shape of the curve in this region can be completely defined by the quantity E_0/E_r . E_0 and E_r are defined as indicated in Sketch b. The subscript r is for "reference" and is used here for consistency with earlier Lockheed work. E_u (u for ultimate) denotes the frequency of exceedance of a load of 1.5 times limit.



Examination of a wealth of calculated wing-bending moment exceedance curves indicates that values of E_0/E_r tend to run between 10^4 and 10^5 . 10^4 is perhaps a more representative value than 10^5 .

Figure H.1a shows upbending and downbending exceedance curves for this value of E_0/E_r (10^4) and $L_{net}/l_{1-g} = 2.5$. The horizontal coordinate is relative load. The scale shown is for *incremental* load (zero for 1-g level flight) in terms of relative U_σ (continuous-turbulence gust velocity, Sec. 5.3.2). The ultimate loads for both upbending and downbending are taken as 1.5 times the respective limit loads. The ratio of ultimate to limit gust capability in terms of frequency of exceedance is seen to be

$$\text{Upbending} \quad E_u/E_r = 10^{-3.33}$$

$$\text{Downbending} \quad E_u/E_r = 10^{-0.57}$$

Figure H.1b shows the corresponding lateral gust case

$$\text{Lateral gust} \quad E_u/E_r = 10^{-2.00}$$

Figure H.1c shows the effect of superimposing a steady maneuver load of one-half the 1-g steady flight load on the gust loads. Curves *A* are the curves of Fig. H.1a. Curves *B* (long dash) are these curves shifted to the right by one-half the 1-g load. The ultimate frequency of exceedance is now the same for both upbending and downbending; $E_u/E_r = 10^{-2.00}$.

What would appear to be a still more realistic picture is provided by curves *C* (short-dash lines). With the limit design frequency of exceedance taken as 2×10^{-5} c/h (the usual value, Sec. 5.3.1), the frequency of exceedance of ultimate load per curves *B* is 2×10^{-7} c/h; airplanes are not lost this often. Curves *C* were obtained from curves *B* by reducing the slopes, defined as $\Delta U_\sigma / \Delta \log N(y)$, in the ratio $9/11 = 0.82$. This reduces the ultimate $N(y)$ by a factor of 21.5, giving a value of about 10^{-8} , a much more plausible value. The reduction in gust velocity at any given frequency of exceedance, moreover, is consistent with operational load factor data obtained from both the NASA digital VGH program and Lockheed's Airline Usage Data Program. For curves *C* as for curves *B*, the ultimate frequency of exceedance capability is the same for upbending and downbending.

The corresponding lateral gust picture is shown in Fig. H.1d. Adding the symmetric maneuver does not affect the lateral gust loads. So case *B* is the same as case *A*. The ultimate frequency of exceedance is the same as given for wing loads by line *B* in Fig. H.1c. With gust velocities reduced in the ratio $9 : 11$ (curve *C*), the ultimate frequency of exceedance capability is again the same as for wing loads.

A still more realistic picture is that shown in Fig. H.1e. Certainly, the severity of the pull-up maneuver should depend on the gust velocity; in Fig. H.1c, the same $\frac{1}{2}$ -g maneuver is present at all frequencies of exceedance. In Fig. H.1e, the upbending and downbending loads at the ultimate level, and the ultimate frequency of exceedance, are the same as in Fig. H.1c (curve *C*), but the maneuver load is assumed to vary in direct proportion to the gust load. The lateral gust picture is shown in Fig. H.1f (curve *C*); this is the same as shown in Fig. H.1d (curve *C*).

If L_{net}/L_{1-g} is 2.0 instead of 2.5, the result is as shown in Figs. H.1g and H.1h. These figures correspond to Figs. H.1e and f, respectively. Numerical values change—for example E_u/E_r goes from $10^{-3.33}$ to $10^{-4.00}$. But the qualitative relations are identical. In particular, the maneuver increment at the ultimate level is still one-half of the 1-g load, and the ultimate frequency of exceedance is identical for upbending, downbending, and lateral gust.

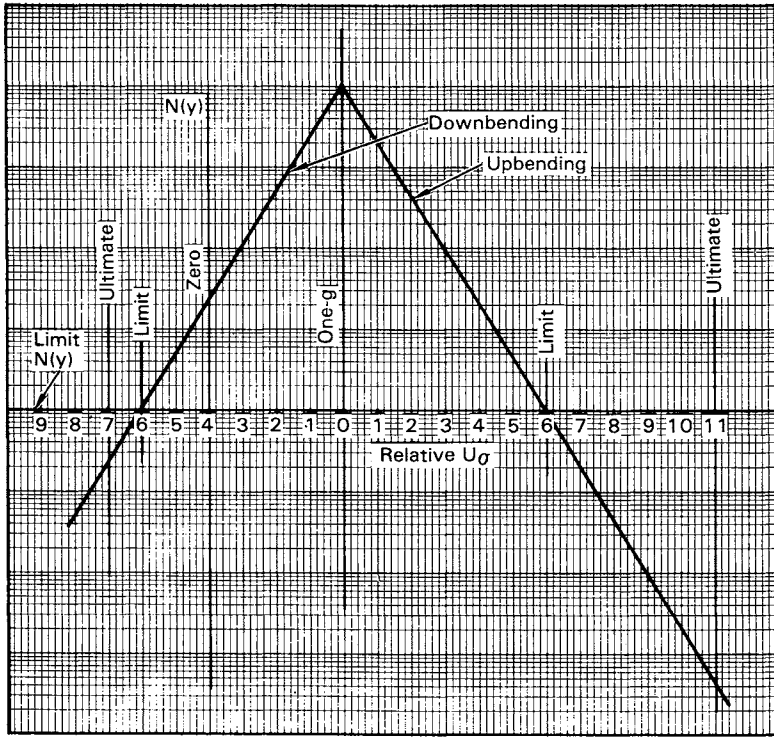
The effect of changing E_0/E_r from 10^4 to 10^5 is shown in Figs. H.1i and j. Again, numerical values change (E_0/E_r goes from $10^{-3.33}$ to $10^{-4.17}$) but the qualitative relations are identical.

Values of E_u/E_r , the ratio of ultimate to limit frequency of exceedance, for various values of E_0/E_r and L_{net}/L_{1-g} are summarized in the following table:

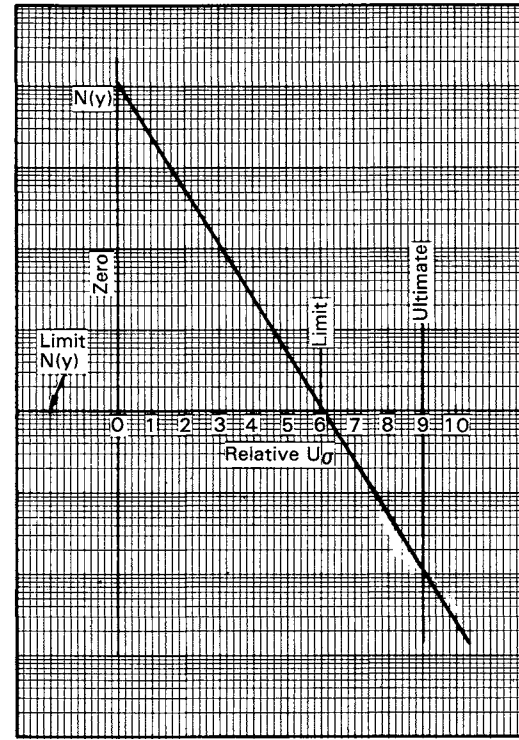
L_{net}/L_{1-g}	$E_{1.5 \text{ lim}}/E_{lim}$	
	$E_0/E_r = 10^4$	$E_0/E_r = 10^5$
2.5	$10^{-3.33}$ (e)	$10^{-4.17}$ (i)
2.0	$10^{-4.00}$ (g)	$10^{-5.00}$

(The first three of the four values are taken from Figs. H.1e, g, and i, as indicated; the fourth is obtained by mentally modifying the right-hand line *A* in Fig. H.1g.)

The foregoing discussion is not intended to lead to new criteria, in which gust and maneuver loads are separately computed and superimposed, although such a possibility is not ruled out. Instead, the intent is to show that loads resulting from a truly rational combination of gust and maneuver might be surprisingly close to those given by present criteria.

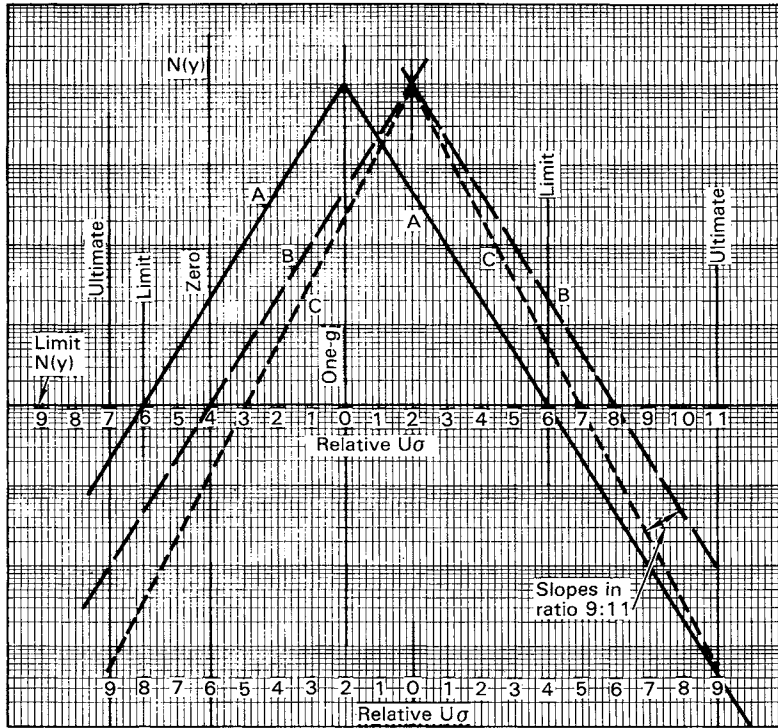


a) Current criteria, vertical gust: $E_0/E_r = 10^4$; $L_{net}/L_{1-g} = 2.5$

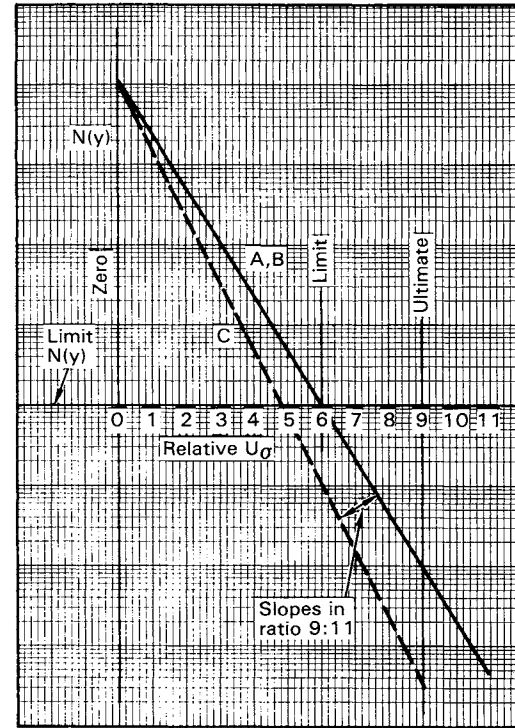


b) Current criteria, lateral gust: $E_0/E_r = 10^4$; $L_{net}/L_{1-g} = 2.5$

Fig. H.1 Idealized frequency of exceedance curves.

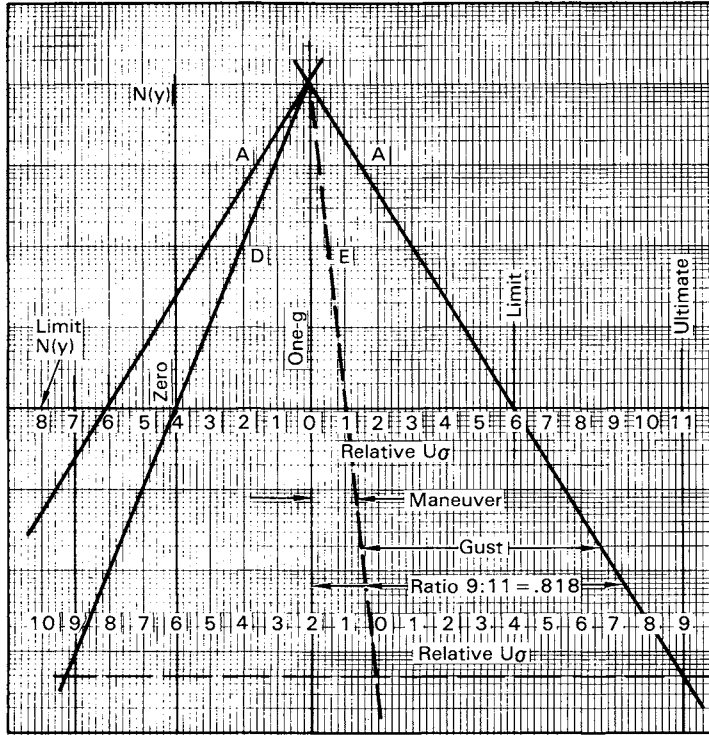


c) Reinterpretation of current criteria, vertical gust: $E_0/E_r = 10^4$; $L_{net}/L_{1-g} = 2.5$

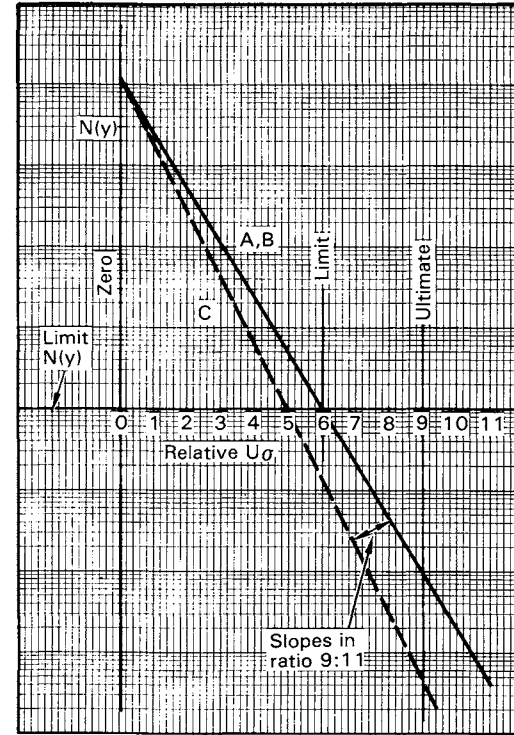


d) Reinterpretation of current criteria, lateral gust: $E_0/E_r = 10^4$; $L_{net}/L_{1-g} = 2.5$

Fig. H.1 (continued) Idealized frequency of exceedance curves.

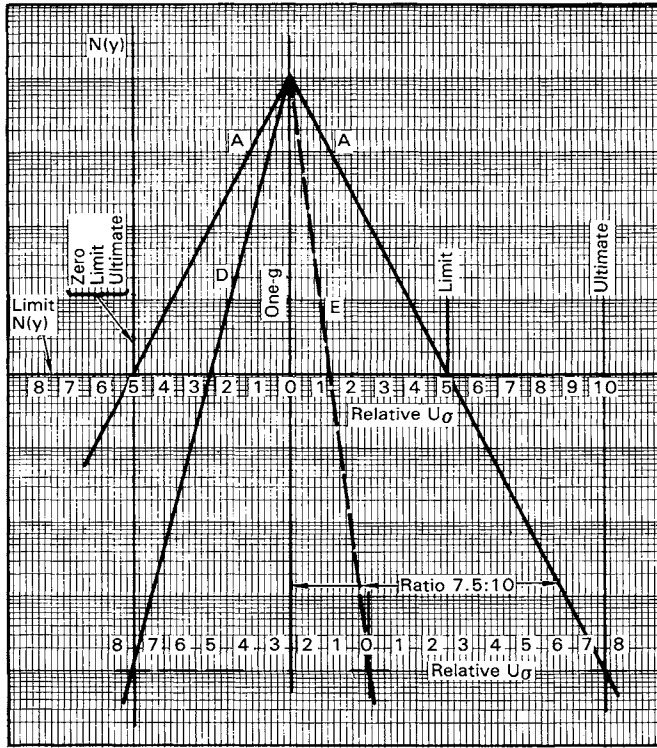


e) Preferred reinterpretation of current criteria, vertical gust: $E_0/E_r = 10^4$; $L_{net}/L_{1-g} = 2.5$

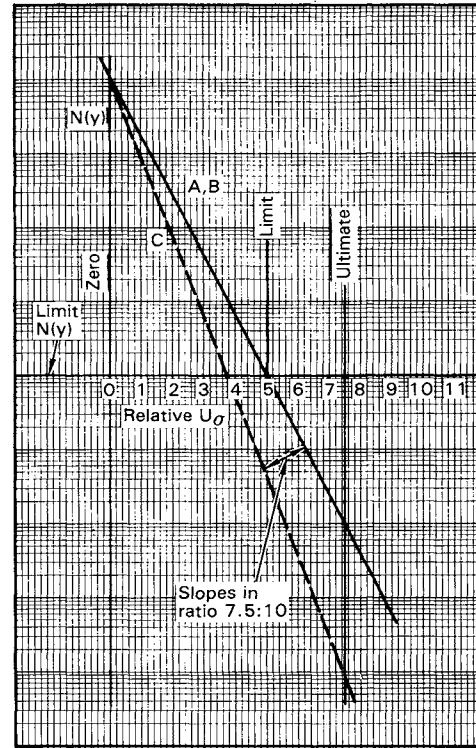


f) Preferred reinterpretation of current criteria, lateral gust: $E_0/E_r = 10^4$; $L_{net}/L_{1-g} = 2.5$

Fig. H.1 (continued) Idealized frequency of exceedance curves.

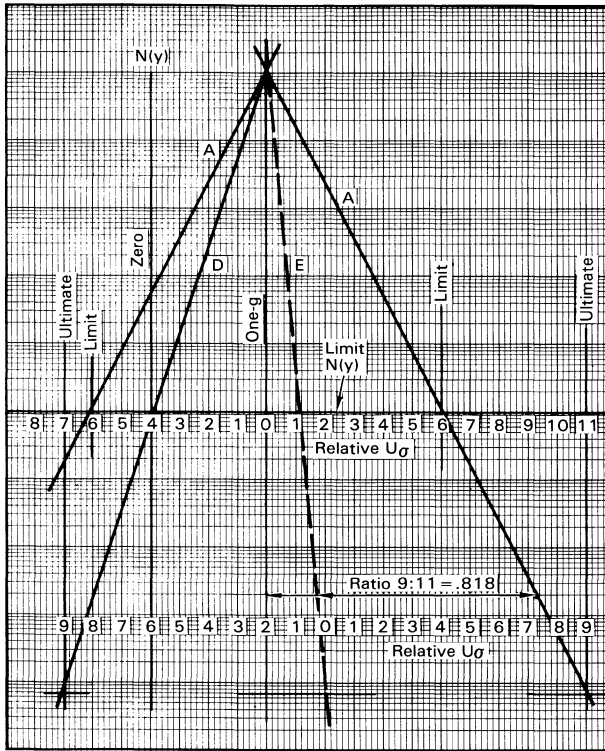


g) Preferred reinterpretation of current criteria, vertical gust: $E_0/E_r = 10^4$; $L_{net}/L_{1-g} = 2.0$

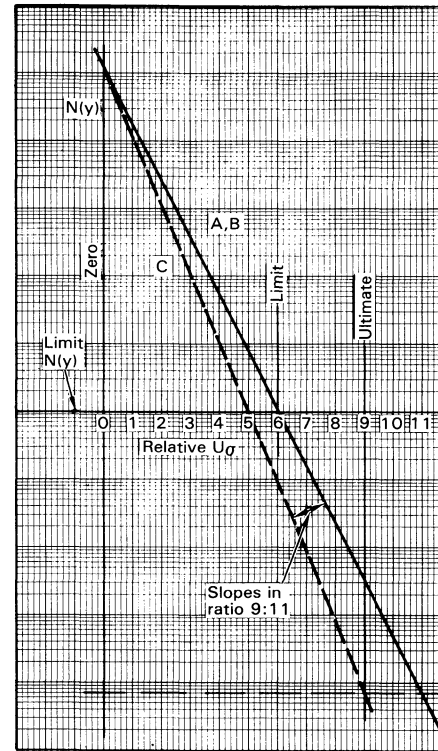


h) Preferred reinterpretation of current criteria, lateral gust: $E_0/E_r = 10^4$; $L_{net}/L_{1-g} = 2.0$

Fig. H.1 (continued) Idealized frequency of exceedance curves.



i) Preferred reinterpretation of current criteria, vertical gust:
 $E_0/E_r = 10^5$; $L_{net}/L_{1-g} = 2.5$



j) Preferred reinterpretation of current criteria, lateral gust: $E_0/E_r = 10^5$; $L_{net}/L_{1-g} = 2.5$

Fig. H.1 (continued) Idealized frequency of exceedance curves.

APPENDIX I

MOST LIKELY σ_w VALUE ASSOCIATED WITH A PARTICULAR LOAD LEVEL

I.1 INTRODUCTION AND RESULTS

This appendix treats three loosely related subjects. All have to do with extracting additional useful information from the continuous turbulence model described in Sec. 4.7.

In this model, as indicated in Sec. 4.7.1, the atmosphere is first considered to be made up of discrete patches of continuous turbulence, each of which is stationary and Gaussian. These patches are of various root-mean-square intensities, σ_w . This discrete-patch model is then replaced by a model that has a continuously varying distribution of σ_w . This variation is considered to be gradual enough so that the relations of output to input developed for a stationary Gaussian process still apply. The probability distribution of this varying σ_w is defined in a particular mathematical form given by Eq. (4.26). This form utilizes four constants, P_1 , P_2 , b_1 , and b_2 , the values of which depend on altitude.

Generalized exceedance curves are derived from this model in Sec. 4.7 and Appendix G. These are in the form of plots of $N(y)/N_0$ vs y/\bar{A} , where for many purposes y/\bar{A} can be considered equivalent to the gust velocity w .*

*The equivalence of w and y/\bar{A} is alluded to in Sec. 4.7.5 and 5.3.2. It can be established as follows. For any particular response quantity y_1 ,

$$y_1 = \left(\frac{y}{\bar{A}}\right) \bar{A}_{y_1}$$

If we consider w to be just another “response” quantity, it follows that

$$w = \left(\frac{y}{\bar{A}}\right) \bar{A}_w = \left(\frac{y}{\bar{A}}\right) \left(\frac{\sigma_w}{\sigma_w}\right) = \left(\frac{y}{\bar{A}}\right) (1) = \frac{y}{\bar{A}}$$

Care must be taken, however, in dealing with *exceedance* data for w . In converting the *generalized exceedance* rate, $N(y)/N_0$, to an *actual* exceedance rate, $N(y)$, one multiplies by N_0 . N_0 for an actual response quantity usually has a fairly well-defined value, but for gust velocity, the computed value is usually infinite. See discussion in Appendix E, Sec. E.1. Accordingly, although for simplicity we may use the notation $N(w)$, this should be thought of as actually designating $N(y/\bar{A})$.

For any given exceedance curve (say for a particular altitude), the frequency of exceedance is the sum of the contributions from all of the various σ_w levels. The generation of exceedance data has been the most widely recognized specific use to which this model has been put.

Cross plots of the generalized exceedance curves are shown in Figs. 5.3 and 5.4. These have been used to establish a rational variation of design gust velocity with altitude.

Probability distributions of σ_w associated with this model have been computed and are shown in Appendix F. These have an application in ride quality evaluations.

In this appendix, three other types of information are developed and presented. In all of this work, only the storm turbulence term in Eq. (4.26) is included. Because only a single term is used, the subscripts 1 and 2 are no longer needed. Accordingly, b_2 becomes simply b . The notation P_2 is retained, however, so that P alone (without a subscript) can be used to denote probability in general, as in Sec. 4.3 and Appendix B. With only the storm turbulence term included, the results are valid only at load levels approaching and beyond the limit level.*

First, a curve is obtained that gives the *fraction of time* that the gust velocity w is above w_1 , as a function of w_1 . This is also the *probability* that, at any instant, w is above w_1 . This curve, like the generalized exceedance curves, is obtained as the sum of contributions from *all σ_w levels*.

Such information, as far as is known, has not been published. It is not necessary for most loads work. There may be circumstances, however, in which the fraction-of-time data may be more significant than frequency of exceedance data. For fatigue analysis of helicopter rotor systems, for example, or of propeller blades, the loading might be idealized as a “varying” load at blade rotation frequency superimposed on a “mean” load that varies more slowly as a result of the turbulence encounter and the response of the vehicle. The fraction of time at various mean loads would then require knowledge of the fraction of time at which w is greater than w_1 .

A curve providing this information was obtained at Lockheed as early as 1965. This has more recently (1982) been recomputed, using an alternate integration sequence and a possibly more accurate numerical integration scheme. It also has been extended to much higher gust velocities.

This curve is shown in Figs. I.1a and b. The corresponding generalized exceedance curve is shown for comparison.

Second, curves are obtained for a series of values of gust velocity w_1 (generalized as w_1/b) showing, for each w_1/b value, the *relative contributions of various σ_w levels to the fraction of time* for which w is above w_1 . These curves are shown in Figs. I.2a–d.

*Alternately, the results can be used when only the nonstorm term is pertinent. Some fatigue and ride quality applications could conceivably fall into this category. Also, it would appear that the results could be applied separately to storm and nonstorm turbulence and the results for the two categories of turbulence added.

Similar curves, less accurately computed and plotted, were obtained in 1971. They were generated "by hand" for fewer w_1/b values and were not normalized to unit area.

The equation utilized in generating the 1971 curves was formulated in 1968. This formulation was the outgrowth of work beginning in 1966 to assign individual numerical values to σ_w and η_d , the component parts of the design gust velocity, $U_\sigma = \sigma_w \eta_d$. The intent was to assign a single value to η_d ; values of σ_w could then be obtained as U_σ / η_d for any given value of U_σ . This breakdown was needed, first, to establish a design probability value for use with the joint probability design technique (Sec. 6.2.4). It is also needed in order to establish design σ_w 's for use in continuous turbulence time-history analyses; such analyses are a key step in determining the effect on loads of active control system saturation. As early as March 1966, it was recognized that η_d should be a function of w_1/b , and available data were plotted in this way beginning at that time. The initial data were taken from the 1966 Lockheed work.

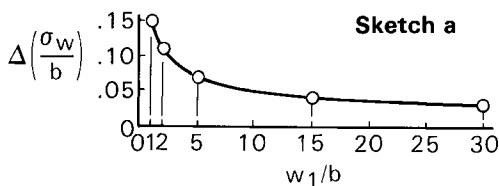
Third, curves are obtained for a series of values of w_1 (generalized as w_1/b), showing, for each w_1/b value, the *relative contributions of various σ_w levels to the number of exceedances* of w_1 by w . The resulting curves are shown in Figs. I.3a-d.

The equation on which these curves were based was formulated in January 1979, and two trial cases run. The curves differed only slightly from the corresponding fraction-of-time curves, so there appeared to be little urgency in preparing the complete set. It would appear, however, that for most applications Fig. I.3 is actually more pertinent than Fig. I.2.

A comparison of representative cases from Figs. I.2 and I.3 is shown in Fig. I.4. It is seen that the "exceedance" curves differ only slightly from the "fraction-of-time" curves. Additional observations from Figs. I.2 and I.3 are:

1) The bandwidths are virtually the same for all the curves shown, with a value at midheight of approximately 1.2. In Fig. I.2, the actual value varies from 1.25 at $w_1/b = 1$ to 1.20 at $w_1/b = 5$ to 1.17 at $w_1/b = 30$. In Fig. I.3, it is 1.17 for all values of w_1/b .

2) The curves are not symmetric, although they become more nearly so as w_1/b increases. As a result, the location of the peak is not actually the best measure of the effective σ_w/b associated with each curve. An arbitrary but probably better measure of the effective σ_w/b is provided by the midpoint taken at midheight. This σ_w/b value is greater than the σ_w/b value of the peak by the following amounts:



These values apply to both Figs. I.2 and I.3.

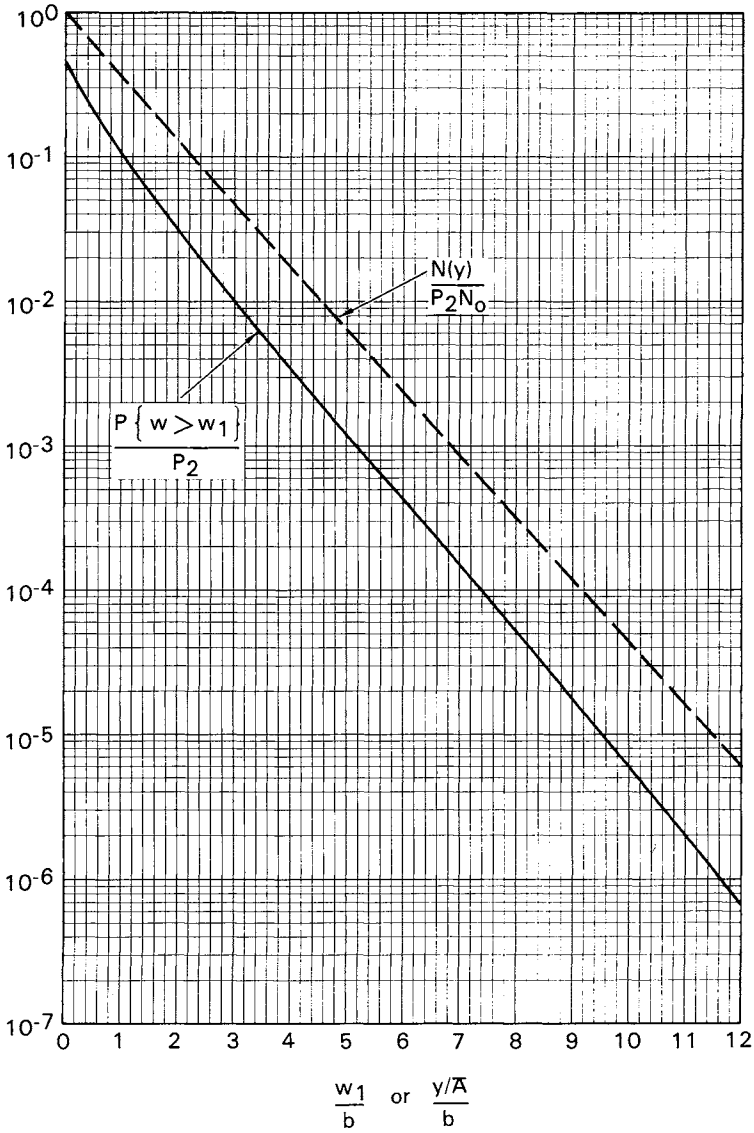


Fig. I.1 Fraction of time that $w > w_1$.
a) $w_1/b = 0-12$

Downloaded by RMIT UNIV BUNDOORA on June 4, 2013 | http://arc.aiaa.org | DOI: 10.2514/4.861888

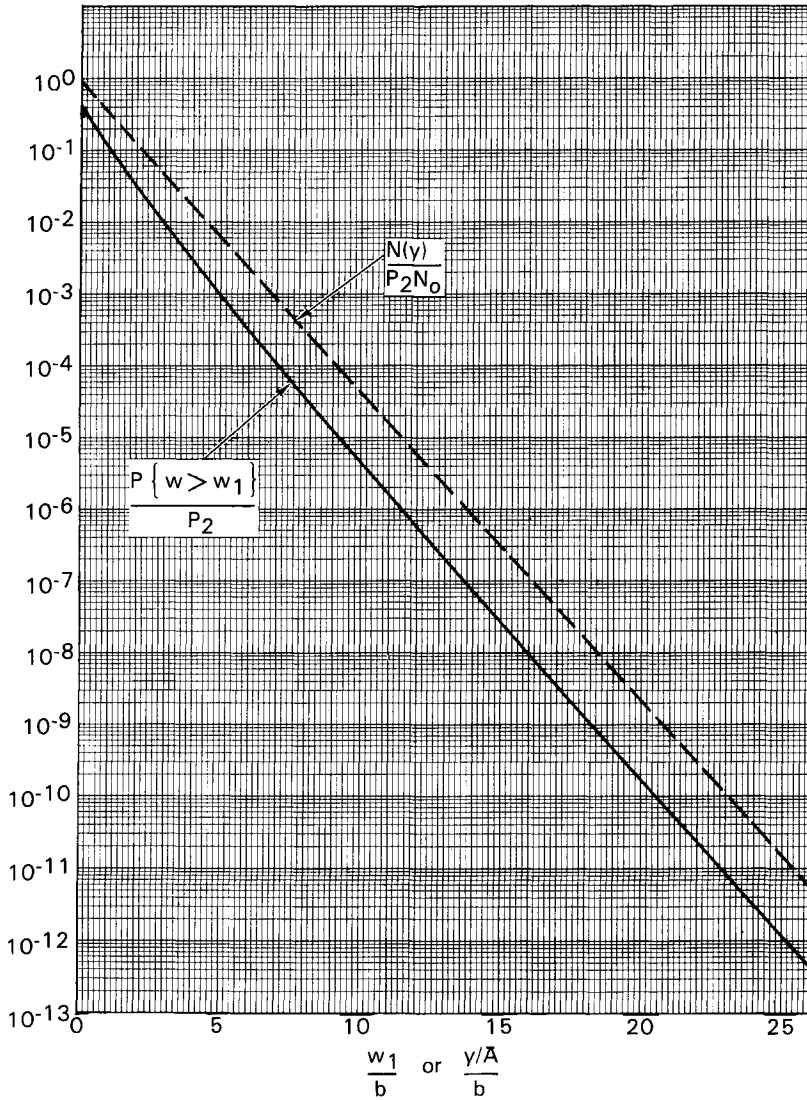
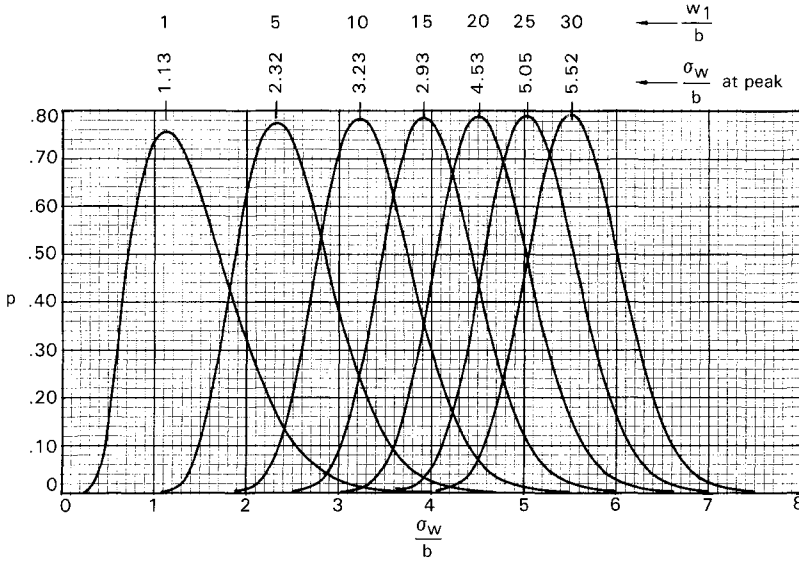
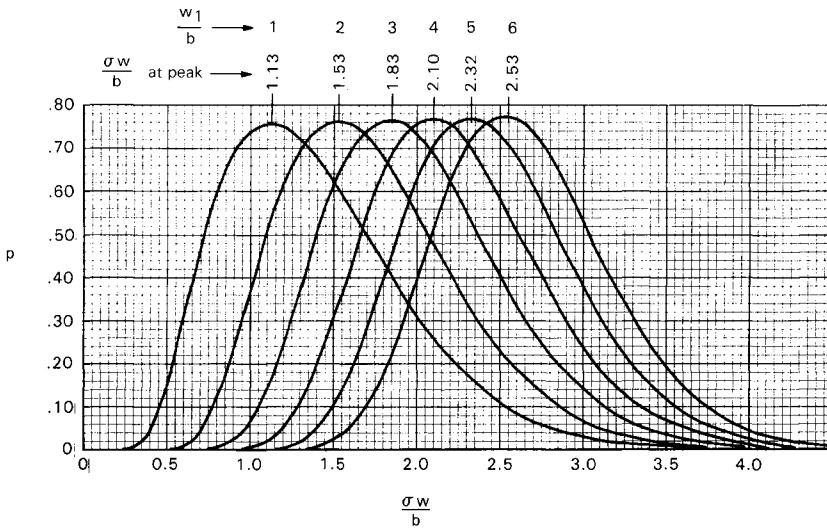


Fig. I.1 (continued) Fraction of time that $w > w_1$.
b) $w_1/b = 0-26$

Downloaded by RMIT UNIV BUNDOORA on June 4, 2013 | http://arc.aiaa.org | DOI: 10.2514/4.861888



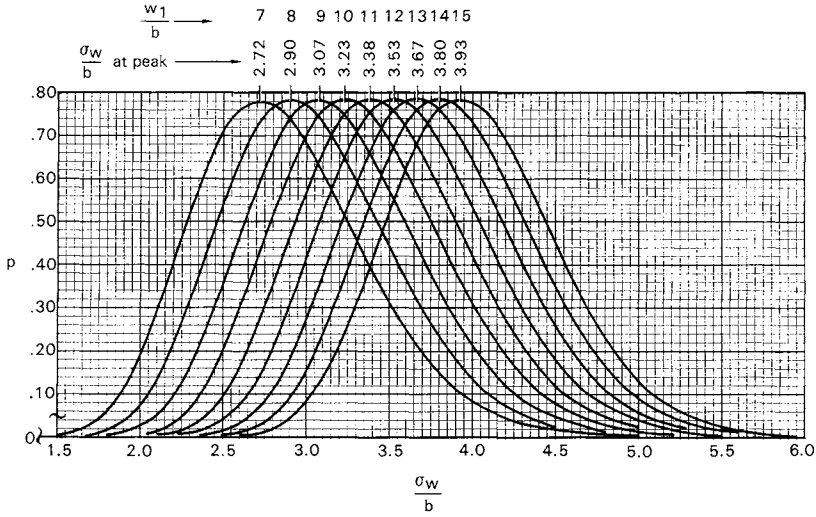
a) Overview



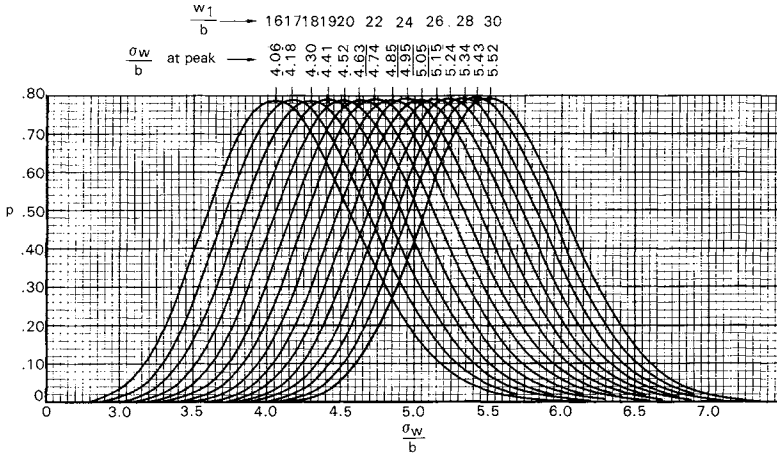
b) $w_1/b = 1-6$

Fig. I.2 Relative contribution of various σ_w levels to fraction of time above particular w_1/b values.

APPENDIX I



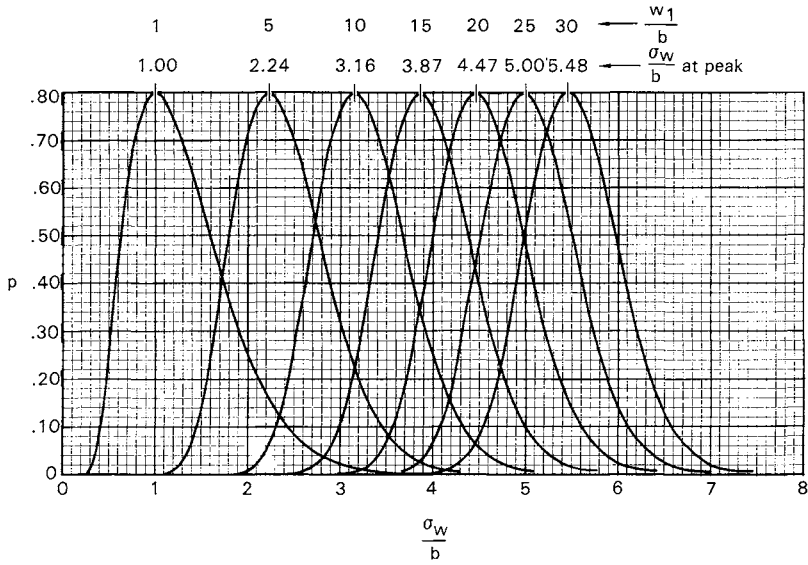
c) $w_1/b = 7-15$



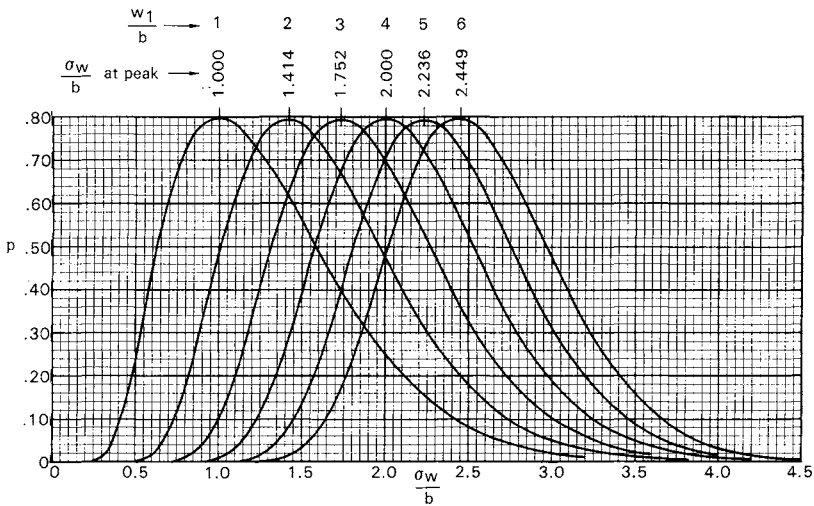
d) $w_1/b = 16-30$

Fig. I.2 (continued) Relative contribution of various σ_w levels to fraction of time above particular w_1/b values.

Downloaded by RMIT UNIV BUNDOORA on June 4, 2013 | http://arc.aiaa.org | DOI: 10.2514/4.861888



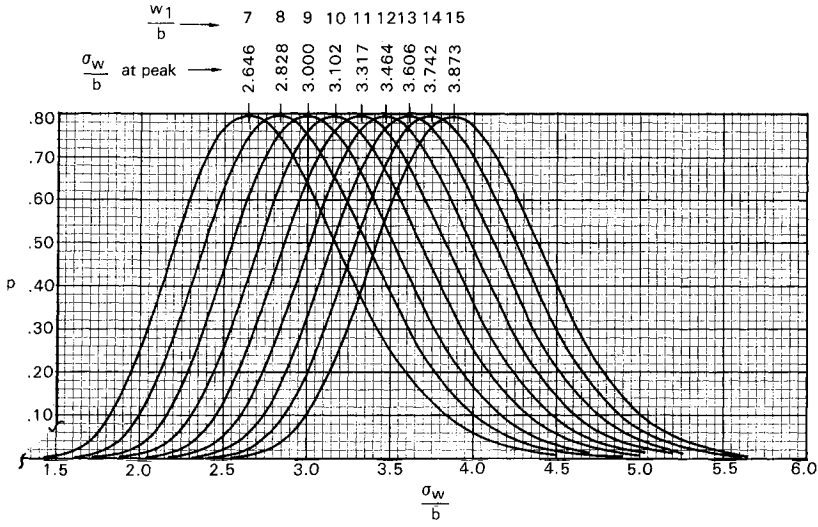
a) Overview



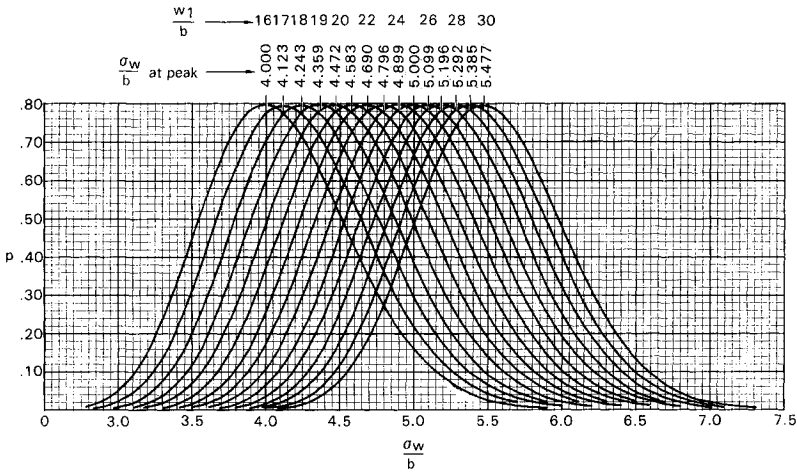
b) $w_1/b = 1-6$

Fig. I.3 Relative contribution of various σ_w levels to exceedances of particular w_1/b values.

APPENDIX I



c) $w_1/b = 7-15$



d) $w_1/b = 16-30$

Fig. I.3 (continued) Relative contribution of various σ_w levels to exceedances of particular w_1/b values.

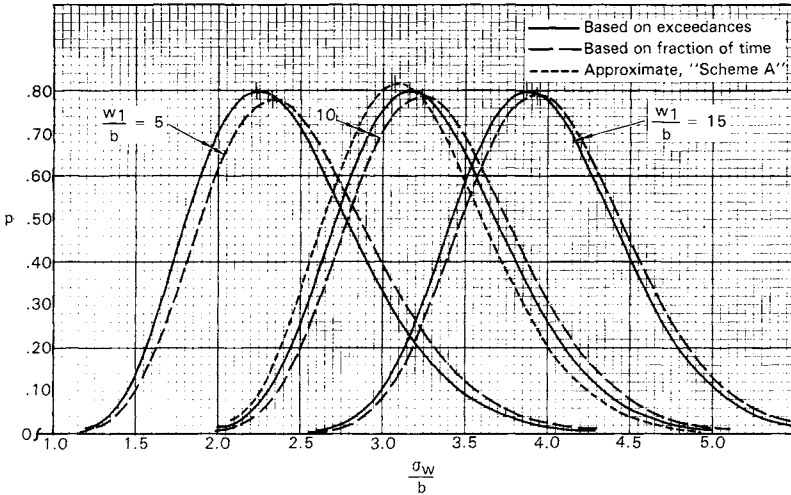


Fig. I.4 Relative contribution of various σ_w levels to exceedances of w_1 and to fractions of time above w_1 comparison.

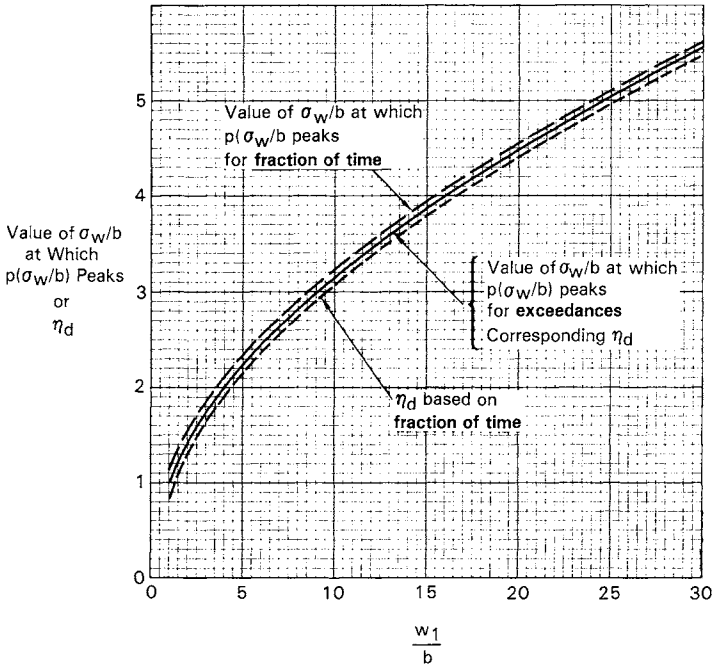


Fig. I.5 Relation of σ_w and η_d to $\sigma_w \eta_d$ (or U_σ or w_1).

Plots of η_d vs w_1/b based both on fraction of time (Fig. I.2) and on exceedances (Fig. I.3) are shown in Fig. I.5. Also shown are plots of the values of σ_w/b at which the curves in Figs. I.2 and I.3 peak. Values of η_d were obtained as

$$\eta_d = \frac{(\sigma_w \eta_d)}{\sigma_w} = \frac{w_1}{\sigma_w} = \frac{w_1/b}{\sigma_w/b} = \frac{w_1/b}{\text{most likely } \sigma_w/b}$$

$$= \frac{w_1/b}{\sigma_w/b \text{ at which curve peaks}}$$

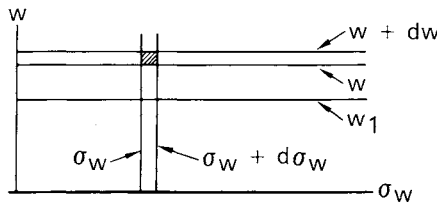
There would have been some merit in increasing the denominator in this expression by the $\Delta(\sigma_w/b)$ value shown in Sketch a. The effect on the numbers obtained, however, would have been very small.

For the exceedances basis, it is shown in Ref. 71, and also in Sec. I.3.3 following, that the location of the peak is given by $\sqrt{w_1/b}$. This likewise, then, is the value of η_d :

$$\eta_d = \frac{w_1/b}{\sqrt{w_1/b}} = \sqrt{w_1/b}$$

I.2 INTEGRATIONS OF JOINT PROBABILITY DENSITY OF w AND σ_w

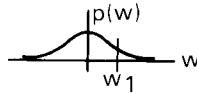
I.2.1 Equation for Joint Probability Density



It is evident that for every value of σ_w (0 to ∞), w can have any value from $-\infty$ to ∞ . Hence, there exists a nonzero joint probability density of σ_w and w for all values of w and all positive values of σ_w .

The probability density of w , for a constant σ_w , is simply the Gaussian probability density [Eq. (4.4)]

$$p(w) = \frac{1}{\sqrt{2\pi}} \frac{1}{\sigma_w} e^{-\frac{1}{2} \left(\frac{w}{\sigma_w}\right)^2} \tag{I.1}$$



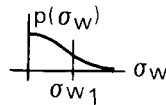
From this, as a matter of interest only,

$$P\{w > w_1\} = \int_{w_1}^{\infty} \frac{1}{\sqrt{2\pi} \sigma_w} \frac{1}{\sigma_w} e^{-\frac{1}{2}\left(\frac{w}{\sigma_w}\right)^2} dw \tag{I.2}$$

where $P\{\}$ denotes “probability of $\{\}$ occurring” or “probability that.”

The probability density of σ_w , as described by Eq. (4.26), if we consider only the storm turbulence term, is

$$p(\sigma_w) = P_2 \frac{1}{b} \sqrt{\frac{2}{\pi}} e^{-\frac{1}{2}\left(\frac{\sigma_w}{b}\right)^2} \tag{I.3}$$



From this, again as a matter of interest only,

$$P\{\sigma_w > \sigma_{w_1}\} = \int_{\sigma_{w_1}}^{\infty} P_2 \frac{1}{b} \sqrt{\frac{2}{\pi}} e^{-\frac{1}{2}\left(\frac{\sigma_w}{b}\right)^2} d\sigma_w \tag{I.4}$$

From Eq. (I.1), the probability that w is between w and $w + dw$, for a given σ_w , is

$$P\{w \text{ is in } dw, \text{ given } \sigma_w\} = \frac{1}{\sqrt{2\pi} \sigma_w} \frac{1}{\sigma_w} e^{-\frac{1}{2}\left(\frac{w}{\sigma_w}\right)^2} dw \tag{I.5}$$

Similarly, from Eq. (I.3), the probability that σ_w is between σ_w and $\sigma_w + d\sigma_w$ is

$$P\{\sigma_w \text{ is in } d\sigma_w\} = P_2 \frac{1}{b} \sqrt{\frac{2}{\pi}} e^{-\frac{1}{2}\left(\frac{\sigma_w}{b}\right)^2} d\sigma_w \tag{I.6}$$

If we consider two events A and B , defined as follows:

- A : σ_w is in $d\sigma_w$
- B : w is in dw

Downloaded by RMIT UNIV BUNDOORA on June 4, 2013 | http://arc.aiaa.org | DOI: 10.2514/4.861888

the probability that both occur, designated $P\{AB\}$, is given by

$$P\{AB\} = P\{A\} P\{B|A\} \quad (I.7)$$

$\begin{matrix} \uparrow & & \uparrow & \uparrow \\ \sigma_w \text{ in } & w \text{ in } & \sigma_w \text{ in} \\ d\sigma_w & dw & d\sigma_w \end{matrix}$

where $P\{B|A\}$ denotes the probability of B given A ("fifth axiom," p. 16 of Ref. 72).

But $P\{A\}$ is given by Eq. (I.6) and $P\{B|A\}$ by Eq. (I.5). Consequently, substituting Eqs. (I.5) and (I.6) into Eq. (I.7) yields

$$P\{w \text{ is in } dw \text{ and } \sigma_w \text{ is in } d\sigma_w\} = \frac{P_2}{b\pi\sigma_w} e^{-\frac{1}{2}\left(\frac{w}{\sigma_w}\right)^2} dw e^{-\frac{1}{2}\left(\frac{\sigma_w}{b}\right)^2} d\sigma_w \quad (I.8)$$

Nondimensionalizing w and σ_w by dividing by b , we get

$$P\left\{\frac{w}{b} \text{ is in } d\frac{w}{b} \text{ and } \frac{\sigma_w}{b} \text{ is in } d\frac{\sigma_w}{b}\right\} = \frac{P_2}{\pi\frac{\sigma_w}{b}} e^{-\frac{1}{2}\left(\frac{w/b}{\sigma_w/b}\right)^2} d\frac{w}{b} e^{-\frac{1}{2}\left(\frac{\sigma_w/b}{b}\right)^2} d\frac{\sigma_w}{b} \quad (I.9)$$

The probability density p is then obtained by dividing by dw/b $d\sigma_w/b$.

$$p\left(\frac{w}{b}, \frac{\sigma_w}{b}\right) = P_2 \frac{1}{\pi} \frac{1}{\sigma_w/b} e^{-\frac{1}{2}\left[\left(\frac{w/b}{\sigma_w/b}\right)^2 + \left(\frac{\sigma_w}{b}\right)^2\right]} \quad (I.10)$$

1.2.2 Integrations to Give $P\{w > w_1\}$

The total fraction of time that $w > w_1$ is obtained by the multiple integration

$$P\{w > w_1\} = P_2 \int_{\frac{w}{b} = \frac{w_1}{b}}^{\infty} \int_{\frac{\sigma_w}{b} = 0}^{\infty} \underbrace{\frac{1}{\pi} \frac{1}{\sigma_w/b} e^{-\frac{1}{2}\left[\left(\frac{w/b}{\sigma_w/b}\right)^2 + \left(\frac{\sigma_w}{b}\right)^2\right]}}_{\text{Integrand}} d\frac{\sigma_w}{b} d\frac{w}{b} \quad (I.11)$$

This can be carried out numerically in either of two ways, scheme A and scheme B .

1.2.3 Scheme A

1) First, integrate over σ_w/b , from 0 to ∞ , for a series of values of w/b . This involves, for each value of w/b , selecting a series of values of σ_w/b , computing the integrand for each, and summing. If the values of σ_w/b are uniformly and closely spaced, simply add the values obtained and multiply by $\Delta(\sigma_w/b)$; otherwise, plot and obtain the area.

2) Then, integrate over w , from w_1 to ∞ . This is done by integrating over w_1 from ∞ to 0, reading out values at a series of values of w , each of which is considered a value of w_1 . If the selected values of w/b , in the preceding step, were uniformly and closely spaced, simply add the values obtained in the first step and multiply by $\Delta(w/b)$; otherwise, plot and obtain areas.

The number of integrations required to obtain $P\{w/b > w_1/b\}$ vs w_1/b is then

$$\begin{array}{ccc} \text{(number of values of } w/b) & + & 1 \\ \text{Step 1} & & \text{Step 2} \end{array}$$

This is the scheme that was used in the 1965 Lockheed work.

It is interesting to note that if, in Step 1, the values of the integrand for a given w/b are plotted vs σ_w/b , the curve looks very much like the curves in Figs. I.2 and I.3. A sample, for $w/b = 10$ only, has been added to Fig. 1.4 (short-dash line). This added curve shows the relative contribution of various σ_w levels to the fraction of time at w_1 instead of above w_1 . As expected, therefore, this curve falls slightly to the left of the long-dash curve. It was data obtained in this way that led to the March 1966 plots of η_d vs w/b referred to earlier.

1.2.4 Scheme B

This involves reversing the order of integration, so that Eq. (I.11) becomes

$$\begin{aligned} P\{w > w_1\} &= P_2 \int_{\sigma_w/b=0}^{\infty} \int_{w/b=w_1/b}^{\infty} \frac{1}{\pi} \frac{1}{\sigma_w/b} \\ &\times \exp\left\{-\frac{1}{2}\left[\left(\frac{w/b}{\sigma_w/b}\right)^2 + \left(\frac{\sigma_w}{b}\right)^2\right]\right\} d\frac{w}{b} d\frac{\sigma_w}{b} \quad (\text{I.12}) \end{aligned}$$

For reasons that will become apparent, this equation is then rearranged to the form

$$\begin{aligned} P\{w > w_1\} &= P_2 \int_{\sigma_w/b=0}^{\infty} \sqrt{\frac{2}{\pi}} \exp\left[-\frac{1}{2}\left(\frac{\sigma_w}{b}\right)^2\right] \left\{ \int_{w/b=w_1/b}^{\infty} \frac{1}{\sqrt{2\pi}} \frac{1}{\sigma_w/b} \right. \\ &\times \exp\left[-\frac{1}{2}\left(\frac{w/b}{\sigma_w/b}\right)^2\right] d\frac{w}{b} \left. \right\} d\frac{\sigma_w}{b} \quad (\text{I.13}) \end{aligned}$$

Then,

1) First, integrate over w/b , from w_1/b to ∞ , for a series of values of σ_w/b . This is the operation enclosed in $\{ \}$'s. The expression within braces can be recognized as the cumulative Gaussian distribution, $1 - P(y)$, of the quantity w/b . (See Secs. 4.3.1 and 4.3.2.) Consequently, it can be read from tables

or computed from empirical equations derived to approximate the tabulated values. Thus, the actual integration is avoided.

2) Then, integrate over σ_w/b , from 0 to ∞ , separately for each value of w_1/b . This involves calculating the value of the “integrand” of Eq. (I.13) for each value of σ_w/b and summing. (If the values of σ_w/b are uniformly and closely spaced, simply add the values obtained and multiply by $\Delta(\sigma_w/b)$; otherwise, plot and obtain the area.)

The number of actual integrations required to obtain $P\{w/b > w_1/b\}$ vs w_1/b is then

$$\begin{array}{l} \text{None} + (\text{Number of values of } w_1/b) \\ \text{Step 1} \qquad \qquad \qquad \text{Step 2} \end{array}$$

This is the scheme that was used to obtain Figs. I.1 and I.2 here.

It is noted that P_2 in Eq. (I.13) is a constant multiplier and does not affect the shape of the curves plotted in Figs. I.1 and I.2.

The curves in Fig. I.2 are of the integrand of Eq. (I.13), normalized to give unit areas under the curves. The areas under the curves before normalizing are listed in Table I.1. They were obtained by means of a rectangular integration scheme. These are the values plotted in Fig. I.1.

Either scheme *A* or *B* could equally well have been used to obtain Fig. I.1. The great advantage of scheme *B* is that it makes available as a byproduct the very useful data presented in Fig. I.2, probably of far greater value than the end product appearing as Fig. I.1.

I.2.5 Scheme B: Details of Calculations

The calculations required in the preparation of Figs. I.1 and I.2 were carried out using an Apple II+ personal computer. For each of the 30 curves (30 values of w_1/b), the value of the integrand in Eq. (I.13) was calculated over 80 values of σ_w/b , varying from 0.1–8.0 in increments of 0.1. The area under each curve (before normalizing) was obtained from the computed values of the integrand using a rectangular integration scheme. Computer time, including printing, was about 45 s per w_1/b value.

Values of the cumulative Gaussian probability distribution, the bracketed quantity in Eq. (I.13), were obtained by two different procedures. Over the range $y/\sigma = 0-5$, values were computed from empirical expressions fitted separately to the tabulated data over the ranges $y/\sigma = 0-0.52$, $0.52-1$, $1-2$, $2-3$, $3-4$, and $4-5$. Each of these expressions represented a parabola on semilog coordinates, passing through the two end points and the center point of the interval. The maximum error in $1 - P(y)$ was about 0.07%. The formulas used to obtain these empirical expressions are derived in Sec. I.4. For y/σ greater than 5, values were computed from Eq. (C.11), Appendix C, using the first four terms of the series. The maximum error was less than 0.03%.

Table I.1 Key Results, Fraction-of-Time-Data

$\frac{w_1}{b}$	Area Under Curve	Location of peak (σ_w/b)	Value at Peak	η_d^a
1	0.1045 E-0	1.129	0.7584	0.886
2	0.3092 E-1	1.528	0.7656	1.309
3	0.9820 E-2	1.835	0.7697	1.635
4	0.3230 E-2	2.095	0.7734	1.909
5	0.1085 E-2	2.323	0.7767	2.152
6	0.3698 E-3	2.532	0.7787	2.370
7	0.1273 E-3	2.724	0.7803	2.570
8	0.4419 E-4	2.904	0.7816	2.755
9	0.1543 E-4	3.072	0.7828	2.930
10	0.5416 E-5	3.231	0.7842	3.095
11	0.1908 E-5	3.384	0.7851	3.251
12	0.6749 E-6	3.529	0.7859	3.400
13	0.2393 E-6	3.669	0.7864	3.543
14	0.8509 E-7	3.803	0.7870	3.681
15	0.3032 E-7	3.932	0.7875	3.815
16	0.1082 E-7	4.057	0.7881	3.944
17	0.3871 E-8	4.179	0.7886	4.068
18	0.1386 E-8	4.298	0.7891	4.188
19	0.4972 E-9	4.412	0.7895	4.306
20	0.1785 E-9	4.525	0.7898	4.420
21	0.6418 E-10	4.634	0.7901	4.532
22	0.2310 E-10	4.740	0.7903	4.641
23	0.8319 E-11	4.845	0.7905	4.747
24	0.2999 E-11	4.947	0.7909	4.851
25	0.1082 E-11	5.047	0.7912	4.953
26	0.3906 E-12	5.146	0.7913	5.052
27	0.1411 E-12	5.242	0.7914	5.151
28	0.5102 E-13	5.336	0.7916	5.247
29	0.1846 E-13	5.429	0.7919	5.342
30	0.6680 E-14	5.520	0.7921	5.435

^a $n_d = (w_1/b)/(\sigma_w/b)$.

Values of σ_w/b at which the respective $p(\sigma_w/b)$ curves peak were determined by fitting a parabola to the highest three points and equating the derivative to zero

$$y = A + Bx + Cx^2$$

$$\frac{dy}{dx} = B + Cx = 0$$

$$x = -B/C$$

Where the two highest points were nearly equal, the operation was repeated with the three points selected such as to center on the next-to-highest point instead of the highest point. A weighted average of the two results was then used. The curve-fitting procedure was essentially the same as used to fit the cumulative Gaussian probability distribution, described here and in Sec. I.4. The results are included in Table I.1.

I.3 INTEGRATIONS OF RICE'S EQUATION $\times p(\sigma_w)$

I.3.1 Expression for Exceedances with σ_w Varying

From Eq. (G.1) of Appendix G, taking only the last term, dropping the subscript on b , and replacing y/\bar{A} with w_1 , we obtain

$$N(y) = N_0 P_2 \sqrt{\frac{2}{\pi}} \frac{1}{b} \int_{\sigma_w=0}^{\infty} e^{-\frac{1}{2}\left(\frac{\sigma_w}{b}\right)^2} e^{-\frac{1}{2}\left(\frac{w_1}{\sigma_w}\right)^2} d\sigma_w \quad (\text{I.14})$$

Nondimensionalizing w_1 and σ_w by dividing by b yields

$$N(y) = N_0 P_2 \int_{\frac{\sigma_w}{b}=0}^{\infty} \underbrace{e^{-\frac{1}{2}\left(\frac{\sigma_w}{b}\right)^2}}_{\text{Rice's eq.}} \underbrace{\sqrt{\frac{2}{\pi}} e^{-\frac{1}{2}\left(\frac{w_1/b}{\sigma_w/b}\right)^2}}_{p(\sigma_w/b)} d \frac{\sigma_w}{b} \quad (\text{I.15})$$

Integrand

In Appendix G, this integration, actually in the form indicated by Eq. (I.14), is carried out to give the familiar expression

$$N(y) = N_0 P_2 e^{-\frac{w_1}{b}} \quad (\text{I.16})$$

1.3.2 Distribution of $N(y)$ with σ_w

It is also of interest, however, to examine the distribution of $N(y)$ with σ_w/b for various specific values of w_1/b . For this purpose, values of the integrand have been calculated for a series of values of σ_w/b , for each of a series of values of w_1/b . The resulting curves, normalized to unit area under the curve, are plotted in Fig. I.3. It is noted that P_2 and N_0 in Eq. (I.15) are constant multipliers and do not affect the shape of the curves plotted in Fig. I.3.

1.3.3 Value of σ_w/b at Which Integrand Peaks

The value of σ_w/b at which the integrand peaks is given simply by

$$\left(\frac{\sigma_w}{b}\right)_{\text{peak}} = \sqrt{\frac{w_1}{b}}$$

This simple relation was pointed out in Ref. 71. Its derivation involves differentiating the integrand in Eq. (I.15) with respect to σ_w/b and equating to zero:

$$\frac{d}{d(\sigma_w/b)} \left[e^{-\frac{1}{2}\left(\frac{\sigma_w}{b}\right)^2} \sqrt{\frac{2}{\pi}} e^{-\frac{1}{2}\left(\frac{w_1/b}{\sigma_w/b}\right)^2} \right] = 0$$

or

$$\frac{d}{d(\sigma_w/b)} \left[e^{-\frac{1}{2}\left(\frac{\sigma_w}{b}\right)^2 - \frac{1}{2}\left(\frac{w_1/b}{\sigma_w/b}\right)^2} \right] = 0$$

Utilizing the relation

$$\frac{d}{dx} e^u = e^u \frac{du}{dx}$$

we obtain

$$e^{-\frac{1}{2}\left(\frac{\sigma_w}{b}\right)^2 - \frac{1}{2}\left(\frac{w_1/b}{\sigma_w/b}\right)^2} \left[-\frac{\sigma_w}{b} - \frac{1}{2}\left(\frac{w_1}{b}\right)^2 \left(-2\right) \left(\frac{1}{\sigma_w/b}\right)^3 \right] = 0$$

$$-\frac{\sigma_w}{b} + \left(\frac{w_1}{b}\right)^2 \frac{1}{(\sigma_w/b)^3} = 0$$

$$\left(\frac{\sigma_w}{b}\right)^4 = \left(\frac{w_1}{b}\right)^2$$

$$\frac{\sigma_w}{b} = \sqrt{\frac{w_1}{b}} \quad (\text{I.17})$$

The value of the integrand at the peak can be found by substituting Eq. (I.17) into Eq. (I.15)

$$\begin{aligned} \text{Integrand} &= \sqrt{\frac{2}{\pi}} e^{-\frac{1}{2} \frac{w_1}{b}} e^{-\frac{1}{2} \frac{w_1}{b}} \\ &= \sqrt{\frac{2}{\pi}} e^{-\frac{w_1}{b}} \end{aligned}$$

To normalize to unit area, it is noted that the area under the curve is simply $\exp(-w_1/b)$, as indicated by Eq. (I.16). Accordingly, after normalizing, the peak value of the integrand is given by

$$\text{Integrand} = \frac{\sqrt{\frac{2}{\pi}} e^{-\frac{w_1}{b}}}{e^{-\frac{w_1}{b}}} = \sqrt{\frac{2}{\pi}} = 0.7979$$

1.3.4 Details of Calculations

The calculations required in the preparation of Fig. I.3 were carried out using an Apple II+ personal computer. The values of w_1/b and σ_w/b for which the integrand in Eq. (I.15) was calculated were the same as utilized in preparing Figs. I.1 and I.2. The areas needed for normalizing the curves to unit area were obtained using a rectangular integration scheme. These could better have been calculated exactly in closed form as $\exp(-w_1/b)$, but the accuracy achieved by the numerical integration was later found to be excellent, generally within one unit in the fifth significant figure!

1.4 DERIVATION OF FORMULAS FOR FITTING PARABOLIC CURVES TO TABULATED DATA

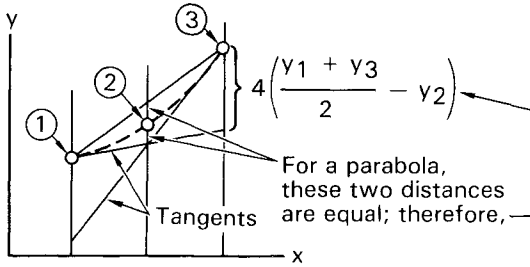
Curves of the cumulative Gaussian probability distribution, in the form of semilog plots of $1 - P(y/\sigma)$ vs y/σ , are shown in Appendix C. It is apparent that it should be possible to represent these curves closely, over particular bands of y/σ , by parabolas.

To facilitate this curve fitting, formulas were first developed for fitting a parabola

$$y = A + Bx + Cx^2 \tag{I.18}$$

to three points equally spaced in x . These formulas were then adapted for application to the semilog plots. The development follows.

GUST LOADS ON AIRCRAFT



$$\begin{aligned}
 y &= y_1 + \frac{(y_3 - y_1) - 4\left(\frac{y_1 + y_3}{2} - y_2\right)}{x_3 - x_1} (x - x_1) + 4\left(\frac{y_1 + y_3}{2} - y_2\right) \left(\frac{x - x_1}{x_3 - x_1}\right)^2 \\
 &= y_1 + \frac{y_3 - y_1 - 2y_1 - 2y_3 + 4y_2}{x_3 - x_1} (x - x_1) + (2y_1 + 2y_3 - 4y_2) \left(\frac{x - x_1}{x_3 - x_1}\right)^2 \\
 &= y_1 + (-3y_1 - y_3 + 4y_2) \frac{x - x_1}{x_3 - x_1} + 2(y_1 - 2y_2 + y_3) \left(\frac{x - x_1}{x_3 - x_1}\right)^2 \\
 &= y_1 - \frac{(-3y_1 - y_3 + 4y_2)x_1}{x_3 - x_1} + 2 \frac{(y_1 - 2y_2 + y_3)x_1^2}{(x_3 - x_1)^2} \\
 &\quad + \left(\frac{-3y_1 - y_3 + 4y_2}{x_3 - x_1} - 4 \frac{(y_1 - 2y_2 + y_3)x_1}{(x_3 - x_1)^2}\right) x + \left(2 \frac{y_1 - 2y_2 + y_3}{(x_3 - x_1)^2}\right) x^2
 \end{aligned}$$

Let

$$\left. \begin{aligned}
 y_4 &= -3y_1 - y_3 + 4y_2 \\
 y_5 &= y_1 - 2y_2 + y_3 \\
 x_4 &= x_3 - x_1
 \end{aligned} \right\} \quad (I.19)$$

Then,

$$y = \underbrace{\left(y_1 - \frac{y_4 x_1}{x_4} + 2 \frac{y_5 x_1^2}{x_4^2}\right)}_A + \underbrace{\left(\frac{y_4}{x_4} - 4 \frac{y_5 x_1}{x_4^2}\right)}_B x + \underbrace{\left(2 \frac{y_5}{x_4^2}\right)}_C x^2 \quad (I.20)$$

or

$$y = A + Bx + Cx^2$$

where *A*, *B*, and *C* are the coefficients indicated.

Equation (I.20) is applied to the semilog plots of $1 - P(y/\sigma)$ vs y/σ as follows:

Let

$$x = y/\sigma \tag{I.21}$$

Let

$$P = 1 - P(y/\sigma) = 1 - P(x) \tag{I.22}$$

Let

$$y = \log_{10} P = \log_e(P/2.3026) \tag{I.23}$$

[The y in Eq. (I.23) is the y in Eqs. (I.18) and (I.20), not the same as the y in Eqs. (I.21) and (I.22).] Then,

Input x_1, x_3, P_1, P_2, P_3 .

Compute y_1, y_2, y_3 from Eq. (I.23).

Compute y_4, y_5, x_4 from Eq. (I.19).

Compute A, B, C from expressions for coefficients in Eq. (I.20).

Input x .

Compute $y = A + Bx + Cx^2$.

Compute $P = 10^y$.

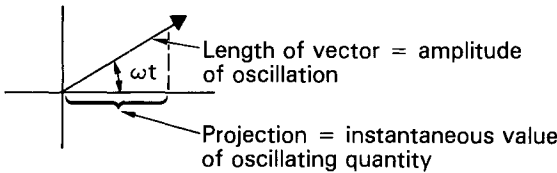
In obtaining the coefficients $A, B,$ and C for each y/σ band, values of $1 - P(y/\sigma)$ at points 1, 2, and 3 were taken from Ref. 66 (Table 2.1 pp. 966–972). As a check, values were then computed from the resulting equation at the same three points, where agreement should be precise, and at approximately the 1/4 and 3/4 points of the interval. Comparison with the tabulated values at the 1/4 and 3/4 points (also from Ref. 66) indicated the accuracy of the fit; the maximum error was 0.07%, as noted in Sec. I.2.5.

This page intentionally left blank

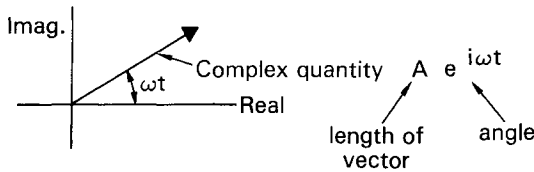
b) *More than one mode*

$$\left. \begin{aligned}
 (m_{11}\ddot{q}_1 + c_{11}\dot{q}_1 + k_{11}q_1) + \dots &= Q_1(t) \\
 (m_{21}\ddot{q}_1 + c_{21}\dot{q}_1 + k_{21}q_1) + \dots &= Q_2(t) \\
 (m_{31}\ddot{q}_1 + c_{31}\dot{q}_1 + k_{31}q_1) & \\
 \vdots & \\
 + (m_{32}\ddot{q}_2 + c_{32}\dot{q}_2 + k_{32}q_2) + (m_{33}\ddot{q}_3 + c_{33}\dot{q}_3 + k_{33}q_3) + \dots &= Q_3(t) \\
 \vdots & \\
 \vdots & \\
 \vdots &
 \end{aligned} \right\} \quad (2)$$

J.2.2 Use of Rotating Vectors to Represent Periodic Phenomena



and complex notation to represent rotating vectors



Addition, subtraction, multiplication, and division of the complex quantities representing the rotating vectors accomplish the corresponding operations on the associated time histories.

J.2.3 Solution of Equations for Case of Steady Oscillating Input

a) *Single equation*

$$m\ddot{q} + c\dot{q} + kq = Q(t) \quad (3)$$

Consider the input to be

$$Q(t) = a U_0 e^{i\omega t} \quad (4)$$

where

a = Product of factors

- relating local forces to gust velocity
- relating generalized force to local forces

U_0 = Amplitude of oscillating gust velocity

$e^{i\omega t}$ = Unit rotating vector

It is seen that the input is considered to be a rotating vector represented by a complex quantity. The real part of this complex quantity is the sinusoidally varying generalized force

$$Q = Q_0 \cos \omega t$$

The steady-state response is then an oscillation at the same frequency but differing in amplitude and phase:

$$\begin{aligned}
 q(t) &= q_0 e^{i(\omega t + \Psi)} \\
 &\quad \uparrow \qquad \qquad \uparrow \\
 &\quad \text{amplitude, a real number} \quad \text{Phase angle} \\
 &= q_0 e^{i\psi} e^{i\omega t} \\
 &\quad \underbrace{\qquad \qquad \qquad} \\
 &\quad \uparrow \\
 &\quad \text{Complex number, } q_c
 \end{aligned}$$

$$q(t) = q_c e^{i\omega t} \tag{5}$$

Again, the physical interpretation is that q is the real part of $q_c e^{i\omega t}$, which is a sine or cosine curve of defined amplitude and phase relative to the input.

It follows that

$$\dot{q}(t) = i\omega q(t) = i\omega q_c e^{i\omega t} \tag{6}$$

and

$$\ddot{q}(t) = (i\omega)^2 q(t) = (i\omega)^2 q_c e^{i\omega t} \tag{7}$$

Substituting (4–7) into (3), and noting that every term contains a factor $e^{i\omega t}$ that can therefore be divided out, we obtain

$$[m(i\omega)^2 + c(i\omega) + k]q_c = aU_0 \tag{8}$$

The square matrix on the left-hand side of the equation can be considered to be the sum of matrices as follows:

$$[\quad] = [M] + [K] + [C] + [A_D] + [A_K]$$

Mass	Structural stiffness	Structural damping	Aero due to α resulting from velocity	Aero due to α resulting from displacement
------	----------------------	--------------------	--	--

$[M] =$	$\begin{bmatrix} -M\omega^2 & 0 \\ 0 & -M\rho^2\omega^2 \\ 0 & \end{bmatrix}$	Diagonal matrix, each element = $-m\omega^2$	where m = generalized mass
$[K] =$	$\begin{bmatrix} 0 & \\ 0 & \end{bmatrix}$	Diagonal matrix, each element = $-m\omega_n^2$	where ω_n = natural frequency
$[C] =$	$\begin{bmatrix} 0 & \\ 0 & \end{bmatrix}$	Diagonal matrix, each element = $i\omega(2\zeta m\omega_n)$	where ζ = damping ratio
or	$\begin{bmatrix} 0 & \\ 0 & \end{bmatrix}$	Diagonal matrix, each element = $igm\omega_n^2$	where g = structural damping constant

$[A_D] =$	$\begin{bmatrix} i\omega Z_z & i\omega Z_\theta & i\omega Z_{\dot{q}_1} & i\omega Z_{\dot{q}_2} & \dots & i\omega Z_{\dot{q}_{20}} \\ i\omega M_z & i\omega M_\theta & i\omega M_{\dot{q}_1} & i\omega M_{\dot{q}_2} & \dots & i\omega M_{\dot{q}_{20}} \\ \vdots & \vdots & i\omega \phi_i & \vdots & \vdots & \vdots \\ i\omega Q_{20_z} & i\omega Q_{20_\theta} & \vdots & \vdots & \vdots & \vdots \end{bmatrix}$	Full matrix, each element =	
	$\begin{bmatrix} \vdots & \vdots & \vdots & \vdots & \vdots & \vdots \\ \vdots & \vdots & \vdots & \vdots & \vdots & \vdots \\ \vdots & \vdots & \vdots & \vdots & \vdots & \vdots \\ \vdots & \vdots & \vdots & \vdots & \vdots & \vdots \end{bmatrix}$	AIC	$\left\{ \phi_j \right\}$
	Forces on elastic modes due to rigid-body velocities	Sums local forces to give generalized force	Gives local displacement from generalized displacement
	Forces on elastic modes due to elastic-mode \dot{q} 's	Gives local displacement from generalized displacement	Forces on rigid-body modes due to elastic-mode \dot{q} 's

Downloaded by RMIT UNIV BUNDOORA on June 4, 2013 | http://arc.aiaa.org | DOI: 10.2514/4.861888

$$[A_K] = \begin{bmatrix} 0 & Z_\theta & Z_{q_1} & Z_{q_2} & \dots & Z_{q_{20}} \\ 0 & M_\theta & M_{q_1} & M_{q_2} & \dots & M_{q_{20}} \\ \hline 0 & Q_{1_0} & \text{Full matrix, each element =} \\ \vdots & \vdots & \begin{bmatrix} \phi_i \\ 1,99 \end{bmatrix} \begin{bmatrix} \text{AIC} \\ 99,99 \end{bmatrix} \left\{ \left(\frac{\partial \phi}{\partial x} \right)_j \right\} \\ 0 & Q_{20_0} & \dots & \dots & \dots & \dots \end{bmatrix}$$

↑ Forces on elastic modes due to rigid-body displacements
↑ Sums local forces to give generalized force
↑ Gives local slopes from generalized displacements

↑ Forces on elastic modes due to elastic-mode q 's
↑ Forces on rigid-body modes due to elastic-mode q 's

The column matrix on the right-hand side of the equation is evaluated as follows:

$$\begin{Bmatrix} F_z \\ M_y \\ Q_1 \\ \vdots \\ Q_{20} \end{Bmatrix} = \begin{Bmatrix} \text{Each element =} \\ \begin{bmatrix} \phi_i \\ \text{AIC} \end{bmatrix} \begin{bmatrix} e^{-\frac{\omega x}{V}} \\ \text{Gust penetration lags} \end{bmatrix} \begin{Bmatrix} \phi_z \\ \text{Each element 0 or 1} \end{Bmatrix} \\ \uparrow \text{Sums local forces to give generalized force} \quad \uparrow \text{Gust penetration lags} \end{Bmatrix}$$

Downloaded by RMIT UNIV BUNDOORA on June 4, 2013 | http://arc.aiaa.org | DOI: 10.2514/4.861888

This page intentionally left blank

APPENDIX K C.G. ACCELERATION PSD'S FOR AN IDEALIZED RIGID AIRPLANE FREE TO PITCH AND PLUNGE

C.g. acceleration psd's for a rigid airplane free to plunge and pitch are shown in Fig. K.1. The psd's are shown in nondimensional form for various values of the dimensionless parameters δ/L , \bar{c}/δ , $f_0\tau$, and ζ , as defined in Sec. 8.2.1. The plunge-only case is also included on each sheet. The curves were obtained using the von Kármán shape of gust psd.

In order to depict the shapes of the curves more clearly at very low frequencies, the frequency scale is made logarithmic. The vertical scale is linear, but the psd (in nondimensional form) is multiplied by the frequency (also in nondimensional form). With the vertical scale thus modified, areas under the curve remain undistorted. More specifically, the fraction of the total area between any two given frequencies is the same in this form of plot as in the customary linear plot.*

A short vertical line has been marked on each curve to indicate the short-period undamped natural frequency. This occurs at $f\tau = f_0\tau$. For the plunge-only case, $f_0\tau$ is taken as 0.159, in accordance with the discussion in Sec. 8.2.3.

A striking feature of these plots is the consistency between the plunge-only and free-to-pitch cases, even to the presence of a clear "short-period" peak in the plunge-only case. Inasmuch as the short period mode is usually thought of as essentially a pitching mode, the presence of a short-period peak in the plunge-only case might appear anomalous. Actually, however, the observed consistency is quite reasonable. As noted in Sec. 8.2.3, the motion in the plunge-only case is identical to that in the particular free-to-pitch case for which $f_0\tau$ and ζ have the values $1/2\pi$ and 1.00, respectively. Moreover, physically, the alleviation of load at frequencies below the short-period peak

*The demonstration is as follows:

$$\underbrace{(\phi f)(d \log_{10} f)}_{\substack{\text{Area, modified} \\ \text{plot, between} \\ f \text{ and } f + df}} = (\phi f) (1/f) (\log_{10} e) df = \underbrace{(\log_{10} e)}_{\substack{\text{Constant} \\ = 0.4343}} \cdot \underbrace{\phi df}_{\substack{\text{Area, basic} \\ \text{plot, between} \\ f \text{ and } f + df}}$$

Downloaded by RMIT UNIV BUNDOORA on June 4, 2013 | http://arc.aiaa.org | DOI: 10.2514/4.861888

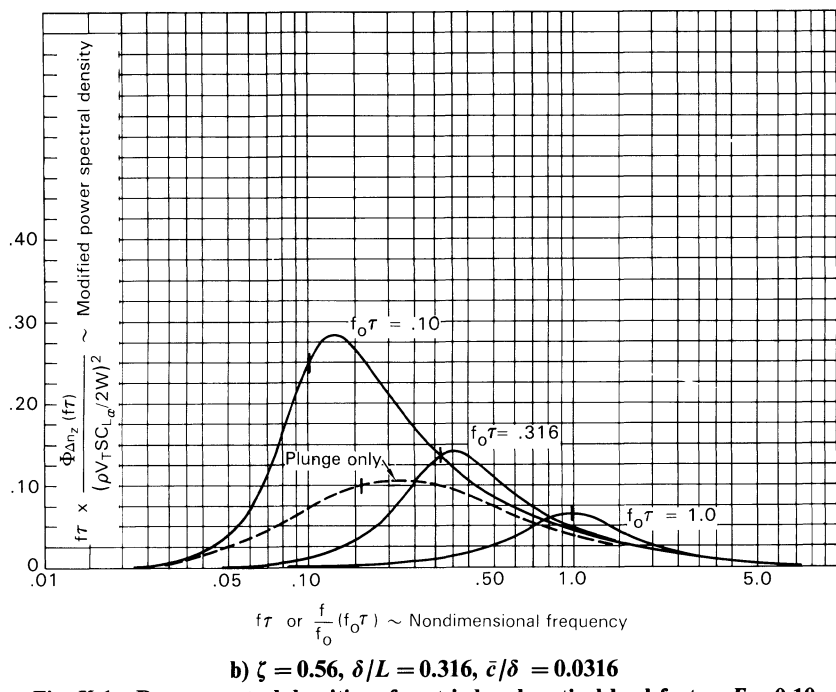
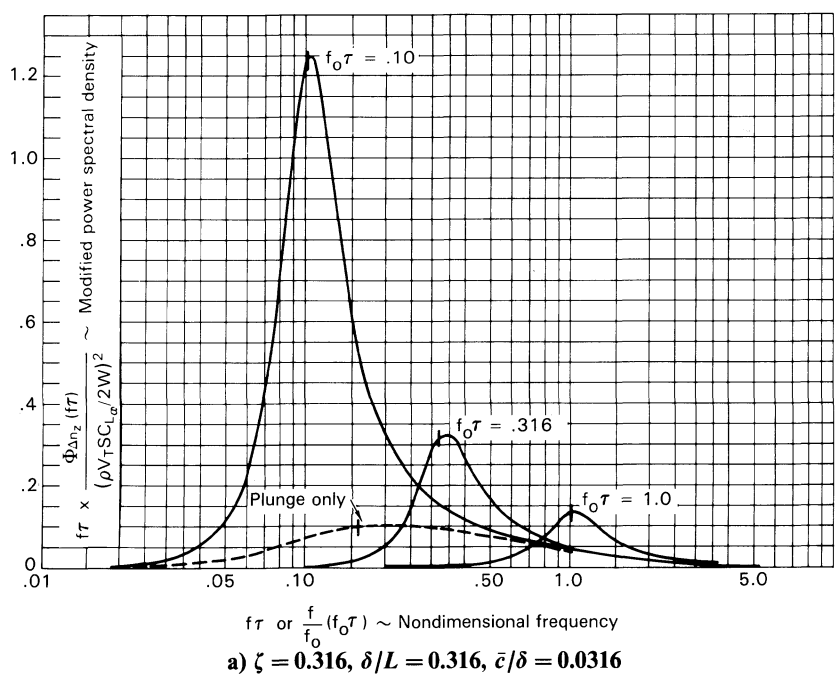


Fig. K.1 Power-spectral densities of gust-induced vertical load factor. $F = 0.10$

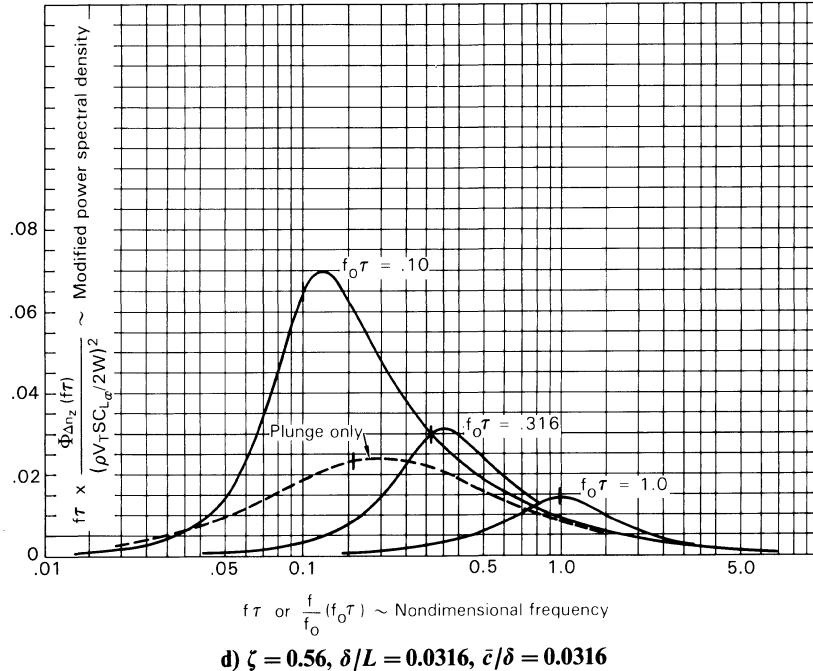
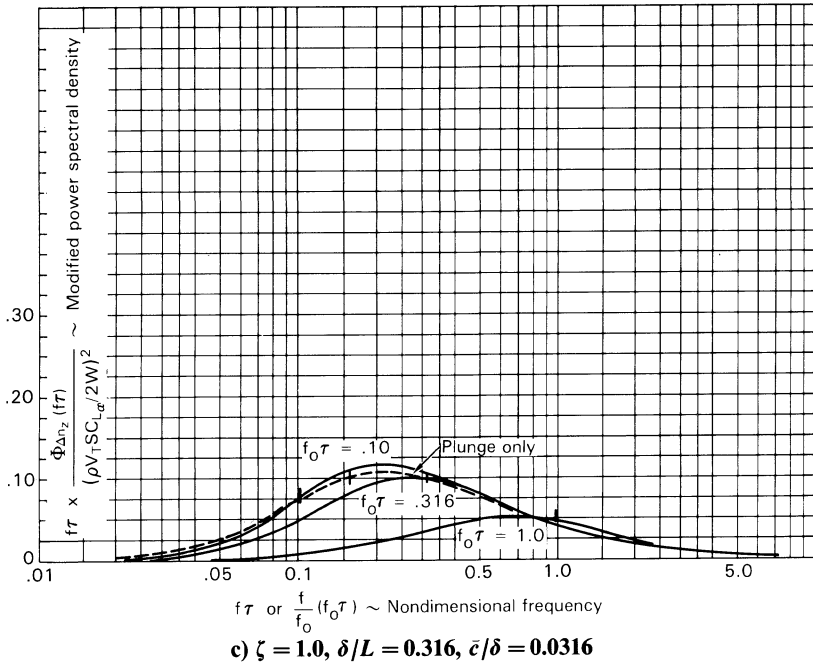
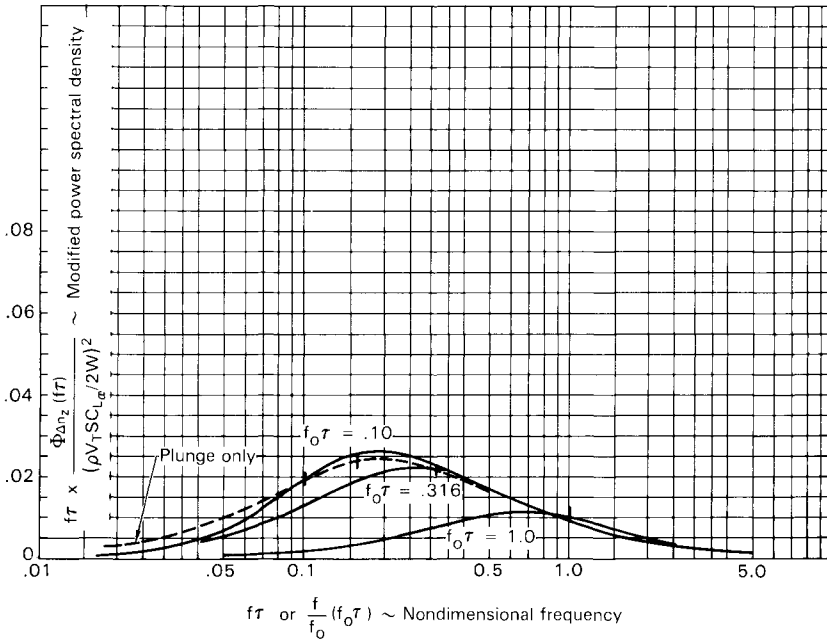


Fig. K.1 (continued) Power-spectral densities of gust-induced vertical load factor. $F = 0.10$



e) $\zeta = 1.0, \delta/L = 0.0316, \bar{c}/\delta = 0.0316$

Fig. K.1 (continued) Power-spectral densities of gust-induced vertical load factor.
 $F = 0.10$

is due to a combination of weathervaning (pitch) and vertical translation; and the fact that weathervaning happens to be absent in one particular case need not alter the basic nature of the response. It might be remarked further that the concept of the short-period mode as a pitching mode arises from the fact that its motion is described by a second-order differential equation in α ; but α , of course, is the sum of pitch and vertical-translation contributions, namely, θ and \dot{z}/V .

APPENDIX L ANNOTATED BIBLIOGRAPHY

The arrangement of entries is as follows:

1) Journals, meeting papers, and books are arranged alphabetically by author.

2) Published reports are arranged alphabetically by organization as abbreviated in the report designation, then alphabetically and numerically by the remainder of the report designation.

The intent has not been to provide an exhaustive list, but rather to include those documents of primary importance to the practitioner of the gust loads art, together with papers of particular historical interest.

Albano and Rodden (Doublet-Lattice)

Albano, E. and Rodden, W. P., "A Doublet-Lattice Method for Calculating Lift Distributions on Oscillating Surfaces in Subsonic Flow," *AIAA Journal*, Vol. 7, Feb. 1969, pp. 279–285.

This and AFFDL-TR-71-5 constitute the basic sources for the doublet-lattice method as used at the Lockheed-California Company.

Blackman and Tukey

Blackman, R. B. and Tukey, J. W., *The Measurement of Power Spectra*, Dover, New York, 1958. Originally published in the *Bell System Technical Journal*, Jan. and March 1958, under the title "The Measurement of Power Spectra from the Point of View of Communications Engineering"; index and preface added.

This is the well-known basic reference for the *Blackman–Tukey* method of computing psd's from measured time histories.

Chen on Rice's Equation

Chen, W.-Y., "Application of Rice's Exceedance Statistics to Atmospheric Turbulence," *AIAA Journal*, Vol. 10, Aug. 1972, pp. 1103–1105.

Contributes significantly to the evaluation of the validity of the stationary-Gaussian model of atmospheric turbulence and calls attention to the requirements for Rice's equation to apply. Derives a simple criterion with which to test specific time histories and applies this to turbulence samples from four sources. Establishes first that the samples are reasonably stationary by

noting that the distribution of $y(t)$ is indeed Gaussian. Finds that the distribution of $z(t) \equiv y(t) - y(t - \tau)$ is *not* Gaussian, indicating that turbulence in general, wind-tunnel as well as atmospheric, tends *not* to meet the requirements for Rice's equation to apply.

This work is generally convincing, although a possible reservation is with respect to the inherent loss of accuracy in taking differences between successive points in the recorded data, which might bias the probability distribution of $z(t)$.

Fung

Fung, Y. C., "Statistical Aspects of Dynamic Loads," *Journal of the Aeronautical Sciences*, Vol. 20, May 1953, pp. 317-330.

This is of historical interest, as the source of the expression for the transfer function modulus used in obtaining Fig. 7 of NACA Rept. 1272 and Fig. 5-2 of Ref. 13. These figures give the continuous turbulence gust response on the assumption of a rigid airplane free to plunge only. It uses Liepmann's¹² approximation for the Kussner effect, and finally, without its being entirely obvious, approximates the Wagner effect by considering lift growth to be instantaneous.

Hoblit (L-1011 Yaw Damper)

Hoblit, F. M., "Effect of Yaw Damper on Lateral Gust Loads in Design of the L-1011 Transport," in *Active Control Systems for Load Alleviation, Flutter Suppression, and Ride Control*, AGARD-AG-175, March 1974 (paper presented October 1973).

Includes treatment of reliability, under both mission analysis and design envelope criteria, and saturation. It also presents flight-test comparison with theory and concludes, incorrectly, that the pilot acts as a fairly effective yaw damper. (Pilot inputs were later found to be in phase with ψ rather than $\dot{\psi}$, and to be very small.)

Liepmann

Liepmann, H. W., "On the Application of Statistical Concepts to the Buffeting Problem," *Journal of the Aeronautical Sciences*, Vol. 19, Dec. 1952, pp. 793-800.

Of historical interest as one of the first published works on the application of power-spectral methods to gust loads studies. Despite the title, the paper is wholly on gust applications. Proposes the Dryden spectrum (although not by name) for describing atmospheric turbulence; gives both the vertical-lateral gust and longitudinal gust forms and the associated autocovariance functions. It also calls attention to Rice's equation.

Moon (Linear Optimization)

Moon, R. N., "Application of Linear Optimization Theory to Development of Design Load Conditions from Statistical Analysis," AIAA Paper

79-0740, AIAA/ASME/ASCE/AHS 20th Structures, Structural Dynamics, and Materials Conference, CP795, St. Louis, MO, April 4–6, 1979.

This paper provides a comprehensive discussion of matching condition generation, with emphasis on the development and use of the Linear Optimization Program for Matching Condition Generation (LOP). This program is a major tool in matching condition generation.

Press and Houbolt

Press, H. and Houbolt, J. C., “Some Applications of Generalized Harmonic Analysis to Gust Loads on Airplanes,” *Journal of the Aeronautical Sciences*, Vol. 22, No. 1, Jan. 1955, pp. 17–26.

Of historical interest as the best overall introduction, at that time, to power-spectral methods and their application to gust loads. Includes extensive summary of Tukey’s work on determination of psd’s from time histories. Also notes that Rice’s equation depends on the disturbance being completely Gaussian.

Press and Tukey

Press, H. and Tukey, J. W., “Power Spectral Methods of Analysis and Their Application to Problems in Airplane Dynamics,” AGARD Flight Test Manual, Vol. 4, Pt. IVC, June 1956.

Of historical interest, it provided an early introduction to power spectral methods from a somewhat mathematical point of view. If this document is to be used, make sure that the 23-item errata sheet is included.

Rice

Rice, S. O., “Mathematical Analysis of Random Noise,” *Bell System Technical Journal*, Vol. XXIII, No. 3, July 1944, pp. 282–332, and Vol. XXIV, No. 1, Jan. 1945, pp. 46–156. Also in Wax, N., “Selected Papers on Noise and Stochastic Processes,” Dover, New York, 1954.

Of historical interest as the source of “Rice’s Equation,” the basis of virtually all analytical generation of frequency of exceedance curves. The key equations are Eqs. 3.3-11 and 3.3-14.

Stauffer and Hoblit

Stauffer, W. A. and Hoblit, F. M., “Dynamic Gust, Landing, and Taxi Loads Determination in the Design of the L-1011,” *Journal of Aircraft*, Vol. 10, Aug. 1973, pp. 459–467.

This paper includes a thorough discussion of dynamic gust loads criteria and their basis; matching condition generation and its basis; and the dynamic taxi loads criteria and methods used in L-1011 loads determination.

Stauffer, Lewolt, and Hoblit

Stauffer, W. A., Lewolt, J. G., and Hoblit, F. M., "Application of Advanced Methods to Design Loads Determination for the L-1011 Transport," *Journal of Aircraft*, Vol. 10, Aug. 1973, pp. 449–458.

This paper, in addition to discussing in detail the generation of static loads conditions, provides extensive general information pertinent to both static and dynamic loads. This includes information on grid systems, use of matrix algebra, sources of data, scanning and stacking, repeated loads spectra, and loads validation tests.

St. Denis and Pierson

St. Denis, M. and Pierson, W. J., "On the Motions of Ships in Confused Seas," *Transactions of the Society of Naval Architects and Marine Engineers*, Vol. 61, 1953, pp. 280–357.

Primarily of historical interest, emphasizing the very narrow timespan over which power-spectral concepts gained attention in various engineering fields. For example, compare the date of this paper (1953) with those of other pioneering papers: Tukey (1949), Liepmann (1952), Press and Mazel-sky (1953), Press and Houbolt (1955), and even Rice (1944–1945).

Included in this work is an excellent discussion of the generation of a stationary-Gaussian process by the superposition of sinusoids. It is interesting to note that application of power-spectral techniques to the response of a ship to waves is far more complex than to the response of an airplane to atmospheric turbulence. The waves are far from isotropic, they are moving (even though the water as a whole is not), and waves of different wavelength move with different speeds. Consequently the ship's course relative to the wave pattern is of great importance and it is impossible to determine the sea state from measurements along a single profile.

Tukey

Tukey, J. W., "The Sampling Theory of Power Spectrum Estimates," Symposium on Applications of Autocorrelation Analysis to Physical Problems, Wood's Hole Oceanographic Institution, Woods Hole, MA, June 1949. (Sponsored by Office of Naval Research, U.S. Navy.)

Included for historical interest. This apparently is the original source for the Blackman–Tukey method of determining psd's from time history-data.

AFFDL-TR-68-127, Vol. 1 (HICAT)

Crooks, W. M., Hoblit, F. M., and Mitchell, F. A., "Project HICAT High Altitude Clear Air Turbulence Measurements and Meteorological Correlations," Air Force Flight Dynamics Laboratory AFFDL-TR-68-127, Vol. 1, Nov. 1968.

This is the final report of the high altitude clear air turbulence measurement program (HICAT) conducted by Lockheed in conjunction with the USAF, using a U-2 airplane to measure the turbulence. In addition to the data on gust psd shape and isotropy, material of particular interest includes:

- 1) Nondimensional plots of Martin-Graham filter characteristics (pp. 188–195).
- 2) Plots of mathematically defined gust psd curves (reduced scale, four per page) (pp. 205–217).
- 3) Stationarity of flight-measured turbulence samples and effect on computed probability distributions of σ_w (pp. 99–109). Clear and comprehensive discussion.

AFFDL-TR-71-5 (Doublet-Lattice)

Giesing, J. P., Kalman, T. P., and Rodden, W. P., *Subsonic Unsteady Aerodynamics for General Configurations: Part II, Application of the Doublet-Lattice Method and the Method of Images to Lifting-Surface/Body Interference*, Air Force Flight Dynamics Laboratory AFFDL-TR-71-5, Vol. I, 1971.

This and the Albano and Rodden paper³³ constitute the basic sources for the doublet-lattice method as used at the Lockheed-California Company.

AFFDL-TR-75-121 (Houbolt Plunge-Pitch Equations)

Houbolt, J. C. and Williamson, G. G., “Spectral Gust Response for an Airplane with Vertical Motion and Pitch,” Air Force Flight Dynamics Laboratory AFFDL-TR-75-121, Oct. 1975.

Gives equations of motion for a rigid airplane free to plunge and pitch. Penetration and unsteady aero effects are included, using as collocation “points” two spanwise lines on the wing and one on the tail (both unswept). Nondimensionalization of the gust input spectrum is confusing; care will be required in use. Computer program listing is believed to be available from NASA.

ASD-TR-61-235 (Optimum Fatigue Spectra)

Neuls, G. S., Maier, H. G., Leverick, T. R., Robb, E. A., and Webster, T. J., “Optimum Fatigue Spectra,” Second Phase Report, USAF Aeronautical Systems Division ASD TR 61-235, 1962.

Of historical interest. The gust loads section contains a redetermination of the P 's and b 's, with the following improvements over the NACA TN 4332¹⁷ data:

- 1) Utilized military data at the higher altitudes in addition to the extensive NASA VGH data.

2) Utilized the original Δn data before conversion to U_{de} ; Δn values were immediately converted to y/\bar{A} and plotted vs $N(y)/N_0$.

3) In determining K_{cs} , used actual lift curve slope instead of 2π in computing mass parameter.

BAC VTO/D/M/257

Card, V., "The Development of the Jones Statistical Discrete Gust Method for the Prediction of Aircraft Gust Loads," British Aircraft Corporation Rept. VTO/D/M/257, Nov. 1976 (apparently not widely distributed).

Despite its title, this report is noteworthy primarily for its coverage of a unique analytical investigation of the validity of psd methods for gust loads determination. Four measured gust velocity profiles were used, varying in length from about 50 s to at least 300 s. Each profile was traversed by a series of six highly idealized airplanes, characterized by a single natural frequency and a range of relative damping values (ζ) from 0.02–0.70. Generalized exceedance curves were obtained from the resulting acceleration time histories, utilizing \bar{A} and N_0 values calculated using a von Kármán gust psd. The degree to which the six exceedance curves for each sample collapsed to a single curve then provided a measure of the validity of the method.

A similar evaluation of the Jones statistical discrete-gust method is also included.

FAA-ADS-53

Hoblit, F. M., Paul, N., Shelton, J. D., and Ashford, F. E., "Development of a Power-Spectral Gust Design Procedure for Civil Aircraft," FAA Tech. Rept. FAA-ADS-53, Jan. 1966.

This report was prepared by the Lockheed-California Company under contract with the FAA. It has become a basic guide worldwide for the establishment of criteria for continuous-turbulence gust loads.

Particular subjects of interest are

- 1) Gust psd as standardized for design use (Sec. 5.2).
- 2) Plots of P 's and b 's vs altitude for design use and of resulting generalized exceedance curves (Sec. 5.3).
- 3) Formal statements of design-envelope, mission analysis, and combined forms of criteria (Chapters 4 and 15).
- 4) Discussion of limit vs ultimate basis for design loads (Chapter 15)
- 5) Discussion of per-hour vs per-mile basis for design frequency of exceedance (Chapter 4).
- 6) Overall procedures for design gust loads determination (Chapter 16);
- 7) The place of the discrete-gust concept, including discussion of a psd gust loads formula (Chapter 17).
- 8) Discussion of basic concepts relating to the 'joint probability' approach of treating combined loads (Chapter 12).

NACA Report 1272

Press, H., Meadows, M. T., and Hadlock, I., "A Reevaluation of Data on Atmospheric Turbulence and Airplane Gust Loads for Application in Spectral Calculations," NASA Rept. 1272, 1956. (Supersedes NACA TN 3362 and TN 3540, 1955.)

Primarily of historical interest this is a landmark paper, which is excellently written. This paper was the first to introduce the concept of determining probability distributions of σ_w from operational c.g. acceleration peak count data, thus paving the way for the more complete and practical approach developed in NACA TN 4332.¹⁷

Includes the first published use of $L = 1000$ ft as a standard value of the scale of turbulence in the Dryden psd equation and of the use of the notation \bar{A} as the ratio of response to gust velocity **rms values**. Also includes the first published curves of K_σ (there denoted $\sqrt{I(K, s)/\pi}$) as a function of mass parameter for various values of \bar{c}/L .

NACA TN 2853

Press, H. and Mazelsky, B., "A Study of the Application of Power-Spectral Methods of Generalized Harmonic Analysis to Gust Loads on Airplanes," NACA TN 2853, Jan. 1953; also, NACA Rept. 1172, 1954.

Of historical interest as the first NACA/NASA publication on the application of power-spectral methods to gust loads studies.

NACA TN 4332

Press, H. and Steiner, R., "An Approach to the Problem of Estimating Severe and Repeated Gust Loads for Missile Operations," NACA TN 4332, 1958.

Primarily of historical interest, this paper builds on the concepts developed in NACA Rept. 1272, and for the first time uses the P 's and b 's form of mathematical expression for σ_w probability distributions and generalized exceedance curves. Also improves on the techniques presented in Rept. 1272 in that it utilizes peak count data in the form of U_{de} 's rather than c.g. Δn 's, thus obviating the need to use average airspeeds in converting from accelerations to gust velocities.

Presents curves of P 's and b 's vs altitude over the altitude range 0–60,000 ft, thus for the first time defining σ_w probability distributions systematically and continuously over the full range of altitudes pertinent (at that time) to aircraft operations.

Despite the title, pertains equally to missile and airplane applications. The only difference is that for missile application, the P_2 values are much higher, reflecting the absence of any attempt at storm avoidance.

NASA CR-2639 (Reeves, Non-Gaussian Turbulence)

Reeves, P. M., Joppa, R. G., and Ganzer, V. M., "A Non-Gaussian Model of Continuous Atmospheric Turbulence for Use in Aircraft Design," NASA CR-2639, Jan. 1976.

This report reviews the stationary-Gaussian model and the evidence of its inadequacies. It then proposes a particular non-Gaussian model and develops a procedure for response calculations.

The proposed model apparently accounts well for variations of σ_w over some 20 h of low-altitude flight under given conditions of terrain and atmospheric stability, as long as the parameter R is adjusted for best fit for each such 20-h sample. The proposed model, however, does not reproduce the probability density of gust velocity *differences*, in comparison with the probability density of the gust velocity itself; in fact, it goes slightly in the wrong direction.

Excellentlly organized and written, this report indicates clearly what the problems are.

NASA CR-159097 (Lockheed-NASA ACS Studies)

Johnston, J. F., et al., *Accelerated Development and Flight Evaluation of Active Controls Concepts for Subsonic Aircraft: Load Alleviation/Extended Span Development and Flight Test*, Vol. 1, NASA CR-159097, Sept. 1979.

This is the final report of the Lockheed-NASA program involving active control system development and flight test for the L-1011.

Section 4.2 provides a general but thorough description, without mathematics, of the Lockheed-California Company VGA and GLP gust loads program systems.

Section 5.7 is a major section, 95 pages, covering the analysis of the gust-response flight-test data. Sections 5.7.1–5.7.7 especially are of general interest; these sections provide a thorough exposition of the principles involved in analyzing continuous turbulence flight-test data. Subjects that may be of special interest are:

- 1) Spectrum-method vs cross-spectrum-method transfer functions (Sec. 5.7.3).
- 2) Comparison of test with theory on basis of psd given by design gust psd times square of modulus of transfer function (Sec. 5.7.6).
- 3) Coherency as measure of quality of data and presence of other inputs; theoretical coherency (Sec. 5.7.6, 5.7.7).
- 4) Measured coherency when true coherency is zero (Fig. 5-102).
- 5) Effect of second input on load reductions achievable by an active control system (Fig. 5-105).

Section 5.7 also includes a thorough discussion of the flight-test findings with respect to pilot use of controls in turbulence.

NASA TR R-199

Houbolt, J. C., Steiner, R., and Pratt, K. G., "Dynamic Response of Airplanes to Atmospheric Turbulence Including Flight Data on Input and Response," NASA TR R-199, June 1964. (Initially presented as an AGARD paper, July 1962.)

This is a thick report, presenting a wealth of information based on the concepts of power-spectral analysis. Apparently, this was the first widely read report proposing the von Kármán spectral shape for use in gust-response work—although it was referred to only as the "isotropic turbulence" spectrum. Earlier, the von Kármán shape was one of six utilized in NACA TN 3920 (1957) for calculating two-dimensional gust response.

This report includes an extensive discussion, in Appendices D and E, of determination of psd data from time histories. Topics treated include prewhitening, aliasing, frequency resolution, coherency, statistical reliability, and selection of parameters such as sample rate and number of lags (Blackman-Tukey procedure). It also includes an extensive bibliography.

RAE TR 73,167 (Jones, 1973 Progress Report)

Jones, J. G., "A Statistical Discrete Gust Theory for Aircraft Loads, Progress Report," Royal Aircraft Establishment TR 73,167, Oct. 1973.

One of a long series of reports by Jones on his development of a more realistic discrete-gust model of atmospheric turbulence for design use.

RAE TM FS 208 (Jones, 1978 Update)

Jones, J. G., "On the Formulation of Gust-Load Requirements in Terms of the Statistical Discrete-Gust Method," Royal Aircraft Establishment TM FS 208, Oct. 1978.

This report provides more details than available in Jones' 1973 report on how the statistical discrete-gust approach might actually be used to determine airplane design loads. Provides for inputs consisting, alternately, of sequences of one, two, four, or eight critically spaced ramp gusts, of magnitude depending on the number of gusts in the sequence. Provides for different design gust velocities U_0 and cluster factors p_n for isolated gusts and continuous turbulence. Realistic treatment is thus provided for lightly damped as well as heavily damped systems. Emphasizes the point suggested in Sec. 12.3.2 herein that, when psd methods are used and design gust velocities are set to provide proper wing loads, the patchiness of real turbulence will result in an overprediction of loads when lightly damped modes predominate. Confined to the design envelope form of criterion.

In setting design gust velocities, for use with either the psd or SDG methods, Jones seems to consider it important that the resulting loads agree closely with those given by existing discrete-gust methods, on the basis of the

satisfactory service record of existing airplanes. He concludes that current U.S. psd criteria give wing loads that are too low and fin loads that are too high. U.S. engineers would tend to disagree with the position that existing discrete-gust methods give proper loads in either case. U.S. transports designed to current U.S. psd requirements have not always met BCAR (except through a rather tenuous interpretation thereof), yet they have experienced a quite satisfactory safety record. Conversely, U.S. experience includes considerable evidence that current discrete-gust load requirements do not provide adequate fin strength because they do not provide for the resonant buildup of load that occurs with a lightly damped Dutch-roll mode.

Included, for various airplanes, are values of psd U_σ required to give the same airplane Δn as a Pratt U_{de} of 50 fps, and also, values of SDG U_0 to give the same airplane Δn as a Pratt U_{de} of 50 fps. These are plotted (separately) vs an airplane "size" parameter, $M/(\rho/2)SC_{L\alpha}$. (This is actually the response parameter δ , introduced in Sec. 8.2.1.) The trends for the psd and SDG data agree closely. The comparison for psd data is very similar to the comparison shown in Table 13.1 herein (although in Table 13.1, ρ is not included in the parameter because the comparison is confined to a single altitude of 20,000 ft). In plotting U_σ for constant U_{de} , however, rather than U_{de} for constant U_σ as in Table 13.1, Jones implies that the newer, more realistic methods of loads determination should be judged by their agreement with the older method; the converse would seem to be more illuminating.

SEG-TR-65-4

Austin, W. H., Jr., "Environmental Conditions to be Considered in the Structural Design of Aircraft Required to Operate at Low Levels," SEG-TR-65-4, 1965.

Of historical interest. Modifies the low-altitude P 's and b 's to reflect F-106 measurements and B-52 structural damage. It is of interest to add to Austin's Fig. 4 the storm turbulence line from Ref. 13, modified to $L = 500$ ft. (This line is defined by y intercept = 4×10^{-3} , x intercept = 112 and goes right through the B-52 points.)

SEG-TR-67-28

Austin, W. H., Jr., "Development of Improved Gust Load Criteria for United States Air Force Aircraft," SEG-TR-67-28, 1967.

Of historical interest. Adapts Ref. 13 for military use by

1) Putting the mission analysis on an ultimate basis [and calling it a rational probability analysis (RPA) per previous USAF usage] and establishing a design ultimate frequency of exceedance of $0.0005/60,000 = 0.833 \times 10^{-8}$ c/h.

2) Reducing L for altitudes below 2500 ft, modifying the b 's accordingly, and retaining the very low altitude b_2 values established in SEG-TR-65-4.

3) Deleting the alternative of a design-envelope analysis only, using conservative U_σ 's.

REFERENCES

¹Etkin, B., *Dynamics of Flight*, Wiley, New York, 1959.

²Federal Aviation Regulations, "Part 25—Airworthiness Standards: Transport Category Airplanes." U.S. Dept. of Transportation, Federal Aviation Administration. Also, Code of Federal Regulations, Title 14, Aeronautics and Space, "Part 25—Airworthiness Standards: Transport Category Airplanes," Sept. 1980.

³Donely, P., "Summary of Information Relating to Gust Loads on Airplanes," NACA Rept. 997, 1950.

⁴Etkin, B., "Turbulent Wind and Its Effect on Flight," *Journal of Aircraft*, Vol. 18, May 1981, pp. 327–345.

⁵Pratt, K. G., "A Revised Formula for the Calculation of Gust Loads," NACA TN 2964, June 1953.

⁶British Civil Airworthiness Requirements, Civil Aviation Authority, Cheltenham, UK.

⁷Jones, J. G., "Statistical Discrete Gust Theory for Aircraft Loads: A Progress Report," Royal Aircraft Establishment TR 73167, Oct. 1973.

⁸Chen, W.-Y., "Application of Rice's Exceedance Statistics to Atmospheric Turbulence," *AIAA Journal*, Vol. 10, Aug. 1972, pp. 1103–1105.

⁹Johnston, J. F., et al., *Accelerated Development and Flight Evaluation of Active Controls Concepts for Subsonic Aircraft: Load Alleviation/Extended Span Development and Flight Test*, Vol. 1, NASA CR-159097, Sept. 1979.

¹⁰Houbolt, J. C., Steiner, R., and Pratt, K. G., "Dynamic Response of Airplanes to Atmospheric Turbulence Including Flight Data on Input and Response," NASA TR R-199, June 1964 (initially presented as an AGARD paper, July 1962).

¹¹Diederich, F. W. and Drischler, J. A., "Effect of Spanwise Variations in Gust Intensity on the Lift Due to Atmospheric Turbulence," NACA TN 3920, April 1957.

¹²Liepmann, H. W., "On the Application of Statistical Concepts to the Buffeting Problem," *Journal of the Aeronautical Sciences*, Vol. 19, 1952, pp. 793–800.

¹³Hoblit, F. M., Paul, N., Shelton, J. D., and Ashford, F. E., "Development of a Power-Spectral Gust Design Procedure for Civil Aircraft," Federal Aviation Agency TR FAA-ADS-53, Jan. 1966.

¹⁴Military Specification, "Airplane Strength and Rigidity: Flight Loads," MIL-A-008861A (USAF), March 1971.

¹⁵Crooks, W. M., Hoblit, F. M., and Mitchell, F. A., "Project HICAT High Altitude Clear Air Turbulence Measurements and Meteorological Correlations," Air Force Flight Dynamics Laboratory TR-68-127, Vol. 1, Nov. 1968, pp. 70 and 205–217.

¹⁶Rice, S. O., "Mathematical Analysis of Random Noise," *Bell System Technical Journal*, Vol. XXIII, No. 3, July 1944, pp. 282–332, and Vol. XXIV, No. 1, Jan. 1945, pp. 46–156; also, in Wax, N., *Selected Papers on Noise and Stochastic Processes*, Dover, New York, 1954.

¹⁷Press, H. and Steiner, R., "An Approach to the Problem of Estimating Severe and Repeated Gust Loads for Missile Operations," NACA TN 4332, 1958.

¹⁸Press, H., Meadows, M. T., and Hadlock, I., "A Reevaluation of Data on Atmospheric Turbulence and Airplane Gust Loads for Application in Spectral Calculations," NACA Rept. 1272, 1956 (supersedes NACA TN 3362 and TN 3540, 1955).

¹⁹Saunders, K. D., *B-66B Low Level Gust Study: Technical Analysis*, WADD TR 60-305, Vol. 1, March 1961.

²⁰Austin, W. H., Jr., "Environmental Conditions to be Considered in the Structural Design of Aircraft Required to Operate at Low Levels," SEG-TR-65-4, 1965.

²¹Feller, W., *An Introduction to Probability Theory and Its Applications*, Vol. 1, Wiley, New York, 1950.

²²Peirce, B. O., *A Short Table of Integrals*, Ginn, Boston, MA, 1929.

²³Stauffer, W. A. and Hoblit, F. M., "Dynamic Gust, Landing, and Taxi Loads Determination in the Design of the L-1011," *Journal of Aircraft*, Vol. 10, Aug. 1973, pp. 459–467.

²⁴Austin, W. H., Jr., "Development of Improved Gust Load Criteria for United States Air Force Aircraft," SEG-TR-67-28, 1967.

²⁵Military Specification, "Airplane Strength and Rigidity—Reliability Requirements, Repeated Loads, and Fatigue," MIL-A-8866 (ASG), May 1960.

REFERENCES

299

²⁶“Aircraft Gust Criteria Survey,” Aerospace Technical Council TR-104, Aerospace Industries Association of America, Aug. 1970.

²⁷Fuller, J. R., Richmond, L. D., Larkins, C. D., and Russell, S. W., “Contributions to the Development of a Power-Spectral Gust Design Procedure for Civil Aircraft,” FAA TR FAA-ADS-54, Jan. 1966

²⁸Hoblit, F. M., “Effect of Yaw Samper on Lateral Gust Loads in Design of the L-1011 Transport,” in *Active Control Systems for Load Alleviation, Flutter Suppression, and Ride Control*, AGARD-AG-175, March 1974 (paper presented Oct. 1973).

²⁹Ramsey, H. D. and Lewolt, J. G., “Design Maneuver Loads for an Airplane with an Active Control System,” AIAA Paper 79-0738, AIAA/ASME/ASCE/AHS 20th Structures, Structural Dynamics, and Materials Conf., St. Louis, MO, April 4–6, 1979.

³⁰Gould, J. D., “Effect of Active Control System Nonlinearities on the L-1011-3 (ACS) Design Gust Loads,” AIAA Paper 85-0755, AIAA/ASME/ASCE/AHS 26th Structures, Structural Dynamics, and Materials Conf., Orlando, FL, April 15–17, 1985.

³¹Moon, R. N., “Application of Linear Optimization Theory to Development of Design Load Conditions from Statistical Analysis,” AIAA Paper 79-0740, AIAA/ASME/ASCE/AHS 20th Structures, Structural Dynamics, and Materials Conf., St. Louis, MO, April 4–6, 1979.

³²Watkins, C. E., Woolston, D. S., and Cunningham, H. J., “A Systematic Kernel Function Procedure for Determining Aerodynamic Forces on Oscillating or Steady Finite Wings at Subsonic Speeds,” NASA TR R-48, 1959.

³³Albano, E. and Rodden, W. P., “A Doublet-Lattice Method for Calculating Lift Distributions on Oscillating Surfaces in Subsonic Flow,” *AIAA Journal*, Vol. 7, Feb. 1969, pp. 279–285.

³⁴Giesing, J. P., Kalman, T. P., and Rodden, W. P., *Subsonic Unsteady Aerodynamics for General Configurations: Part II, Vol. I, Application of the Doublet-Lattice Method and the Method of Images to Lifting-Surface/Body Interference*, Air Force Flight Dynamics Laboratory TR-71-5, 1971.

³⁵Fung, Y. C., “Statistical Aspects of Dynamic Loads,” *Journal of the Aeronautical Sciences*, Vol. 20, May 1953, pp. 317–330.

³⁶Houbolt, J. C., “Design Manual for Vertical Gusts Based on Power Spectral Techniques,” Air Force Flight Dynamics Laboratory TR-70-106, Dec. 1970.

³⁷Taylor, J., *Manual on Aircraft Loads*, Pergamon, New York, 1965.

³⁸Pratt, K. G. and Bennett, F. V., "Charts for Estimating the Effects of Short-Period Stability Characteristics on Airplane Vertical Acceleration and Pitch-Angle Response in Continuous Atmospheric Turbulence," NACA TN 3992, June 1957.

³⁹Peele, E. L., "A Method for Estimating Some Longitudinal and Lateral Rigid-Body Responses of Airplanes to Continuous Atmospheric Turbulence," NASA TN D-6273, Aug. 1971 (first issued in 1968 as a NASA-Langley Working Paper).

⁴⁰Houbolt, J. C. and Williamson, G. G., "Spectral Gust Response for an Airplane with Vertical Motion and Pitch," Air Force Flight Dynamics Laboratory TR-75-121, 1975.

⁴¹Eichenbaum, F. D., "A General Theory of Aircraft Response to Three-Dimensional Turbulence," *Journal of Aircraft*, Vol. 8, May 1971, pp. 353-360.

⁴²Eichenbaum, F. D., "Response of Aircraft to Three-Dimensional Random Turbulence," Air Force Flight Dynamics Laboratory TR-72-28, Oct. 1972.

⁴³Eichenbaum, F. D., "Evaluation of 3-D Turbulence Techniques for Designing Aircraft," Air Force Flight Dynamics Laboratory TR-74-151, March 1975.

⁴⁴Coupry, G., "Effect of Spanwise Variation of Gust Velocity on Airplane Response to Turbulence," *Journal of Aircraft*, Vol. 9, Aug. 1972, pp. 569-574.

⁴⁵Bennett, F. V. and Yntema, R. T., "Evaluation of Several Approximate Methods for Calculating the Symmetrical Bending-Moment Response of Flexible Airplanes to Isotropic Atmospheric Turbulence," NASA Memo 2-18-59L, March 1959.

⁴⁶Kaynes, I. W., "Aircraft Centre of Gravity Response to Two-Dimensional Spectra of Turbulence," Ministry of Aviation, Aeronautical Research Council, R. & M. No. 3665, June 1970.

⁴⁷Eichenbaum, F. D., "The Application of Matrix Methods to Clear Air Turbulence Measurement," AIAA Paper 66-967, Nov. 1966.

⁴⁸Press, H. and Tukey, J. W., "Power Spectral Methods of Analysis and Their Application to Problems in Airplane Dynamics," in *AGARD Flight Test Manual*, Vol. 4, Pt. IVC, June 1956.

⁴⁹Soovere, J., "Smoothing Errors in Fourier Transform Based Modal Data Analysis," Society of Automotive Engineers Aerospace Technology Conf., Long Beach, CA, Oct. 14-17, 1985.

⁵⁰Keisler, S. R. and Rhyne, R. H., "An Assessment of Prewhitening in Estimating Power Spectra of Atmospheric Turbulence at Long Wavelengths," NASA TN D-8288, Nov. 1976.

REFERENCES

301

- ⁵¹Mark, W. D., "Characterization of Nongaussian Atmospheric Turbulence for Prediction of Aircraft Response Statistics," NASA CR-2913, Dec. 1977.
- ⁵²Burns, A., "On the Nature of Large Clear Air Gusts Near Storm Tops," Aeronautical Research Council CP 1248, 1973.
- ⁵³Jones, J. W., "High Intensity Gust Investigation (WFT 1217 R3)," Boeing-Wichita Rept. D-13273-333A, Oct. 1964.
- ⁵⁴Reeves, P. M., Joppa, R. G., and Ganzer, V. M., "A Non-Gaussian Model of Continuous Atmospheric Turbulence for Use in Aircraft Design," NASA CR-2639, Jan. 1976.
- ⁵⁵Gould, D. G. and MacPherson, J. I., "A Suggested Method for Estimating Patch Length from Turbulence Measurements Using Results from Low Altitude Flights by a T-33 Aircraft," National Academy of Engineering Rept. LR-562, National Research Council of Canada, Aug. 1972.
- ⁵⁶Strom, A. J. and Weatherman, T. G., *NB-66-B High Altitude Gust Survey: Vol. I, Technical Analysis, and Vol. III, Time Series*, USAF ASD-TR-63-145, June 1963.
- ⁵⁷Card, V., "The Development of the Jones Statistical Discrete Gust Method for the Prediction of Aircraft Gust Loads," British Aircraft Corp. Rept. VTO/D/M/257, Nov. 1976.
- ⁵⁸Houbolt, J. C. and Williamson, G., "A Direct Time History Study of the Response of an Airplane to Nonstationary Turbulence," Air Force Flight Dynamics Laboratory TR-74-148, Jan. 1975.
- ⁵⁹Reeves, P. M., "A Non-Gaussian Turbulence Simulation," Air Force Flight Dynamics Laboratory TR-69-67, Nov. 1969.
- ⁶⁰Reeves, P. M., Campbell, G. S., Ganzer, V. M., and Joppa, R. G., "Development and Application of a Non-Gaussian Atmospheric Turbulence Model for Use in Flight Simulators," NASA CR-2451, Sept. 1974.
- ⁶¹Tomlinson, B. N., "Developments in the Simulation of Atmospheric Turbulence," Paper 19 in AGARD-CP-198, June 1976 (paper presented Oct. 1975).
- ⁶²Coles, W. W. and Porter, R. W., "Non-Spectral Turbulence," Hawker-Siddeley Stress Office Rept. 142, May 1973.
- ⁶³Noback, R., "Comparison of Discrete and Continuous Gust Methods for Airplane Design Loads Determination," *Journal of Aircraft*, Vol. 23, March 1986, pp. 226-231.

⁶⁴Coupry, G., "Analyse Critique de la Méthode de Jones," Office National d'Etudes et de Recherches Aérospatiales Rept. 10/5108 RY OR, March 1978.

⁶⁵Noback, R., "Comparison Between the Statistical Discrete Gust Method and the Power-Spectral Density Method," NLR TR 75158U (The Netherlands), Nov. 1975.

⁶⁶*Handbook of Mathematical Functions with Formulas*, U.S. Department of Commerce, Washington, D.C.

⁶⁷Burington, R. S. and May, D. C., Jr., *Handbook of Probability and Statistics with Tables*, Vol. 81. Handbook Publishers, Sandusky, OH, 1953.

⁶⁸Kenney, J. F., *Mathematics of Statistics*, Van Nostrand, New York, 1939.

⁶⁹Taylor, J., "Atmospheric Loads on Aircraft," *Aeronautical Journal*, Dec. 1977.

⁷⁰Taylor, J., "The Energy and Pressure Spectra of Homogeneous Isotropic Turbulence," Royal Aircraft Establishment TR 66346, 1966.

⁷¹Stapleford, R. L. and DiMarco, R. J., "Evaluation of a Describing Function Approach to Nonlinear Gust Loads Analysis," *Journal of Aircraft*, Vol. 17, Feb. 1980, pp. 87-94.

⁷²Arley, N. and Buch, K. R., *Introduction to the Theory of Probability and Statistics*, Wiley, New York, 1950.

Index

- Active control systems, 95–96, 121, 169–171
 Active failure, 95
 Aerodynamic data, 118
 Aerodynamic forces, 16, 118, 279–281
 Airplane motions, 4–5
 Albano, E., 287
 Aliasing, 185
 Alleviation factor, 12
 Amplitude ratio, 35–37
 Austin, W. H., Jr., 296
 Autocorrelation function, 32–34
 Autocovariance function, 32–34
- b*'s and *P*'s:
 design values, 56–59
 determination, 62–65
 relation to *L*, 65
 sources of data, 65
- Blackman, R. B., 287
 Blackman–Tukey procedure, 34, 177, 178, 290
 Burns, Anne, 187, 190
- Card, V., 292
 Characteristic frequency, (*see* N_0)
 Check flights, 84
 Checks for error, 121–122
 Chen, Wen-Yuan, 29, 190, 192, 287
 Circumscribing octagons, 100, 101–102, 108, 110
 Coherency function, 176
 Combined criterion, 77
 Combined vertical and lateral gust loads, 92–94
 how to combine, 92
 mission analysis application, 94
 when to combine, 92–94
 Comparative analysis, 19–20
 Correlation coefficient, 101–102
 Coupling, 16
 Coupry, G., 126, 166, 195
 Criteria, 69–96
 Crooks, W. M., 290
 Cross-spectrum method, 166, 176
 Cross-transfer function, 166
 Cruise altitude, 83
- Design envelope criterion, 72–77, 79–81
 definition, 72–73
 design values of U_σ at V_B and V_D , 81
 design values of U_σ at V_C , 79–81
 effect of N_0 , 90–92, 233–234
 FAR Appendix G requirements, 80
 Design gust velocities, 9, 11, 12, 19–20, 72–75, 79–81, 95
 Design load levels, 77–81
 Design speeds, 9
 Discrete gust idealization, 7–12, 194–195
 one-minus-cosine, 7, 12
 ramp, 9, 11
 sharp-edge, 8, 11
 Discrete-gust dynamic loads, 15–20, 197–198
 Discrete-gust static loads, 7–14, 198–202
 Dryden spectrum, 42–46, 70, 125, 129, 171, 227–228, 293
 Dynamic loads, 15
- Eichenbaum, Frederick D., 165, 167, 175
 Elementary distributions, 109
 Engine loads, 93
 Ensemble average, 23
 Equal probability ellipses, 101–102, 105–106
 Equations of motion, 11, 12, 115–122, 203–207, 275–281
 Exceedances, exceedance curves, 51–66
- Failures, active vs passive, 95
 FAR (Federal Aviation Regulations):
 continuous turbulence, 15, 69–70, 77, 80–81
 discrete-gust dynamic loads, 15, 17
 gust loads formula, 8–11
 history, 11–13
 static gust requirements, 7–11
 Fatigue, xii, 70, 87
 FFT (fast Fourier transform) procedure, 34, 177, 179
 Fictitious structural element concept, 103–106
 Filters, 171, 291
 Flight testing, 173–186
 averaging of data, 180–182
 basic approach, 174
 gust velocity determination, 175
 psd calculations, 175–177, 183–186
 psd parameter selection, 177–182
 purpose, 173–174
 sample selection, 174
 use of psd's, 175–177
 Flutter, 122
 Fourier series, 30–31

- Frequency of exceedance, 51–66, 70–72
 Frequency-response function, 35–37, 120–121, 276–281
 Frequency, spatial vs temporal, 34
 Fung curves, 123–125
 Fung, Y. C., 125, 288
 Fuselage loads, 93–94
- Gaussian probability distribution:
 definition, 21, 25–26
 numerical values, 26, 217–223
 significance, 27–28
- Generalized coordinates, 15, 115–116, 120, 279
 Generalized damping constant, 276
 Generalized exceedance curves, 59–62
 Generalized mass, 119, 275–276
 Generalized spring constant, 276
 Giesing, J. P., 291
 Gould, J. D., 170, 171
 Gradient distance, 7, 9, 10, 16–18, 195, 198, 205
 Grid systems for analysis, 116–117
 Gust velocity (*see also* gust velocity psd's)
 continuous turbulence (U_{σ}), 72–75, 79–81
 derived equivalent (U_{de}), 8, 9, 12
 design values, 9, 11, 12, 72–75, 79–81
 Gust velocity psd's:
 constant- σ_w vs constant-asymptote families, 48–50
 design, 42–46
 Dryden, 42–46, 129, 171, 227–228
 generation of time histories, 170–171
 geometric properties, 45
 L , (*see* scale of turbulence)
 mathematically defined shapes, 51
 measured shapes, 39, 47
 vertical-lateral vs longitudinal, 42, 44, 50–51
 von Kármán, 42–50, 71, 73, 123, 126, 129, 167, 171, 177, 227–228
- Hadlock, I., 293
 Hall formula, 126
 Hall, J., 126
 Hanning, 183
 Head-on gust, 2–5
 Hoblit, F. M., 288, 289, 290
 Hoblit plunge-pitch curves, 129–145
 Horizontal tail loads, 87, 93
 Houbolt, J. C., 156–157, 194, 235, 289, 291, 295
 Hours vs miles, 71
- Input-output relation, 37–38
 Integrated loads, 16, 120
 Integration of joint probability density of w and σ_w , 263–269
 Intermittency, 187
 Internal loads, 107–108
 Isotropy, 6
- Joint probability density, 28–29, 101, 105–106, 111–112, 263–269
 Joint probability technique, 111–113
 Jones, J. G., 18, 194–195, 295
- Kalman, T. P., 291
 Kussner function,
 definition, 125, 204
 effect on loads, 157
 Liepmann expression, 125, 133, 153, 154–156
 Peele expression, 148, 149, 153, 154–156
- Lag in buildup of lift, 7, 125, 203
 Lateral gust loads, 1, 4, 92–94, 134, 146
 Level crossings, 52–53, 63–64
 Lewolt, J. G., 290
 Liepmann, H. W., 42, 125, 288
 Lift growth assumptions, 125, 133, 148, 149, 153, 154–156, 157, 203–204
 Limit vs ultimate loads criteria, 71
 Loads for stress analysis, 107–113
- Mass data, 117, 119
 Mass parameter, 8, 123
 Mass-spring-damper system, 4
 Matching condition technique, 108–111
 Matrix algebra, 119–120, 275–282
 Mazelski, Bernard, 293
 Meadows, M. T., 293
 Military requirements:
 static discrete gust, 14
 continuous turbulence, 70
 Mission analysis criterion, 70–72, 73, 75–77, 78, 82–89
 airspeeds, 83
 check flights, 84
 cruise altitude, 83
 definition, 70, 71
 design frequency of exceedance, 78
 effect of N_0 on loads, 60, 233–234
 flaps-extended segments, 84, 87
 flight profile generation, 82–89
 fuel weights, 84
 payload, 83–84

- typical vs maximum values, 82
- use of average values, 88–89
- weight empty, 83
- Modes
 - elastic, 15–16, 115–116
 - rigid-body, 15–16, 115–116
- Moon, R. N., 288
- Neuls, G. S., 291
- N_0 , 54
 - definition, 54
 - computation, 54, 121, 229–235
 - effect on design envelope loads, 90–92, 233–234
 - effect on mission analysis loads, 60, 233–234
- Nonback, R., 195
- Non-Gaussian turbulence, 187–192
- Nonlinear systems, 96, 169–171
- Nonstationary turbulence, 187–192
- Nyquist frequency, 177, 178, 179, 185
- One-dimensional gust analysis (vs 3-D), 165–167
- One-g load, 18, 62, 70, 74, 243–252
- Passive failure, 95
- Patchiness, 187
- Peaks, peak counts, 51–52, 63–64
- Peele curves, 145–156
- Phase angle, 35–37, 278
- “Phasing” of design loads, 97–106
- Pierson, W. J., 290
- Pilot training flights, 84
- Plunge-only curves, 123–129
- Plunge-only data from plunge-pitch curves, 156
- Plunge-pitch curves, 129–156
- Power-spectral density, (*see* PSD)
- Power-spectral methods, xii, 21–38, 51–62
- Pratt, K. G., 295
- Press, Harry, 289, 293
- Prewhitening, 185–186
- Probability
 - density, 23
 - distribution, 23 25
 - notation, 23, 24
 - of exceedance, 65
 - theory of, 27, 209–215
- Psd (power-spectral density), 29–41
 - c.g. acceleration, 283–286
 - changes in the frequency argument, 34–35
 - definitions, 31–32
 - determination from time histories, 32–34, 177–186
 - gust velocity (*see* gust velocity psd's)
 - one-sided vs two-sided, 72
 - physical significance, 31
 - relation to rms value, 31
 - terminology, 31
 - typical shapes, 39–41
- Ratio of design to rms load (η_d), 73, 111–113, 262, 263
- Reeves, P. M., 192, 294
- Reliability, 95
- Repeated loads spectra, xi, 70, 87
- Resolution, 180
- Rice, S. O., 289
- Rice's equation, 29, 52–54, 55, 187, 188, 190, 191
- Rms (root-mean-square) value, 22–23
- Rms gust velocity (σ_w):
 - relation to psd curve, 31
 - most-likely value, 112, 253–273
 - probability distribution, 56–60, 62–65, 156
- Rodden, W. P., 287, 291
- Rotating vectors, 36, 277
- Saturation, 95, 96, 169–171
- Scale of turbulence (L):
 - design values, 46, 70
 - determination, 47
 - significance, 45, 46–50
- Segmentation of profiles, 54, 84, 86–88
- Short-cut methods, 123–164
 - empirical adjustments, 157–159
 - plunge-only curves, 123–129
 - plunge-only data from plunge-pitch curves, 156
 - plunge-pitch curves, 129–156
 - simplified equations, 156–157
- Simplified equations of motion, 156–157
- Single-variable vs multiple-variable
 - treatment of combined loads, 113
- Soovere, J., 184
- Sources of turbulence, 6
- Spanwise variation of gust velocity (*see* 3-D gust analysis)
- Spectral window, 183–184
- Spectrum method, 176
- Spring-mass-damper system, 4
- Stability augmentation system, 95–96, 121, 169–171
- Standard deviation, 22–23
- Static aeroelastic deformation, 13–14

- Static discrete-gust loads, 7–14, 198–202
- Stationarity, 63, 174, 190–192, 194
- Stationary Gaussian model of turbulence, 21, 187–194
- Stationary Gaussian random process, 21–22, 28–29
- Statistical discrete gust model of turbulence, 194–195
- Statistical reliability, 180
- Stauffer, W. A., 289, 290
- St. Denis, M., 290
- Steiner, R., 293, 295
- Stiffness data, 117–118
- Stresses, 107–108, 111–113
- Superposition of sinusoids, 29–31

- Three-dimensional gust analysis, 165–167
 - applications, 165–166
 - effect of L , 166–167
 - effects on loads, 166
 - theory, 165
- Transfer function, 35–37 (*see also* frequency-response function)
- Tukey, J. W., 287, 289, 290
- Tuned discrete-gust analysis, 16–17, 197–198
- Turbulence (atmospheric):
 - characteristics, 5–6, 197
 - clear air, 6
 - continuous, xi, 5
 - cumulus cloud, 6
 - nonstorm, 56
 - sources, 6
 - storm, 6, 56
 - terminology, 5, 6
- Typical gust profile, 5

- Ultimate gust velocity capability, 243–252
- Ultimate vs limit loads criteria, 71
- Unavailability, 95
- Upper limit of integration, 121, 229–235

- Variance, 22–23
- Vertical gust loads, 1
- Von Kármán spectrum, 42–50, 71, 73, 123, 126, 129, 167, 171, 177, 227–228

- Wagner function
 - definition, 125, 204
 - effects on loads, 157
- Wilson, E. B., 11

- Zero crossings, (*see* N_0)